

**THREE-PHASE DYNAMIC DISPLACEMENT MEASUREMENTS
OF RELATIVE PERMEABILITY IN POROUS MEDIA
USING THREE IMMISCIBLE LIQUIDS**

1991

LEE W. THOMAS, JR.

The Pennsylvania State University

The Graduate School

Department of Mineral Engineering

**THREE-PHASE DYNAMIC DISPLACEMENT MEASUREMENTS
OF RELATIVE PERMEABILITY IN POROUS MEDIA
USING THREE IMMISCIBLE LIQUIDS**

A Thesis in

Petroleum and Natural Gas Engineering

by

Lee W. Thomas, Jr.

Submitted in Partial Fulfillment
of the Requirements
for the Degree of

Master of Science

May 1991

T253529

Thesis
T 4174
C.1

I grant The Pennsylvania State University the nonexclusive right to use this work for the University's own purposes and to make single copies of the work available to the public on a not-for-profit basis if copies are not otherwise available.

We approve the thesis of Lee W. Thomas Jr.

ABSTRACT

An experimental investigation is conducted to examine the simultaneous motion of three phases in porous media. Limited research has been done in this area; therefore, the work is exploratory in nature. Experimental apparatus is constructed to enable the flow of three immiscible fluids through a one-dimensional, horizontal glass bead packed core. The fluids used are water, benzyl alcohol and decane, representing water, oil, and gas phases respectively. The apparatus allows the core to be brought to any combination of saturations of the three phases through steady-state and unsteady-state (dynamic displacement) experiments.

The main objective of the research is to map the relative permeabilities of the fluids in the interior region of the ternary diagram through a series of dynamic displacement water floods. Fluid relative permeabilities and saturations during the dynamic displacement experiments are calculated from the three-phase extension of the two-phase dynamic displacement theory of Welge's permeability ratios, and Johnson, Bossler and Naumann's two-phase method of determining individual relative permeabilities. Steady-state relative permeabilities are determined from Darcy's law.

The interior region of the ternary diagram cannot be mapped by a dynamic water flood originating along the residual water saturation line. The piston-like displacement of decane and the development of a benzyl alcohol (oil) bank create a Buckley-Leverett saturation jump which follows the residual water saturation line down to the dynamic residual decane saturation line. The saturation trajectory then follows the dynamic residual decane saturation line down to residual benzyl alcohol and decane saturations in the presence of water, bypassing the central region of the

ternary diagram. A difference in residual decane saturations is seen between the steady-state and the dynamic displacement floods.

Exact graphical matching of the core-end saturation change is seen between the displaced decane and the oil bank. This observation lends credence to the extension of the two-phase dynamic displacement theory to three phases.

Further investigation will be required to examine the mechanism behind the development of the oil bank and the difference in the residual decane saturations of the two types of floods.

Implications of the discovered oil bank phenomena include examining alternative methods for mapping the interior of the ternary diagram and possible applications to oil recovery.

TABLE OF CONTENTS

	<u>Page</u>
LIST OF FIGURES	vii
LIST OF TABLES.....	xii
NOMENCLATURE	xiv
ACKNOWLEDGMENTS.....	xviii
Chapter 1. INTRODUCTION	1
Chapter 2. REVIEW OF THE THEORY AND LITERATURE.....	3
2.1 Steady-State and Dynamic Relative Permeability Measuring Techniques	3
2.2 History of Three-Phase Relative Permeability Determination.....	4
2.3 Extension of the Welge/JBN Theory to Three Phases.....	6
2.4 Analysis Procedure	10
Chapter 3. PROBLEM STATEMENT	14
Chapter 4. EXPERIMENTAL APPARATUS	15
4.1 Apparatus Capabilities and Overview.....	15
4.2 Fluids.....	23
4.3 Injection System	24
4.4 Porous Medium and Core Holder	26
4.5 Pressure Monitoring System	28
4.6 Collection System.....	29
4.7 Additional Equipment.....	30
Chapter 5. EXPERIMENTAL PROCEDURE	31
5.1 System Core and Tubing Volume Determination	31
5.2 Pump Calibration	31
5.3 Core Preparation	31
5.4 Determination of Porosity.....	32
5.5 Determination of Core Linearity	34
5.6 Determination of Absolute Permeability.....	35
5.7 Steady-State Experiments	36

5.8 Dynamic Displacement Experiments	38
5.9 Fractional Recovery Analysis.....	40
Chapter 6. ERROR ANALYSIS.....	42
6.1 Error Analysis for Porosity.....	42
6.2 Error Analysis for Saturation	45
6.2.1 Error Analysis for Steady-State Saturations	45
6.2.2 Error Analysis for Non-Steady-State Saturations	47
6.3 Error Analysis for Absolute Permeability.....	49
6.4 Error Analysis for Relative Permeability.....	50
6.4.1 Error Analysis for Steady-State Relative Permeability	50
6.4.2 Error Analysis for Dynamic Relative Permeability.....	51
6.5 Relative Error Analysis.....	51
6.6 Pump Flow Rates.....	52
Chapter 7. RESULTS.....	56
7.1 Three-Phase Decane Flood Experiments	57
7.2 Two-Phase Water-Benzyl Alcohol Relative Permeability Experiments....	69
7.3 Two-Phase Benzyl Alcohol-Decane Relative Permeability Experiments..	98
7.4 Three-Phase Water Flood Experiments.....	120
7.5 Unacceptable Core Linearity Runs.....	143
Chapter 8. DISCUSSION.....	146
8.1 Verification.....	146
8.2 Apparatus.....	146
8.3 Exploratory Findings.....	148
8.4 Questions Raised From the Research.....	154
8.5 Implications.....	154
Chapter 9. CONCLUSIONS AND RECOMMENDATIONS	156
REFERENCES	158
Appendix A: TABULATED RUN DATA.....	160
Appendix B: COMPUTER PROGRAMS.....	180
B.1 READPT.BAS.....	181
B.2 DATAFRAC.F.....	183
B.3 PVST.F.....	188
B.4 VARIQ.F.....	190

LIST OF FIGURES

	<u>Page</u>
Figure 2.1: Recovery of Two Phases Displaced by a Third Phase as a Function of PVI.....	11
Figure 2.2: Normalized Pressure Drop as a Function of PVI	13
Figure 4.1: Flooding Capabilities of the Apparatus; Single-Phase Injection	16
Figure 4.2: Flooding Capabilities of the Apparatus; One-Phase into One-Phase	17
Figure 4.3: Flooding Capabilities of the Apparatus; One-Phase into Two-Phases.....	18
Figure 4.4: Flooding Capabilities of the Apparatus; Two-Phases into Two-Phases.....	19
Figure 4.5: Flooding Capabilities of the Apparatus; One-Phase into Three-Phases.....	19
Figure 4.6: Flooding Capabilities of the Apparatus; Two-Phases into Three-Phases.....	20
Figure 4.7: Flooding Capabilities of the Apparatus; Three-Phases into Three-Phases.....	20
Figure 4.8: Apparatus Schematic	22
Figure 4.9: Core Pressure Tap Schematic	27
Figure 6.1: Water Pump - Actual vs. Specified Flow Rates	53
Figure 6.2: BA Pump - Actual vs. Specified Flow Rates.....	54
Figure 6.3: Decane Pump - Actual vs. Specified Flow Rates	55
Figure 7.1: Core Linearity Check Pressure Profile; Run 2.....	58
Figure 7.2: Dynamic Flood Recovery Curves; Run 2	59
Figure 7.3: Expanded Dynamic Flood Recovery Curves; Run 2.....	60

Figure 7.4: Saturation History and Trajectories; Run 2.....	62
Figure 7.5: Dynamic Flood Normalized Pressure Profile; Run 2.....	63
Figure 7.6: Core Linearity Check Pressure Profile; Run 3.....	65
Figure 7.7: Dynamic Flood Recovery Curves; Run 3	66
Figure 7.8: Expanded Dynamic Flood Recovery Curves; Run 3.....	67
Figure 7.9: Saturation History and Trajectories; Run 3.....	68
Figure 7.10: Dynamic Flood Normalized Pressure Profile; Run 3.....	70
Figure 7.11: BA Relative Permeabilities vs. BA Saturation; Run 3	71
Figure 7.12: Decane Relative Permeabilities vs. Decane Saturation; Run 3	72
Figure 7.13: Water Relative Permeabilities vs. Water Saturation; Run 3.....	73
Figure 7.14: Core Linearity Check Pressure Profile; Run 9.....	74
Figure 7.15: Saturation History and Trajectories; Run 9 - First Dynamic Water Flood	76
Figure 7.16: Expanded Dynamic Flood Recovery Curves; Run 9 - First Dynamic Water Flood	77
Figure 7.17: Normalized Pressure Drop (Fixed q) vs. PVI; Run 9 - First Dynamic Water Flood	78
Figure 7.18: Normalized Pressure Drop (Variable q) vs. PVI; Run 9 - First Dynamic Water Flood	80
Figure 7.19: Fixed vs. Variable Normalized Pressure Drop Comparison; Run 9 - First Dynamic Water Flood	81
Figure 7.20: Oil and Water Relative Permeabilities vs. Water Saturation; Run 9 - First Dynamic Water Flood	82
Figure 7.21: Saturation History and Trajectories; Run 9 - Second Dynamic Water Flood	83
Figure 7.22: Expanded Dynamic Flood Recovery Curves; Run 9 - Second Dynamic Water Flood	85
Figure 7.23: Normalized Pressure Drop (Fixed q) vs. PVI; Run 9 - Second Dynamic Water Flood	86

Figure 7.24:	Normalized Pressure Drop (Variable q) vs. PVI; Run 9 - Second Dynamic Water Flood	87
Figure 7.25:	Oil and Water Relative Permeabilities vs. Water Saturation; Run 9 - Second Dynamic Water Flood	88
Figure 7.26:	Relative Permeability Comparison; Run 9 - First and Second Dynamic Water Floods. A = Oil Relative Permeability, Second Dynamic Flood B = Oil Relative Permeability, First Dynamic Flood C = Water Relative Permeability, First Dynamic Flood D = Water Relative Permeability, Second Dynamic Flood.....	90
Figure 7.27:	Saturation History and Trajectories; Run 9 - Third Dynamic Water Flood	91
Figure 7.28:	Expanded Dynamic Flood Recovery Curves; Run 9 - Third Dynamic Water Flood	92
Figure 7.29:	Normalized Pressure Drop (Fixed q) vs. PVI; Run 9 - Third Dynamic Water Flood	94
Figure 7.30:	Normalized Pressure Drop (Variable q) vs. PVI; Run 9 - Third Dynamic Water Flood	95
Figure 7.31:	Fixed vs. Variable Normalized Pressure Drop Comparison; Run 9 - Third Dynamic Water Flood	96
Figure 7.32:	Oil and Water Relative Permeabilities vs. Water Saturation; Run 9 - Third Dynamic Water Flood	97
Figure 7.33:	Relative Permeability Comparison; Run 9 - Second and Third Dynamic Water Floods. A = Oil Relative Permeability, Second Dynamic Flood B = Oil Relative Permeability, First Dynamic Flood C = Water Relative Permeability, First Dynamic Flood D = Water Relative Permeability, Second Dynamic Flood.....	99
Figure 7.34:	Core Linearity Check Pressure Profile; Run 8	100
Figure 7.35:	Overall Saturation History; Run 8	102
Figure 7.36:	Steady-State Drainage Saturation History; Run 8.....	103
Figure 7.37:	Oil Saturation vs. Oil Fractional Flow	105
Figure 7.38:	Decane and Oil Relative Permeabilities vs. Oil Saturation; Run 8 - Steady-State Drainage Series	106
Figure 7.39:	Steady-State Imbibition Saturation History; Run 8.....	107

Figure 7.40: Decane and Oil Relative Permeabilities vs. Oil Saturation; Run 8 - Steady-State Imbibition Series.....	110
Figure 7.41: Comparison of Relative Permeabilities; Run 8 - Drainage and Imbibition Series.....	111
Figure 7.42: Saturation History and Trajectories; Run 8 - Dynamic Decane Flood	112
Figure 7.43: Dynamic Flood Recovery Curves; Run 8 - Dynamic Decane Flood	113
Figure 7.44: Expanded Dynamic Flood Recovery Curves; Run 8 - Dynamic Decane Flood	114
Figure 7.45: Normalized Pressure Drop vs. PVI; Run 8 - Dynamic Decane Flood	116
Figure 7.46: Expanded Normalized Pressure Drop vs. PVI; Run 8 - Dynamic Decane Flood	117
Figure 7.47: Comparison of Dynamic and Steady-State Calculated Relative Decane Permeabilities; Run 8	118
Figure 7.48: Comparison of Dynamic and Steady-State Calculated Relative Oil Permeabilities; Run 8	119
Figure 7.49: Core Linearity Check Pressure Profile; Run 4	121
Figure 7.50: Dynamic Flood Recovery Curves; Run 4.....	122
Figure 7.51: Expanded Dynamic Flood Recovery Curves; Run 4	123
Figure 7.52: Saturation History and Trajectories; Run 4.....	125
Figure 7.53: Normalized Pressure Drop vs. PVI; Run 4	126
Figure 7.54: Core Linearity Check Pressure Profile; Run 5	127
Figure 7.55: Dynamic Flood Recovery Curves; Run 5.....	129
Figure 7.56: Expanded Dynamic Flood Recovery Curves; Run 5	130
Figure 7.57: Saturation History and Trajectories; Run 5.....	131
Figure 7.58: Normalized Pressure Drop vs. PVI; Run 5	133
Figure 7.59: Oil Relative Permeabilities; Runs 4 and 5	134
Figure 7.60: Water Relative Permeabilities; Runs 4 and 5.....	136

Figure 7.61: Oil and Water Relative Permeabilities; Runs 4 and 5.....	137
Figure 7.62: Dynamic Water Flood Recovery Curves; Run 8.....	138
Figure 7.63: Expanded Dynamic Water Flood Recovery Curves; Run 8	139
Figure 7.64: Saturation History and Trajectories; Run 8 - Dynamic Water Flood	141
Figure 7.65: Normalized Pressure Drop vs. PVI; Run 8 - Dynamic Water Flood	142
Figure 7.66: Core Linearity Check Pressure Profile; Run 6.....	144
Figure 7.67: Core Linearity Check Pressure Profile; Run 7	145
Figure 8.1: Comparison of Saturation Trajectories; Run 3 (marked as A) vs. Grader and O'Meara (1988) Run 15 (marked as B).....	147
Figure 8.2: Core Saturation Profile at Breakthrough; Run 4	150
Figure 8.3: Core Saturation Profile at Breakthrough; Run 5	151
Figure 8.4: Core Saturation Profile at Breakthrough; Run 8.....	152

LIST OF TABLES

	<u>Page</u>
Table 4.1: Summary of Fluid Properties	23
Table 4.2: Screen Analysis of Glass Beads.....	26
Table 7.1: Summary of Run 8 Drainage Experiments.....	104
Table 7.2: Summary of Run 8 Imbibition Experiments	108
Table A.1: Fractional Collection Analysis Summary; Run 2.....	161
Table A.2: Relative Permeability Analysis Summary; Run 2	162
Table A.3: Fractional Collection Analysis Summary; Run 3.....	163
Table A.4: Relative Permeability Analysis Summary; Run 3	164
Table A.5: Relative Permeability Analysis Summary; Run 9 - First Dynamic Water Flood.....	165
Table A.6: Fractional Collection Analysis Summary; Run 9 - First Dynamic Water Flood.....	166
Table A.7: Relative Permeability Analysis Summary; Run 9 - Second Dynamic Water Flood	167
Table A.8: Fractional Collection Analysis Summary; Run 9 - Second Dynamic Water Flood	168
Table A.9: Relative Permeability Analysis Summary; Run 9 - Third Dynamic Water Flood	169
Table A.10: Fractional Collection Analysis Summary; Run 9 - Third Dynamic Water Flood	170
Table A.11: Relative Permeability Analysis Summary; Run 8 - Dynamic Decane Flood	171
Table A.12: Fractional Collection Analysis Summary; Run 8 - Dynamic Decane Flood	172
Table A.13: Fractional Collection Analysis Summary; Run 4	173

Table A.14: Relative Permeability Analysis Summary; Run 4	174
Table A.15: Fractional Collection Analysis Summary; Run 5	175
Table A.16: Relative Permeability Analysis Summary; Run 5	176
Table A.17: Fractional Collection Analysis Summary; Run 8 - Dynamic Water Flood.....	177
Table A.18: Relative Permeability Analysis Summary; Run 8 - Dynamic Water Flood.....	178
Table A.19: Run Core Characteristics	179

NOMENCLATURE

Roman

A	= cross-sectional area
E	= error
f_i	= fractional flow of fluid i
f_j	= fractional flow of fluid j
H_1	= top liquid interface height in reservoir
H_2	= bottom liquid interface height in reservoir
k	= effective permeability
k_{abs}	= absolute permeability
k_r	= relative permeability
l	= length of core
L	= pore volumes recovered
n	= number collection tubes
N_{tubes}	= number of tubes penetrating reservoir fluid
Q	= cumulative pore volumes injected
q	= total flow rate
q_{act}	= total actual flow rate
q_i	= actual flow rate of fluid i
q_j	= actual flow rate of fluid j
R_i	= cumulative recovered pore volumes of fluid i
S	= saturation
S_{ro}	= residual oil saturation

S_{rw}	= irreducible water saturation
t	= time
v	= fluid velocity
V	= volume of fluid
V_{bulk}	= bulk volume
V_{dead}	= core volume without glass beads subject to fluid flow
V_{pore}	= pore volume
V_{surge}	= surge suppressor volume
V_i	= volume of fluid i in a collection tube
V_{ti}	= cumulative volume of fluid i collected
V_{tt}	= total cumulative volume of all fluids collected
V_{tubing}	= volume of fluid displaced by tubing in the reservoir
x	= position measured from the inlet end of the core
\hat{X}	= dimensionless position scaled by the length of the core

Greek

ΔP	= pressure drop across core
ΔP_{a-b}	= pressure drop across taps a and b
Δt	= elapsed time
ΔV	= change in fluid volume
η	= similarity variable
λ	= mobility ratio
μ	= fluid viscosity
ϕ	= porosity

- Φ = normalized pressure drop
 $\bar{\Phi}$ = average normalized pressure drop
 ρ = density
 ψ = defined by Equation (2.16)

Subscripts

- a = arbitrary pressure tap
 abs = absolute
 act = actual
 b = arbitrary pressure tap
 d = decane
 f = fluid
 final = final
 i = arbitrary fluid
 in = initial
 inj = injected
 j = arbitrary fluid
 o = oil (benzyl alcohol)
 r = relative
 rec = recovered
 w = water

Abbreviations

- atm = atmospheres

BA	= benzyl alcohol
° c	= degrees celsius
cc	= cubic centimeters
cm	= centimeters
D	= decane
g	= grams
H ₂ O	= water
in	= inch
min	= minutes
mL	= milliliter
psi	= pounds per square inch
pvi	= pore volume injected
sec	= seconds
wt	= weight

ACKNOWLEDGMENTS

The author acknowledges the United States Navy, for providing funding for the graduate education program culminating with this research.

The author wishes to express sincere appreciation to Dr. Abraham S. Grader, whose assistance, encouragement, and guidance made the completion of this work possible. Much gratitude is also extended to the members of the committee, Dr. Turgay Ertekin, and Dr. Robert Watson, for their constructive comments and suggestions.

The author is grateful to his wife, Rebecca Ann Thomas, for her patience and support throughout the duration of this project. Sincere thanks is offered to the author's parents, Lee and Mildred Thomas, for their endless support and encouragement throughout the years.

Chapter 1

INTRODUCTION

The objective of this research is to further our understanding of the simultaneous motion of three phases in porous media. This is to include hysteretical effects and to specifically quantify and qualify immiscible three-phase relative permeabilities.

Multi-phase flow in porous media occurs in many engineering fields, such as ground water hydrology, hazardous waste disposal sites, surface spills, and petroleum hydrocarbon reservoirs. As the upper crust of the earth is being taxed more and more with sophisticated processes, a need for a better understanding of transport phenomena in porous media is required. We have a responsibility to preserve the functionality of fluid bearing formations, and to be able to accurately predict and optimize the outcome of prospective production or injection projects. In the case of contamination, we must have the ability to design a cleanup process, minimizing damage and danger.

One of the key parameters used to describe the motion of various fluids in porous media is relative permeability. The relative permeability parameter is used to determine the energy needed to move the fluids through the porous media, and the relative flow rates of each phase present. Knowledge of the permeability of a formation rock to a given fluid is an essential input for numerical models used to predict and optimize aquifer and reservoir performance, and for the designing of efficient and effective mobilization or utilization systems.

Several examples of three-phase flow in subsurface formations are:

- A surface spill of a non-aqueous solution, not miscible with water, that seeps into the ground under gravity. This non-aqueous solution then mixes with rain water and air, to form a three-phase mixture flowing simultaneously in a porous medium.
- A non-aqueous fluid might be introduced into a disposal well that penetrates an aquifer containing air or a non-condensable gas such as carbon dioxide. Again, the result is a three-phase flow.
- In hydrocarbon production, simultaneous flow of oil, gas and water is common, under both primary or secondary recovery. Three-phase flow is also encountered in enhanced recovery processes.
- Three phases can be created in the subsurface in an effort to control the movement of a contaminant toward a set of producing wells, through the use of some displacement process.

The relative permeability to a given phase is a function of that phase's saturation and possibly, a function of other phase saturations as well. The effective permeability is one of the major non-linear factors in the mass transport equations that are used in both analytical and numerical reservoir models. Due to the highly non-linear nature of the multiphase flow problem, relative permeabilities must be determined experimentally. The results and trends from this exploratory experimental research have application to multiple disciplines. Therefore, in this work a very idealized system consisting of a one dimensional core, simple fluids, and relatively homogeneous porous media are used.

Chapter 2

REVIEW OF THE THEORY AND LITERATURE

One-dimensional single-phase flow through porous media is described by Darcy's equation (Darcy 1856), shown as:

$$v = - \frac{k}{\mu} \frac{\partial p}{\partial x} \quad (2.1)$$

Darcy's law applied to all phases (capillary pressure neglected) is:

$$v_i = - \frac{k_i}{\mu_i} \frac{\partial p}{\partial x} \quad (2.2)$$

where k_i is the effective permeability of phase i .

Relative permeability is defined as:

$$k_{ri} = \frac{k_i}{k_{abs}} \quad (2.3)$$

where k_{ri} is the relative permeability of phase i .

2.1 Steady-State and Dynamic Relative Permeability Measuring Techniques

There are two major methods involving continuous injection of fluids for determining relative permeabilities: the steady-state method and the unsteady-state method. In the Penn State steady-state injection technique, a fixed fractional flow of fluids is injected into the core, until the same fractional flow of fluids is produced from the core. At this point it is assumed that steady-state is achieved. The pressure drop across the core is measured and Equation (2.2) is used to determine the effective permeabilities followed by Equation (2.3) to determine the relative permeabilities of each of the injected phases.

The unsteady-state method of relative permeability determination (dynamic displacement) involves the injection of (usually) one fluid phase into an iso-saturated core. The fluids recovered from the core, and the pressure drop along the core, are measured as functions of the pore volumes injected. From this data the core-end saturations and the associated fluid relative permeabilities are determined. The specific method of determining these values is derived by extending, from two-phases to three-phases, the two-phase dynamic displacement theory of Welge's permeability ratios with Johnson, Bossler and Naumann's (JBN) two-phase method of determining individual relative permeabilities (Welge 1950; Johnson et al. 1959). The actual derivation and extension of the theory is presented by Grader and O'Meara (1988) and is summarized in section 2.3.

2.2 History of Three-Phase Relative Permeability Determination

A large number of papers relating to the determination of relative permeabilities in porous media is found in the literature. Honarpour et al. (1986) presented a review of the subject.

Leverett and Lewis (1941) presented a study of three-phase relative permeabilities using the steady-state method. Their conclusion is that the water relative permeability is solely a function of the water saturation in an unconsolidated sand pack.

The steady-state method for determining three-phase relative permeabilities was used by Caudle et al. (1951), Corey et al. (1956), Snell (1962), and Oak et al. (1988). Caudle et al. (1951) found that for a consolidated core, each relative permeability depends on the saturation of the three phases.

The few papers listed above used the steady-state method for determining

three-phase relative permeabilities. Measurements of relative permeabilities using the unsteady-state method are presented by Sarem (1966), Donaldson and Dean (1966), and Saraf et al. (1983). Sarem (1966) used a Welge-like method which assumes that each phase relative permeability depends only on its own saturation. As shown by Grader and O'Meara (1988) this assumption is not needed in the development of the extension of the Welge method from two phases to three phases.

Donaldson and Dean (1966) used a variation of Sarem's method (Sarem 1966) in that the relative permeabilities depend on the saturation of the three phases in the core. For the three-phase case, they used the Welge method (Welge 1950) by replacing the fractional flow of oil, by the sum of the fractional flow of oil and water. They do not, however, present a derivation or the assumptions made for the application of the Welge method to three phases. In the paper the three-phase relative permeabilities for Berea sandstone and Arbuckle limestone are presented. These two rock types show high residual water and oil saturations, limiting the size of the three-phase region on the ternary diagram available for mapping. Saraf et al. (1983) also make use of an extension of the Welge method.

Summary tables with some of the three-phase relative permeability work described in the literature are presented by Honarpour et al. (1986), Oak et al. (1988), and Donaldson and Kayser (1981).

The difficulty in determining three-phase relative permeabilities using either the steady-state or unsteady-state methods justifies the need for a three-phase relative permeability model which uses only two-phase relative permeability data. Baker (1988) presents a comprehensive summary of the various three-phase relative permeability models.

2.3 Extension of the Welge/JBN Theory to Three Phases

The Welge/JBN method discussed in this section is based on the work of Grader and O'Meara (1988) which extends the Welge/JBN theory from two phases to three phases. The theory is simplified to the non-gravity case. In the following derivation, the standard simplifying assumptions are made: incompressible, one-dimensional, isothermal, and immiscible three-phase flow with no capillary pressure effects. The material balance equation and Darcy's Law equation describing the velocity of fluid flow in a porous medium are:

$$\phi \frac{\partial S_j}{\partial t} + \frac{\partial v_j}{\partial x} = 0 \quad (2.4)$$

$$v_j = -\lambda_j \frac{\partial p}{\partial x} \quad (2.5)$$

where $j = 1, 2, 3$, $S_1 + S_2 + S_3 = 1$, $\lambda_j = k_j / \mu_j$, and the rest of the terms are defined in the Nomenclature. By summing the three material balance equations we can show that v , the total fluid velocity, is independent of x , and is therefore, at most only a function of time (we will show later in the Chapter 7 how the variable rate does not affect the validity of the proposed solution). Summation of Darcy's Law equations for the three fluids provides an expression for the pressure gradient in terms of v , which can then be substituted into Eq. (2.2) to obtain:

$$v_j = v f_j (S_1, S_2) \quad (2.6)$$

where

$$f_j = \frac{\lambda_j}{\lambda} \quad (2.7)$$

$$\lambda = \lambda_1 + \lambda_2 + \lambda_3 \quad (2.8)$$

Notice that, for a given choice of fluids, f_j is a function only of saturation. Also, note that there are only two independent volume equations for two phases, as the

third phase volumetrics are complimentary, and dependent. Substituting Equation (2.6) into Equation (2.4) yields the following differential equation (neglecting gravity effects):

$$\phi \frac{\partial S_j}{\partial t} + \left[v \frac{\partial f_j}{\partial S_1} \right] \frac{\partial S_1}{\partial x} + \left[v \frac{\partial f_j}{\partial S_2} \right] \frac{\partial S_2}{\partial x} = 0 \quad \text{for } j = 1, 2 \quad (2.9)$$

For suitable initial and boundary conditions (iso-saturation at initial time, and a constant fractional flow at the injection face), the solution to Equation (2.9) is self similar. A natural choice for the similarity variable, η , is $\frac{Q}{\hat{X}}$ where \hat{X} denotes the dimensionless position scaled by 1, the length of the core and Q denotes the cumulative pore volume of total fluid injected:

$$Q = \frac{1}{\phi l} \int_0^t v(t') dt' \quad (2.10)$$

Substitution of η into Eq. (2.9) yields:

$$\left[\left[\frac{\partial f_1}{\partial S_1} \right] \eta - 1 \right] \frac{\partial S_1}{\partial \eta} + \left[\frac{\partial f_1}{\partial S_2} \right] \eta \frac{\partial S_2}{\partial \eta} = 0 \quad (2.11)$$

$$\left[\frac{\partial f_2}{\partial S_1} \right] \eta \frac{\partial S_1}{\partial \eta} + \left[\left[\frac{\partial f_2}{\partial S_2} \right] \eta - 1 \right] \frac{\partial S_2}{\partial \eta} = 0 \quad (2.12)$$

Letting S_j^o denote the initial saturation of phase j in the porous medium and S_j^i denote its initial saturation at the inlet end of the core, we obtain the initial condition:

$$S_j = S_j^o \quad \text{at } \eta = 0 \quad (2.13)$$

and the boundary condition:

$$S_j = S_j^i \quad \text{at } \eta \rightarrow \infty \quad (2.14)$$

The fluid mobilities and consequently, the permeabilities are calculated from the following equation that is obtained from Equation (2.5):

$$\lambda_j = \frac{\psi_j}{\Phi} \quad (2.15)$$

where

$$\psi_j = \frac{v_j}{v} \quad (2.16)$$

$$\Phi = - \frac{\left[\frac{\partial p}{\partial x} \right]}{v} \quad (2.17)$$

ψ_j and Φ are functions of only the fluid saturations and, thereby, η . Our task then reduces to experimentally determining the functional dependency of S_j , ψ_j , and Φ on η . We assume that the conditions for self-similarity prevail. Then from Equations (2.6) and (2.16) we obtain:

$$\psi_j = f_j(S_1, S_2) \quad (2.18)$$

Substitution of Equation (2.6) into Equation (2.5) shows that Φ also depends only on fluid saturations. Therefore, for a self-similar system, S_j , ψ_j and Φ each depend solely on η .

Let L_j represent the cumulative pore volume of fluid j collected at the outflow end ($\hat{X} = 1$) of the porous medium. Then ψ_j is simply the derivative of the L_j vs. Q curve where $\eta = Q$, the fractional flow of fluid j :

$$\psi_j = \frac{\frac{dL_j}{dt}}{\frac{dQ}{dt}} = \frac{dL_j}{dQ} \quad \text{for } \eta = Q \quad (2.19)$$

The average saturation of fluid j between the injection point ($x = 0$) and x is:

$$\bar{S}_j = \frac{\int_0^x S_j dx'}{x} \quad (2.20)$$

Upon differentiating Equation (2.20) we obtain:

$$S_j = \bar{S}_j + x \frac{\partial \bar{S}_j}{\partial x} \quad (2.21)$$

Equation (2.21) relates the saturation at a particular point to the average saturation between the point and the injection end of the core. Since S_j and, therefore, \bar{S}_j depends only on η this equation can be transformed in terms of the pore volumes injected as:

$$S_j = \bar{S}_j - \eta \frac{d\bar{S}_j}{d\eta} \quad (2.22)$$

The average saturations in the core, \bar{S}_j , can be obtained via mass balance:

$$\bar{S}_j = S_j^o + \psi_j^i Q - L_j \quad (2.23)$$

where ψ_j^i is the fraction of fluid j in the inflow stream. On substituting Equation (2.23) into Equation (2.21) for $\eta = Q$ we obtain:

$$S_j = S_j^o - L_j + Q \frac{dL_j}{dQ} \quad (2.24)$$

or:

$$S_j = S_j^o - L_j + Q \psi_j \quad (2.25)$$

Equations (2.24) and (2.25) describe the Welge method for determining the saturation at the down stream end of the core. Johnson et al. (1959) showed that the pressure gradient at the end of the core is needed in order to determine the individual relative permeabilities at the saturation values. Since Φ is also a function of η , it too can be obtained from the measurement of its average:

$$\Phi = \bar{\Phi} - \eta \frac{d\bar{\Phi}}{d\eta} \quad (2.26)$$

At the end of the core $\hat{X} = 1$, $\eta = Q$, the pore volumes injected. Hence, Equation (2.26) simplifies for pressure drops measured between the two ends of the core:

$$\Phi = \bar{\Phi} - Q \frac{d\bar{\Phi}}{dQ} \quad (2.27)$$

Finally, Equation (2.15) is simplified for the zero gravity case and for using the saturation and pressure gradients at the downstream end of the core:

$$\lambda_j = \frac{f_j}{\Phi} \quad (2.28)$$

Where f_j is the fractional flow of phase j , and Φ is the normalized pressure gradient at the end of the core. The application of the JBN method for determining the individual relative permeabilities can be used for a three-phase system, in the same way it is used for a two-phase system.

2.4 Analysis Procedure

The analysis procedure for determining the individual phase relative permeabilities and their corresponding saturations is similar to the two-phase procedure. This procedure was presented for three phases by Grader and O'Meara (1988) and is summarized here. The recovery of the three phases and the overall pressure drop between the injection and the production ends of the core must be measured as a function of time. The saturations and permeabilities are computed for the conditions at the end of the core. Figure 2.1 presents two synthetic recovery curves for two of the three phases in the system. The solid dots represent breakthrough. The Welge tangent construction method is described in this figure, similar to the method presented by Jones and Roszelle (1978). For a certain value of pore volume of fluid injected, the recovery of a given phase at the intersection of the tangent and the recovery axis is the change in the saturation of that phase at the end of the core. Note that there is no mathematical reason preventing this saturation change from being negative, indicating an increase in the saturation of the phase. The slope of the recovery curve with respect to the pore volume injected is the fractional flow

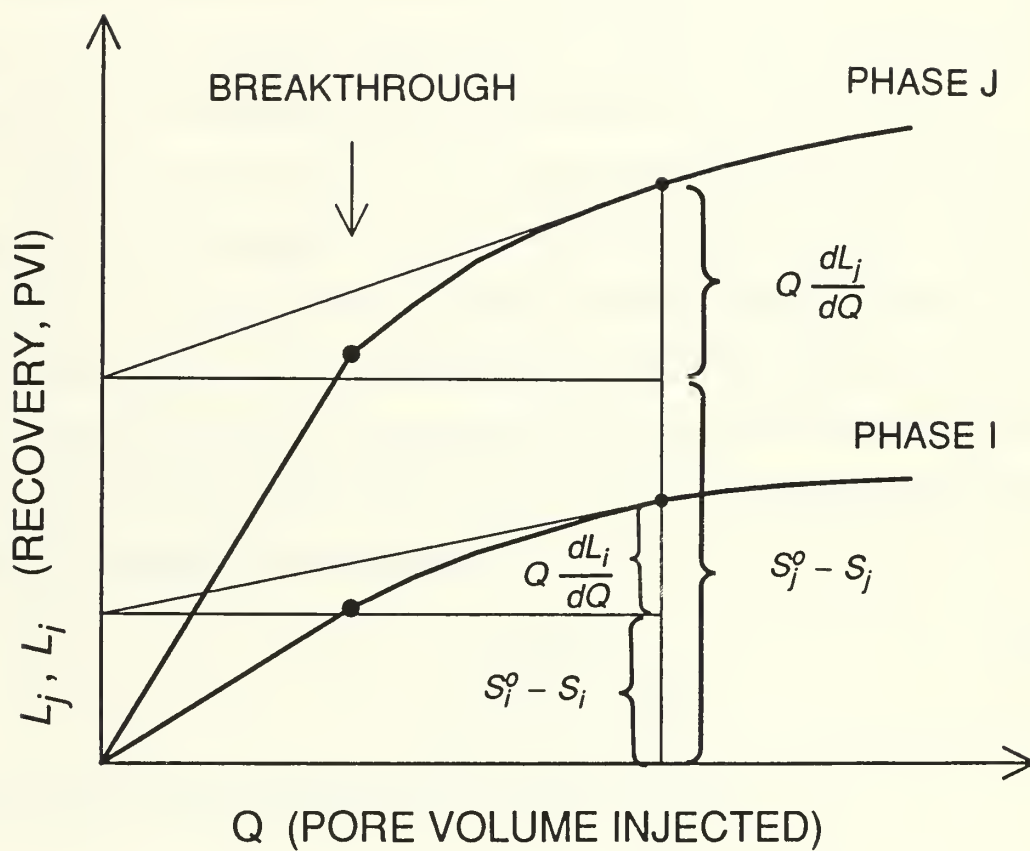


Figure 2.1: Recovery of Two Phases Displaced by a Third Phase as a Function of PVI.

value for a phase. We use the tangent construction method for two phases, using the individual recovery curves. The saturation of the third phase is determined using the material balance equation as well as its fractional flow value. Hence, Equation 2.24 is used to evaluate S_j at the end of the core.

Figure 2.2 presents the normalized pressure drop as a function of pore volume injected (the pressure drop is divided by the flow rate). In some cases discussed in the Chapter 7, the instantaneous flow rate was used, as the overall injection rate was not constant. For a given value of pore volume injected, the tangent construction method proposed by Johnson et al. (1959) (the JBN method) is applied. The intersection point of the tangent with the normalized pressure drop axis yields the value of the spatial gradient of the normalized pressure drop at the downstream end of the core. This local gradient at the downstream end of the core is then used in conjunction with Equation (2.28) and the slope of the recovery curve to determine the relative permeabilities of the three phases:

$$k_{rj} = \frac{f_j l_{\text{core}} \mu_j}{k_{\text{abs}} A_{\text{core}} \left[l_{\text{core}} \frac{\partial p}{\partial x} \right]} \quad (2.29)$$

Note that by using the definition of the similarity variable,

$$\left[l_{\text{core}} \frac{\partial p}{\partial x} \right] = \bar{\Phi} - Q \frac{d\bar{\Phi}}{dQ} \quad (2.30)$$

This is clearly shown in Figure 2.2.

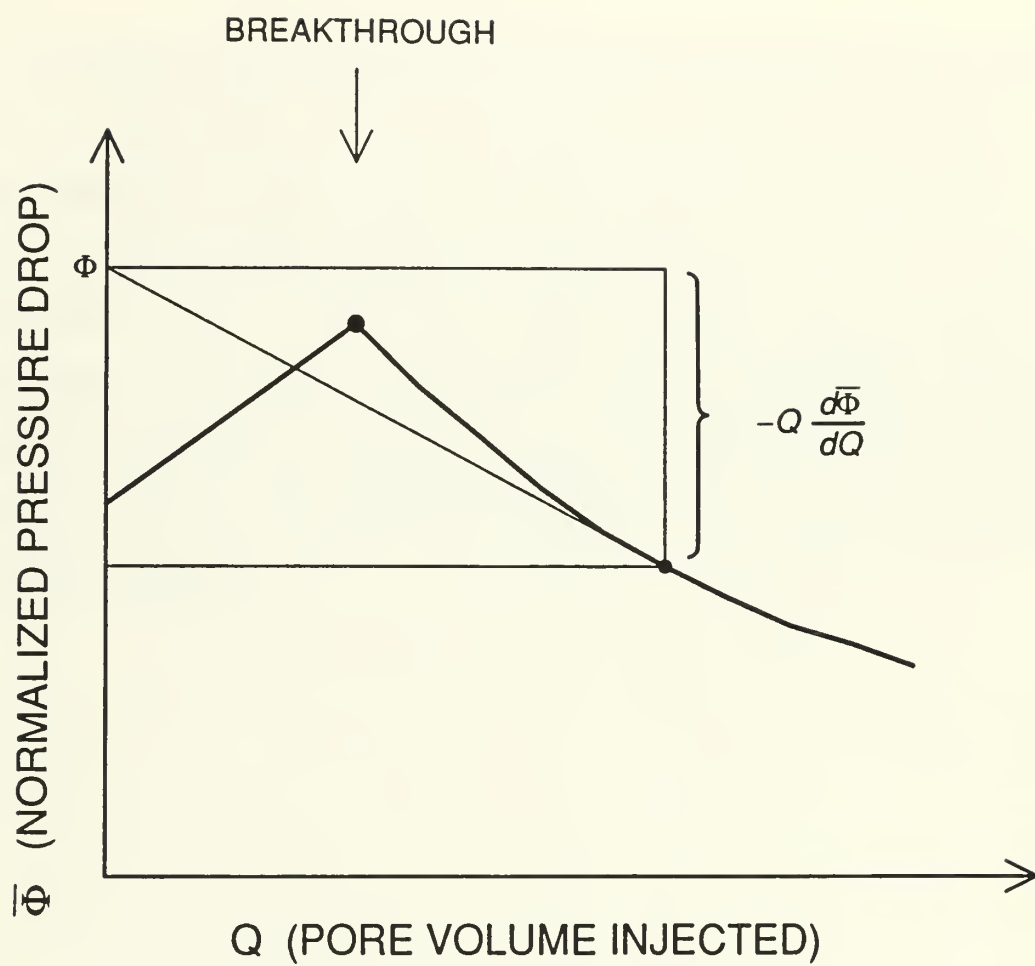


Figure 2.2: Normalized Pressure Drop as a Function of PVI.

Chapter 3

PROBLEM STATEMENT

The purpose of this research is to investigate the simultaneous motion of three phases in porous media. A series of laboratory experiments are conducted in a highly idealized environment, using; three immiscible fluids of similar densities and interfacial tensions, and a horizontal one-dimensional glass bead pack. The objective of this work is to quantify and qualify immiscible three-phase relative permeabilities. This is achieved by performing experiments to determine three-phase relative permeabilities using steady-state and non-steady-state methods, and by applying the frontal advance three-phase theory in the mapping of the ternary three-phase diagram.

Chapter 4

EXPERIMENTAL APPARATUS

4.1 Apparatus Capabilities and Overview

The apparatus allows the performance of both steady-state and unsteady-state multi-phase flow experiments. The possible types of experiments include:

- a. one-phase injection
- b. two-phase Penn-State steady-state
- c. three-phase Penn-State steady-state
- d. two-phase Welge dynamic classical displacement
- e. three-phase Welge dynamic classical displacement

Specific core saturations can be obtained through these types of experiments. Figures 4.1 through 4.7 show the apparatus' capabilities through the relation of the injected phase(s), initial core saturation, and resulting core saturation. The initials of the water, decane, benzyl alcohol used in the apparatus represent the 100% saturation points of the fluids on the ternary diagrams.

Single-phase injections and saturations are shown by figure 4.1. The open dots are the injected phase and the resulting saturation of the core.

Two-phase final saturations are possible through the injection scenarios shown in figures 4.2 through 4.4. Single-phase flooding into an existing single-phase saturation is shown in figure 4.2. The open dots are the existing phase saturations at the beginning of the flood and the solid dots represent the injected single-phase and

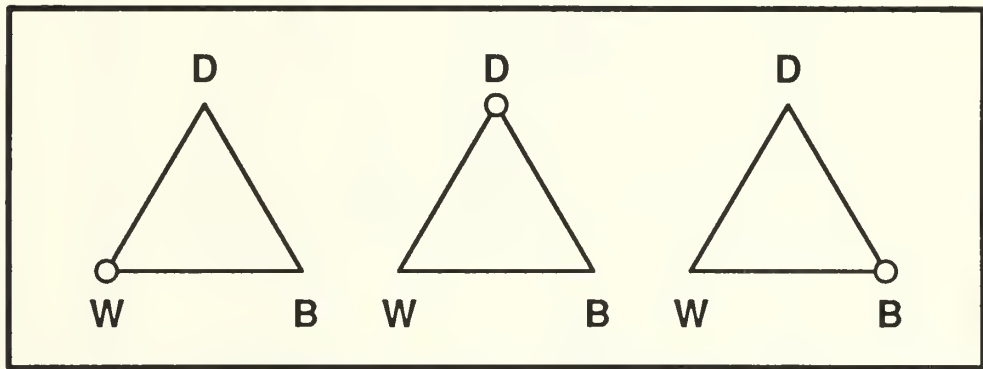


Figure 4.1: Flooding Capabilities of the Apparatus; Single-Phase Injection

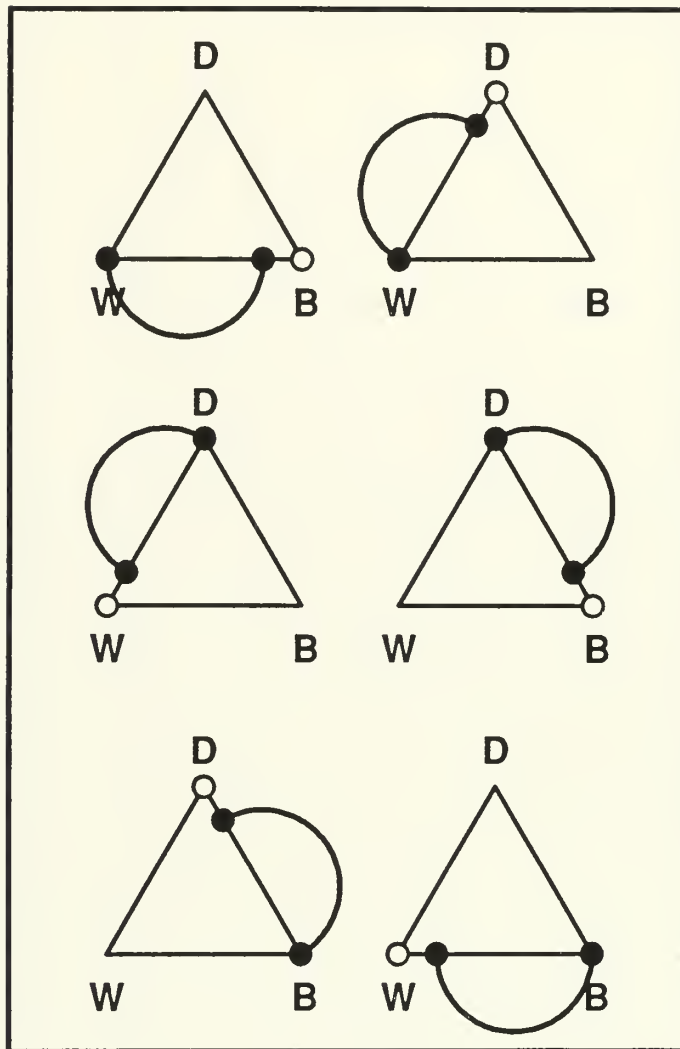


Figure 4.2: Flooding Capabilities of the Apparatus; One-Phase into One-Phase

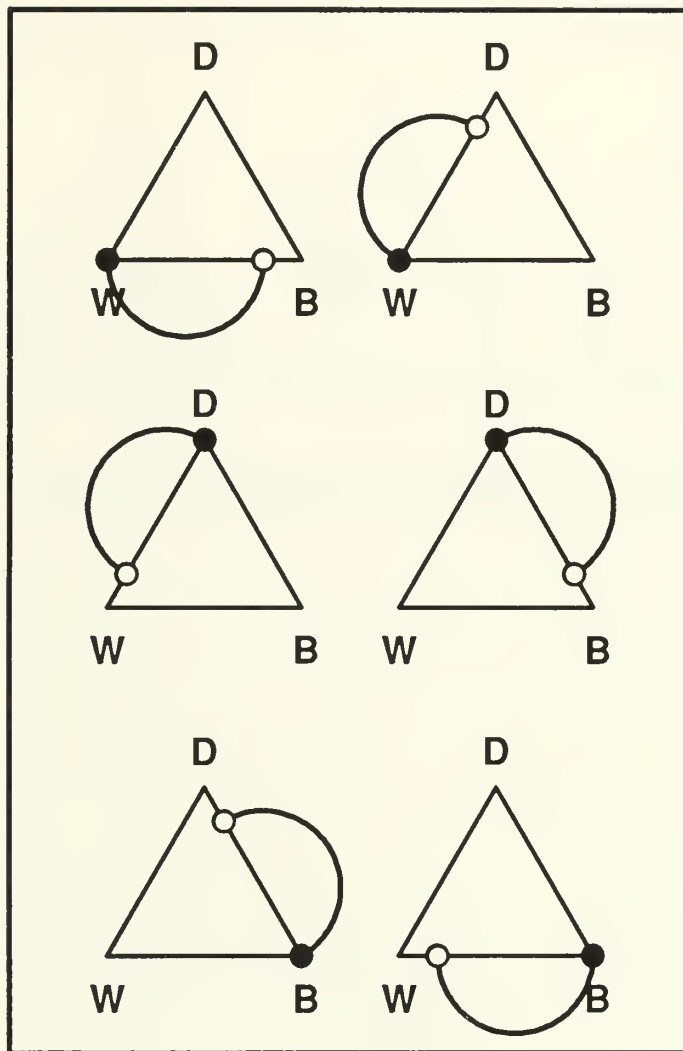


Figure 4.3: Flooding Capabilities of the Apparatus; One-Phase into Two-Phases

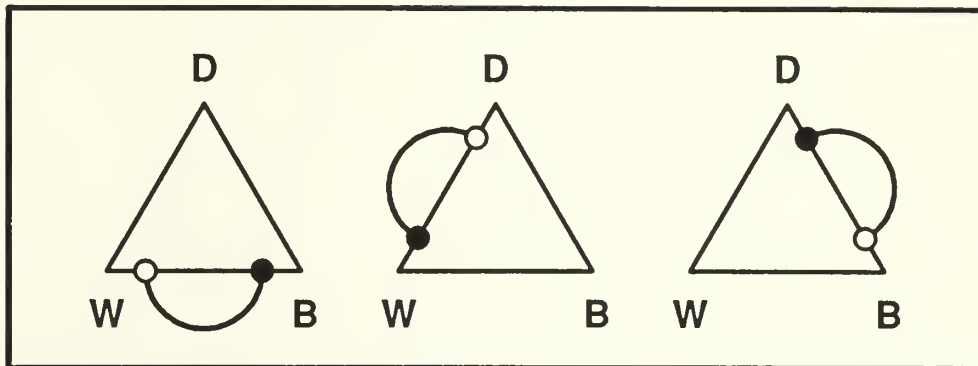


Figure 4.4: Flooding Capabilities of the Apparatus; Two-Phases into Two-Phases

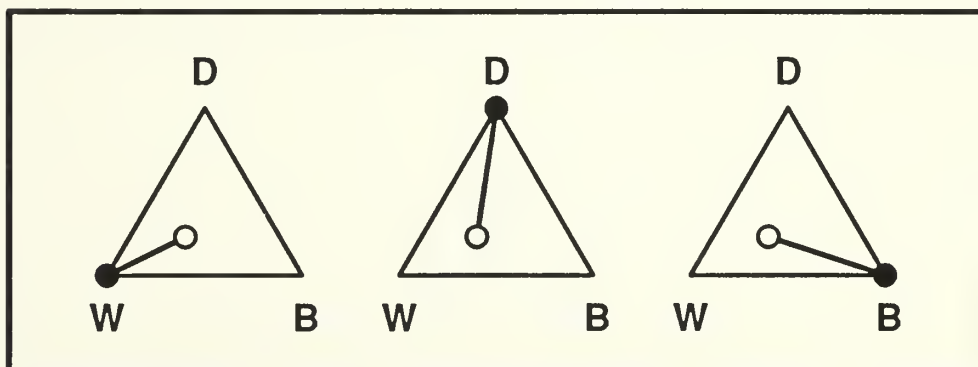


Figure 4.5: Flooding Capabilities of the Apparatus; One-Phase into Three-Phases

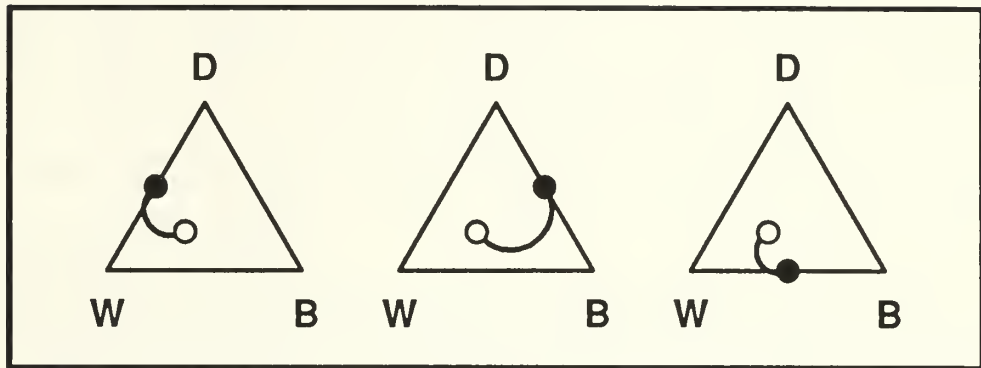


Figure 4.6: Flooding Capabilities of the Apparatus; Two-Phases into Three-Phases

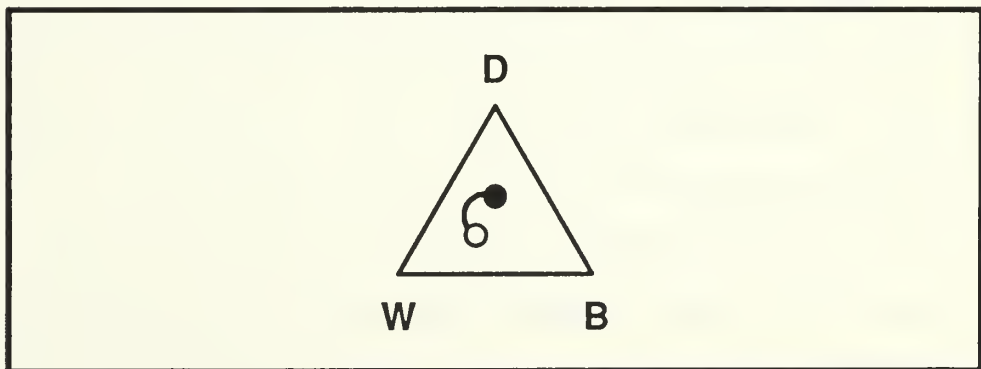


Figure 4.7: Flooding Capabilities of the Apparatus; Three-Phases into Three-Phases

the resulting two-phase saturations. Figure 4.3 diagrams the possibilities of a single-phase, shown by a closed dot, being injected into a two-phase saturated core and the resulting two-phase saturation, shown by an open dot. Two-phase saturations can be changed by injecting different fractional flows of the two fluids. Figure 4.4 shows the two-phase saturation (open dot), being changed to a new two-phase saturation, (closed dot).

Three-phase saturation paths are shown on figures 4.5 through 4.7. In figure 4.5, a three-phase saturation, shown by an open dot can be achieved by injection of a single-phase, shown by a closed dot, into an existing two-phase or three-phase saturation. Three-phase saturations can be achieved or altered as shown in figure 4.6 by the injection of a two-phase mixture into an existing two-phase or three-phase saturation. Three-phase saturations can be altered by the injection of a new three-phase mixture as shown in figure 4.7.

A schematic representation of the experimental equipment used is given in Figure 4.8. Tubing is represented by thin lines. Valves are represented by dots. Important equipment is outlined by a bold line and described below. The fluid pumps; water (1), decane (2), and benzyl alcohol (3), draw fluid from either a central collection reservoir (4) or their individual fluid storage flasks. Each pump is flanked by a pressure surge suppressor to its left and its fluid storage flask to the right. The fluid injected into the system is kept below 20 psig by the use of a pressure relief valve (6). When pressure testing the system, the pressure is monitored up to 200 psig on the system pressure gauge (7). The pressure drop across the core (8), is measured with a digital pressure transmitter (9). Prior to its first flooding, the core is evacuated by a vacuum pump (10). Fluids leaving the core are returned to the system reservoir (4) or collected in a fraction collector (5). The

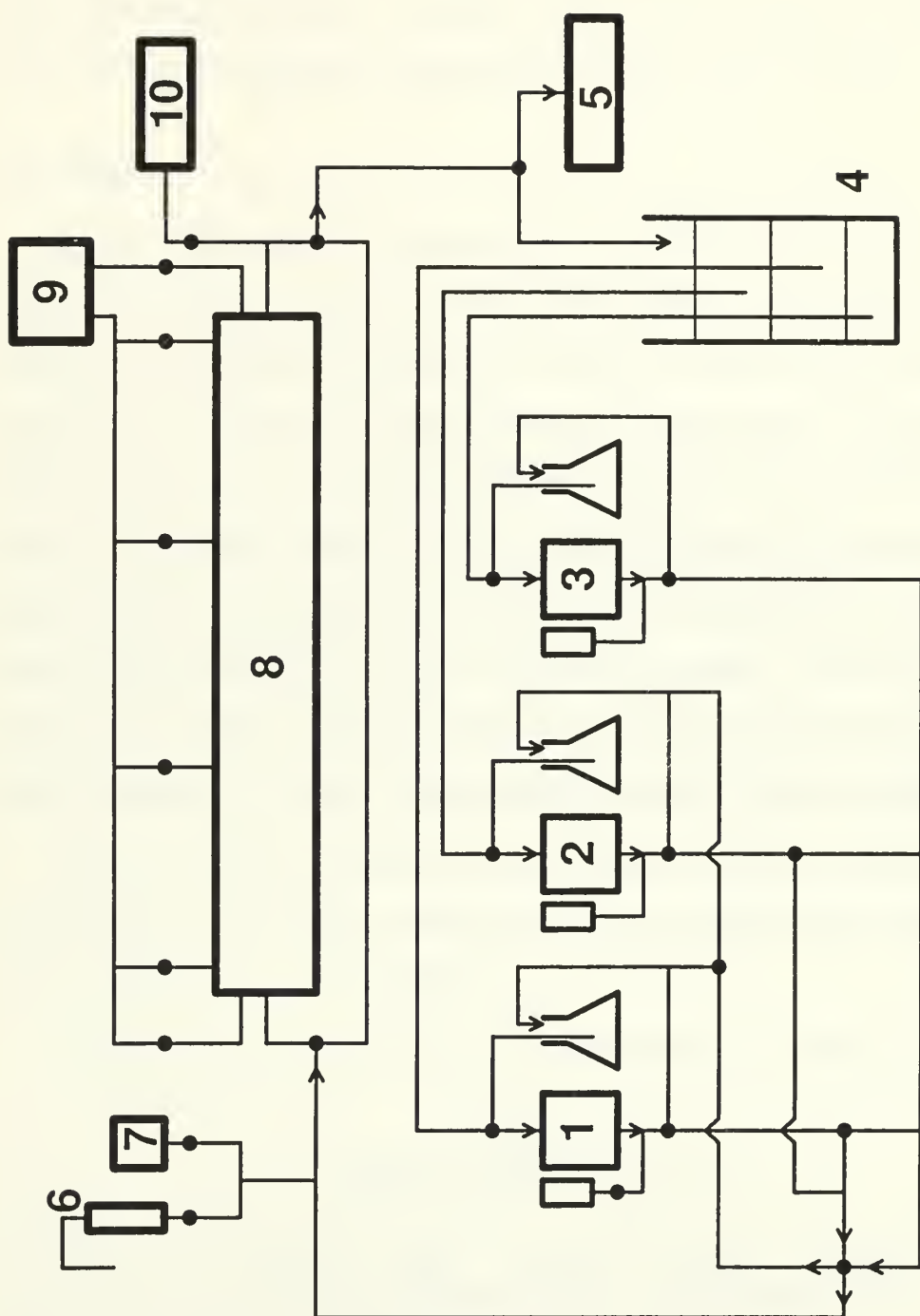


Figure 4.8: Apparatus Schematic.

apparatus can be broken down into four major portions: 1. injection system, 2. porous medium/core holder, 3. collection system, and 4. pressure monitoring system. A detailed description of each portion is presented in this chapter.

4.2 Fluids

The three phases in this experimental work are represented by three immiscible liquids. The three liquids used are distilled water, benzyl alcohol (Phenyl Methanol), and decane. Distilled water represents a water phase, benzyl alcohol represents an oil phase, and decane represents a gas phase. The terms benzyl alcohol and oil are used interchangeably, as is decane and gas. All fluid storage vessels in the system contain all three liquids. Each pump has its own 2000 mL glass storage flask. Each pump storage flask contains approximately 1000 mL of its specified liquid and 500 mL of each of the other two liquids. The system reservoir consists of a 250 mL graduated cylinder and contains varying amounts of each liquid depending on the stage of the experiment currently being conducted.

Prior to each run the liquids in the storage vessels are circulated to allow presaturation with each other. Presaturation avoids interphase mass transfer during the run, and preserves the mass balance.

The physical properties used for these three liquids are contained in Table 4.1.

Table 4.1
Summary of Fluid Properties

fluid	μ [cp] 15° c	μ [cp] 20° c	μ [cp] 25° c	ρ [g/ml] 15° c	ρ [g/ml] 20° c	ρ [g/ml] 25° c
decane	1.010	0.932	0.863	0.739	0.735	0.731
water	1.346	1.124	1.002	1.042	1.001	1.00
benzyl alcohol	5.83	4.943	4.217	0.992	1.026	1.022

The benzyl alcohol value for density at 15° c is not consistent with the temperature and is questionable. This has no effect as the experiments were conducted at about 23° c in the range where density values are correct.

4.3 Injection System

Three constant rate pumps are used to inject the three different phases, one pump for each phase. The pumps used are Beckman Model 110B Solvent Delivery Modules. These are fluid metering pumps designed primarily for liquid chromatography applications. Each module contains a single-piston pumping mechanism, drive motor, and electronic circuitry in one cabinet. Each pump can deliver from 0.1 to 9.9 mL/min at pressures up to 6000 psi. A digital potentiometer allows selection of specified flow rates in increments of 0.1 mL/min. A comparison of actual versus specified flow rates is contained in the error analysis section, Chapter 6, and each pump flow rate is calculated before each experiment. The pumps can be manually operated or remotely controlled by a suitable system controller. In this research project the pumps are operated in the manual mode.

A valve system was constructed to allow the injection of one, two, or three phases. This valve system is mounted on a 1-foot by 4-foot piece of 1/4-inch plexiglass sheeting to give the system rigidity. Each pump has a three-way inlet valve that allows the pump to draw liquid from the pump's storage flask or from the system reservoir (see figure 4.8). Downstream from each pump's outlet there is a three-way pump outlet valve that allows the liquid to be returned to the pump's storage flask or directed to the liquid selection valves leading to the core (see figure 4.8). These liquid selection valves determine if the liquid is to be mixed with others for multi-phase injection or to be used as the single-phase flooding liquid.

Downstream of the liquid selection valves there is a four-way valve that allows a circulation loop through the core and another simultaneous loop back to a pump storage flask. The fractional flow compositions of the two loops are determined by the liquid selection valves and the flow rates specified by the pumps. Turning the four-way valve diverts the fluid from one loop to the other and vice versa. This permits an uninterrupted interchange of flow from the multi-phase injection stream to the single-phase flood stream at the start of the flood portion of the run.

A pressure relief valve (set to 20 psi) along with a pressure gauge (0-200psi), points (6) and (7) on Figure 4.8, is installed just before the core/bypass inlet valve. The pressure relief valve is a safety measure to protect the pressure transmitter from possible damage due to over pressurization. The pressure gauge allows the system pressure to be read during pressure testing. Both of these devices have valves before them in order to isolate them from the system while the evacuated core is being flooded. This eliminates air from entering the core during this critical flood.

All tubing used to connect the valves is either 1/8-inch stainless steel or 1/8-inch teflon tubing. The valves used are Whitey® two, three, or four-way, 1/8-inch swagelock® connecting valves. Between each pump outlet and the outlet control valve is a filter assembly and a pressure surge suppressor. A 0.5-micron sintered stainless-steel filter element is used in each filter assembly. Each surge suppressor consists of a vertical, graduated glass bulb attached to the outlet stream by a tee and 1/4-inch adapter. Each bulb has an approximate volume of 6 mL. These suppressors are partially filled with fluid and the fluid levels recorded before and after each operation in the run.

4.4 Porous Medium and Core Holder

The porous medium consists of a strongly water-wet glass bead pack enclosed in a stainless steel core holder. The screen analysis of the number 8 glass beads used in run 2, and the number 9 glass beads used in runs 3 through 8 are shown in Table 4.2.

Table 4.2
Screen Analysis of Glass Beads

mesh size	weight % no. 8 beads	weight % no. 9 beads
+70	0.54%	<0.02%
70-100	85.5%	72.8%
100-200	13.81%	27.2%
200-400	0.13%	<0.02%
-400	0.02%	0.0%

Two core holders were constructed of 1-inch O.D. stainless steel pipe, each 36-inches long. One core is used in the apparatus at a time. The second core can be prepared for the next run during slow periods. Figure 4.9 shows the pressure tap and tubing configuration of the core. Holes for 1/8-inch stainless steel pressure taps were drilled symmetrically along the core. These pressure taps are silver soldered in place.

The ends of each core are milled flat. One-inch swagelock® caps seal the ends of the core. Each cap had two holes drilled into it, one for the fluid stream

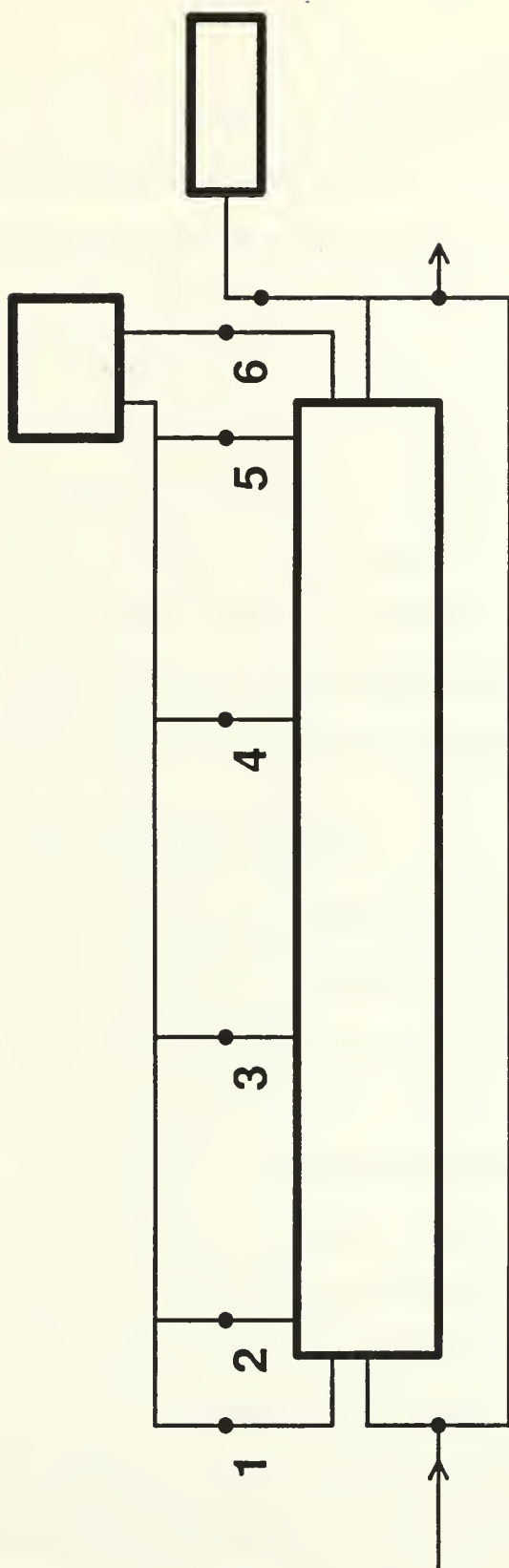


Figure 4.9: Core Pressure Tap Schematic.

inlet or outlet and the other as a pressure port. The stainless steel tubing (1/8 inch) for the inlet or outlet duct and pressure port are silver soldered into these holes. A fine-mesh brass screen wrapped around a disc of 3/16-inch thick sintered brass matting is placed in each core end cap between the end of the core and the core seat in the cap. This screen and disc keeps the glass beads in the core while allowing fluids to enter and leave the core with minimal pressure drop.

Three-way valves located just before and just after the core allow the core to be bypassed. This allows the adjustment of fluid levels in the reservoir without having to pass these fluids through the core.

Plexiglass® stands hold the bypass valves, core, and pressure tap valve manifold in order to give these portions of the system rigidity.

4.5 Pressure Monitoring System

Six symmetrically placed pressure taps along the core, along with unions and shut-off valves for each tap, make up the pressure tap manifold. Figure 4.9 shows the numbering of the pressure taps along the core. The pressure tap manifold is designed to allow the measurement of the pressure differential between an open pressure tap along the core and the end of the core. A Paroscientific Model 1020-D Digiquartz® Intelligent Transmitter is used to measure the pressure differential. The transmitter is connected to a microcomputer by a RS232 serial port card. The transmitter integrates the pressure readings over the sample time selected and corrects for any temperature changes during the sample period. The transmitter also has the capability to measure ambient temperature. Sampling speed (integration time) is set by adjusting the baud rate and pressure resolution. The baud rate for all experiments is set at 1200 and the pressure resolution is adjusted to change the sampling rate. For core linearity measurements and dynamic displacement

experiments the sample time is set at approximately one second. During steady-state runs, the sampling time is set at approximately thirty seconds.

A BASIC program, (readpt.bas) contained in Appendix B, is used during experiments to instruct the transmitter to measure the initial ambient temperature, followed by continuous pressure readings. The program measures and records the elapsed time from when the program is initiated until the measurements are taken. When the program is given the stop command, the final temperature is measured. All pressure, temperature, and corresponding time measurements are displayed on the monitor and written to the microcomputer hard drive. A Paroscientific Model 710 LCD visual display is used to display the pressure data generated by the Model 1020-D transmitter.

4.6 Collection System

A three-way valve following the core/bypass outlet three-way valve, determines if the fluid stream is directed to the fractional collector during dynamic displacement experiments or to the system reservoir during steady-state experiments.

An ISCO Retriever II fraction collector is used to collect the fluids during dynamic displacement experiments. The Retriever II can collect fractions on the basis of time (0.1 to 999 minutes), counted drops (1 to 9990 drops) or other counted events (1-9990). For all runs, the time basis is used. The collection time is set to either 5 minutes or 3 minutes. Tubes used for collection in the Retriever II were 15 mL graduated centrifuge tubes. During a dynamic displacement when most of the core fluids have been displaced, and only small amounts of displaced fluids are being collected, the Retriever II collection method is replaced with hand changed 100 mL centrifuge collection tubes.

4.7 Additional Equipment

In addition to the major equipment described so far, a few auxiliary items and pieces of equipment were required.

In order to evacuate gases from the core prior to initial flooding, a vacuum line is connected by a tee between the core and the core/bypass outlet three-way valve (see figure 4.8). In series, between the core outlet tee and the vacuum pump, are a three-way valve, vacuum transducer, and 2000 mL vacuum flask. The three-way valve permits the vacuum pump to evacuate the core, isolate the core from the vacuum pump, or allow air into the evacuated flask. A Leybold Trivac "A" dual stage rotary vane pump, model D2A, is used as the vacuum pump. A Hastings vacuum gauge, model VT-6B, and vacuum tube, type DV-6R, is used to measure the vacuum drawn on the vacuum system.

An IEC centrifuge, model HN-S II, is used to facilitate quicker separation of phases collected during the dynamic displacement experiments.

Chapter 5

EXPERIMENTAL PROCEDURE

5.1 System Core and Tubing Volume Determination

Prior to any experimental runs, the volumes of tubings and cores are determined. The core volumes are determined through linear measurements. The tubing volumes and core end cap volumes are determined by injecting distilled water into the tubing with a 3-mL syringe and reading the injected volume needed to fill the tubing.

5.2 Pump Calibration

Actual pump flow rates for each pump are determined by measuring the elapsed time, Δt , for a volume of fluid, V , to be displaced from the pump for a variety of specified flow rates. The actual flow rate for a particular specified flow rate is:

$$q_{\text{act}} = \frac{V}{\Delta t} \quad (5.1)$$

The specified flow rate versus actual flow rates for each pump are shown in Chapter 6.

5.3 Core Preparation

The #8 glass beads for run 2 were sieved, and the 70-100 mesh beads used for the packing. All other runs used #9 glass beads that are washed in water, rinsed in distilled water and dried in a core drying oven for 48-72 hours at 50 ° c.

The procedure used to pack the core is as follows:

1. The weights of the empty core holder and flask containing the glass beads are taken and recorded.
2. The outlet end of the core is capped, and the glass beads poured into the core in 80 mL volume lifts. After each lift, a 3/4-in x 36-in aluminum rod is inserted into the core to hold the beads in place. The core is then tapped lightly up and down its length with a rubber headed hammer for several minutes in order to settle and compact the beads uniformly.
3. The core is filled and tapped as described above until the beads are flush with the top of the core. An additional mound of beads approximately 1/8-inch in height is added to account for any additional settling. The inlet cap is then screwed into place and tightened.
4. The weights of the full core holder and bead flask are again taken and recorded. After final tightening of the end caps, the threaded joint on each end cap, as well as each core/cap joint, is sealed with a fillet of vacuum grease.

5.4 Determination of Porosity

After each core is packed, and prior to conducting any experimental runs, the core's porosity is determined. By definition

$$\phi = \frac{V_{\text{pore}}}{V_{\text{bulk}}} \quad (5.2)$$

The pore volume of each core glass bead pack is determined as follows:

1. The core is first evacuated. This is accomplished by the following sequence of events. The core is isolated from the rest of the apparatus by closing all of the valves leading to the core. The valve leading from the core outlet to the vacuum pump is opened, and the core is then evacuated to a vacuum of not

greater than 100 microns of mercury. The vacuum pump normally runs overnight to achieve this level of vacuum.

2. The apparatus is then set to flood the core with water while measuring the volume of water needed to accomplish the flood. This is accomplished by the following sequence of events. The core inlet and outlet valves are set to bypass. The liquid selection valves are set for a water flood. The water surge suppressor, pressure relief valve, and pressure gauge are isolated from the system by closing the appropriate valves. All other valves are then set to a no-flow position in order to minimize possible vacuum loss and/or fluid contamination of the core. The reservoir is filled from the water flask via the bypass with a minimum of one core bulk volume of water. This ensures that the injection tubing network contains only water and that there is enough water in the reservoir to fill the core. The water pump feed valve is then set to draw water from the reservoir so that a loop is established from the reservoir to the pump through the bypass and back to the reservoir. The initial reservoir fluid levels and tubing heights, and surge suppressor fluid volumes are recorded.
3. The core is then flooded. This is accomplished as follows: The water pump flow rate is set to 5.0 mL/min. The vacuum valve is closed and the core inlet valve is turned from bypass to the core, thereby pumping water from the reservoir into the evacuated core. The pump is stopped at a volume several mL from the predicted volume needed to fill the core, and water is allowed to be pulled through the pump by the remaining vacuum. Once the water level has stabilized in the reservoir, the water surge valve is slowly and carefully opened to see if the reservoir water level drops indicating that a vacuum still remains. If the level drops, water is pumped one mL at a time into the core and the

surge test repeated until there is no further drop in the surge fluid level. The core outlet valve is then opened and the system pressures and fluid levels allowed to equilibrate.

4. The final reservoir and surge fluid levels, and tubing heights are recorded. Tubing displacement volume is determined by measuring the linear difference between the initial and final fluid heights multiplied by the number of tubes within the displaced zone and then multiplied by the cross-sectional area of the tubing. The pore volume is equal to the volume of the water that was pumped, minus the dead volume of the core under vacuum, minus the tubing displacement volume in the ΔH_2O displaced, minus the change in the surge volume.

$$V_{\text{pore}} = \Delta V_{H_2O} - V_{\text{dead}} - V_{\text{tubing}} - \Delta V_{\text{surge}} \quad (5.3)$$

The porosity is then determined by the definition given in Equation (5.2).

5. After the final fluid readings are taken, approximately 40 mL of water from the water flask is pumped through the core and into the fraction collector outlet to flush any fines from of the core. Unflushed fines could cause premature clogging of the system's filters. The pressure tap manifold is then flushed and filled with water and the pressure transmitter connected.

5.5 Determination of Core Linearity

Horizontal steady-state linear flow through homogeneous porous media must have a linear pressure drop along the length of the porous media. Core pressure drop linearity is determined as follows:

1. Pressure transmitter sample rate is set to one sample per second. Water pump flow rate is set to less than the flow rate required to inject one pore volume

per hour. The usual specified flow rate for linearity and absolute permeability determinations is 2.0 mL/min.

2. The BASIC data recording program (readpt.bas) shown in Appendix B, is started and pressure drops are recorded across the core at each tap until the pressure stabilizes and a constant reading is observed. A normal recording time is 3-5 minutes per tap. The glass bead pack is used for experiments if the pressure drop across the core's pressure taps are within 10% of each other. The pressure drops used for the test are across taps 2 and 3, ΔP_{2-3} , taps 3 and 4, ΔP_{3-4} , and taps 4 and 5, ΔP_{4-5} (see figure 4.9). As only pressures across a specified tap and tap 6 can be measured, the equation

$$\Delta P_{a-b} = \Delta P_{a-6} - \Delta P_{b-6} \quad (5.4)$$

is used to determine the pressure drop across the taps of interest.

5.6 Determination of Absolute Permeability

For horizontal steady-state linear flow it can be shown from Darcy's Law that absolute permeability k_{abs} is

$$k_{abs} = \frac{q \mu l}{\Delta P A} \quad (5.5)$$

where;

q: water flow rate in mL/sec

μ : water viscosity in cp at the final run temperature

l: length of core in cm

ΔP : final pressure drop across the entire core in atm

A: cross-sectional area of core in cm^2

5.7 Steady-State Experiments

Steady-state experiments are run to achieve specific core saturations and determine the effective and relative permeabilities at those saturations. A specific fractional fluid flow is injected into the core until the same fractional flow is produced from the core. Steady-state is assumed to be achieved at this point. Darcy's law is used to determine the effective permeabilities and material balances are used to determine the core saturations.

After the core characteristics are found, the core is brought to residual water saturation through a steady-state oil flood. From residual water saturation, the core is taken to a desired two-phase or three-phase saturation through a multi-phase steady-state flood. All steady-state experiments follow essentially the same procedure, only the fractional flow of the injected fluids change from experiment to experiment. The following procedure is used for steady-state floods.

1. The reservoir is charged, through the bypass, with enough of each fluid to reach the desired core saturation without expending all of any of the reservoir fluids being flooded.
2. The apparatus valves are adjusted so that the flooding fluids are looped from the reservoir, to the pumps, through the multi-phase injection portion of the fluid injection valve system, on through the bypass and back to the reservoir.
3. The pumps of the flooding fluids are set to achieve the desired fractional flow rates. The pumps are run until the multiphase injection, bypass, and reservoir return tubings are filled with the new fraction of fluids. All fluid levels in the reservoir and surge tubes, along with the tubing heights are taken and recorded. These readings are called the initial readings.

4. The pressure tap manifold valves are set to measure the pressure drop across the entire core (taps 1 and 6 are the only open valves). The pressure transmitter sampling rate is set. The rate used for all steady-state runs is one sample each thirty seconds. The BASIC data recording program, (readpt.bas) contained in appendix B, is begun and both core inlet and outlet valves are simultaneously turned from bypass to core.
5. A minimum of three pore volumes of fluid is allowed to flow through the core. The pressure and reservoir fluid levels are monitored. Once the pressure and fluid levels have stabilized, steady-state is assumed to have been reached. The pumps are shut off and all valves switched to the no-flow positions. All fluid levels and tubing heights are again taken and recorded. These are known as the final readings.

Saturations of the liquids and their effective and relative permeabilities are then determined. The following quantities are defined and used to determine saturations and permeabilities.

1. Fractional flow of fluid i, f_i ; where q_i and q_j are the actual individual fluid flow rates and q_t is the total flow rates of the pumps.

$$f_i = \frac{q_i}{q_t} = \frac{q_i}{q_i + q_j} \quad (5.6)$$

2. Tubing volume, V_{tubing} ; where H_1 and H_2 are the top and bottom liquid interface heights in the reservoir measured in cm, A_{tubing} is the cross-sectional area of the tubing, and N_{tubes} is the number of tubes,

$$V_{\text{tubing}} = (H_1 - H_2) A_{\text{tubing}} N_{\text{tubes}} \quad (5.7)$$

3. Initial and final fluid volumes; where V_{reading} is the raw reservoir fluid column

volume reading in mL.

$$V_i = V_{\text{top reading}} - V_{\text{bottom reading}} - V_{\text{tubing}} \quad (5.8)$$

4. Change in surge volume;

$$\Delta V_{\text{surge}} = V_{\text{surge initial}} - V_{\text{surge final}} \quad (5.9)$$

5. Change in fluid volume;

$$\Delta V_i = V_{i \text{ initial}} - V_{i \text{ final}} - V_{i \text{ tubing}} - \Delta V_{i \text{ surge}} - (f_i V_{\text{dead}}) \quad (5.10)$$

6. New core fluid volume, $V_{i,\text{new,core}}$; where $V_{i,\text{old,core}}$ is the fluid volume in the core before the last flood,

$$V_{i,\text{new,core}} = V_{i,\text{old,core}} - \Delta V_i \quad (5.11)$$

7. Core saturations, S_i ;

$$S_i = \frac{V_{i,\text{new,core}}}{V_{\text{pore}}} \quad (5.12)$$

8. Effective permeability of each liquid at the final core saturation;

$$k_i = \frac{q_i \mu_i l}{\Delta P A} \quad (5.13)$$

9. Relative permeability of each liquid at the final core saturation;

$$k_{r,i} = \frac{k_i}{k_{\text{abs}}} \quad (5.14)$$

5.8 Dynamic Displacement Experiments

The dynamic displacement experiments are conducted to reduce the number of experiments needed to map the saturation region. In all dynamic displacement experiments a single phase is injected. Runs 2 and 3 end with a dynamic decane flood to verify the results with previous work. Runs 4 and 5 end with a dynamic water flood. In run 8, a dynamic decane flood is conducted prior to the dynamic

water flood in order to compare with the results of run 8's earlier steady-state experiments.

The following procedure is used for dynamic displacement experiments:

1. Steady-state flow through the core is established to reach the desired initial core saturations. The injection into the core is through the four-way valve's multiphase inlet and core injection outlet line. The valves for the single-phase injecting fluid are set to establish a loop from the flask, through the pump, into the four-way valve's single-phase inlet and flask return outlet, and then back to the flask.
2. A minimum of 5 pore volumes of flooding fluid is established in the flooding fluid flask. The specified flow rate of the flooding fluid pump is set to match the total specified flow rate of the steady-state flow rate.
3. The pressure transmitter sampling rate is set to one sample per second. The BASIC data collection program (readpt.bas, found in Appendix B) is started and the fraction collector is set to the specified sample rate. In all runs except run 2, the fraction collector sample rate is set to 3 minutes. The reservoir/fraction collector selection valve is set to the fraction collector and at least 6 mL of the steady-state fluid fraction is pumped through the line to purge it.
4. The dynamic flood is started by simultaneously turning the four-way valve to direct the single-phase flood to the core, advancing the fraction collector to the first dynamic displacement collection tube, and recording the elapsed time from the data collection program.
5. The 15 mL collection tubes are used until the displaced core fluid volumes can no longer be read accurately. Normally this occurs when the oil volume is

below 0.1 mL per tube. At this point the Retriever II fraction collector is shut off and 100 mL centrifuge tubes are placed by hand to collect the fluid. The empty and full weights of the 100 mL collection tubes and the elapsed collection time of each tube are recorded. The filled fraction collection tubes are numbered and run through the centrifuge to separate the phases. The top fluid level reading for each fluid is recorded for each tube. The total fluid volume for the 100 mL tubes is determined by multiplying the weight difference of the full and empty tube by the density of the displacing fluid.

$$V_{t \text{ 100 mL tube}} = \Delta wt_{\text{tube}} \rho_{\text{displacing fluid}} \quad (5.15)$$

The total fluid volume for the 100 mL tubes may also be determined by multiplying the weight difference of the full and empty tube by the density of the displacing fluid if the flow rate during the collection is constant and equal to the calculated rate.

$$V_{100 \text{ mL tube}} = q_{\text{actual}} \Delta t \quad (5.16)$$

5.9 Fractional Recovery Analysis

The raw fluid level data for each dynamic displacement experiment is used by a FORTRAN analysis program (datafrac.f), listed in Appendix B, to determine the actual fluid volumes in each tube, V_i , the cumulative individual fluid collected volumes for each tube, V_{ti} , the total cumulative fluid collected volume for each tube, V_{tt} , the cumulative pore volumes recovered for each fluid, R_i , and the pore volumes injected, Q . Pore volumes recovered are defined as

$$R_i = \frac{V_{ti}}{V_{\text{pore}}} \quad (5.17)$$

where V_{ti} accounts for the fluid dead volumes in the core and tubing leading to the

fraction collector.

$$V_{ti} = \sum_1^n V_i - f_i V_{\text{dead}} \quad (5.18)$$

Pore volumes injected are defined as

$$Q = \frac{V_u}{V_{\text{pore}}} \quad (5.19)$$

where

$$V_u = \sum_1^n V_{ti} \quad (5.20)$$

The fluid recoveries are then plotted against the respective pore volume injected.

The pressure data is converted by another FORTRAN program (pvst.f), contained in Appendix B, into the normalized pressure drop, Φ , and plotted against the pore volumes injected, Q . The normalized pressure drop is defined as

$$\Phi = \frac{\Delta P}{q_{\text{calc}}} \quad (5.21)$$

The program has the capability of averaging any specified number of the pressure data points in order to smooth the curve. Another FORTRAN program (variq.f), contained in appendix B, is a modified version of pvst.f that calculates the actual flow rates during the collection time of a collection vessel by dividing the actual collected volume by the time collected. This data is then used to determine the true normalized pressure drop and the actual pore volumes injected. This program is used if there is a varying flow rate during the dynamic flood experiment.

Chapter 6

ERROR ANALYSIS

In this section, the errors in calculating the following four quantities are discussed:

1. Porosity
2. Saturation
3. Absolute Permeability
4. Relative Permeability

The general approximation for the error is:

$$\Delta G = \sum_{i=1}^n \left| \frac{\delta G}{\delta x_i} \right| \Delta x_i \quad (6.1)$$

where $G = f(x_1, x_2 \cdots x_i)$.

6.1 Error Analysis for Porosity

The equation for porosity calculation is:

$$\phi = \frac{V_{\text{pore}}}{V_{\text{bulk}}} \quad (6.2)$$

where

$$V_{\text{pore}} = \Delta V_{\text{H}_2\text{O}} - V_{\text{dead}} - V_{\text{tubing}} - \Delta V_{\text{surge}} \quad (6.3)$$

$$V_{\text{pore}} = V_{\text{in,H}_2\text{O}} - V_{\text{final,H}_2\text{O}} - V_{\text{dead}} - V_{\text{tubing}} - V_{\text{in,surge}} + V_{\text{final,surge}} \quad (6.4)$$

$$V_{\text{pore}} = V_{\text{in,H}_2\text{O}} - V_{\text{final,H}_2\text{O}} - \sum_{i=1}^6 \Delta V_{\text{dead}} - \left[H_{\text{in}} - H_{\text{final}} \right] \pi r_t^2 N - V_{\text{in,surge}} + V_{\text{final,surge}} \quad (6.5)$$

where r_t is the tubing radius and N is the number of tubes in the domain that is changing.

$$V_{\text{bulk}} = \pi r_{\text{core}}^2 L_{\text{core}} \quad (6.6)$$

hence:

$$\phi = \frac{\left[V_{\text{i,H}_2\text{O}} - V_{\text{final,H}_2\text{O}} - \sum_{i=1}^6 \Delta V_{\text{dead}} - \left[H_{\text{final}} - H_{\text{i}} \right] \pi r_t^2 N - V_{\text{i,surge}} + V_{\text{final,surge}} \right]}{\pi r_{\text{core}}^2 L_{\text{core}}} \quad (6.7)$$

The summation term for the dead volume has six different values. Hence, the summation is from 1 to 6. We will take the worst case of $N = 4$. We will compute the individual errors, EV_{pore} , and EV_{bulk} ; then we will compute the error in porosity.

$$\begin{aligned} EV_{\text{pore}} = & EV_{\text{in,H}_2\text{O}} + EV_{\text{final,H}_2\text{O}} + \sum_{i=1}^6 E\Delta V_{\text{dead}} \\ & + 4\pi \left[r_t^2 \left[EH_{\text{in}} + EH_{\text{final}} \right] + \left[H_{\text{final}} - H_{\text{in}} \right] 2r_t \cdot Er_t \right] + EV_{\text{in,surge}} + EV_{\text{final,surge}} \end{aligned} \quad (6.8)$$

$$EV_{\text{bulk}} = \pi \left[2 r_{\text{core}} l_{\text{core}} Er_{\text{core}} + r_{\text{core}}^2 El_{\text{core}} \right] \quad (6.9)$$

$$E\phi = \frac{EV_{\text{pore}}}{V_{\text{bulk}}} + \frac{V_{\text{pore}}}{V_{\text{bulk}}^2} \cdot EV_{\text{bulk}} = \phi \cdot \left[\frac{EV_{\text{pore}}}{V_{\text{pore}}} + \frac{EV_{\text{bulk}}}{V_{\text{bulk}}} \right] \quad (6.10)$$

The individual E values are controlled by the measurement techniques, and given below:

$$EV_{\text{in,H}_2\text{O}} = 0.5 \text{ cc}$$

$$EV_{\text{final,H}_2\text{O}} = 0.5 \text{ cc}$$

$$E\Delta V_{\text{dead}} = 0.02 \text{ cc}$$

$$EH_{\text{in}} = 0.05 \text{ cm}$$

$$EH_{\text{final}} = 0.05 \text{ cm}$$

$$Er_t = 0.002 \text{ cm}$$

$$EV_{\text{in,surge}} = 0.01 \text{ cc}$$

$$EV_{\text{final,surge}} = 0.01 \text{ cc}$$

$$Er_{\text{core}} = 0.002 \text{ cm}$$

$$El_{\text{core}} = 0.002 \text{ cm}$$

Typical measured values are:

$$H_{\text{in}} = 0.0 \text{ cm}$$

$$H_{\text{final}} = 15.0 \text{ cm}$$

$$r_t = 0.3175 \text{ cm}$$

$$r_{\text{core}} = 1.0895 \text{ cm}$$

$$l_{\text{core}} = 91.46 \text{ cm}$$

$$\phi = 0.38$$

$$V_{\text{bulk}} = 341.0 \text{ cc}$$

$$V_{\text{pore}} = 134.0 \text{ cc}$$

Applying the errors and typical values to Equations 6.8 and 6.9 yields:

$$\begin{aligned} EV_{\text{pore}} &= 0.5 + 0.5 + 6 \cdot 0.02 \\ &+ 4 \pi \left[1.0895^2 \left[0.05 + 0.05 \right] + \left[15.0 - 0.0 \right] 2 \cdot 1.0895 \cdot 0.002 \right] \\ &+ 0.01 + 0.01 = 1.968 \approx 1.97 \text{ cc} \end{aligned}$$

$$\begin{aligned} EV_{\text{bulk}} &= \pi \left[2 \cdot 1.0895 \cdot 91.46 \cdot 0.002 + 1.0895^2 0.002 \right] \\ &= 1.259 \approx 1.26 \text{ cc} \end{aligned}$$

Substituting EV_{pore} and EV_{bulk} into Equation 6.10 yields typical porosity error:

$$\begin{aligned} E\phi &= 0.38 \left[\frac{1.97}{134.0} + \frac{1.26}{341.0} \right] \\ &= 0.00699 \end{aligned}$$

In percentage units $\approx 0.7\%$ error.

6.2 Error Analysis for Saturation

There are two different procedures for saturation determination: the steady-state and the non-steady-state. These two procedures are discussed next.

6.2.1 Error Analysis for Steady-State Saturations

The basic equation for average core saturations is:

$$S_j = \frac{V_{j,\text{core}}}{V_{\text{pore}}} \quad (6.11)$$

where $V_{j,\text{core}}$ is the volume of phase j in the core. Recall that $EV_{\text{pore}} = 1.97$ cc.

Now:

$$V_{j,\text{core}} = V_{j,\text{old,core}} - \Delta V_{j,\text{core}} \quad (6.12)$$

Let us assume that for the first time fluid j is introduced to the core

$$V_{j,\text{old,core}} = 0 \pm 0.0.$$

Therefore:

$$V_{j,\text{core}} = -\Delta V_i \quad (6.13)$$

$$\Delta V_j = V_{j,\text{in}} - V_{j,\text{final}} - V_{j,\text{tubing}} - V_{j,\text{in,surge}} + V_{j,\text{final,surge}} - f_j V_{\text{dead}} \quad (6.14)$$

This is very similar to the Equation 6.4 except for the f_j term. Let us take f_j at the upper limit of 1. Then $EV_{j,\text{core}} \approx EV_{\text{pore}} \approx 1.97$ at the upper limit of complete phase displacement. Hence:

$$ES_j = S_j \left[\frac{EV_{j,\text{core}}}{V_{j,\text{core}}} + \frac{EV_{\text{pore}}}{V_{\text{pore}}} \right] \quad (6.15)$$

Typical saturation values are $0.1 - 0.8$ and typical $V_{j,\text{core}}$ values are $134.0 \cdot 0.1 - 134.0 \cdot 0.8 = 13.4 - 107.2$.

Hence, for $S_j \approx 0.1$

$$ES_j = 0.1 \left[\frac{1.97}{13.4} + \frac{1.97}{134.0} \right] = 0.0162 \approx 1.6\%$$

For $S_j \approx 0.8$

$$ES_j = 0.8 \left[\frac{1.97}{107.2} + \frac{1.97}{134.0} \right] = 0.0264 \approx 2.6\%$$

In summary, $ES_j \approx 1\% - 3\%$. For cases that $V_{j,\text{old,core}} \neq 0$, the errors do not simply add up as the same fluid is used over and over. For example, the first oil

flood is done in a closed loop and $V_{oil,old,core} = 0$. Now, the second steady-state oil-water flood (as in runs 2 and 3) is done without adding fluids to the cycling reservoir. Since the interfaces in the graduated cylinder are read in the same fashion every time, the errors cannot accumulate for one-phase independently. If the error increases for one phase it decreases for the other, hence, if the reading technique is constant, the errors should stay constant at about 1–2%. If new conditions are established in the cycling reservoir, the errors for phases existing in the core should double.

6.2.2 Error Analysis for Non-Steady-State Saturations

The determination of the saturation error for this case is rather difficult. The dynamic displacement saturation that we calculate using the Buckley-Leverett theory is assigned to the output end of the core and given by:

$$S_j = S_{j,in} + \left[R_j - Q \frac{\partial R_j}{\partial Q} \right] \quad (6.16)$$

where R_j is the recovery in pore volumes of phase j , and $\frac{\partial R_j}{\partial Q} = R_j'$. Let us assume that $ES_{j,in}$ is of the same order of the error we had before $\approx 1-2\%$. The error in R_j depends on the number of tubes we read and the individual error in the tubes. If we can reduce $EV_{j,tube} \approx 0.1$ cc then for the 15th tube (at about 1.2 – 1.5 PVI), $EV_{j,total \text{ produced}} = 1.5$ cc. This error can be reduced by knowing the overall injected volume.

Since

$$R_j = \frac{V_{j,total \text{ produced}}}{V_{pore}} \quad (6.17)$$

$$ER_j = R_j \left[\frac{EV_{j,\text{total produced}}}{V_{\text{pore}}} + \frac{EV_{\text{pore}}}{V_{\text{pore}}} \right] \quad (6.18)$$

If a typical value for $R_j \approx 0.3$ then:

$$ER_j = 0.3 \left[\frac{1.5}{0.3 \cdot 134.0} + \frac{1.97}{134.0} \right] = 0.0156 \approx 1.6 \%$$

If the recovery is smaller, then the errors are smaller too.

The term Q (PVI) is:

$$Q = \frac{V_{\text{inj,total}}}{V_{\text{pore}}} = \frac{V_{\text{prod,total}}}{V_{\text{pore}}} \quad (6.19)$$

and

$$EQ = Q \left[\frac{EV_{\text{inj,total}}}{V_{\text{inj,total}}} + \frac{EV_{\text{pore}}}{V_{\text{pore}}} \right] \quad (6.20)$$

The error in total fluid produced can be reduced to ≈ 0.5 cc, at about 1 PVI (≈ 150 cc), by considering pump rates and accumulations. At 1 PVI we use about 10–15 tubes. If we use these tubes for a PVI calculation, then $EV_{\text{prod,total}} \approx 1.0 - 1.5$ cc. We will use $EV_{\text{prod,total}} \approx 0.5$ cc. Hence:

$$EQ = 1.0 \left[\frac{0.5}{134.0} + \frac{1.97}{134.0} \right] = 0.0184 \approx 1.8 \%$$

Typical slopes are on the order of $0.1 \left[\frac{PV_{\text{rec}}}{\text{PVI}} \right]$. The error in the slope is difficult to assess as we are using eye construction. Let us assume that $ER_j \approx 0.01$. Hence:

$$ES_j = ES_{j,\text{in}} + ER_j + R_j' EQ + Q ER_j' \quad (6.21)$$

$$ES_j = (1\% - 3\%) + 1.0 \% + (0.1) \cdot 1.8\% + 1 \cdot 1\% = 3.18\% - 5.18\%$$

This error varies based upon what stage of the flood it is computed for, and can be reduced by consistent fluid level measurements and overall material balance corrections.

6.3 Error Analysis for Absolute Permeability

The error analysis for absolute permeability was documented by Obut (1989) and is summarized here. The absolute permeability is given by:

$$k_{\text{abs}} = \frac{q \mu l}{A \Delta P} \quad (6.22)$$

The error is defined by:

$$Ek_{\text{abs}} = k_{\text{abs}} \left[\frac{Eq}{q} + \frac{E\mu}{\mu} + \frac{El}{l} + \frac{EA}{A} + \frac{E\Delta P}{\Delta P} \right] \quad (6.23)$$

The typical individual experimental measurements and their error values are:

$$q = 2.00 \text{ cc/min}$$

$$Eq = 0.01 \text{ cc/min}$$

$$\mu = 1.00 \text{ cp}$$

$$E\mu = 0.01 \text{ cp}$$

$$l = 90.00 \text{ cm}$$

$$El = 0.02 \text{ cm}$$

$$A = 3.729 \text{ cm}^2$$

$$EA = 0.02 \text{ cm}^2$$

$$\Delta P = 1.0 \text{ psi}$$

$$E\Delta P = 0.001 \text{ psi}$$

$$k_{\text{abs}} \approx 20 \text{ darcy}$$

$$\begin{aligned} Ek_{\text{abs}} &= 20.0 \left[\frac{0.01}{2.0} + \frac{0.01}{1.0} + \frac{0.02}{90.0} + \frac{0.02}{3.729} + \frac{0.01}{1.0} \right] \\ &= 0.612 \text{ darcy: or } \approx 3\% \text{ error} \end{aligned}$$

6.4 Error Analysis for Relative Permeability

In this project, steady-state and dynamic relative permeabilities are calculated. We consider these two cases next.

6.4.1 Error Analysis for Steady-State Relative Permeability

The equation used for steady-state relative permeability of phase i is:

$$k_{r,i} = \frac{k_i}{k_{\text{abs}}} \quad (6.24)$$

The error is defined by:

$$Ek_{r,i} = k_{r,i} \left[\frac{Ek_i}{k_i} + \frac{Ek_{\text{abs}}}{k_{\text{abs}}} \right] \quad (6.25)$$

We assume that $Ek_i = Ek_{\text{abs}}$ as the k_i equation is identical in format to the k_{abs} equation. If $k_{r,i} = 0.1$, $Ek_i = 0.0375$ darcy, and $k_{\text{abs}} = 20.0$ darcy, then:

$$\begin{aligned} Ek_{r,i} &= 0.1 \left[\frac{0.612}{10.0} + \frac{0.612}{20.0} \right] \\ &= 0.009 \text{ or } \approx 9\% \end{aligned}$$

6.4.2 Error Analysis for Dynamic Relative Permeability

The Welge equation for the relative permeability as modified by Johnson, Bossler, and Naumann, (JBN) is:

$$k_{r,j} = \frac{k_j}{k_{abs}} = \frac{1}{k_{abs}} \cdot \frac{f_j l \mu_j}{A \left[\frac{1}{q} \cdot \frac{\partial P}{\partial x} \right]} = \frac{1}{k_{abs}} \cdot \frac{f_j l \mu_j}{A \Phi} \quad (6.26)$$

where $\left[\frac{1}{q} \cdot \frac{\partial P}{\partial x} \right] = \Phi$ is the distance between the intercept of the tangent with the y-axis, as shown in Figure 2.1. Then:

$$Ek_{r,i} = k_{r,i} \left[\frac{Ek_{abs}}{k_{abs}} + \frac{Ef_i}{f_i} + \frac{E l}{l} + \frac{E \mu_i}{\mu_i} + \frac{E A}{A} + \frac{E \Phi}{\Phi} \right] \quad (6.27)$$

Let us assume that $E \cdot \left[\Phi \right] = 0.02 \Phi$. The error in the fractional flow is the error in the slope of the recovery curve. We assumed before that this error is on the order of 1–2%. The error in the viscosity is about 1%. The error in the area is about 0.1%. Hence:

$$\begin{aligned} Ek_{r,i} &= k_{r,i} \left[0.0187 + 0.01 + 0.002 + 0.01 + 0.006 + 0.02 \right] \\ &= k_{r,i} \left[0.068 \right] \\ &\approx 6\% \end{aligned}$$

The basic way to reduce this error is to reduce the error in the slopes.

6.5 Relative Error Analysis

The relative error does not consider constant errors that are added to the absolute error. For example, the error in measuring k_{abs} does not have any effect on the

individual dynamic relative permeability errors of Equation 6.27. Only the actual measurements take part in the relative error. For example:

$$E_r k_{r,i} = k_{r,i} \left[\frac{E f_i}{f_i} + \frac{E \Phi}{\Phi} \right] \quad (6.28)$$

Hence:

$$E_r k_{r,i} = k_{r,i} [0.03] \approx 3\%$$

These errors should be expected, and are reasonable in magnitude considering the equipment used for this project.

6.6 Pump Flow Rates

The error for the pump flow rates is discussed in Section 6.3. Figures 6.1 through 6.3 are the relationships between the specified pump flow rates and the actual pump flow rates. The fluid flow path used in the determination of these relations is the following: flow from the fluid flask through the individual pump, through the core-bypass and out the fractional flow collection outlet. The dots in these figures represent the actual data points taken.

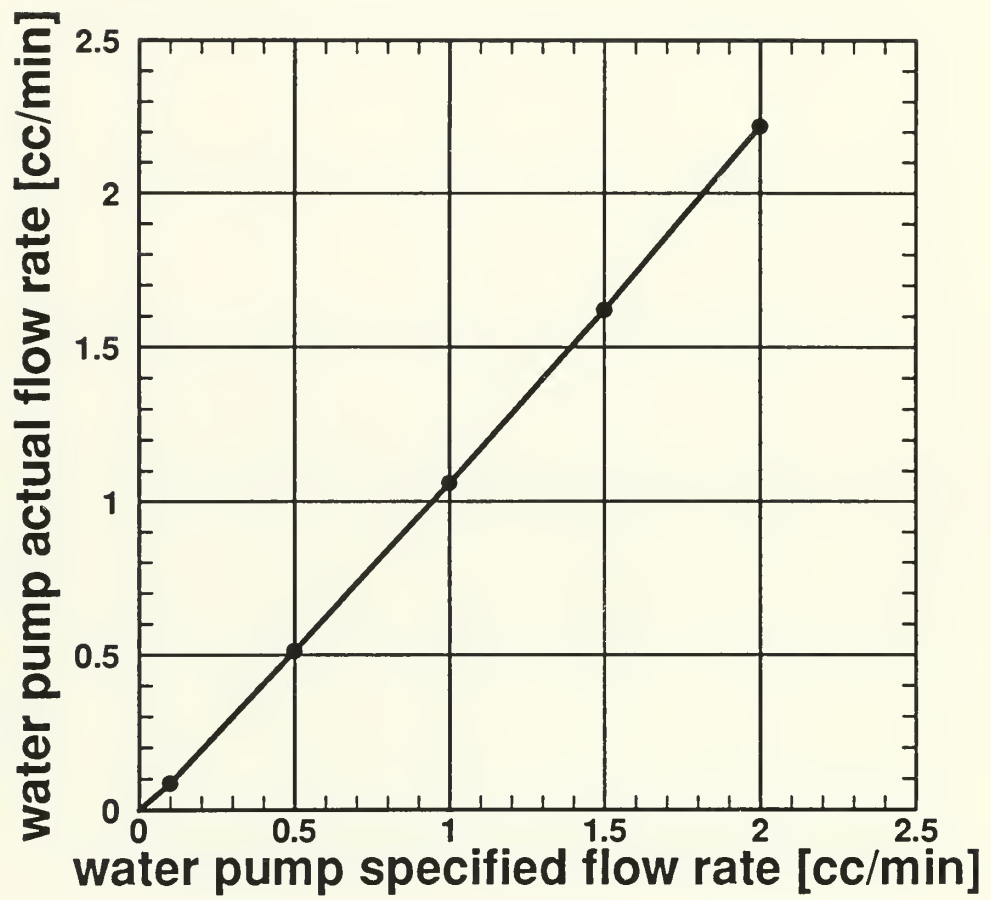


Figure 6.1: Water Pump - Actual vs. Specified Flow Rates

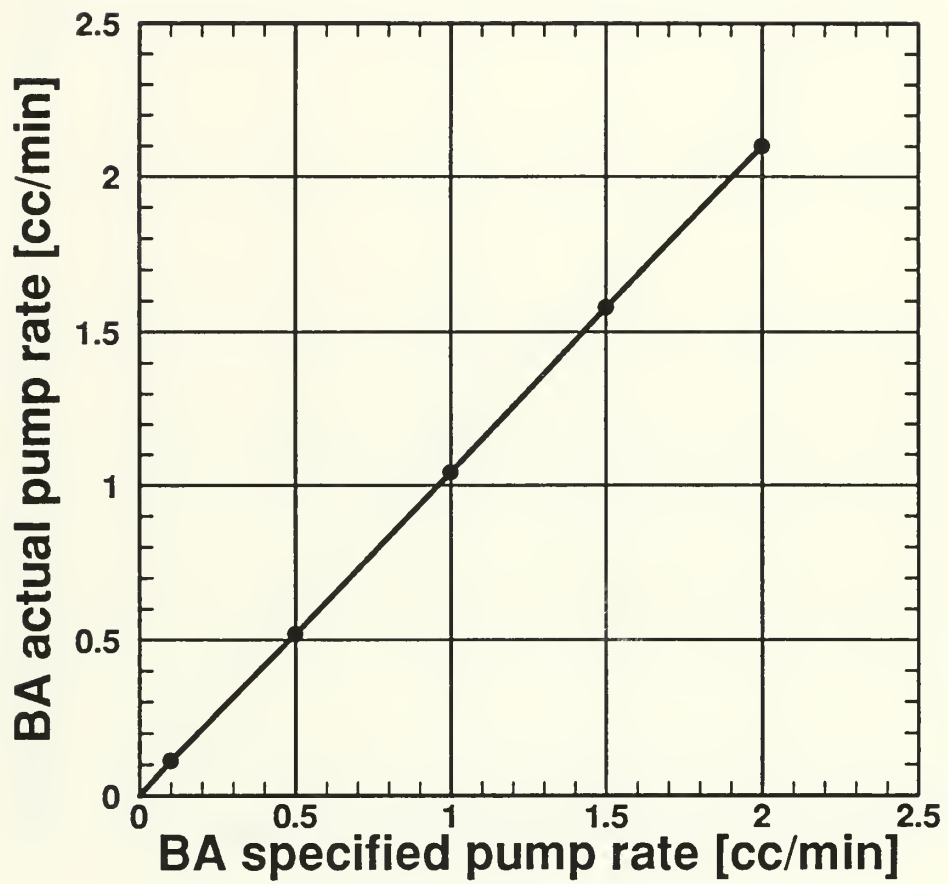


Figure 6.2: BA Pump - Actual vs. Specified Flow Rates

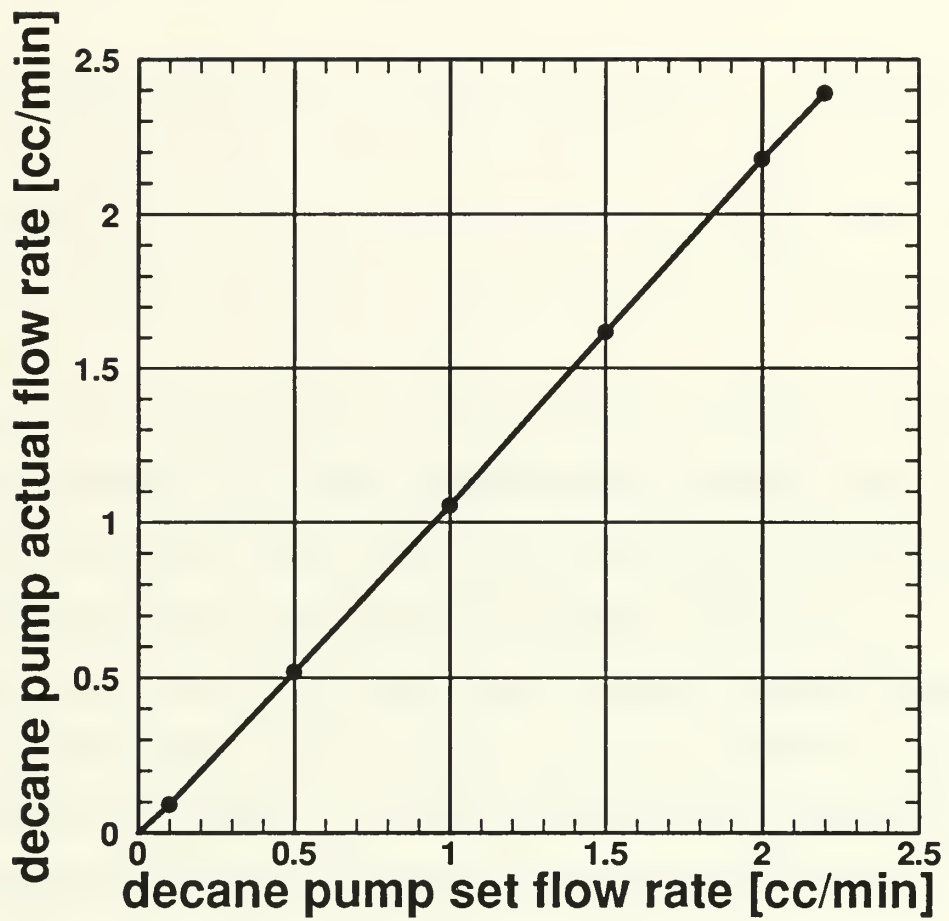


Figure 6.3: Decane Pump - Actual vs. Specified Flow Rates

Chapter 7

RESULTS

Nine experimental runs were conducted in this research. A run consisted of a series of experiments using the same packed glass bead core. Run 1 was an equipment familiarity run. In run 1, the apparatus contained only distilled water. Multiple phase experiments began in run 2, consequently there are no multiphase results from run 1.

Runs 2 and 3 were conducted to verify the apparatus. This was accomplished by running dynamic decane flooding experiments under conditions similar to those reported by Grader and O'Meara (1988). Run 2 was primarily a multiphase familiarity run. Run 3 was a repeat of Grader and O'Meara's (1988) run 15.

Runs 4 and 5 were the first dynamic water flood runs. They were designed to enter the ternary diagram in the interior region of the irreducible water iso-saturation line. The objective was to provide insight into the general trends of dynamic water floods and give a background for selecting subsequent runs.

Runs 6 and 7 were abandoned after initial water flooding because of non-linear pressure drops across the glass bead pack.

Run 8 was designed to obtain data along the irreducible water iso-saturation line. The initial steady-state experiments were conducted to travel up and down the irreducible water iso-saturation line with the following objectives: to obtain a fractional fluid flow ratio versus core saturation plot, to examine the effects of hysteresis, to provide benzyl alcohol and decane relative permeabilities, and to provide comparison with data obtained through dynamic displacement experiments. Run 8

concluded with a dynamic water flood originating at irreducible water saturation and residual oil saturation in the presence of decane. This provided data from a water flood at the upper limit of decane saturation.

Run 9 was designed to obtain data along the two-phase water/benzyl alcohol saturation line (0% decane saturation), and along the residual decane iso-saturation line. These experiments provided data on the effect of decane in the system and provided data from a water flood at the lower limit of decane saturation.

7.1 Three-Phase Decane Flood Experiments

This section discusses the results of experimental runs 2 and 3. These two runs were used to test and fine-tune the apparatus. They were also used to validate the apparatus by comparing the results with previous work. Tables A.1 through A.4 in Appendix A summarize the fluid recovery data and relative permeability data of these runs.

Figure 7.1 is the pressure profile of the core linearity check for run 2. The plateaus in the profile show the pressure drop between the labeled core taps. In this linearity test each tap along the core was opened for 100 seconds. There is an unexplained discrepancy in this profile as the pressure drop between taps 2 and 6 cannot be lower than the the drop between 3 and 6. The core is not completely linear as there is not equal drop between the three equally spaced taps, 2-3, 3-4, and 4-5. The run was continued despite this nonlinearity just to gain familiarity with the equipment and to use the data as a comparison. There was no attempt to use this run for verification saturation mapping.

Figures 7.2 and 7.3 show the recovery curves for the benzyl alcohol and the water with the injected decane. The initials of the recovered fluids identify the

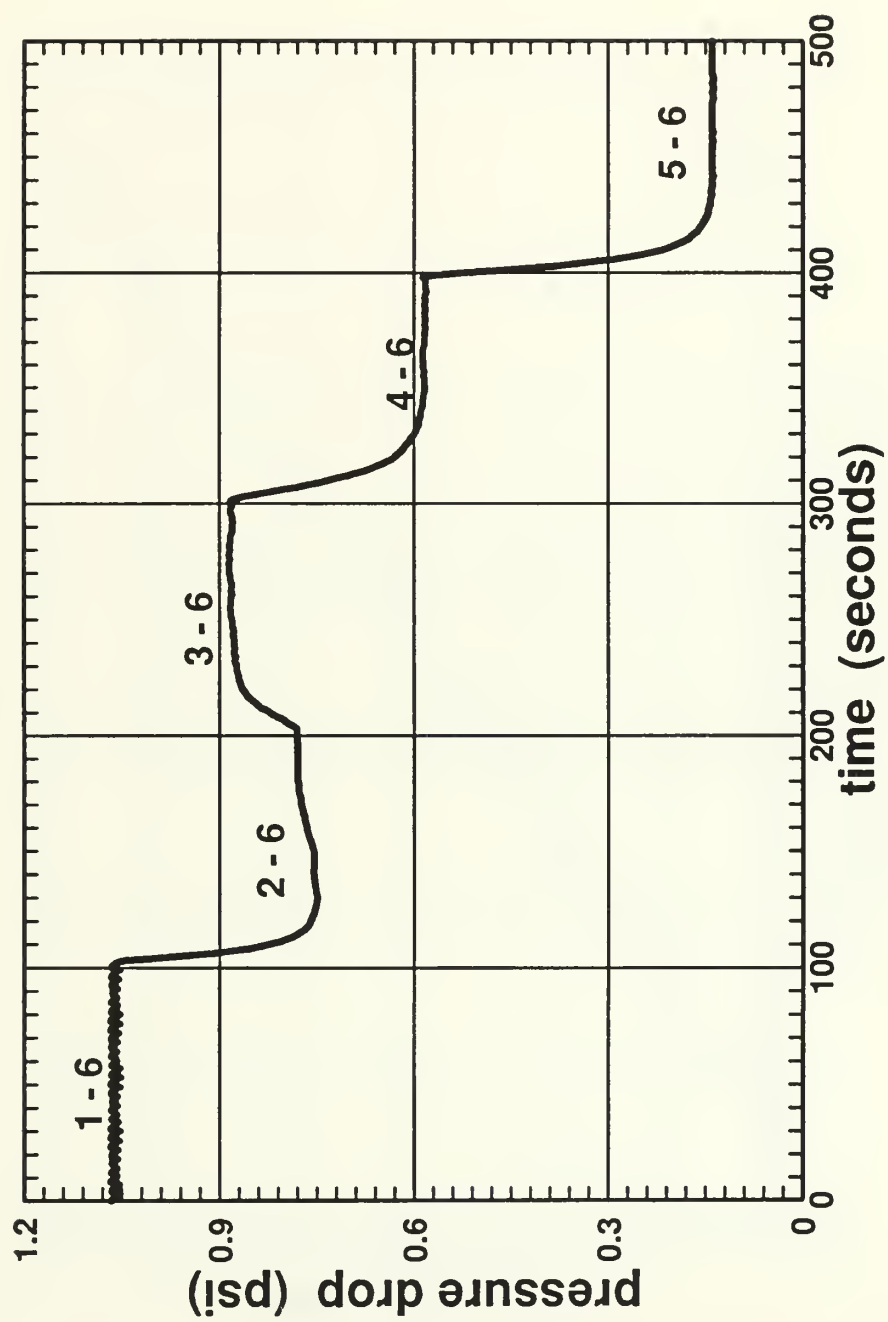


Figure 7.1: Core Linearity Check Pressure Profile; Run 2.

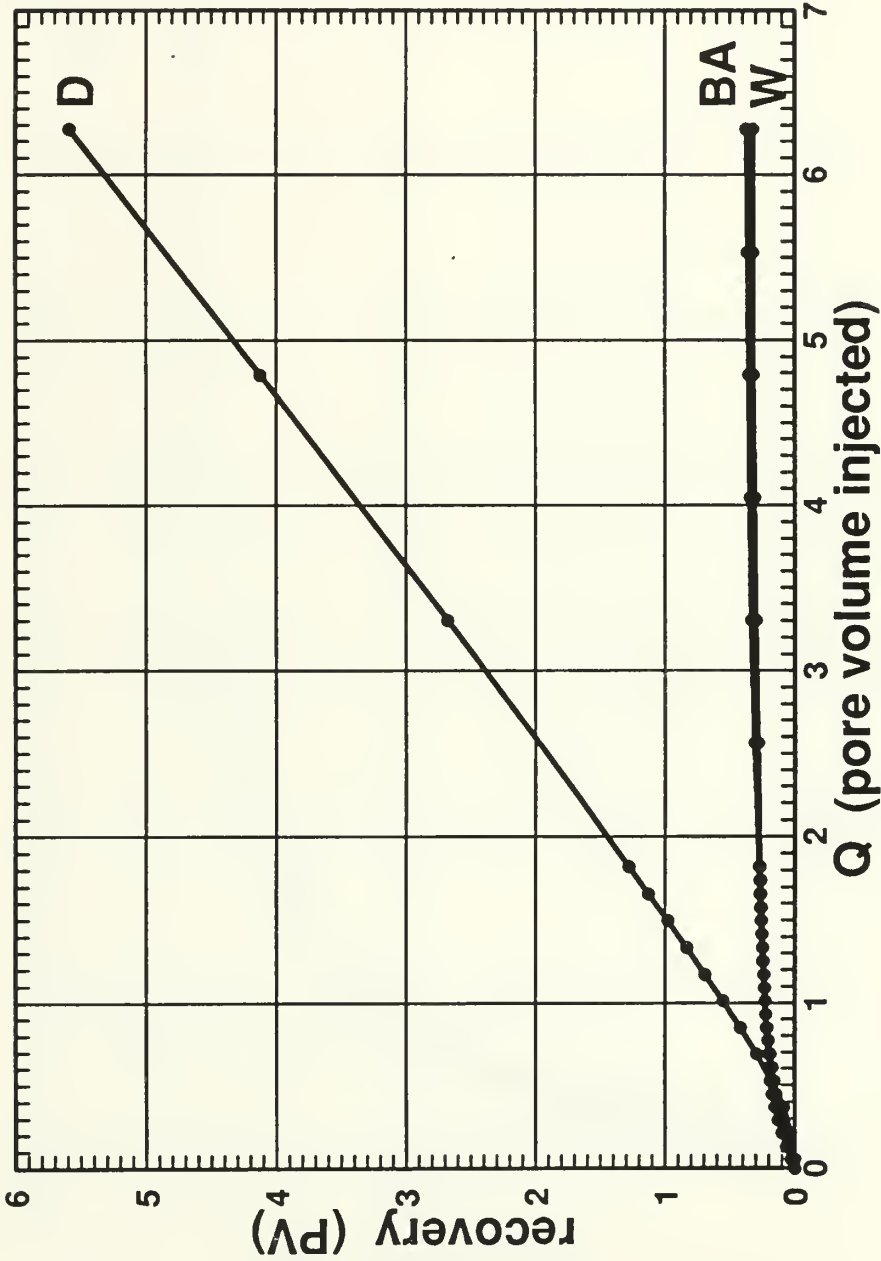


Figure 7.2: Dynamic Flood Recovery Curves; Run 2.

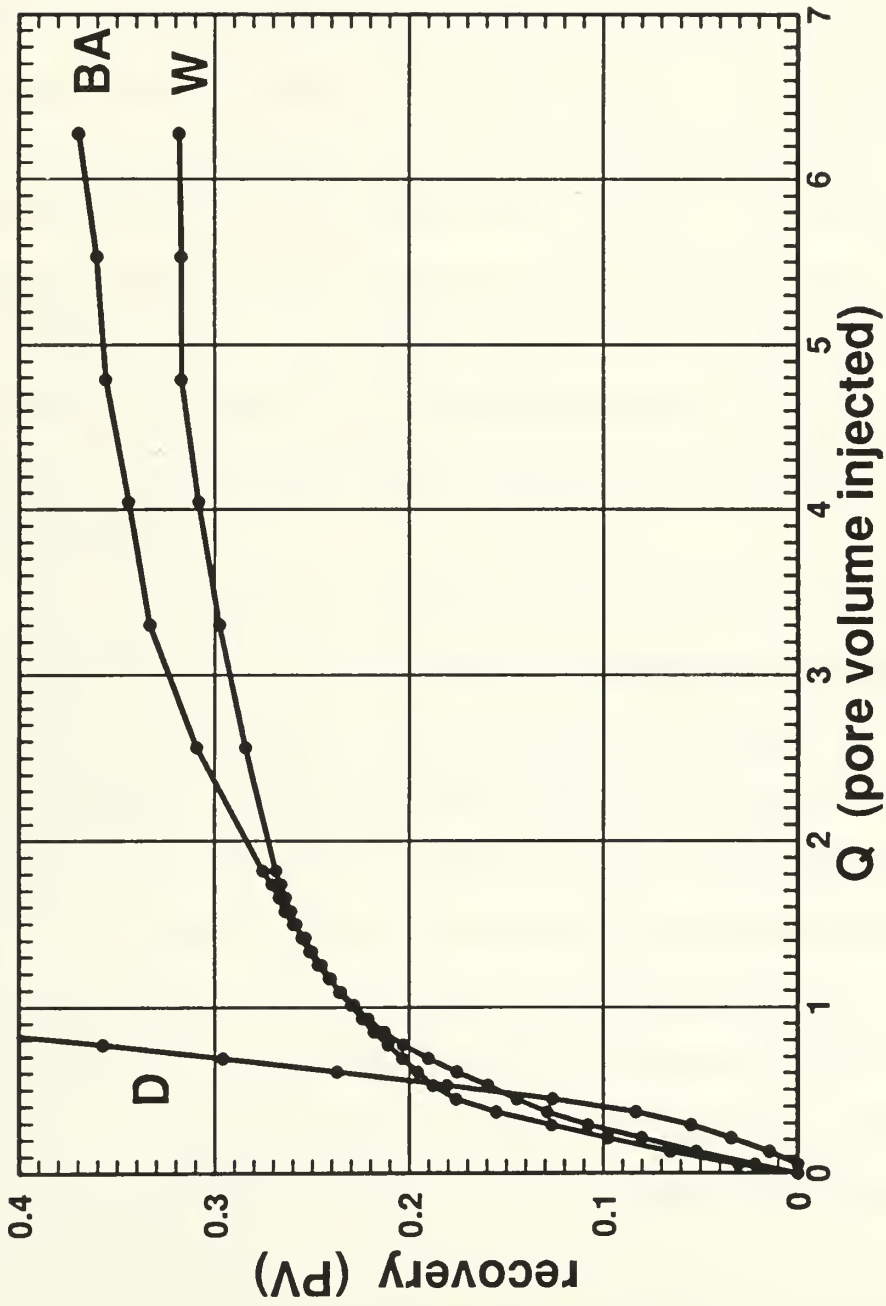


Figure 7.3: Expanded Dynamic Flood Recovery Curves; Run 2.

recovery curves. The dots on the figures are the actual data points representing the data from each collection vessel. The data for these figures is found in Table A.1. Figure 7.2 shows the entire recovery curves for all three phases, while Figure 7.3 enlarges the recovery curves of the water and alcohol. Breakthrough of the decane occurred at approximately 0.06 pore volumes injected as shown by the departure of the decane recovery curve from the x-axis at this point. The smooth transitions of both the water and alcohol curves after breakthrough indicate there is no fluid bank developed for either of these fluids during the flood and there will be little to no saturation shock jump. Why this condition developed is unclear and normally is related to fluid bypassing the glass bead pack along the interface of the case and glass bead pack.

The saturation history of this run is shown in Figure 7.4. The glass bead pack was flooded with water (1), then flooded to residual water saturation with benzyl alcohol (2), and brought to a core saturation (3) of 49% water and 51% alcohol by a steady-state 1:1 water-benzyl alcohol flood. The saturation trajectory of the dynamic decane flood is shown by points (3) to (5). The Buckley-Leverett shock is shown by the jump from point (3) to point (4). The continuous saturation trajectory after breakthrough is shown by the line from point (4) to point (5). The dots along the trajectory are the saturations calculated at various pore volumes injected. The data for these points are contained in Table A.2 in Appendix A. The saturation trajectory was determined using the dynamic displacement trajectory technique presented in Chapter 2.

The flow-rate normalized pressure drop versus the pore-volumes injected plot is shown as Figure 7.5. The pressure was normalized to the single calculated actual flow set on the decane pump. The sample rate was set at one sample per second

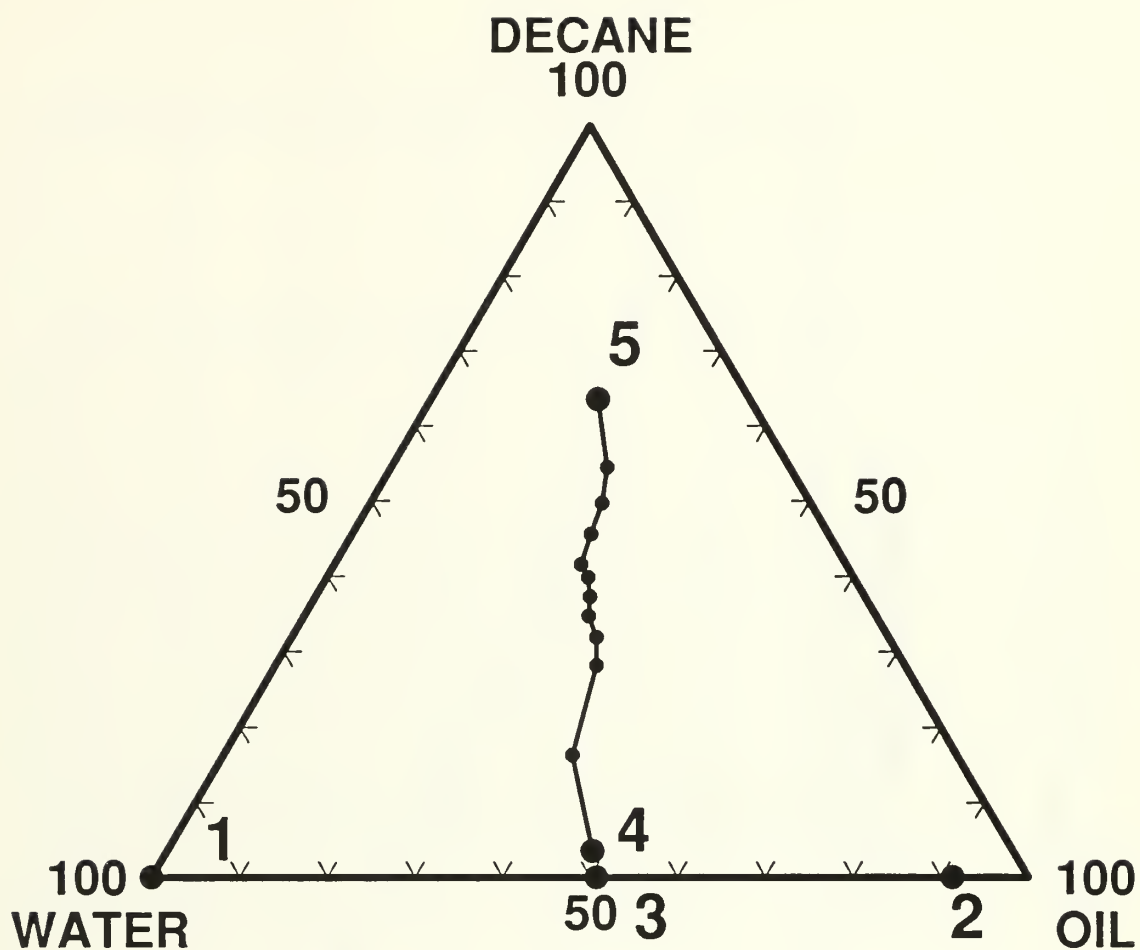


Figure 7.4: Saturation History and Trajectories; Run 2.

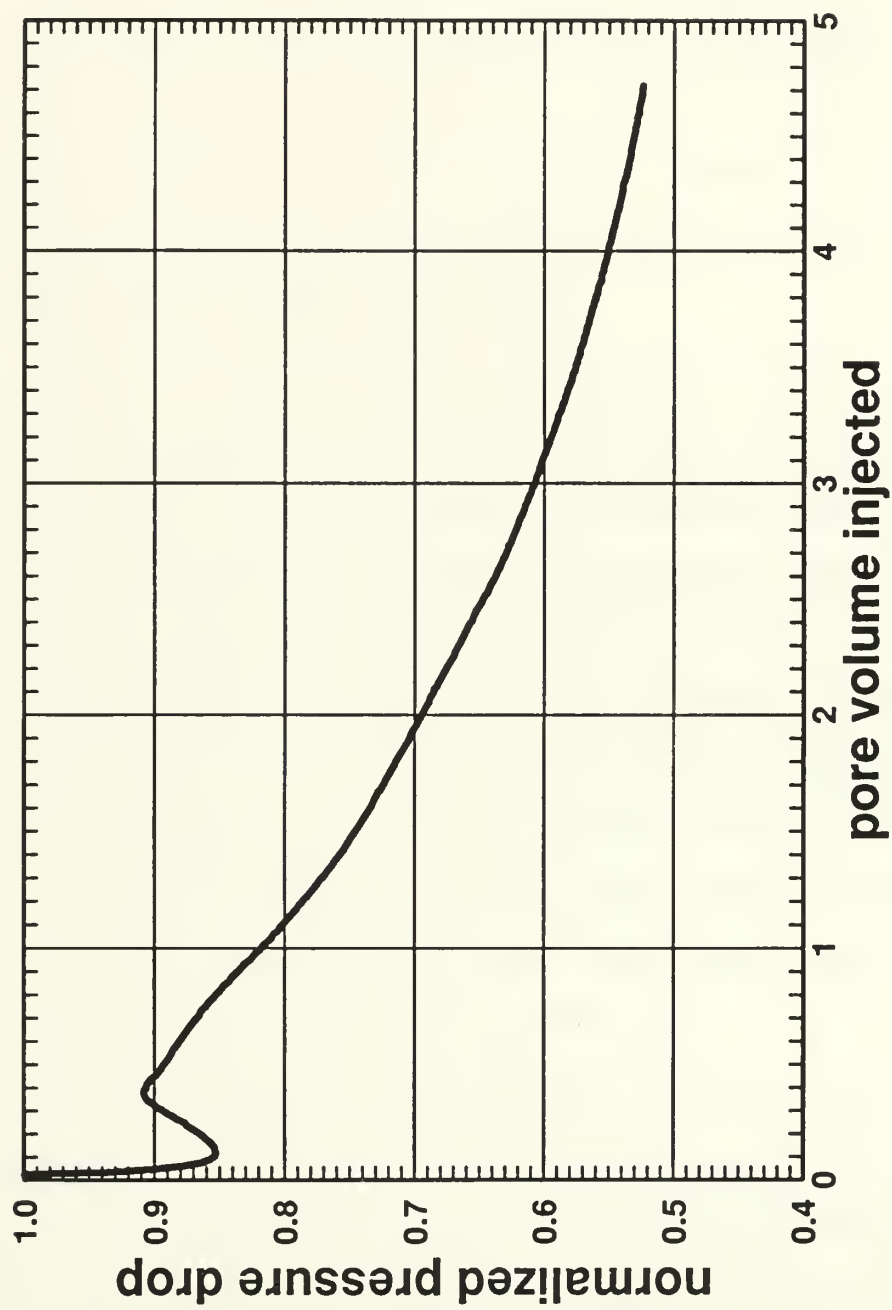


Figure 7.5: Dynamic Flood Normalized Pressure Profile; Run 2.

and one hundred data points were averaged to make one point on the graph.

Figure 7.6 is the pressure profile of the core linearity check for run 3. The plateaus of the profile show the pressure drop between the labeled core taps. In this linearity test each tap along the core was opened for 5 minutes (300 seconds). Sample time was one second. The core had a maximum pressure difference of 8.2% between zones ΔP_{3-4} and ΔP_{4-5} . Other differences were 6.7% between ΔP_{2-3} and ΔP_{3-4} , and 0.9% between ΔP_{2-3} and ΔP_{4-5} .

Figures 7.7 and 7.8 show the recovery curves for the benzyl alcohol and the water with the injected decane. The initials of the recovered fluids identify the recovery curves. The dots on the figures are the actual data points representing the data from each collection vessel. This data is contained in Table A.3 of Appendix A. Figure 7.7 shows the entire recovery curves for all three phases, while Figure 7.8 enlarges the recovery curves of the water and alcohol. Breakthrough of the decane occurred at approximately 0.5 pore volumes injected as shown by the departure of the decane recovery curve from the x-axis at this point. The abrupt decline of the slope of both the water and alcohol curves at breakthrough indicate there is no fluid bank developed for either of these fluids during the flood, however, there will be a significant Buckley-Leverett saturation shock.

The saturation history of this run is shown in Figure 7.9. The glass bead pack was flooded with water (1), then flooded to residual water saturation, S_{rw} , with benzyl alcohol (2), and brought to a core saturation (3) of 63.6% water and 36.4% alcohol by a steady-state 10:1 water-alcohol flood. The saturation trajectory of the dynamic decane flood is shown by points (3) to (5). The Buckley-Leverett shock is shown by the jump from point (3) to point (4). The continuous saturation trajectory after breakthrough is shown by the line from point (4) to point (5). The dots along

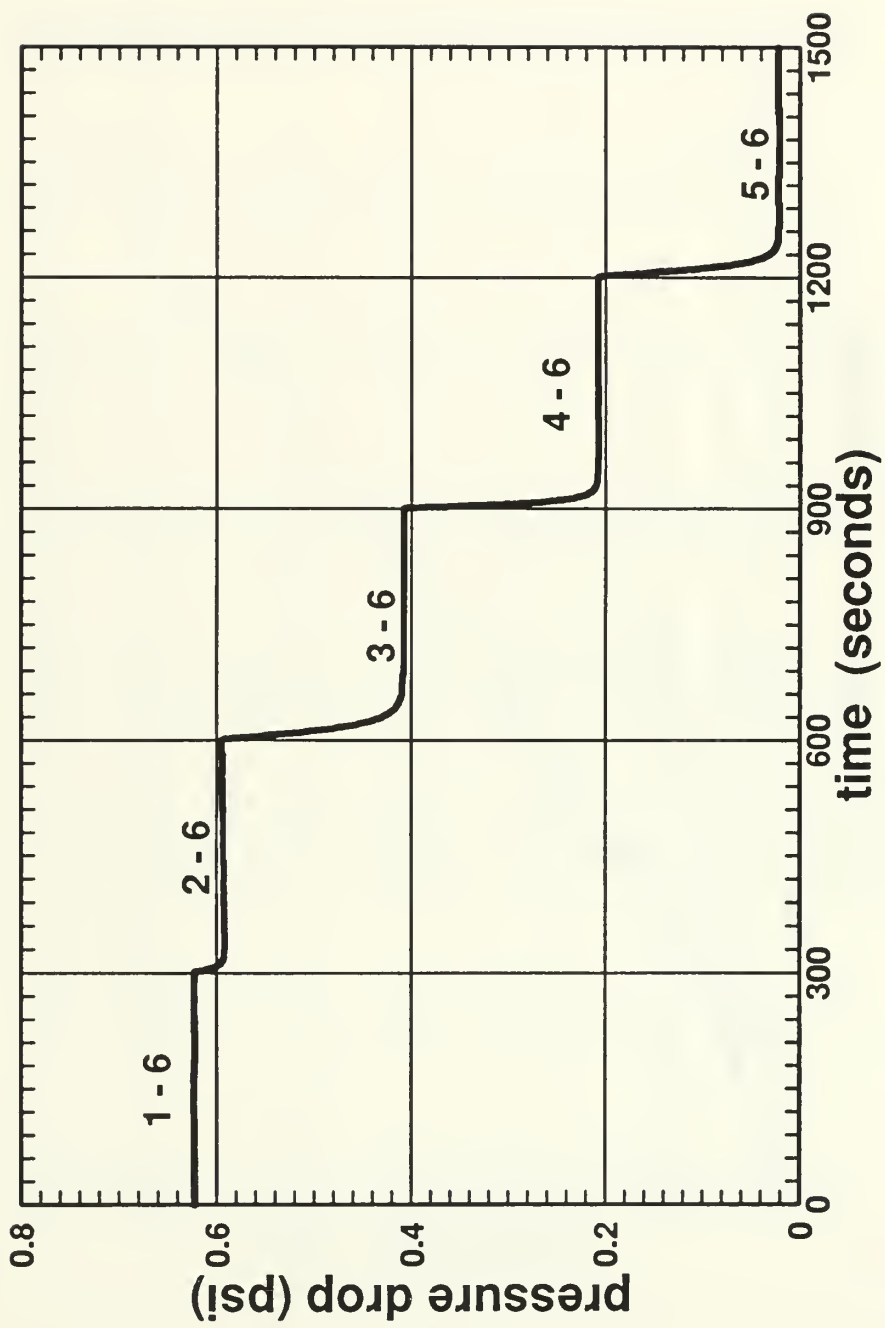


Figure 7.6: Core Linearity Check Pressure Profile; Run 3.

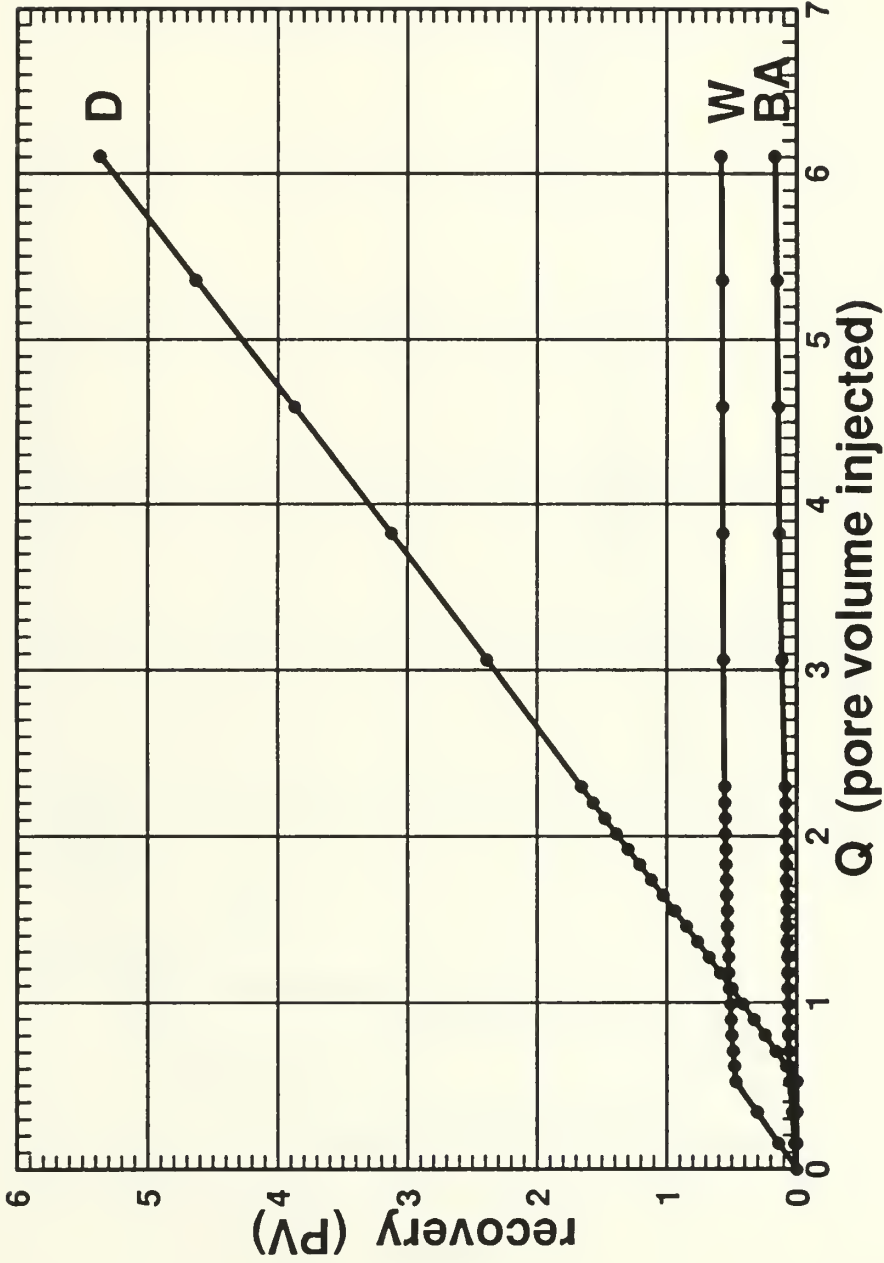


Figure 7.7: Dynamic Flood Recovery Curves; Run 3.

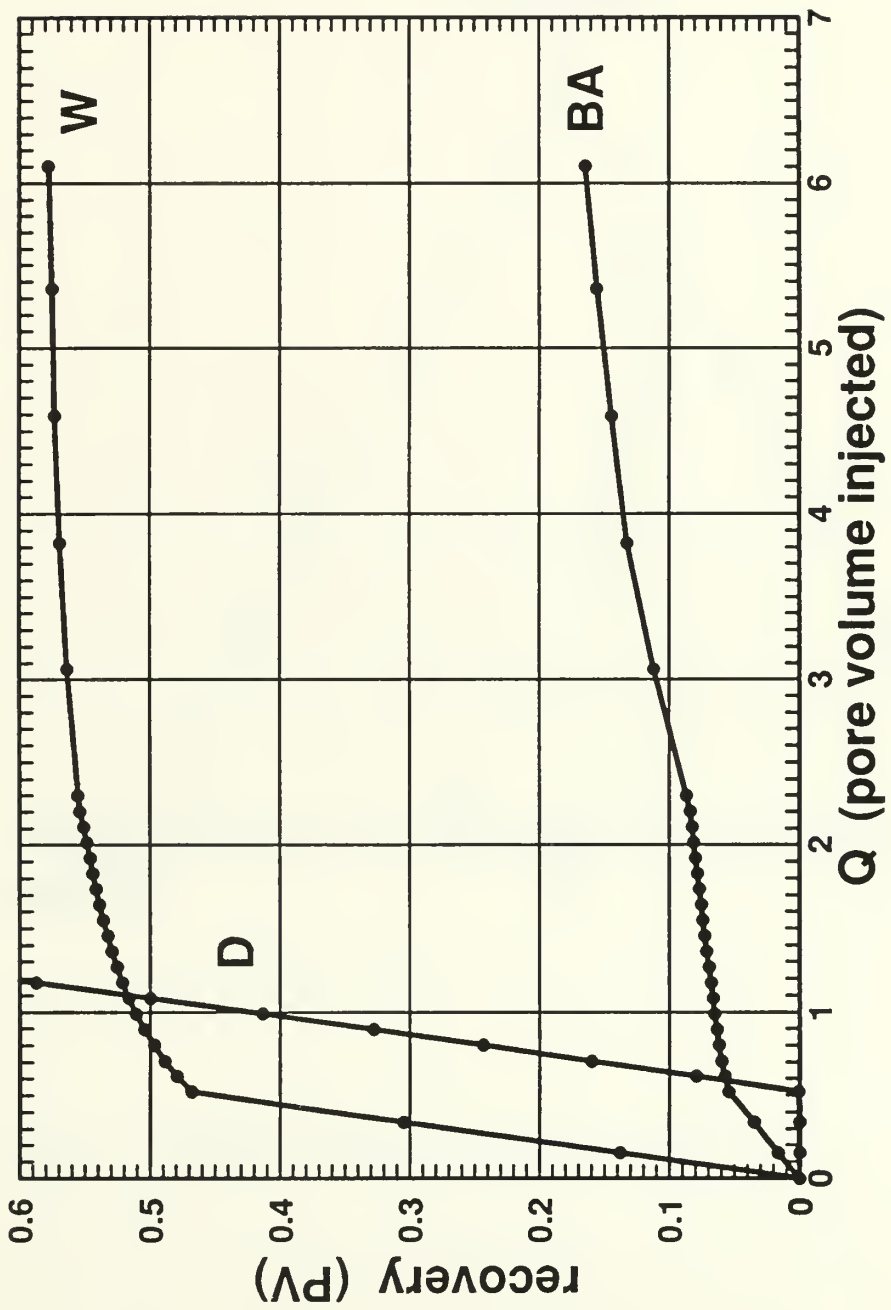


Figure 7.8: Expanded Dynamic Flood Recovery Curves; Run 3.

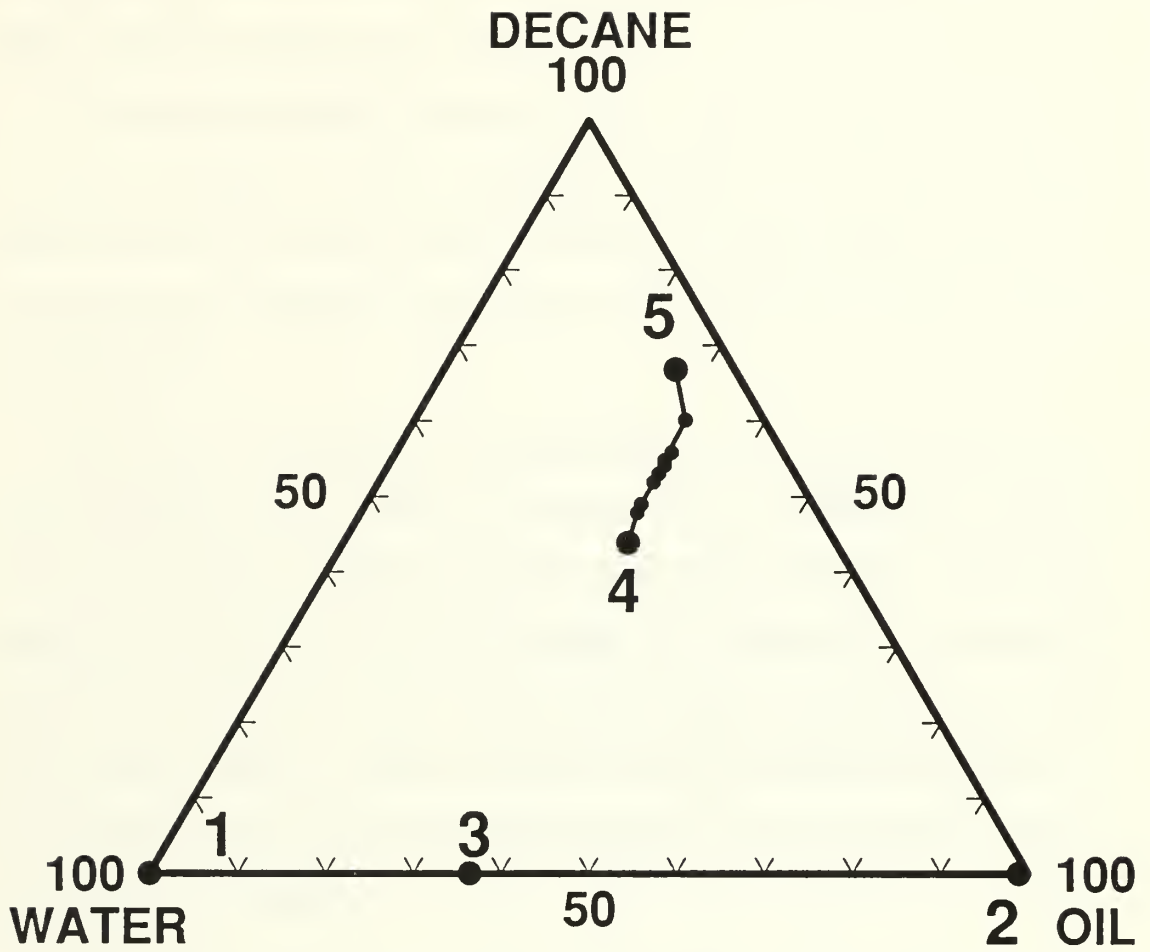


Figure 7.9: Saturation History and Trajectories; Run 3.

the trajectory are the saturations calculated at various pore volumes injected. This data is contained in Table A.4 of Appendix A.

The flow-rate normalized pressure drop versus the pore-volumes injected plot is shown as Figure 7.10. The pressure was normalized to the single calculated actual flow set on the decane pump. The pressure sample rate was one sample per second. Every one-hundred pressure points were averaged and plotted to make the pressure profile.

The water, oil and decane relative permeabilities for runs 2 and 3 are shown in semi-logarithmic plots in Figures 7.11 through 7.13. The dots on the curves are the actual data points calculated at various pore volumes injected. These data are contained in Tables A.2 and A.4 of Appendix A. Different sizes of glass beads were used between runs 2 and 3. Larger, size 8, glass beads were used for run 2. The resulting larger pore spaces and larger absolute permeability may account for the increase in oil and decane relative permeabilities and the resulting decrease in water relative permeability.

The saturation trajectory and relative permeability trends of run 3 are consistent with the work of Grader and O'Meara (1988).

7.2 Two-Phase Water-Benzyl Alcohol Relative Permeability Experiments

The first portion of run 9 was dedicated to determining the two-phase relative permeabilities of a water-benzyl alcohol system. The run then goes on to determine the water-benzyl alcohol relative permeabilities at residual decane saturation. Tables A.5 through A.10 in Appendix A contain summaries of the data from this run.

Figure 7.14 is the pressure profile of the core linearity check for run 9. The

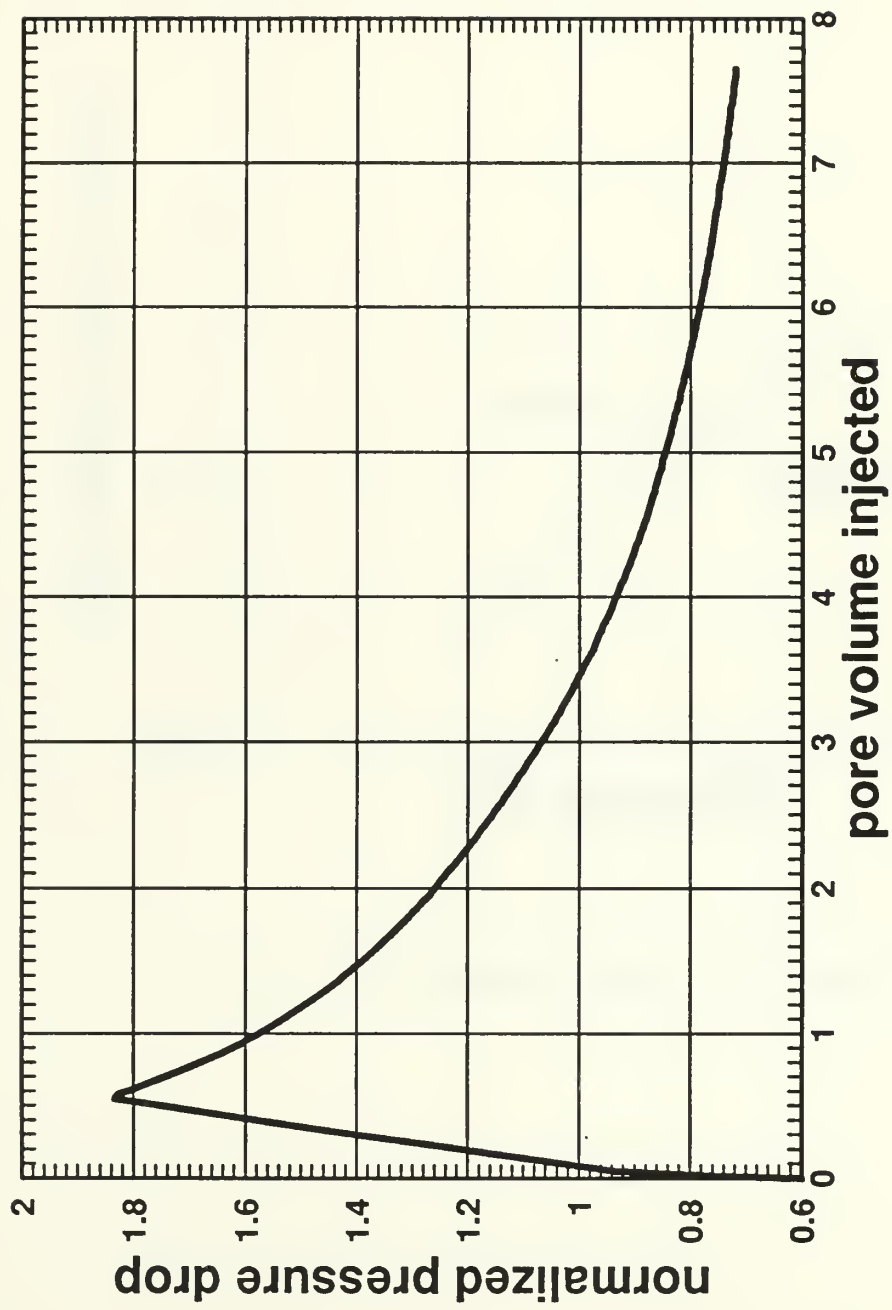


Figure 7.10: Dynamic Flood Normalized Pressure Profile; Run 3.

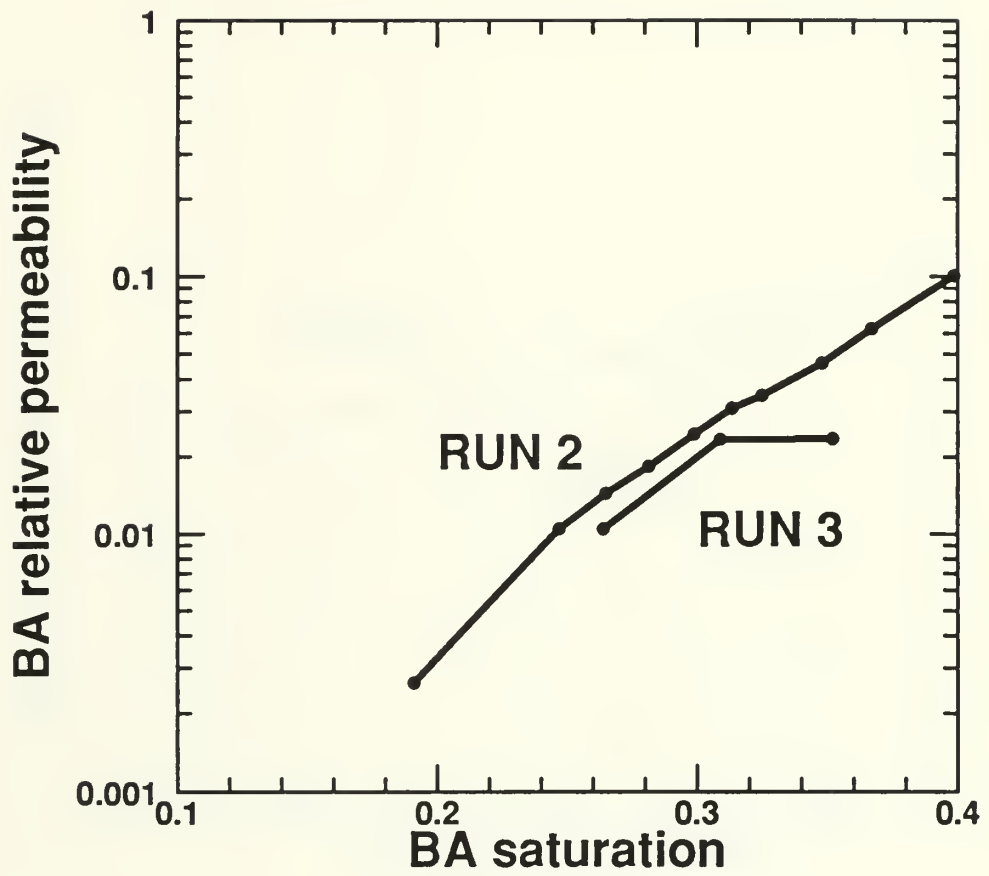


Figure 7.11: BA Relative Permeabilities vs. BA Saturation ; Run 3.

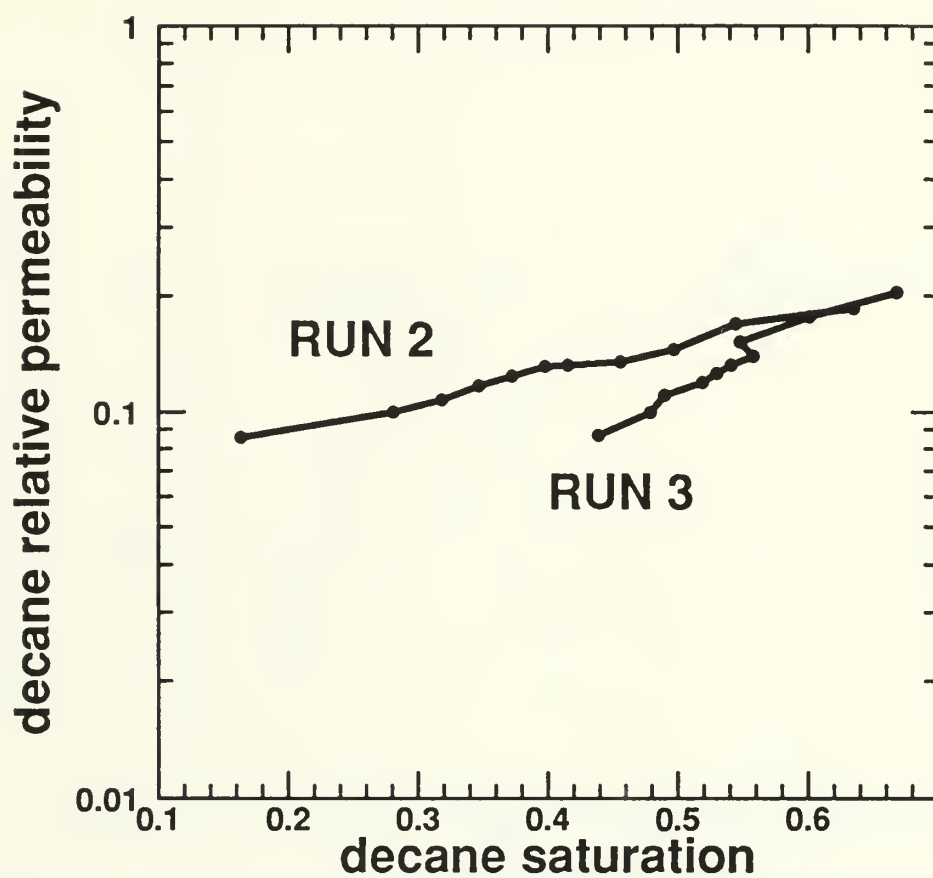


Figure 7.12: Decane Relative Permeabilities vs. Decane Saturation; Run 3.

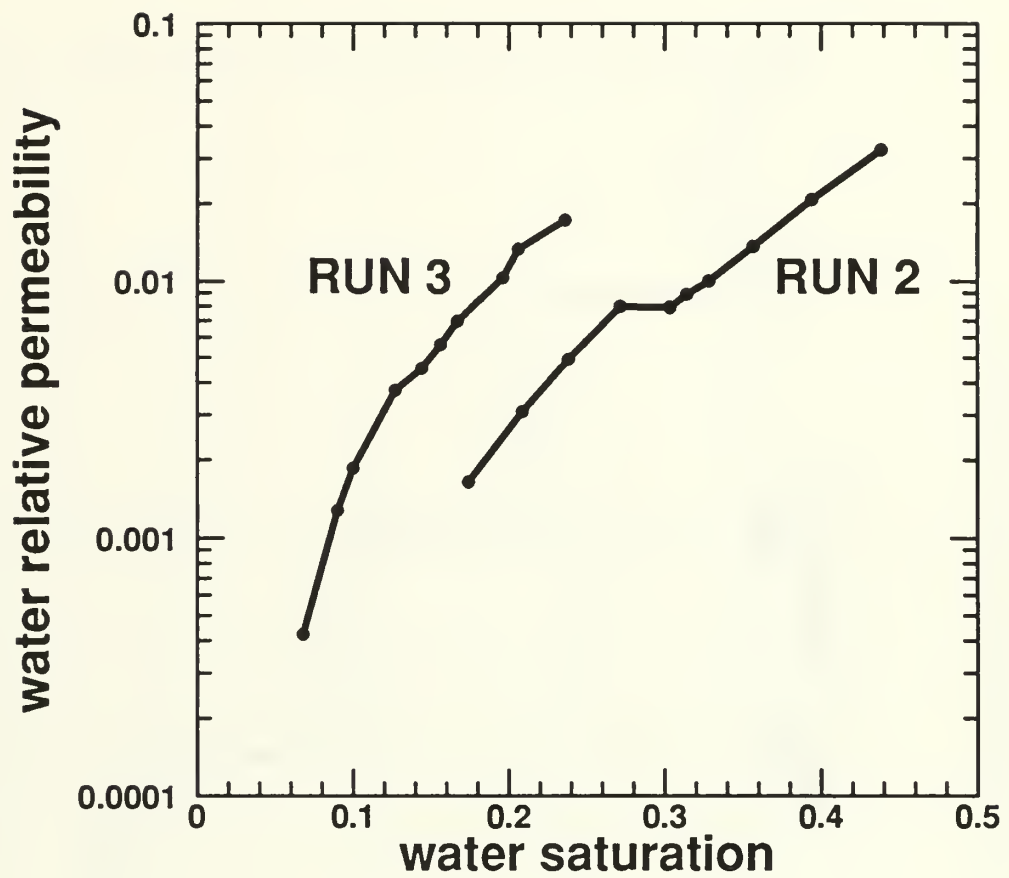


Figure 7.13: Water Relative Permeabilities vs. Water Saturation; Run 3.

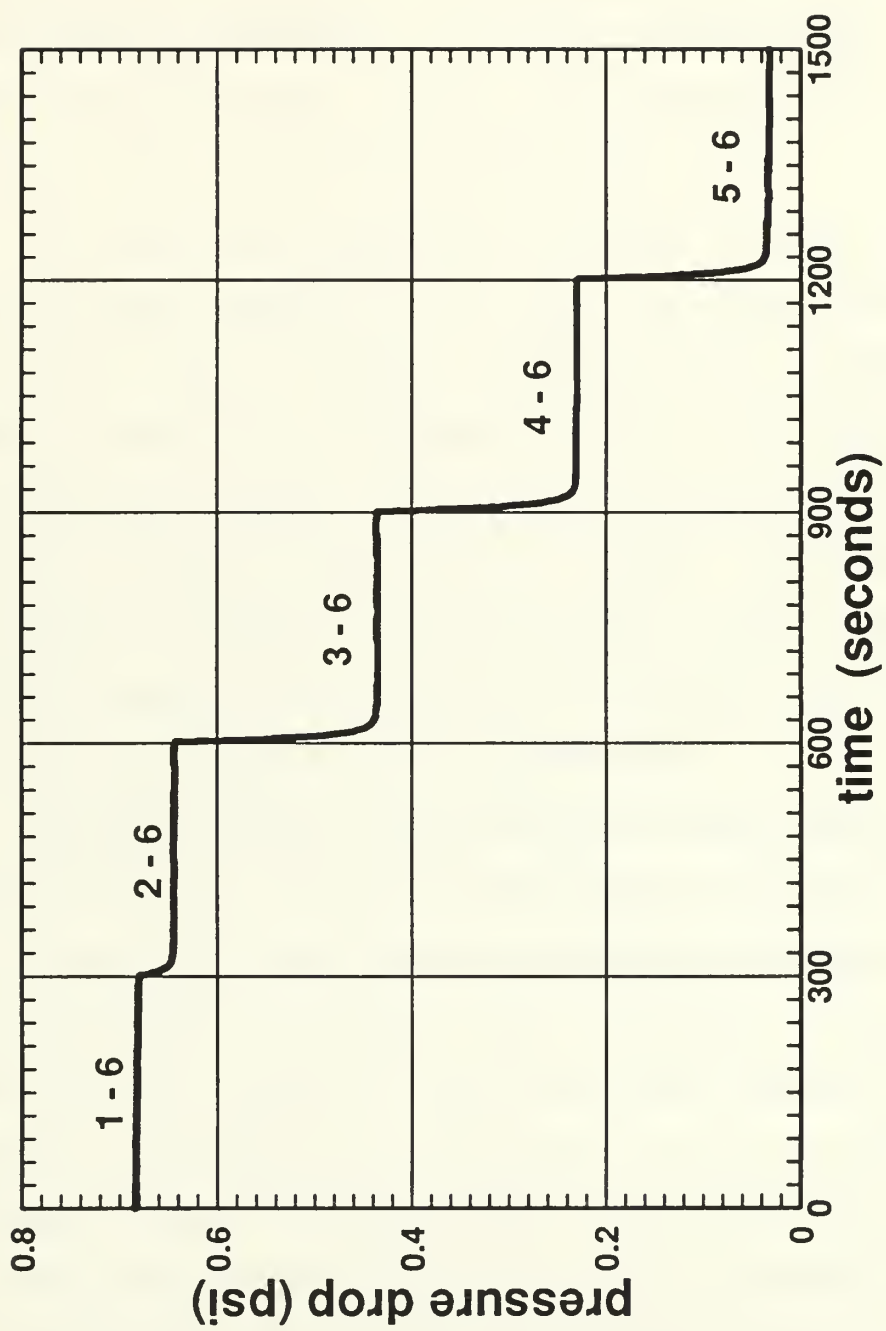


Figure 7.14: Core Linearity Check Pressure Profile; Run 9.

plateaus of the profile show the pressure drop between the labeled core taps. In this linearity test each tap along the core was opened for five minutes (300 seconds). Sample time was one second. The core had a maximum pressure difference of 4.6% between zones ΔP_{2-3} and ΔP_{4-5} . Other differences were 0.95% between ΔP_{2-3} and ΔP_{3-4} , and 3.7% between ΔP_{3-4} and ΔP_{4-5} .

The dynamic water displacement experiment to determine the water-benzyl alcohol relative permeabilities was run twice. The saturation history of the first experiment is shown in Figure 7.15. The glass bead pack was flooded with water, point (1), then flooded to residual water saturation, $S_{rw} = 8.9\%$, with the oil phase (benzyl alcohol) point (2). The oil saturated core was then dynamically water flooded to residual oil saturation (4), $S_{ro} = 11.6\%$. Core-end oil saturation at breakthrough of the Buckley-Leverett shock was $S_o = 44.7\%$, point (3). The dots along the trajectory are the saturations calculated at various pore volumes injected. These data are contained in Table A.5 of Appendix A.

Figure 7.16 shows the recovery curve for the benzyl alcohol and the injected water. The initials of the recovered fluids identify the recovery curves. The dots on the figures are the actual data points representing the data from each collection vessel. These data are contained in Table A.6 of Appendix A. Breakthrough of the water occurred at approximately 0.625 pore volumes injected as shown by the departure of the water recovery curve from the x-axis at this point. The abrupt decline of the slope of the alcohol recovery curve at breakthrough indicates that no oil bank developed during the flood and accounts for the Buckley-Leverett saturation shock jump seen on the ternary saturation trajectory diagram, Figure 7.15.

The pressure drop normalized to a fixed flow rate versus the pore volumes injected plot is shown as Figure 7.17. The pressure was normalized to the single

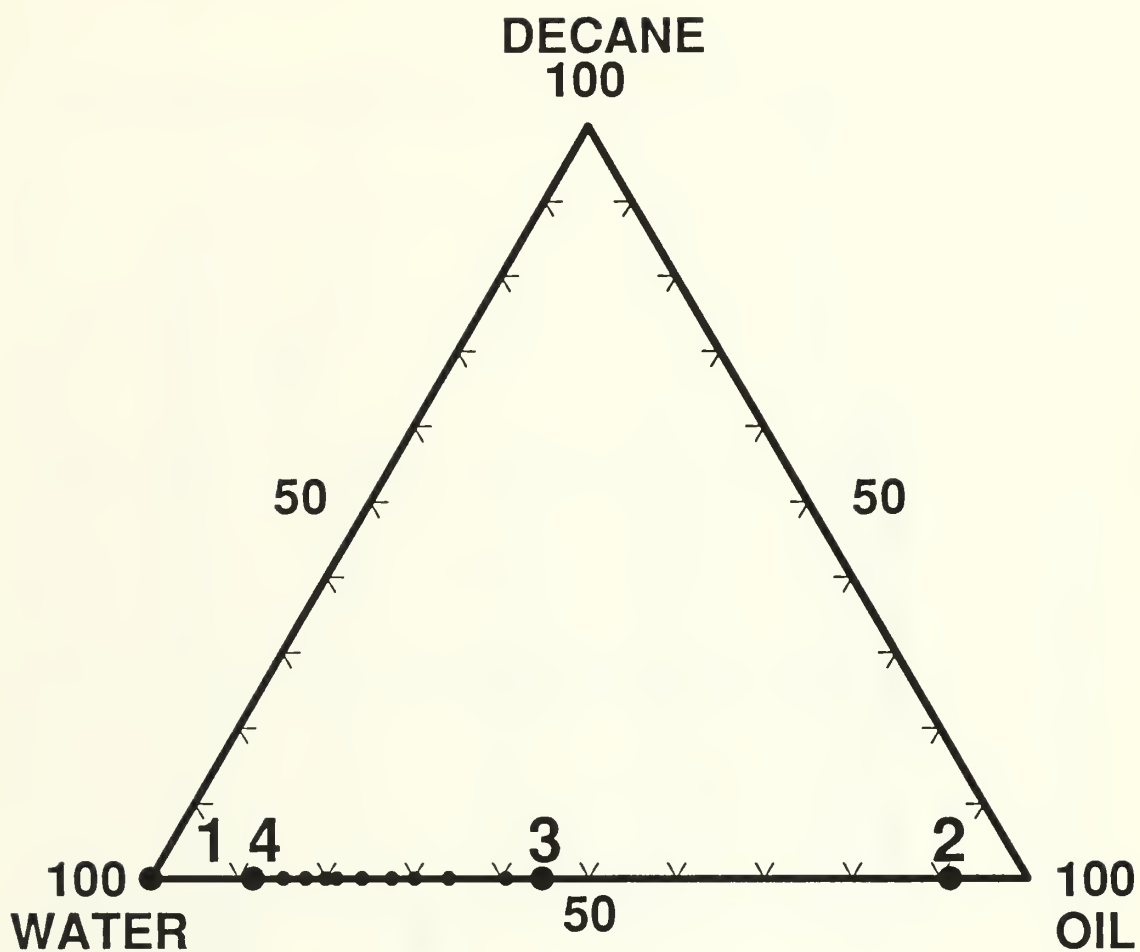


Figure 7.15: Saturation History and Trajectories; Run 9 - First Dynamic Water Flood

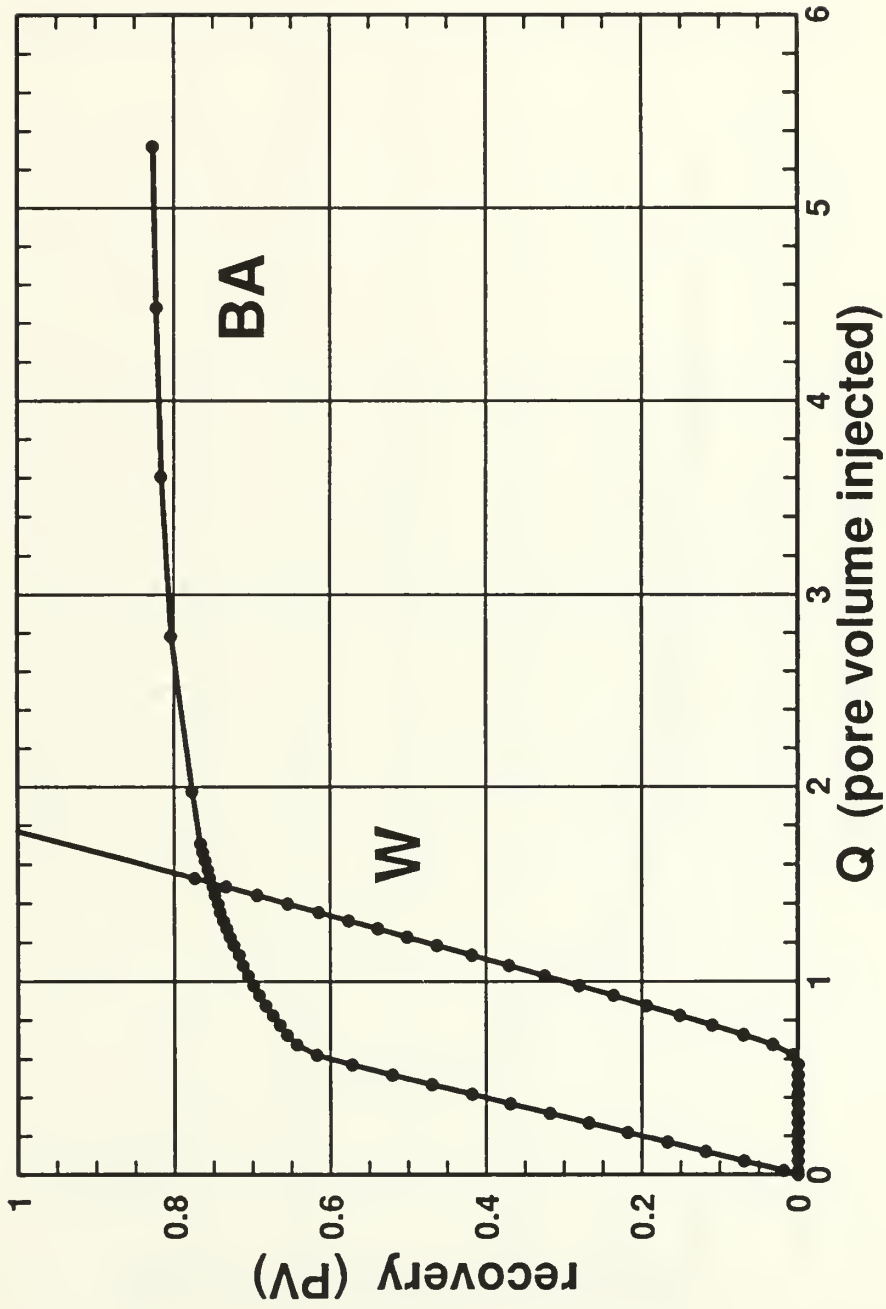


Figure 7.16: Expanded Dynamic Flood Recovery Curves; Run 9 - First Dynamic Water Flood.

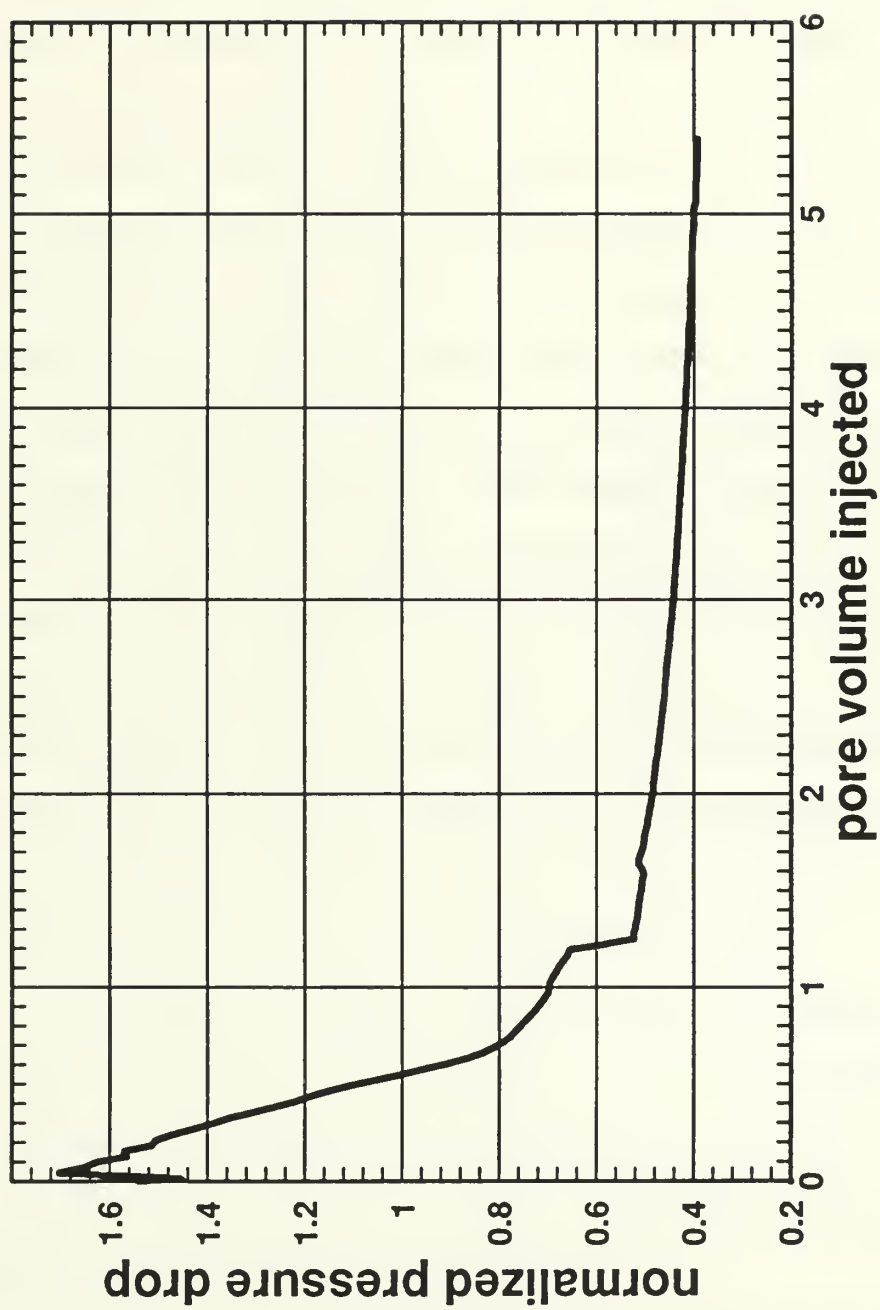


Figure 7.17: Normalized Pressure Drop (Fixed q) vs. PVI; Run 9 - First Dynamic Water Flood.

calculated actual flow set on the water pump. The pressure sample rate was one sample per second. Every one-hundred pressure points were averaged and plotted to make the pressure profile. A drop in the injection flow rate caused the sudden drop in pressure at approximately 1.2 pore volumes. This is believed to be due to a sudden sealing of the water supply flask stopper. This in turn hindered makeup air from entering the flask creating a vacuum and slowing the flow rate of the pump. The fixed flow rate used to calculate the normalized pressure drop could not compensate for this and therefore the dip in curve resulted. The FORTRAN program, `pvst.f`, used to calculate the Φ versus Q data, was upgraded to correct this problem. This updated FORTRAN program (`vari.q.f`) contained in appendix B, calculates the actual flow rates for each collection period by dividing the the actual collected volume by the time collected. This data was then used to determine the true normalized pressure drop and the actual pore volumes injected. The results of this program's analysis is shown in Figure 7.18 and then plotted with the fixed-flow rate normalized pressure drop plot in Figure 7.19. As seen in Figure 7.19 the corrected plot is slightly above the fixed flow-rate plot, also, the corrected normalized pressure drop curve is much smoother than the uncorrected curve.

The two-phase water-benzyl alcohol relative permeabilities of this first dynamic water flood are shown in Figure 7.20. The relative permeabilities were calculated using the variable flow-rate normalized pressure data. The dots on the curves are the actual data points calculated at various pore volumes injected. These data are contained in Table A.5 of Appendix A.

A second dynamic water flood experiment of the oil saturated core at irreducible water saturation was conducted to determine the effect of the flow-rate drop seen in the first dynamic water flood experiment. Figure 7.21 shows the saturation

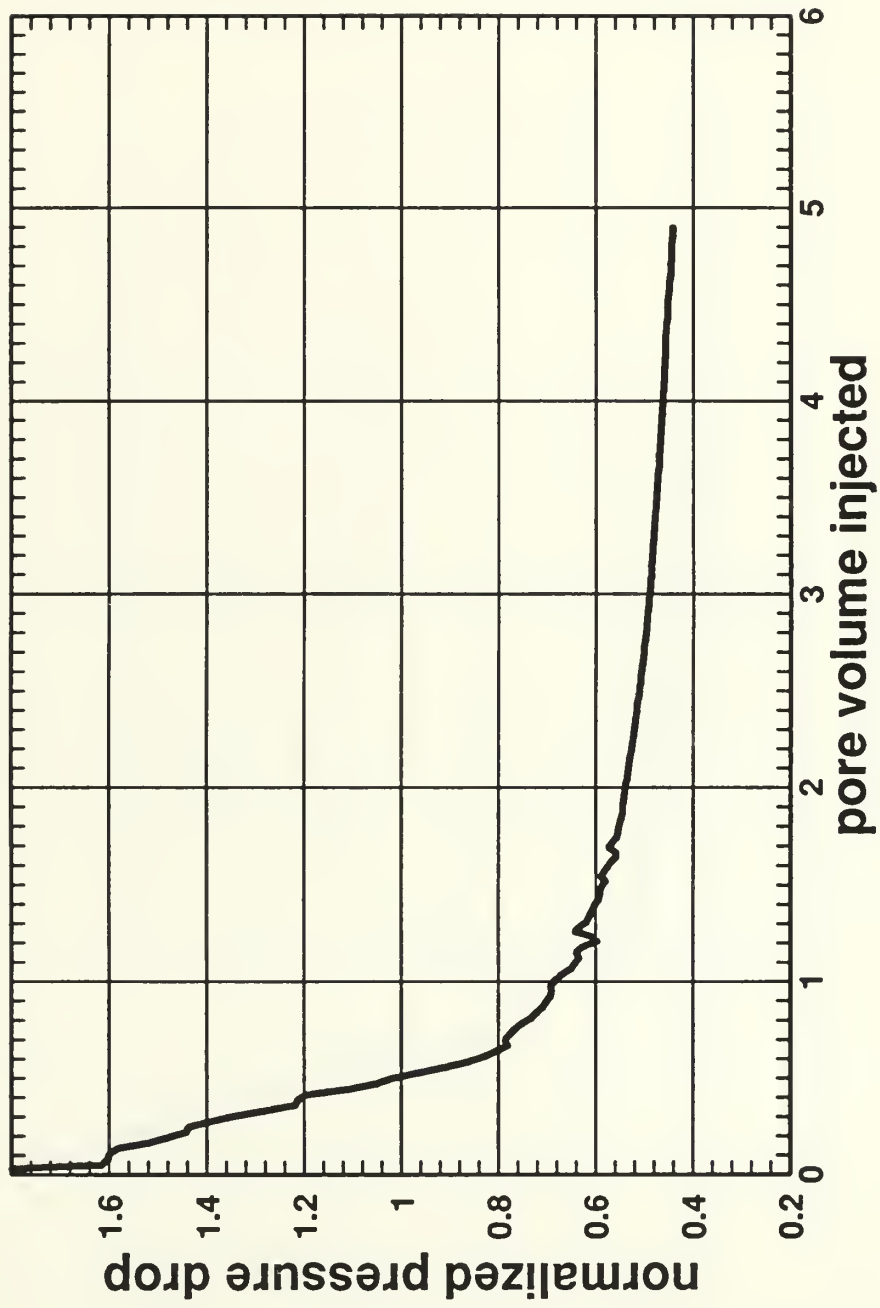


Figure 7.18: Normalized Pressure Drop (Variable q) vs. PVI; Run 9 - First Dynamic Water Flood.

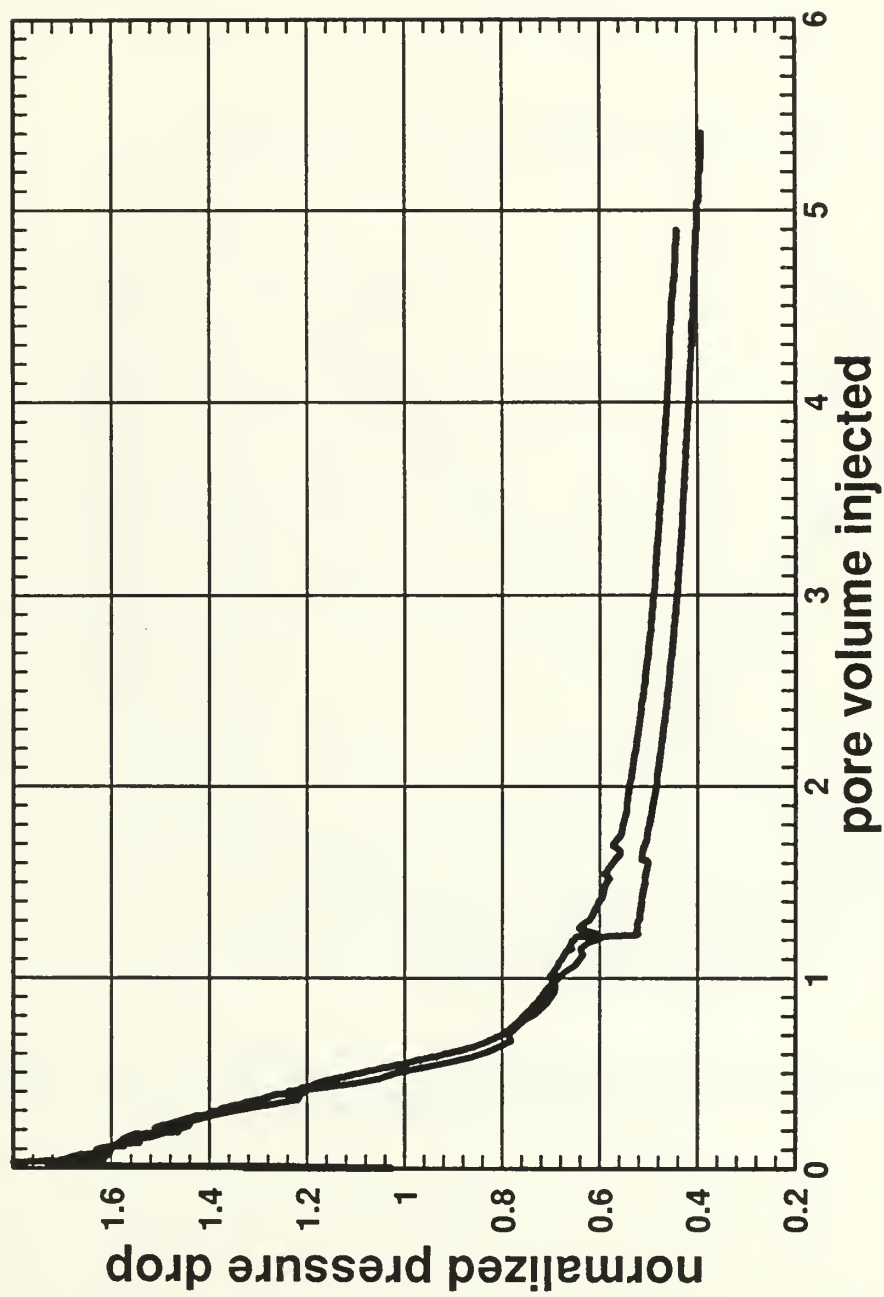


Figure 7.19: Fixed vs. Variable Normalized Pressure Drop Comparison; Run 9 - First Dynamic Water Flood.

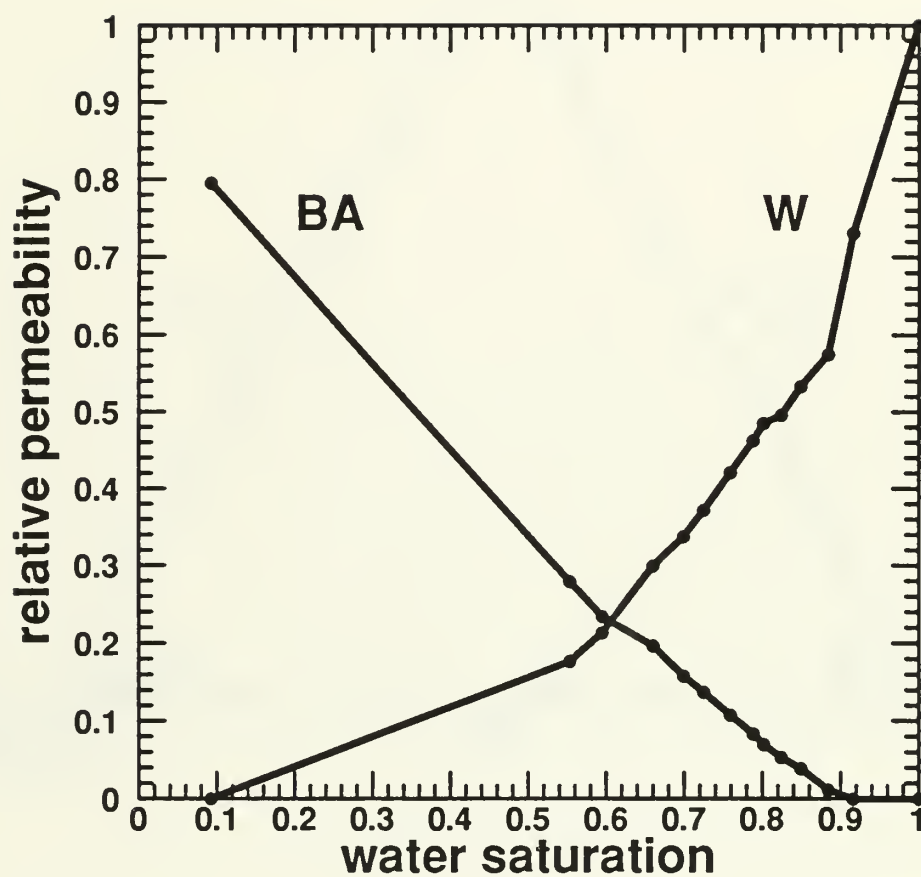


Figure 7.20: Oil and Water Relative Permeabilities vs. Water Saturation;
Run 9 - First Dynamic Water Flood

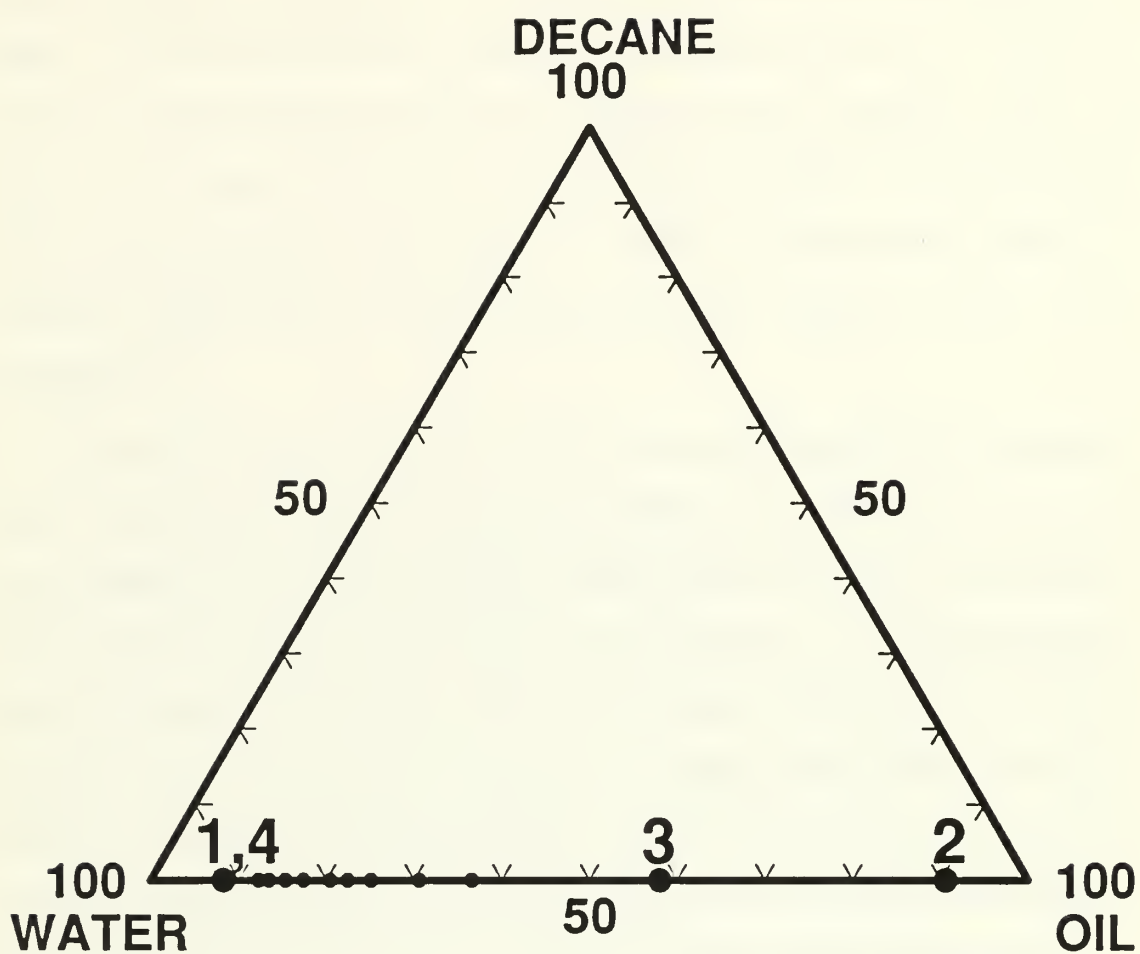


Figure 7.21: Saturation History and Trajectories; Run 9 - Second Dynamic Water Flood

history leading to the dynamic water flood and the saturation trajectory during the flood. The core was taken from residual oil saturation, point (1) $S_{ro} = 8.45\%$, at the end of the first water flood, to irreducible water saturation, point (2) $S_{rw} = 9.44\%$, by an oil flood. The core was then dynamically water flooded with breakthrough, point (3), occurring at $S_w = 42.9\%$. The flood ended at residual oil saturation, point (4) $S_{ro} = 9.16\%$. These data are contained in Table A.7 of Appendix A.

Figure 7.22 shows the recovery curve for the benzyl alcohol and the injected water. The initials of the recovered fluids identify the recovery curves. The dots on the figures are the actual data points representing the data from each collection vessel. These data are contained in Table A.8 of Appendix A. Breakthrough of the water occurred at approximately 0.625 pore volumes injected as shown by the departure of the water recovery curve from the x-axis at this point. The abrupt decline of the slope of the alcohol recovery curve at breakthrough indicates that no oil bank developed during the flood and accounts for the Buckley-Leverett saturation shock jump seen on the ternary saturation trajectory diagram (Figure 7.21).

The pressure drop normalized to a fixed flow rate versus the pore volumes injected plot is shown as Figure 7.23. The pressure was normalized to the single calculated actual flow rate set on the water pump. The pressure sample rate was one sample per second. Every one-hundred pressure points were averaged and plotted to make the pressure profile. The normalized pressure was recalculated using the FORTRAN program *vari.q.f* (contained in Appendix B), and the data plotted in Figure 7.24.

The two-phase water-benzyl alcohol relative permeabilities of this second dynamic water flood are shown in Figure 7.25. The relative permeabilities were

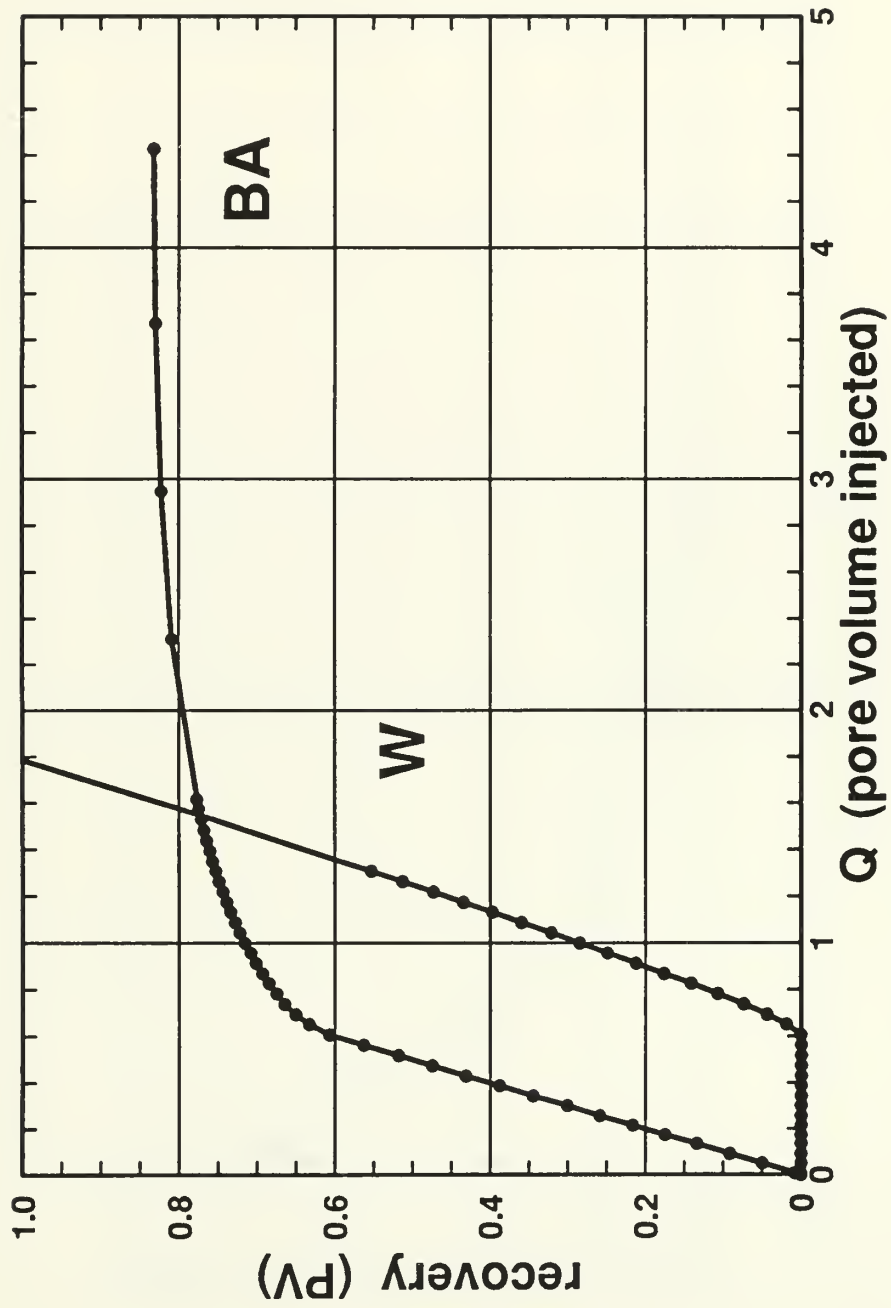


Figure 7.22: Expanded Dynamic Flood Recovery Curves; Run 9 - Second Dynamic Water Flood.

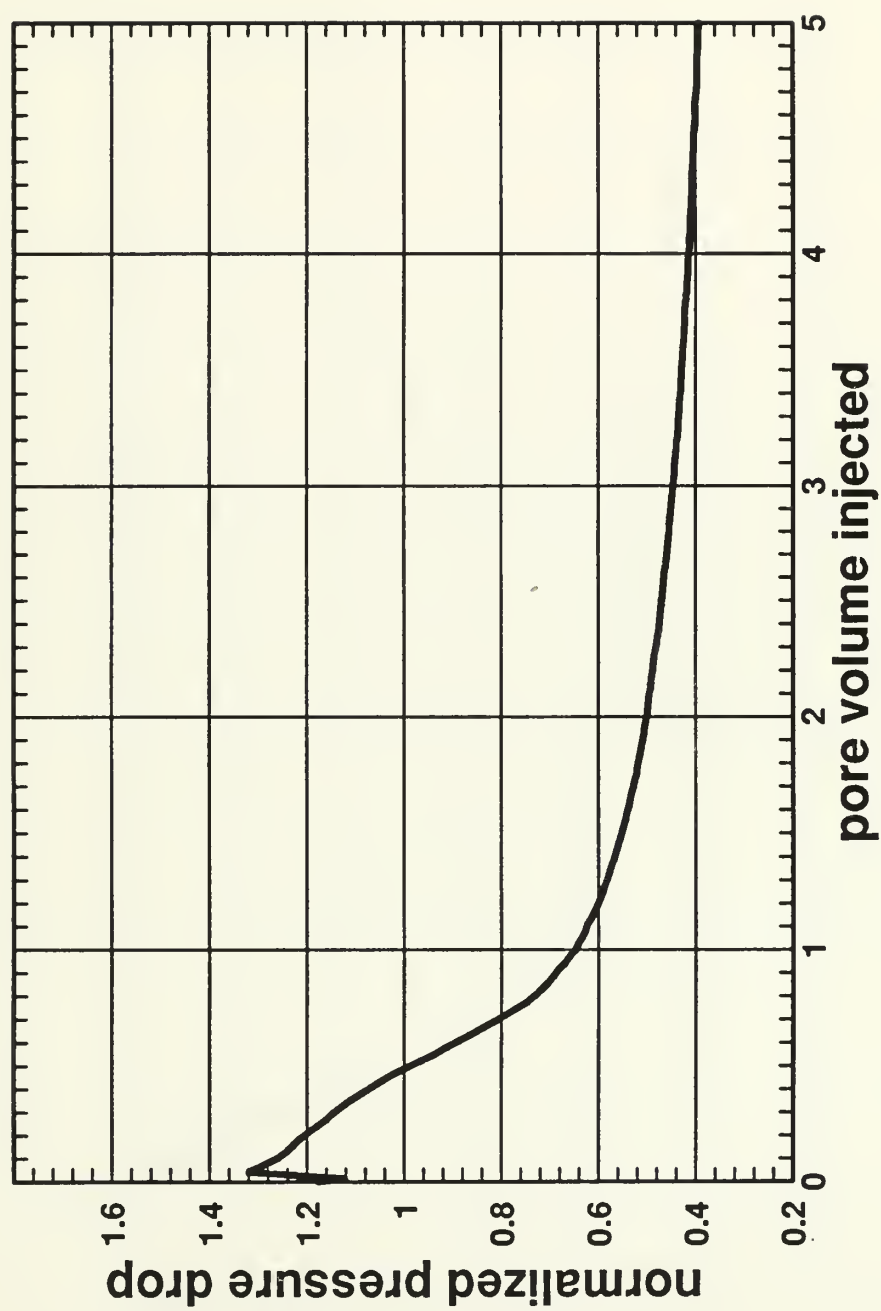


Figure 7.23: Normalized Pressure Drop (Fixed q) vs. PVI; Run 9 - Second Dynamic Water Flood.

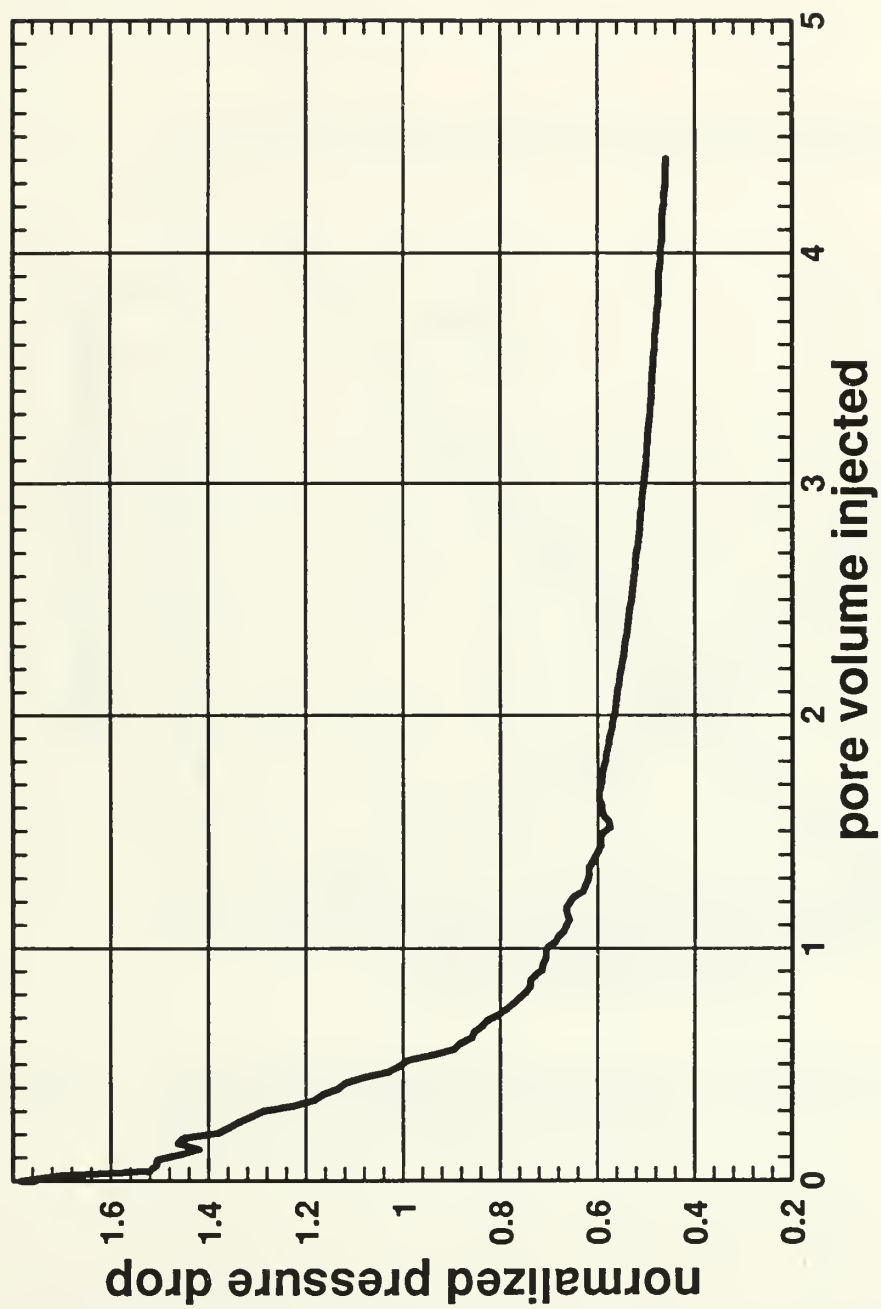


Figure 7.24: Normalized Pressure Drop (Variable q) vs. PVI; Run 9 - Second Dynamic Water Flood.

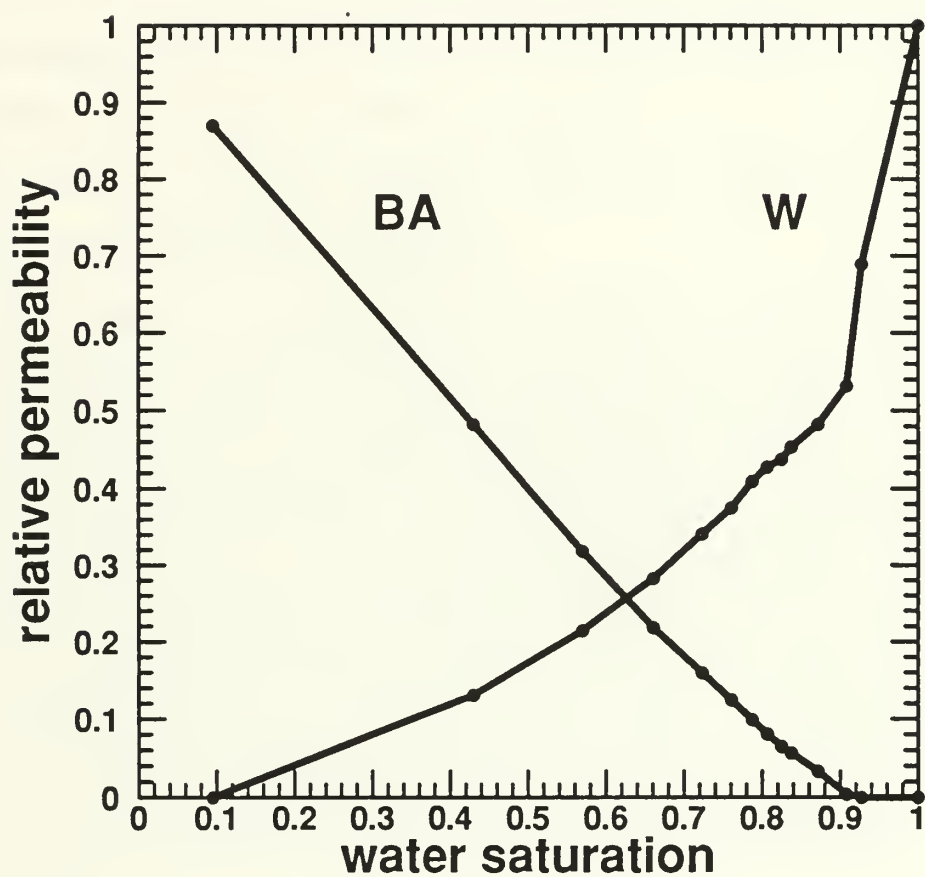


Figure 7.25: Oil and Water Relative Permeabilities vs. Water Saturation
Run 9 - Second Dynamic Water Flood.

calculated using the variable flow rate normalized pressure data shown in Figure 7.24. The dots on the curves are the actual data points calculated at various pore volumes injected. These data are contained in Table A.7 of Appendix A. A comparison of run 9's two-phase water-oil relative permeability data from the first and second dynamic water flood is shown in 7.26. Curves A and D are the second water flood's relative oil permeabilities and relative water permeabilities respectively, while curves B and C are the first water flood's relative oil permeabilities and relative water permeabilities respectively.

The last phase of run 9 consisted of a third dynamic water flood but at residual decane saturation. Figure 7.27 shows the saturation history leading to this third dynamic water flood and the saturation trajectory during the flood. The core was taken from 100% water saturation, point (1) prior to flood 1, to irreducible water saturation, point (2) $S_{rw} = 9.44 \%$, through the series of water and oil floods outlined in the description of dynamic water floods 1 and 2. The glass bead pack was then brought to point (3) by a steady-state decane flood, $S_d = 74.8 \%$, and then back to point (4) by a steady-state oil flood. Point (4) represents residual water, $S_{rw} = 9.5 \%$, and residual decane, $S_{rd} = 8.1 \%$, in the presence of oil, $S_o = 82.4 \%$.

The third dynamic water flood was conducted with breakthrough (5) occurring at $S_w = 33.8 \%$, and a continuous saturation trajectory at residual decane saturation from point (5) to point (6), $S_w = 83.6 \%$ and $S_{ro} = 8.29 \%$. Decane was not produced during this flood. These data are contained in Table A.9 of Appendix A.

Figure 7.28 shows the recovery curve for the benzyl alcohol and the injected water. The initials of the recovered fluids identify the recovery curves. The dots on the figures are the actual data points representing the data from each collection

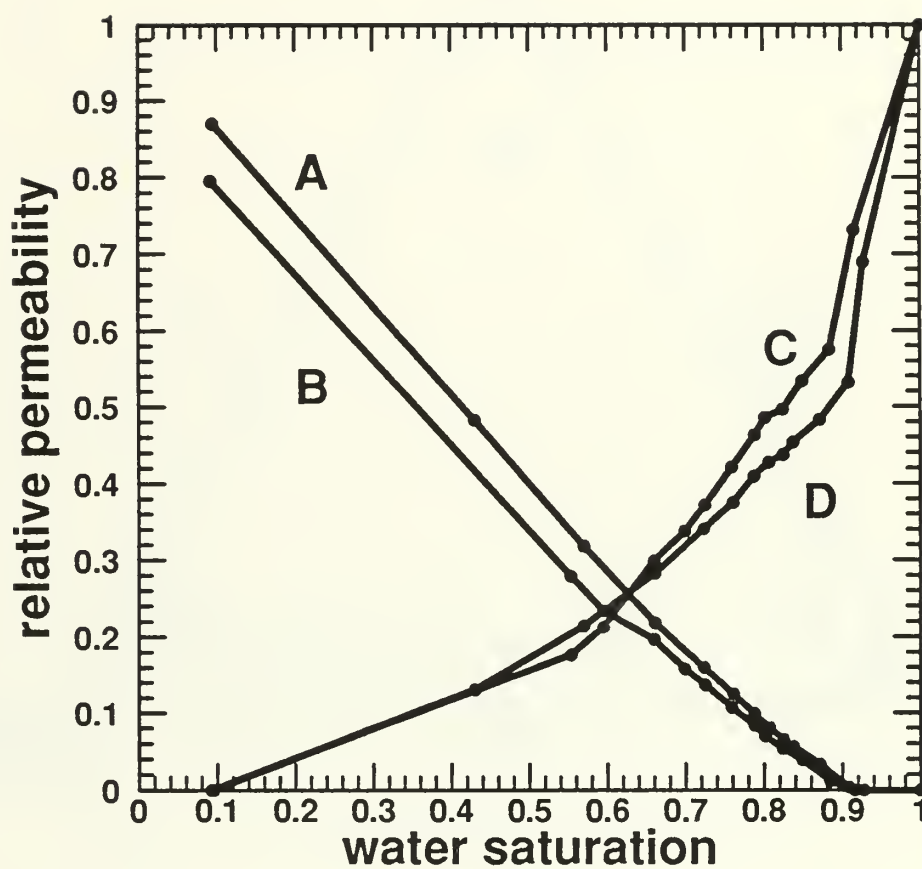


Figure 7.26: Relative Permeability Comparison;
 Run 9 - First and Second Dynamic Water Floods.
 A = Oil Relative Permeability, Second Dynamic Flood
 B = Oil Relative Permeability, First Dynamic Flood
 C = Water Relative Permeability, First Dynamic Flood
 D = Water Relative Permeability, Second Dynamic Flood

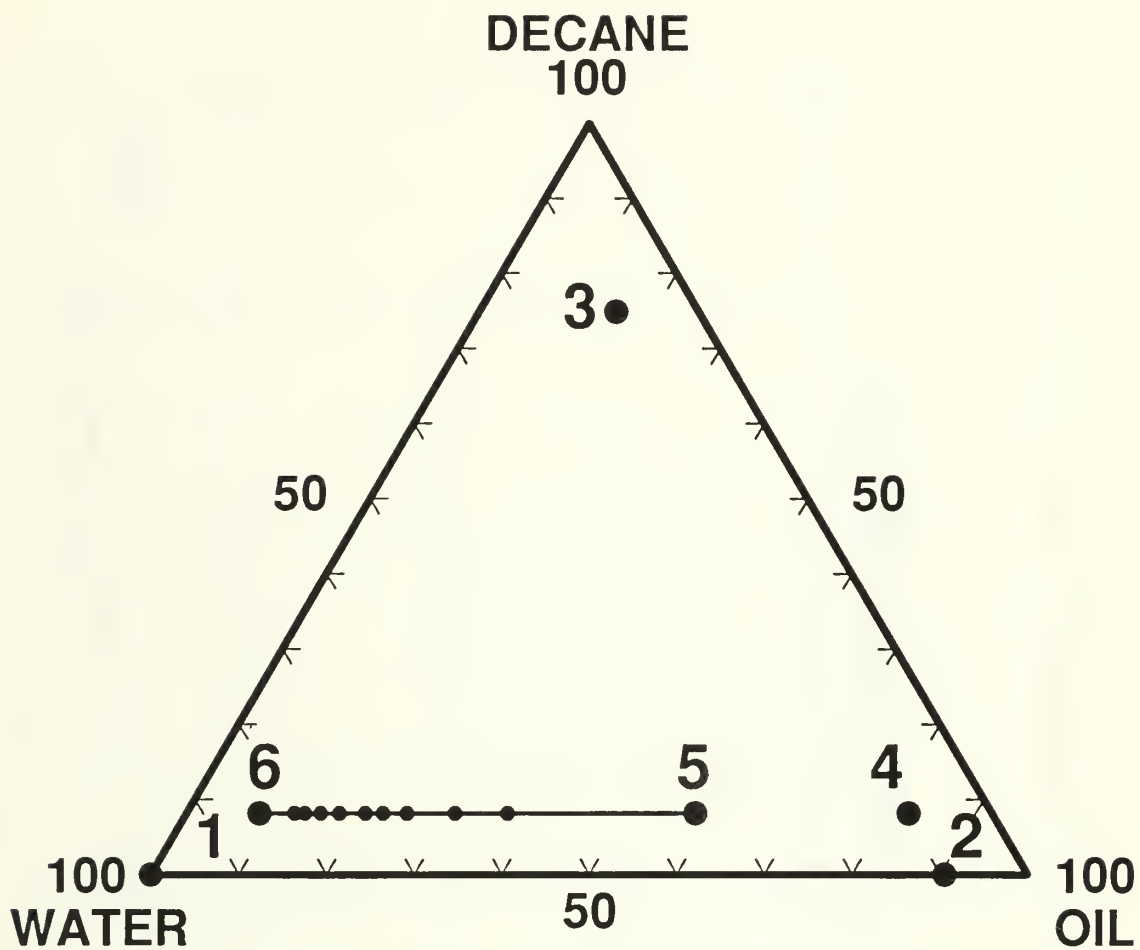


Figure 7.27: Saturation History and Trajectories; Run 9 - Third Dynamic Water Flood

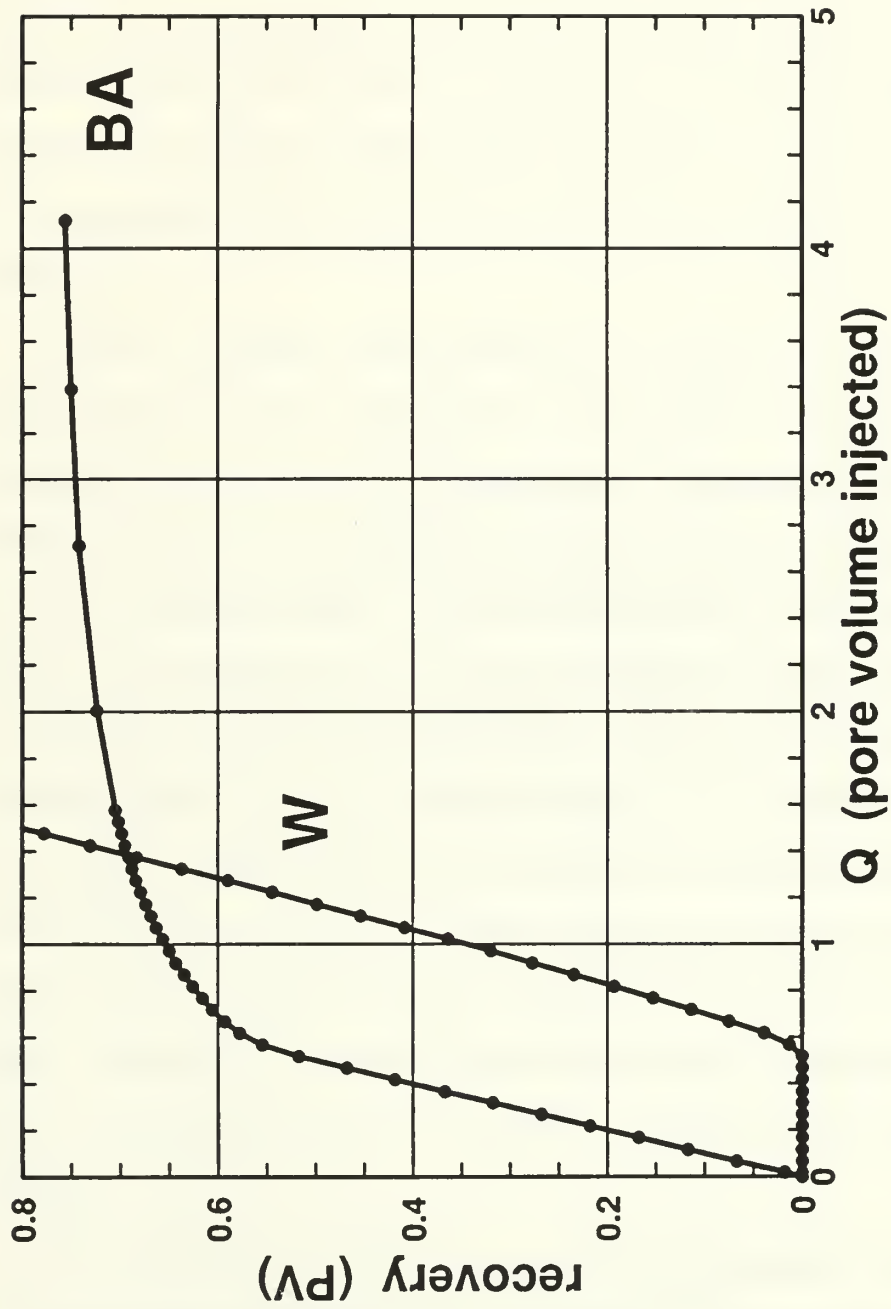


Figure 7.28: Expanded Dynamic Flood Recovery Curves; Run 9 - Third Dynamic Water Flood.

vessel. These data are contained in Table A.10 of Appendix A. Breakthrough of the water occurred at approximately 0.54 pore volumes injected as shown by the departure of the water recovery curve from the x-axis at this point. The abrupt and continuous decline of the slope of the alcohol recovery curve at breakthrough indicates that no oil bank developed during the flood and accounts for the Buckley-Leverett saturation shock jump seen on the ternary saturation trajectory diagram, Figure 7.27.

The plot of pressure drop normalized to a fixed flow rate versus the pore volumes injected is shown as Figure 7.29. The pressure was normalized to the single calculated actual flow set on the water pump. The pressure sample rate was one sample per second. Every one-hundred pressure points were averaged and plotted to make the pressure profile. The normalized pressure was recalculated with the actual varying injected flow rate using the FORTRAN program (variq.f) contained in Appendix B. This data is shown in Figure 7.30. A comparison of the two calculated normalized flow rates is shown in Figure 7.31. The agreement of the pressure profiles is much better than the comparison of pressure profiles in the first water flood shown in Figure 7.19. This is because the flow rates in the third water flood are more consistent and closer to the calculated fixed flow rate of the water pump. This shows that the fixed flow rate analysis used in subsequent data presentations is valid as long as there is no significant deviation from the predicted pump flow rate.

The two-phase water-benzyl alcohol relative permeabilities measured at residual decane saturation during the third dynamic water flood are shown in Figure 7.32. The relative permeabilities were calculated using the variable flow rate normalized pressure data shown in Figure 7.30. The dots on the curves are the actual

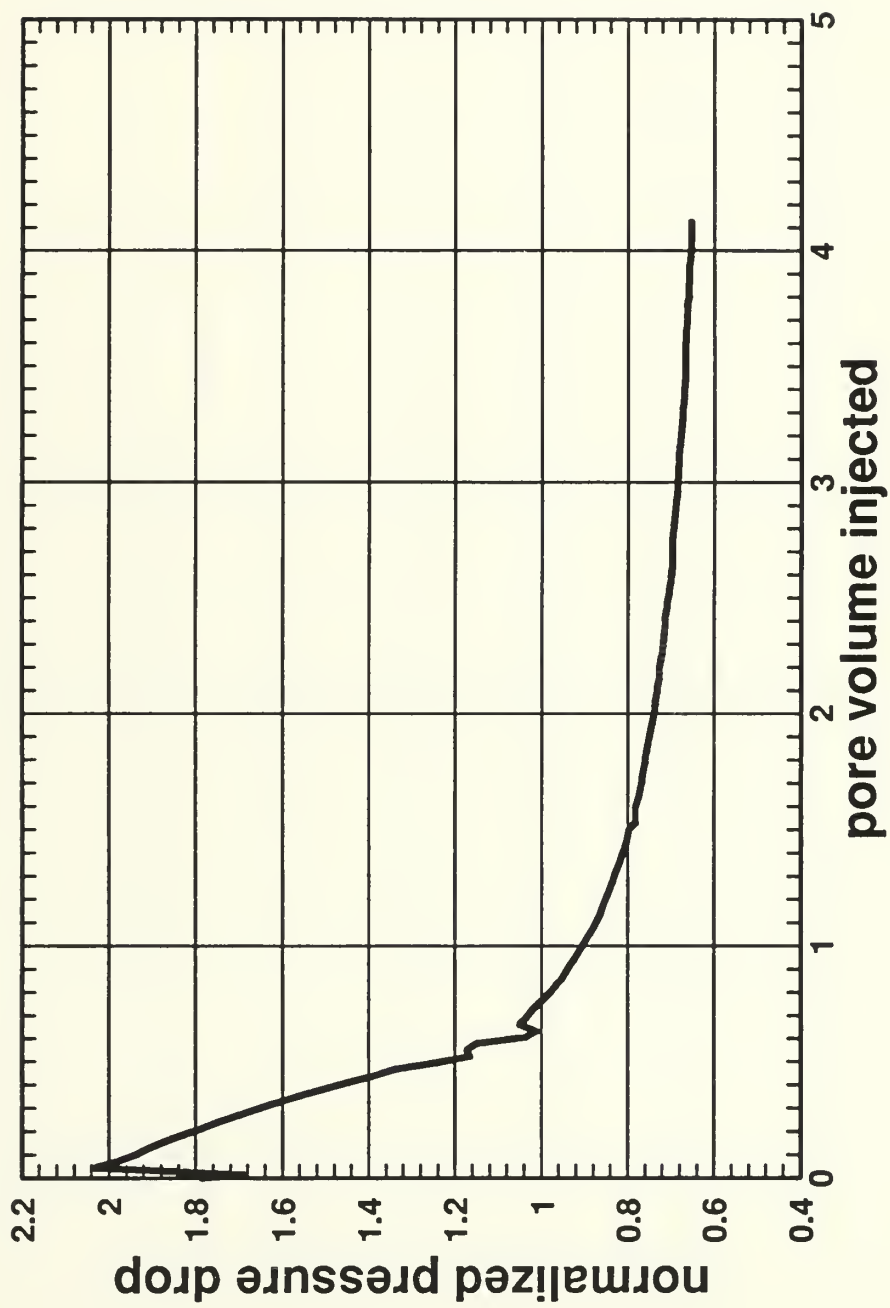


Figure 7.29: Normalized Pressure Drop (Fixed q) vs. PVI; Run 9 - Third Dynamic Water Flood.

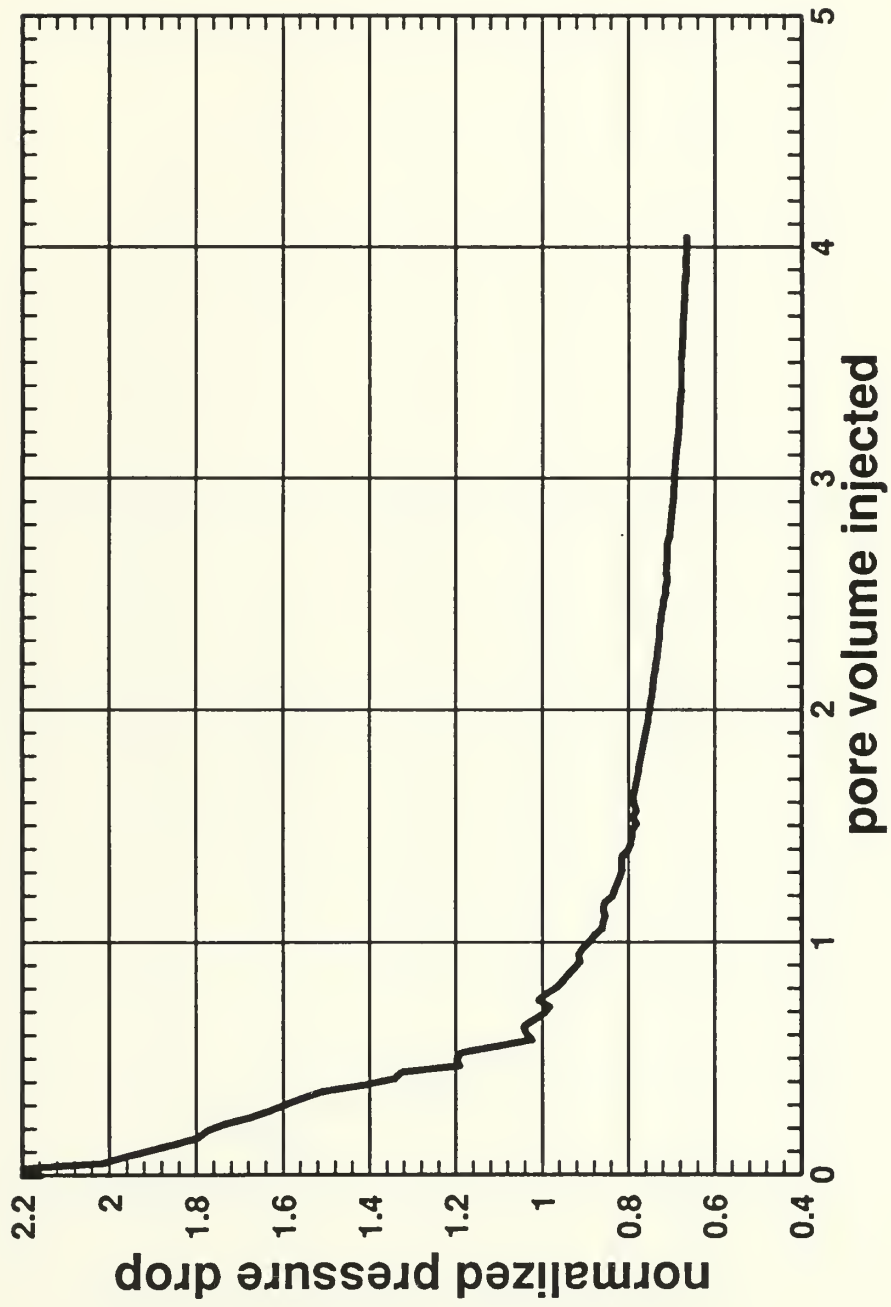


Figure 7.30: Normalized Pressure Drop (Variable q) vs. PVI; Run 9 - Third Dynamic Water Flood.

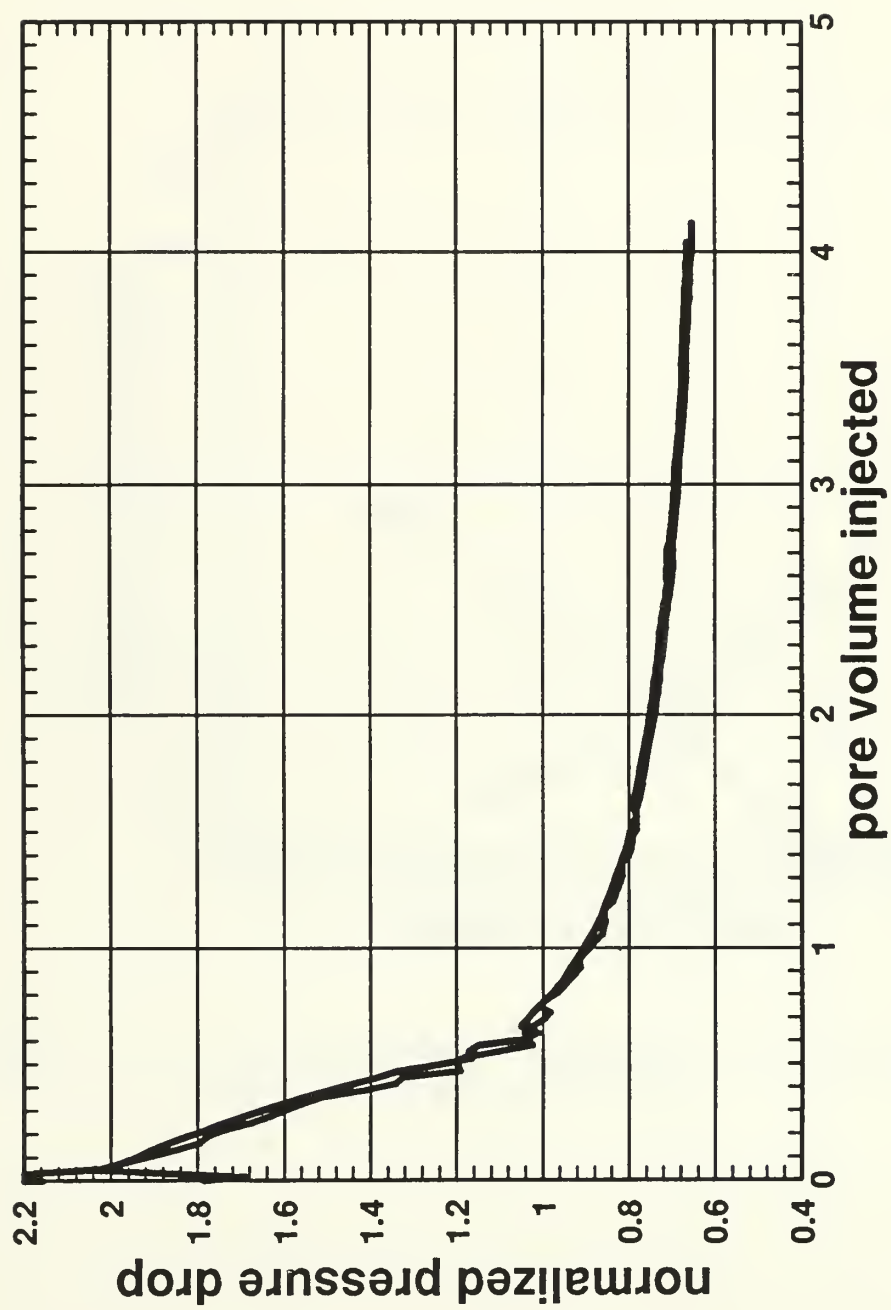


Figure 7.31: Fixed vs. Variable Normalized Pressure Drop Comparison; Run 9 - Third Dynamic Water Flood.

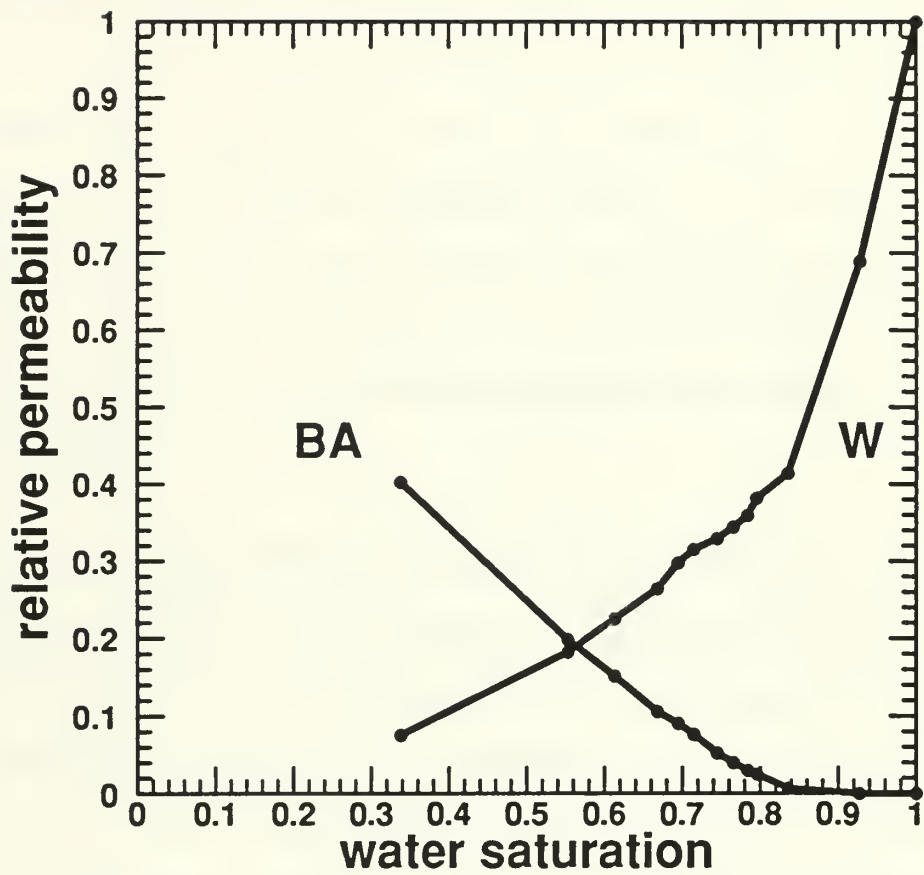


Figure 7.32: Oil and Water Relative Permeabilities vs. Water Saturation; Run 9 - Third Dynamic Water Flood.

data points calculated at various pore volumes injected. These data are contained in Table A.9 of Appendix A. A comparison of run 9's two-phase water-oil relative permeability data from the second dynamic water flood and from the third water flood at residual decane saturation is shown in Figure 7.33. Curves A and C are the second water flood's oil relative permeabilities and water relative permeabilities, respectively, while curves B and D are the third water flood's oil relative permeabilities and water relative permeabilities, respectively. As expected, relative permeabilities of the oil and water are lower in the third water flood because of the presence of residual decane. Note also, the oil relative permeability is reduced more significantly than the water relative permeability by the presence of residual decane saturation.

7.3 Two-Phase Benzyl Alcohol-Decane Relative Permeability Experiments

The first portion of run 8 was designed to determine the two-phase relative permeabilities of a benzyl alcohol-decane system at residual water saturation. This was accomplished through a series of steady-state experiments and a dynamic decane flood. The run concluded with a dynamic water flood of the glass bead pack at residual water saturation and residual oil saturation in the presence of decane.

Figure 7.34 is the pressure profile of the core linearity check for run 8. The plateaus of the profile show the pressure drop between the labeled core taps. In this linearity test each tap along the core was opened for five minutes (300 seconds). Sample time was one second. The core had a maximum pressure difference of 9.4% between zones ΔP_{2-3} and ΔP_{4-5} . Other differences were 3.0% between ΔP_{2-3} and ΔP_{3-4} , and 6.6% between ΔP_{3-4} and ΔP_{4-5} .

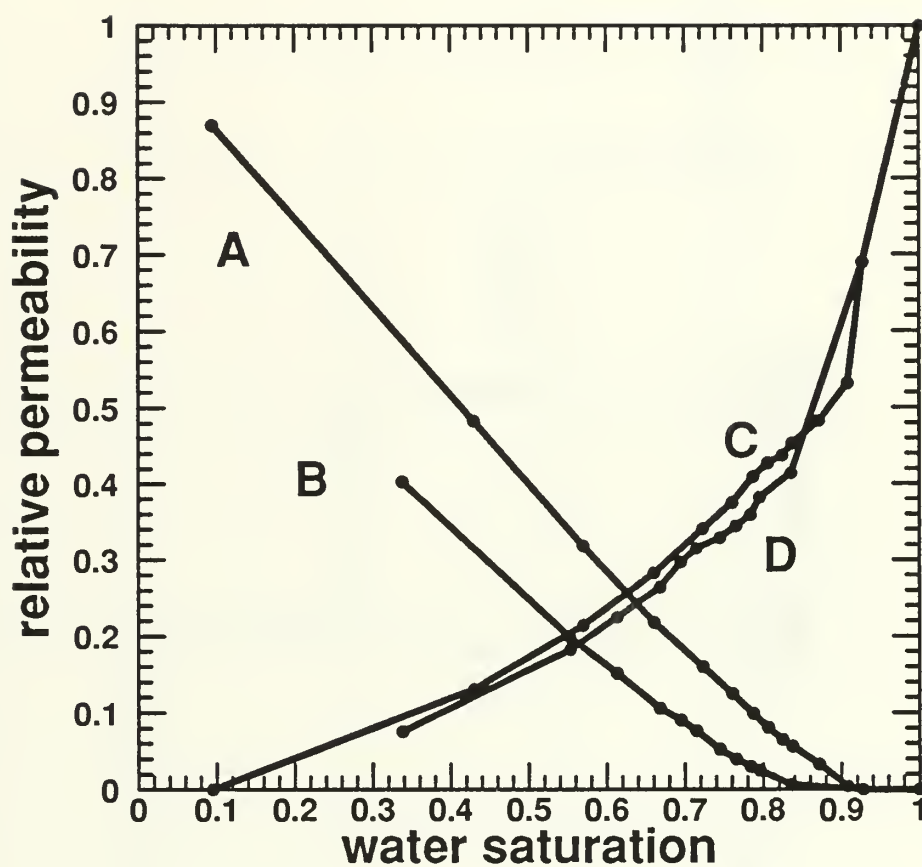


Figure 7.33: Relative Permeability Comparison;
 Run 9 - Second and Third Dynamic Water Floods.
 A = Oil Relative Permeability, Second Dynamic Flood
 B = Oil Relative Permeability, Third Dynamic Flood
 C = Water Relative Permeability, Second Dynamic Flood
 D = Water Relative Permeability, Third Dynamic Flood

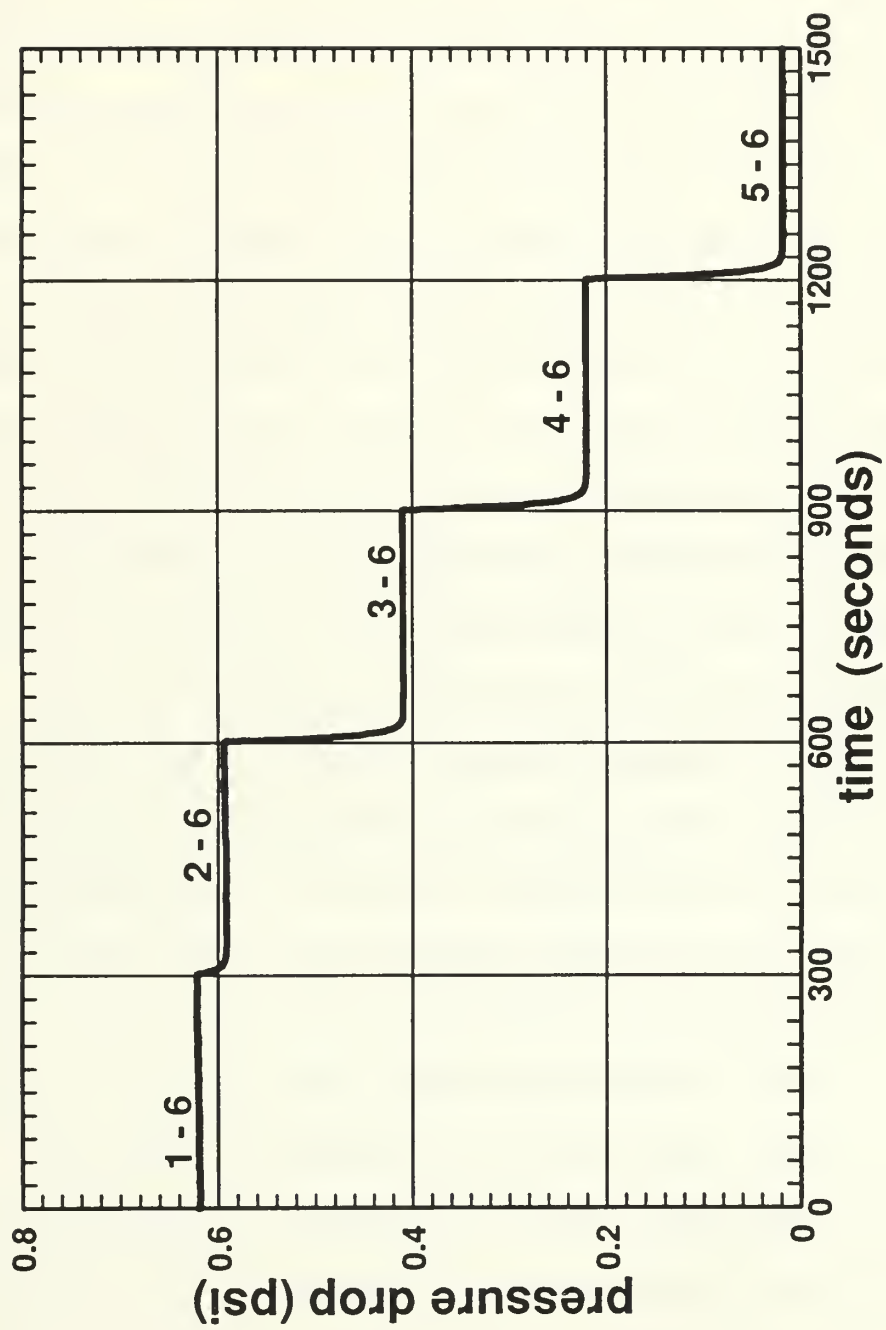


Figure 7.34: Core Linearity Check Pressure Profile; Run 8.

The overall saturation path of run 8 is shown in Figure 7.35. The glass bead pack was flooded with water, point (1), then flooded to residual water saturation with the oil phase (benzyl alcohol), point (2). The oil saturated core was then brought to point (3) by a series of steady-state decane/oil floods, called the drainage series. Point (3) represents residual water saturation and residual oil saturation in the presence of decane. The glass bead pack was then brought down to residual water saturation and residual decane saturation in the presence of oil, point (4), by a series of decane/oil floods in the reverse sequence of fractional flow rates that made up the drainage series of experiments. The series of experiments from point (3) to point (4) is called the imbibition series. To complete the run the glass bead pack was brought back to residual water saturation and residual oil saturation in the presence of decane, point (5), and then dynamically water flooded to point (6).

Figure 7.36 shows the saturation history of the steady-state drainage series of experiments from run 8. Table 7.1 lists the saturations of each point, the fractional flow ratios and actual specified flows that were used to reach the point, and the relative permeabilities at the point. Figure 7.37 plots the fractional flow of oil and the resulting glass bead pack saturations obtained from the results of these steady-state drainage series experiments at residual water saturation. The solid dots are the actual calculated data points. These data are contained in Table 7.1 .

The relative permeability data for oil and decane versus oil saturation from these drainage series of experiments is plotted in Figure 7.38. The solid dots are the actual calculated data points from each experiment and are contained in Table 7.1 .

Figure 7.39 shows the saturation history of the steady-state imbibition series of steady-state experiments from run 8. Table 7.2 lists the saturations of each point,

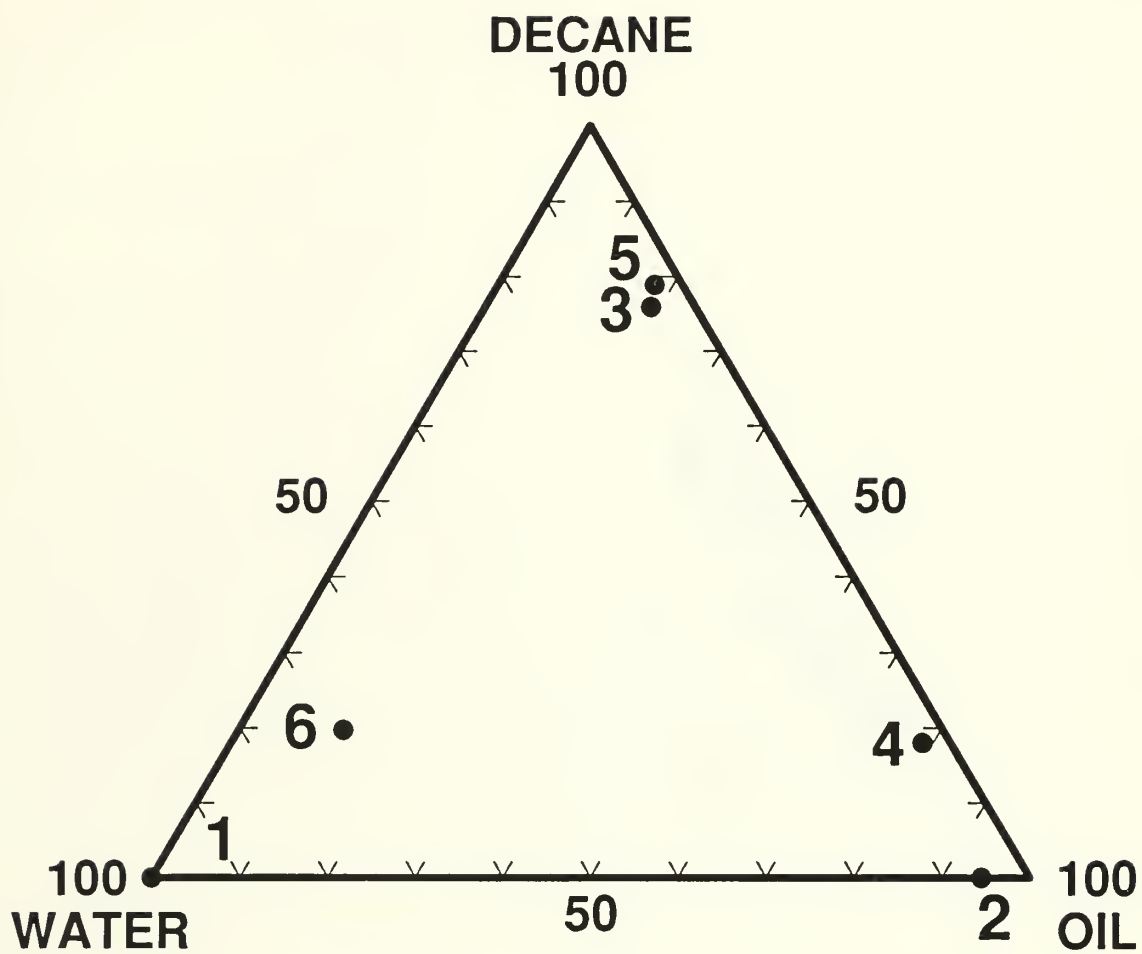


Figure 7.35: Overall Saturation History; Run 8.

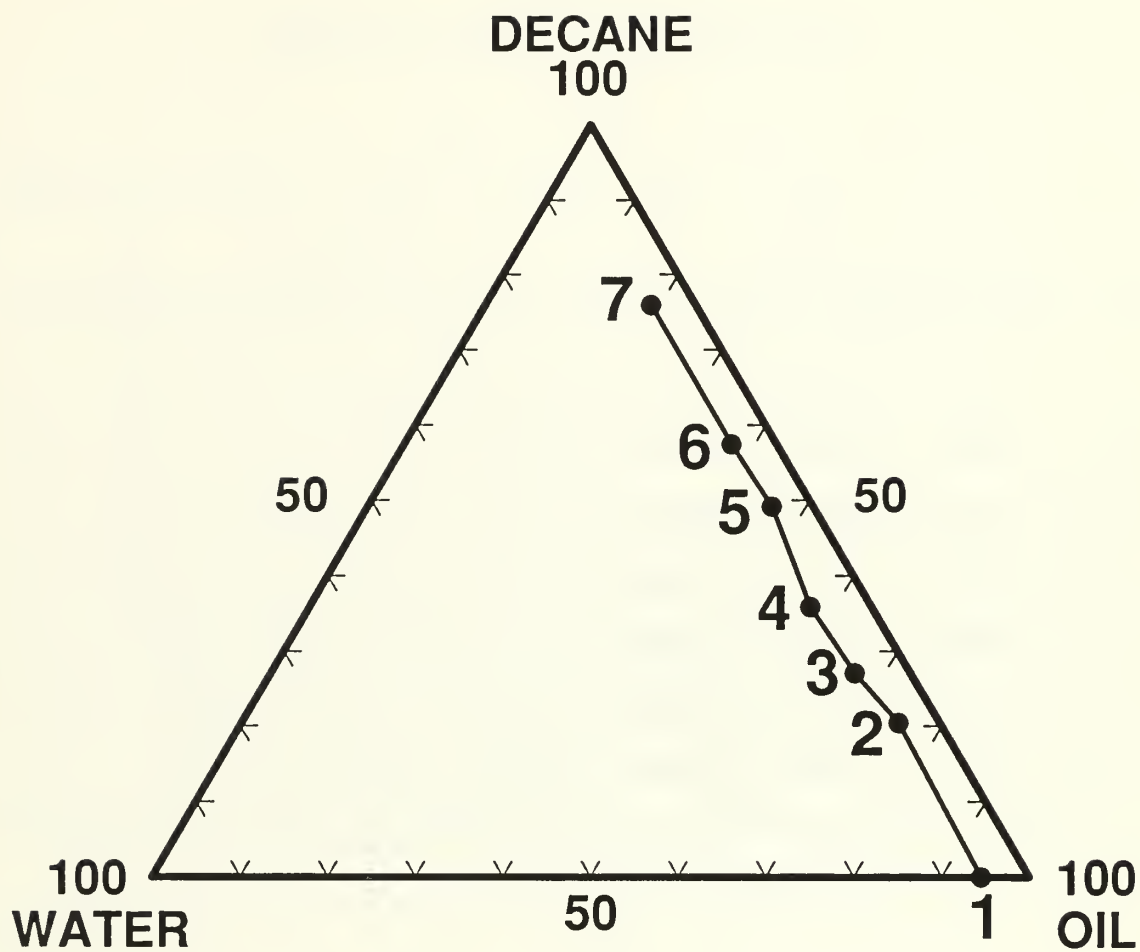


Figure 7.36: Steady-State Drainage Saturation History; Run 8.

Table 7.1
Summary of Run 8 Drainage Experiments

point	$f_{\text{dec}} : f_{\text{oil}}$	$q_{\text{dec}} : q_{\text{oil}}$ [mL/min]	k_{To}	k_{Td}	S_o %	S_d %	S_w %
1	0:1	0.0 : 2.0	0.852	0.0000	94.53	0.00	5.47
2	1:1	1.0 : 1.0	0.430	0.0870	74.90	20.40	4.70
3	2:1	1.0 : 0.5	0.319	0.1296	66.56	27.12	5.92
4	4:1	1.2 : 0.3	0.227	0.1839	57.19	35.88	6.13
5	10:1	1.0 : 0.1	0.119	0.2440	46.14	49.20	4.66
6	20:1	2.0 : 0.1	0.074	0.2900	37.38	57.48	5.14
7	1:0	2.0 : 0.0	0.000	0.4410	18.98	75.97	5.05

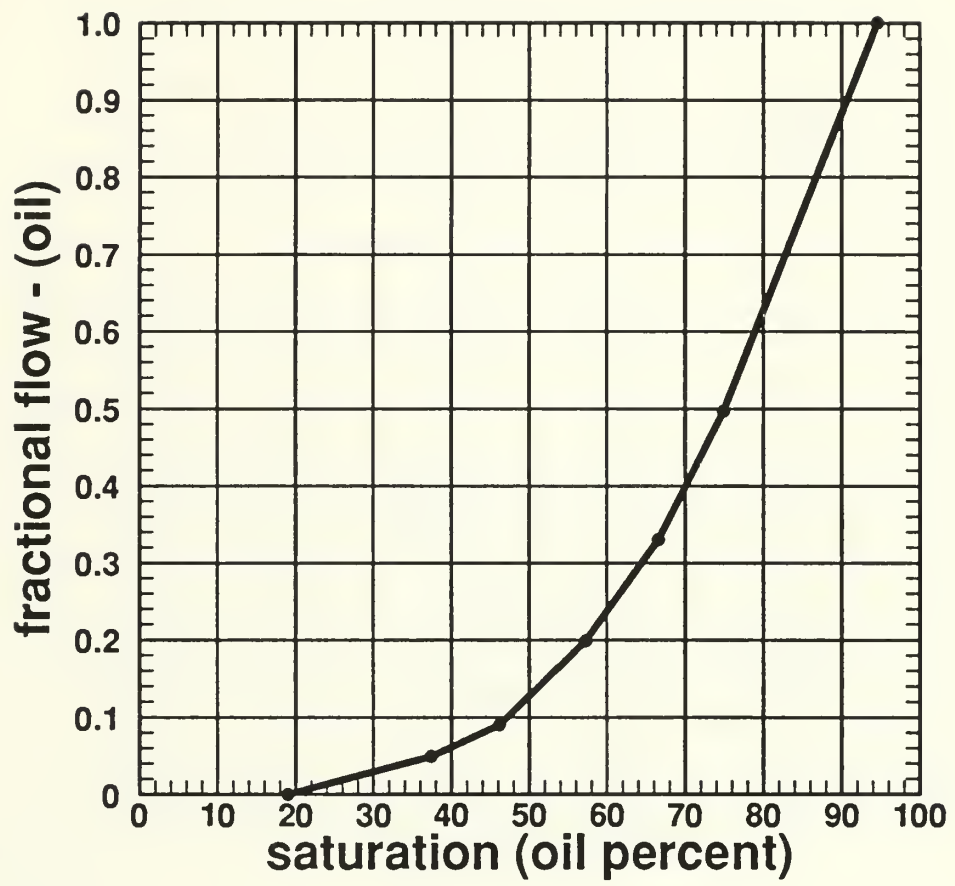


Figure 7.37: Oil Saturation vs. Oil Fractional Flow

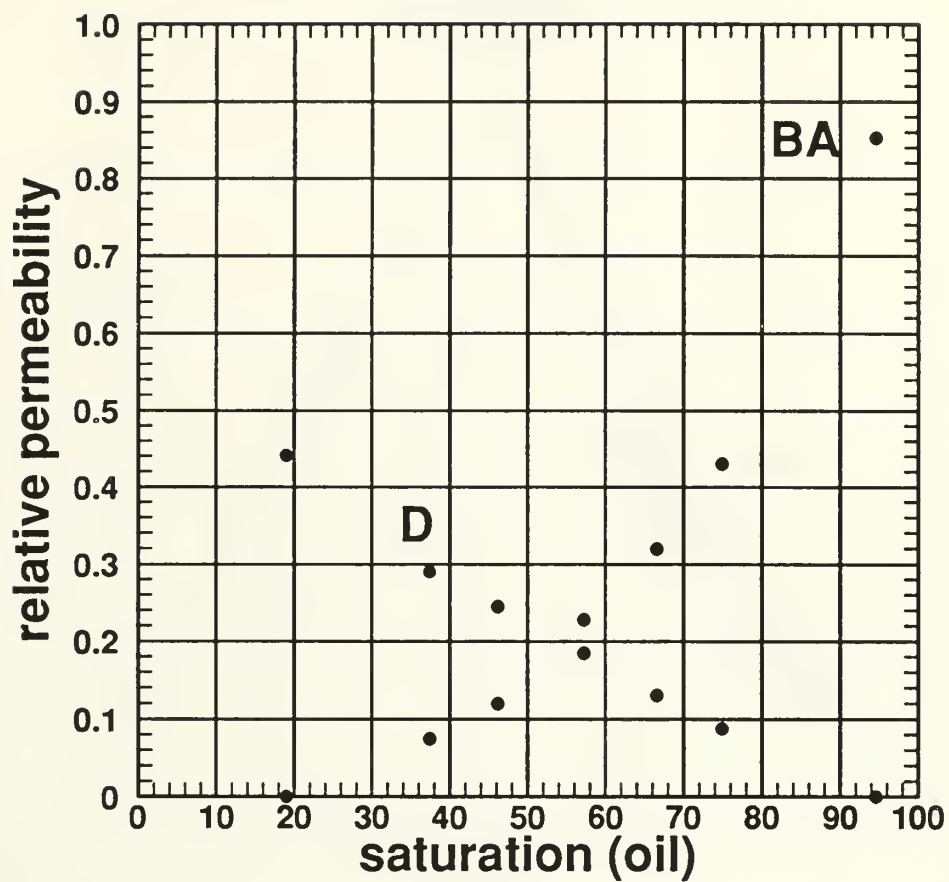


Figure 7.38: Decane and Oil Relative Permeabilities vs. Oil Saturation; Run 8 - Steady-State Drainage Series.

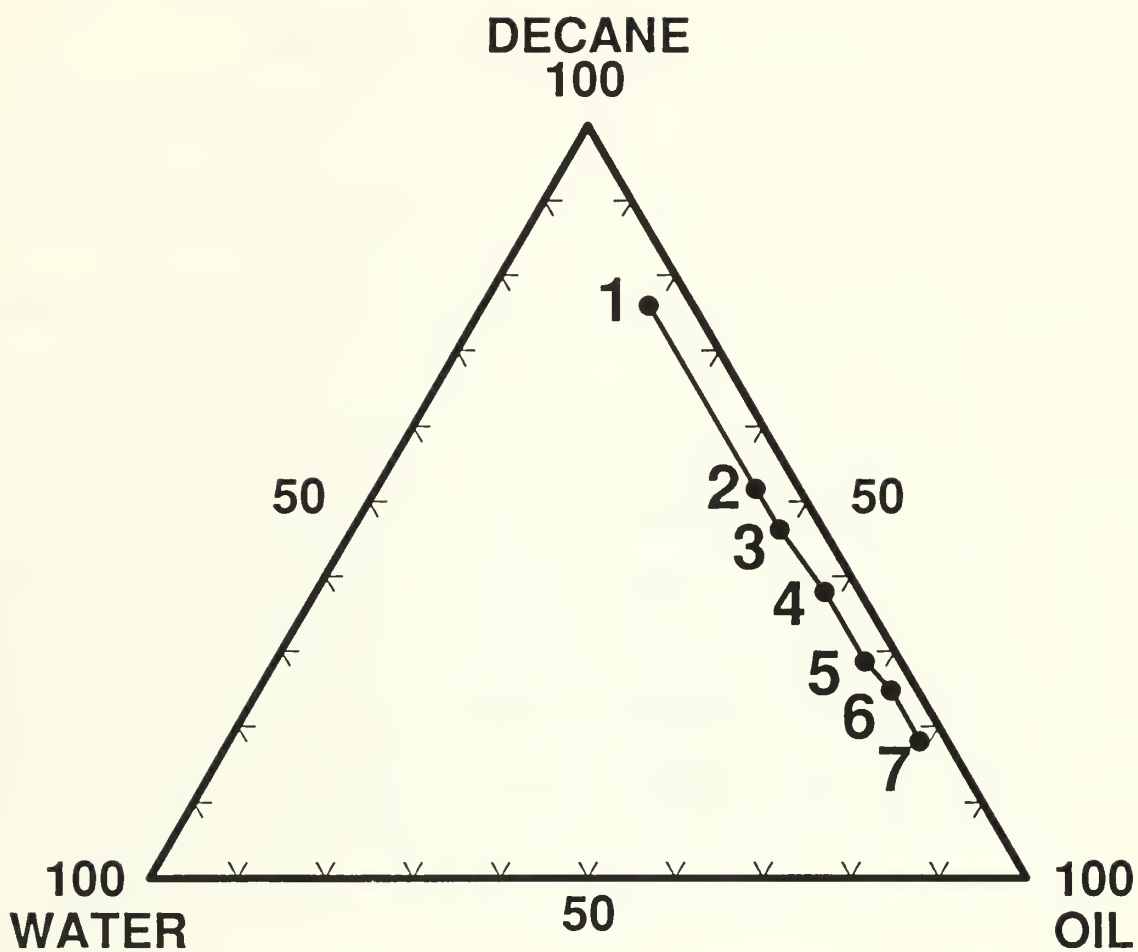


Figure 7.39: Steady-State Imbibition Saturation History; Run 8.

Table 7.2
Summary of Run 8 Imbibition Experiments

point	$f_{\text{dec}} : f_{\text{oil}}$	$q_{\text{dec}} : q_{\text{oil}}$ [mL/min]	k_{To}	k_{Td}	S_o %	S_d %	S_w %
1	1:0	0.0 : 2.0	0.000	0.4410	18.98	75.97	5.05
2	20:1	1.0 : 1.0	0.098	0.3770	43.31	51.69	5.00
3	10:1	1.0 : 0.5	0.144	0.2904	48.78	46.26	4.96
4	4:1	1.2 : 0.3	0.226	0.1816	58.00	37.98	4.02
5	2:1	1.0 : 0.1	0.310	0.1256	67.26	28.63	4.11
6	1:1	2.0 : 0.1	0.341	0.0686	72.18	24.81	3.01
7	0:1	2.0 : 0.0	0.490	0.0000	78.81	18.06	3.12

the fractional flow ratios and specified flow rates that were used to reach the point, and the relative permeabilities at the point. The relative permeability data for oil and decane versus oil saturation from these imbibition series of experiments is plotted in Figure 7.40. The solid dots are the actual calculated data points from each experiment. The comparison of the drainage (small dots) and imbibition (large dots) relative permeabilities is shown in Figure 7.41. Figure 7.41 shows relatively unchanged values for benzyl alcohol relative permeabilities, while the decane curves show some hysteresis effects by shifting their slopes.

The run 8 two-phase decane-benzyl alcohol experiments at residual water saturation concluded with a decane flood of the glass bead pack at residual water saturation, residual decane saturation in the presence of oil. The saturation trajectory of this experiment is projected in Figure 7.42. The starting point of the dynamic decane flood is point (1) representing residual water saturation, $S_{rw} = 3.1 \%$, and residual decane saturation, $S_{rd} = 18.1 \%$, in the presence of oil. The Buckley-Leverett shock breakthrough occurred at point (2), $S_d = 22.1 \%$, the saturation trajectory continues until point (3) representing residual water saturation, $S_{rw} = 3.1 \%$, and residual oil saturation, $S_o = 14.7 \%$, in the presence of decane. The dots are the actual calculated data points from the decane flood experiment and are contained in Table A.11 contained in Appendix A .

Figures 7.43 and 7.44 show the recovery curves for the benzyl alcohol with the injected decane. The initials of the recovered fluids identify the recovery curves. The dots on the figures are the actual data points representing the data from each collection vessel. These data are contained in Table A.12 of Appendix A. Figure 7.43 shows the entire recovery curves for both phases, while Figure 7.44 enlarges the recovery curve of the benzyl alcohol. Breakthrough of the decane

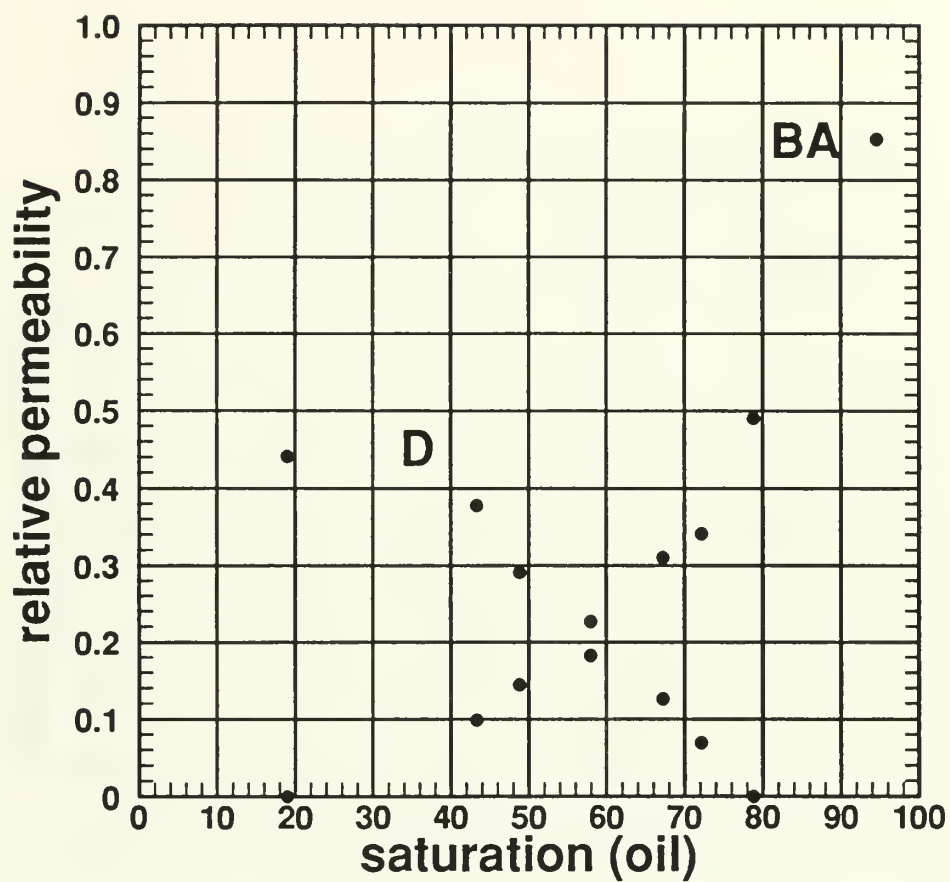


Figure 7.40: Decane and Oil Relative Permeabilities vs. Oil Saturation;
Run 8 - Steady-State Imbibition Series.

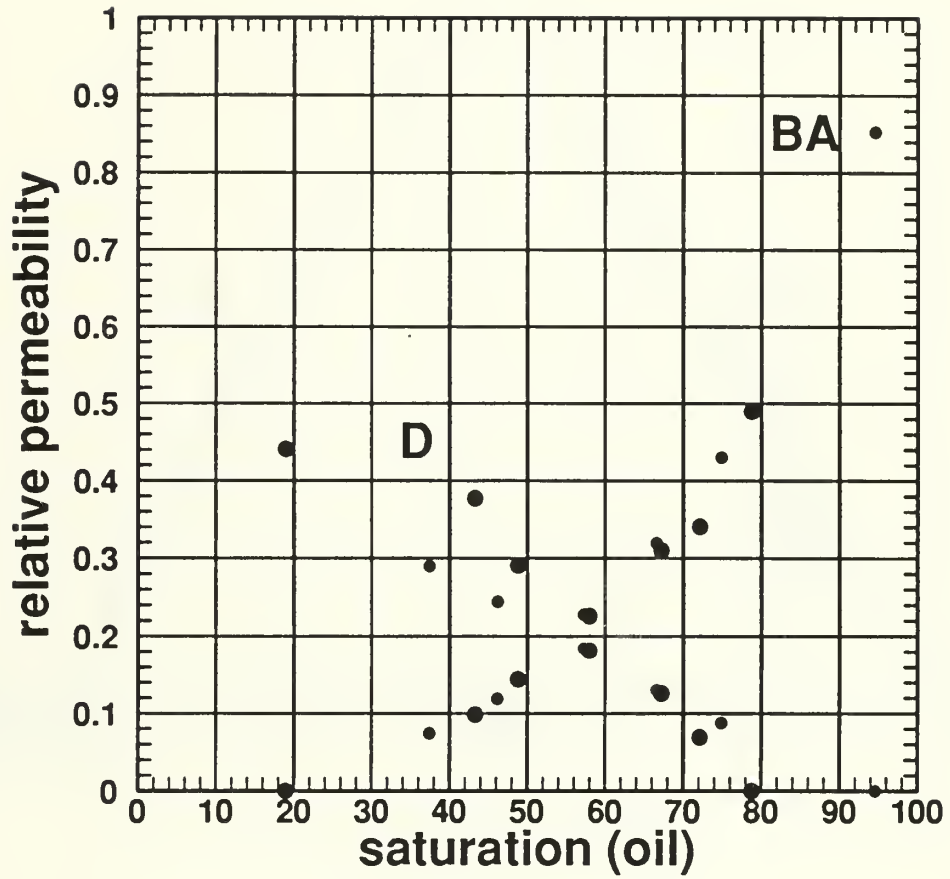


Figure 7.41: Comparison of Relative Permeabilities;
Run 8 - Drainage and Imbibition Series.

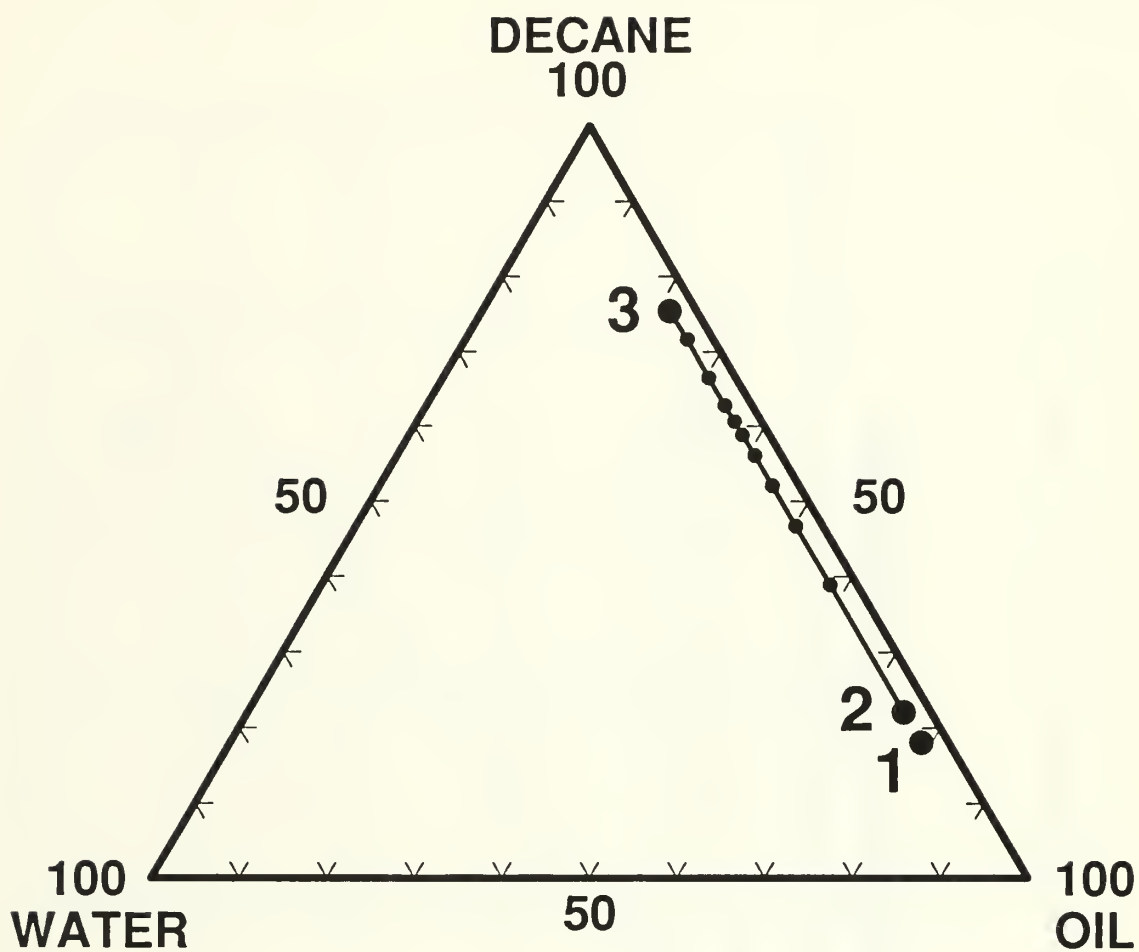


Figure 7.42: Saturation History and Trajectories;
Run 8 - Dynamic Decane Flood.

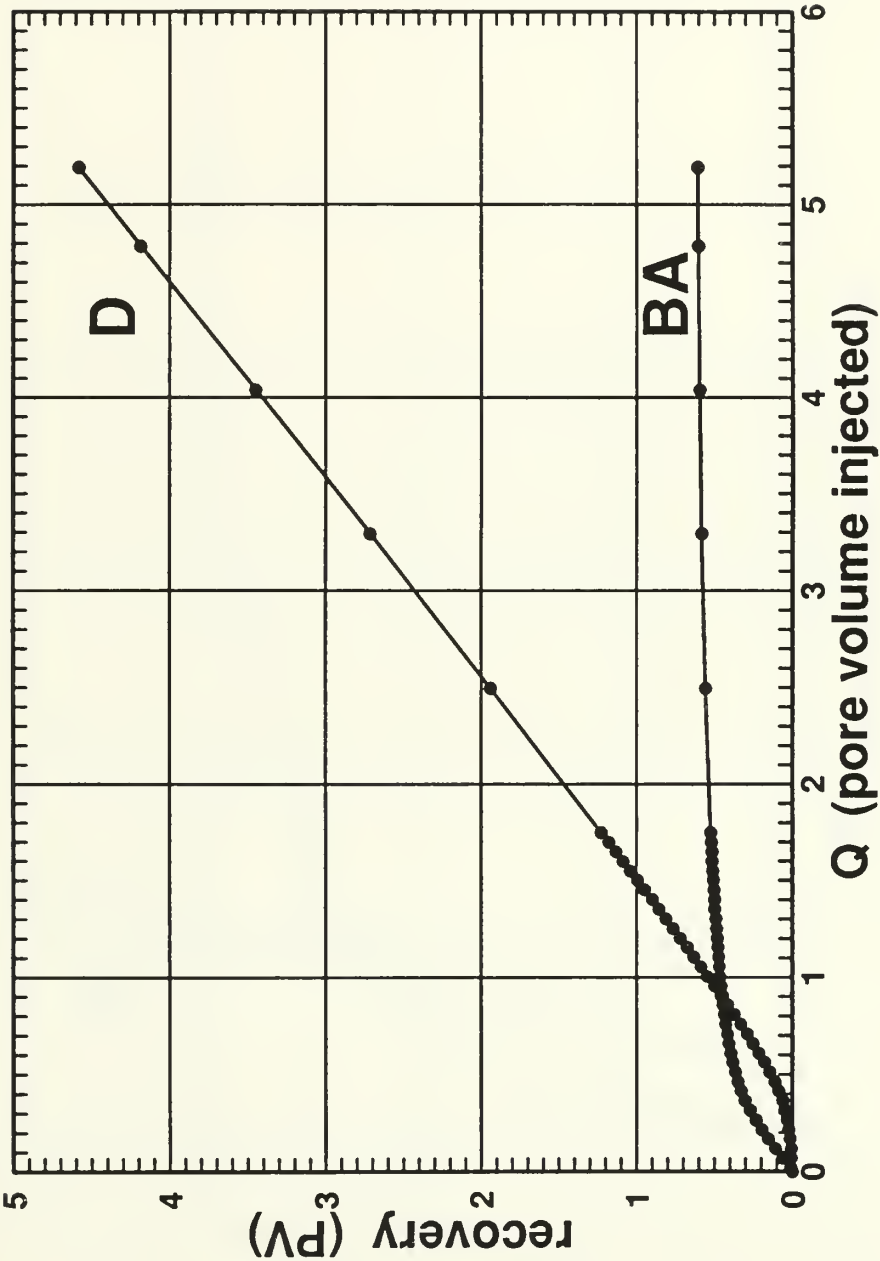


Figure 7.43: Dynamic Flood Recovery Curves; Run 8 - Dynamic Decane Flood.

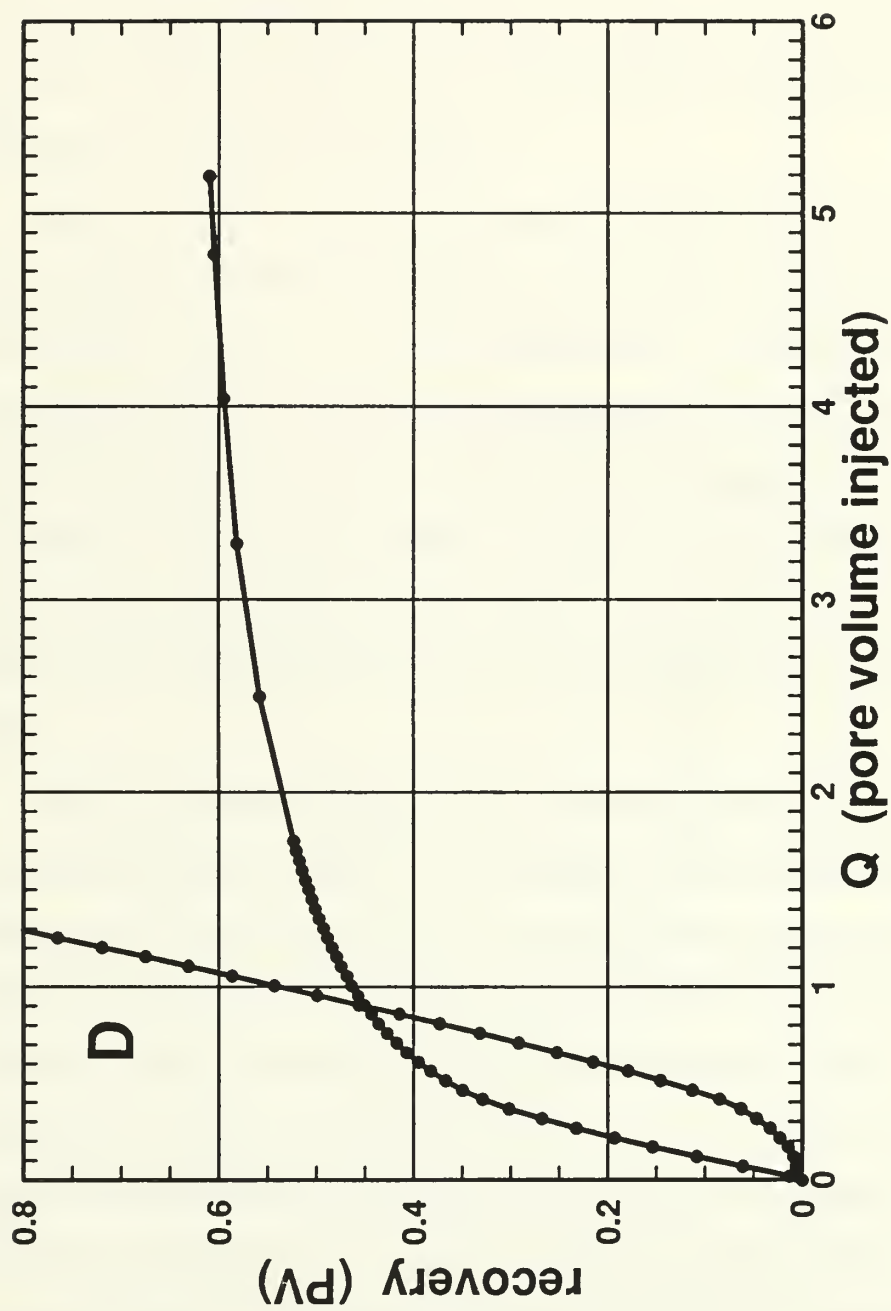


Figure 7.44: Expanded Dynamic Flood Recovery Curves; Run 8 - Dynamic Decane Flood.

occurred at approximately 0.02 pore volumes injected as shown by the departure of the decane recovery curve from the x-axis at this point. The smooth transition of the benzyl alcohol curve after breakthrough indicates that no oil bank developed during the flood and accounts for the small saturation shock jump seen in moving from point (1) to point (2) on Figure 7.42.

The plot of pressure drop normalized to a fixed flow rate versus the pore volumes injected is shown as Figure 7.45. The pressure was normalized to the single calculated actual flow set on the decane pump. The pressure sample rate was one sample per second. Every one-hundred pressure points were averaged and plotted to make the pressure profile. Figure 7.46 is an enlargement of the early portion of Figure 7.45. As seen in Figures 7.43 and 7.44, breakthrough occurred very early at 0.02 pore volumes injected. Figure 7.46 makes it easier to evaluate the slope of the normalized pressure drop curve when determining relative permeabilities.

The two-phase decane-benzyl alcohol relative permeabilities measured at residual water saturation obtained from the drainage (small dots) and imbibition (large dots) series of steady-state experiments and the dynamic decane flood are shown in Figures 7.47 and 7.48. The steady-state data points are the stand alone points while the relative permeability points calculated from the dynamic flood data are connected by a curve. The dynamic flood relative permeabilities were calculated using the fixed flow rate normalized pressure data shown in Figures 7.45 and 7.46. The dots on the curves are the actual data points calculated at various pore volumes injected. These data are contained in Table 7.1 and 7.2 in this chapter and A.11 of Appendix A. The oil relative permeabilities are approximately the same in both the steady-state and dynamic floods, where as the decane relative permeabilities are

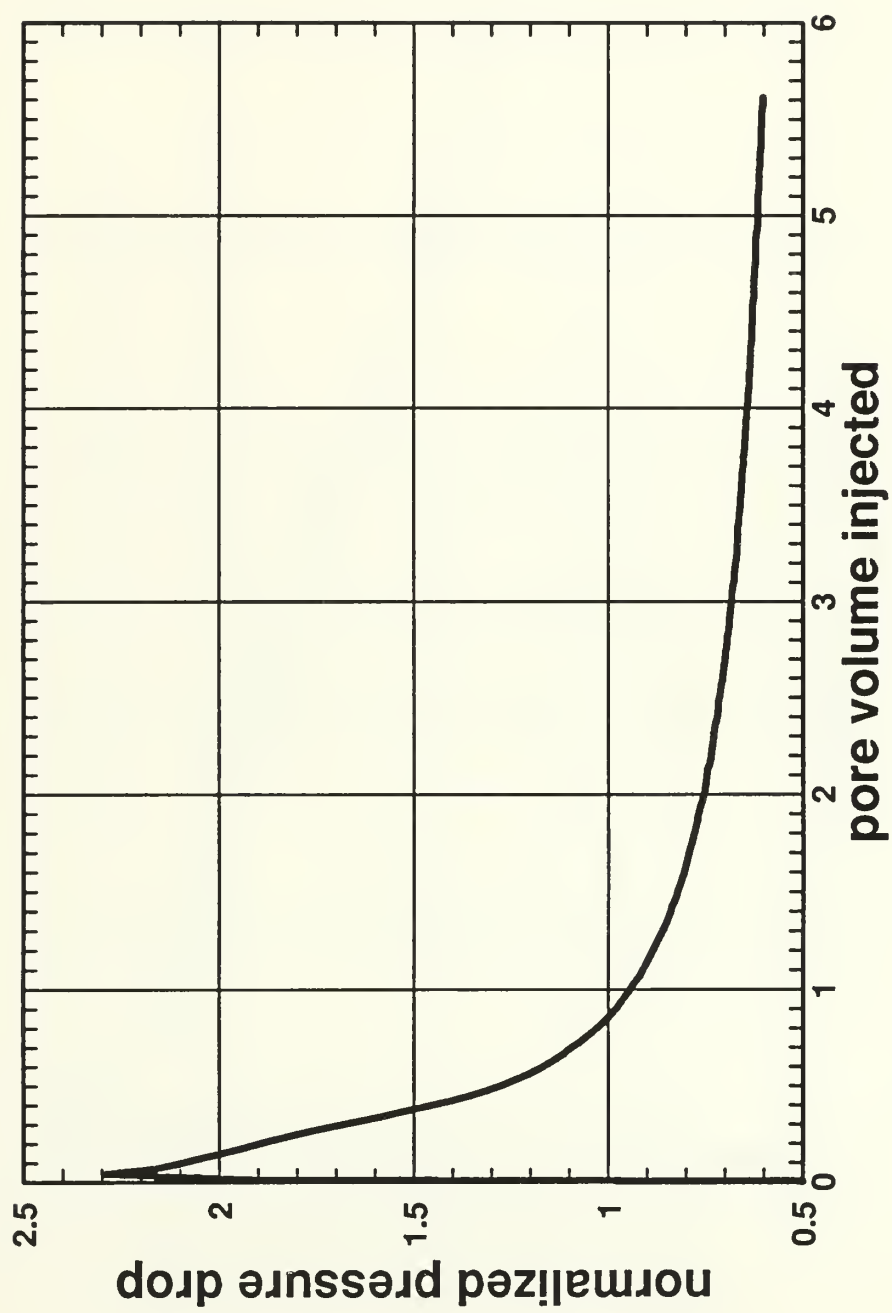


Figure 7.45: Normalized Pressure Drop vs. PVI; Run 8 - Dynamic Decane Flood.

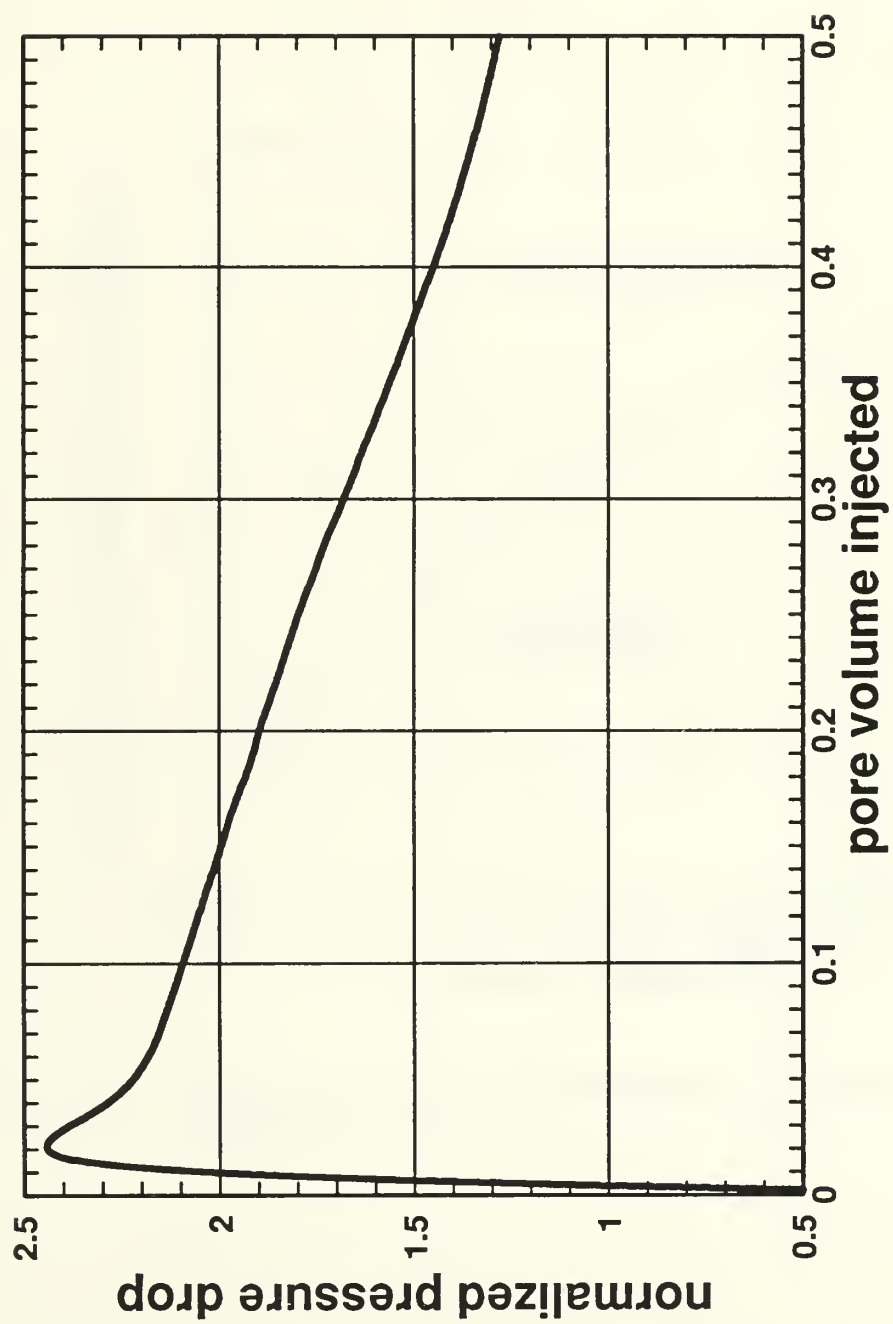


Figure 7.46: Expanded Normalized Pressure Drop vs. PVI; Run 9 - Dynamic Decane Flood.

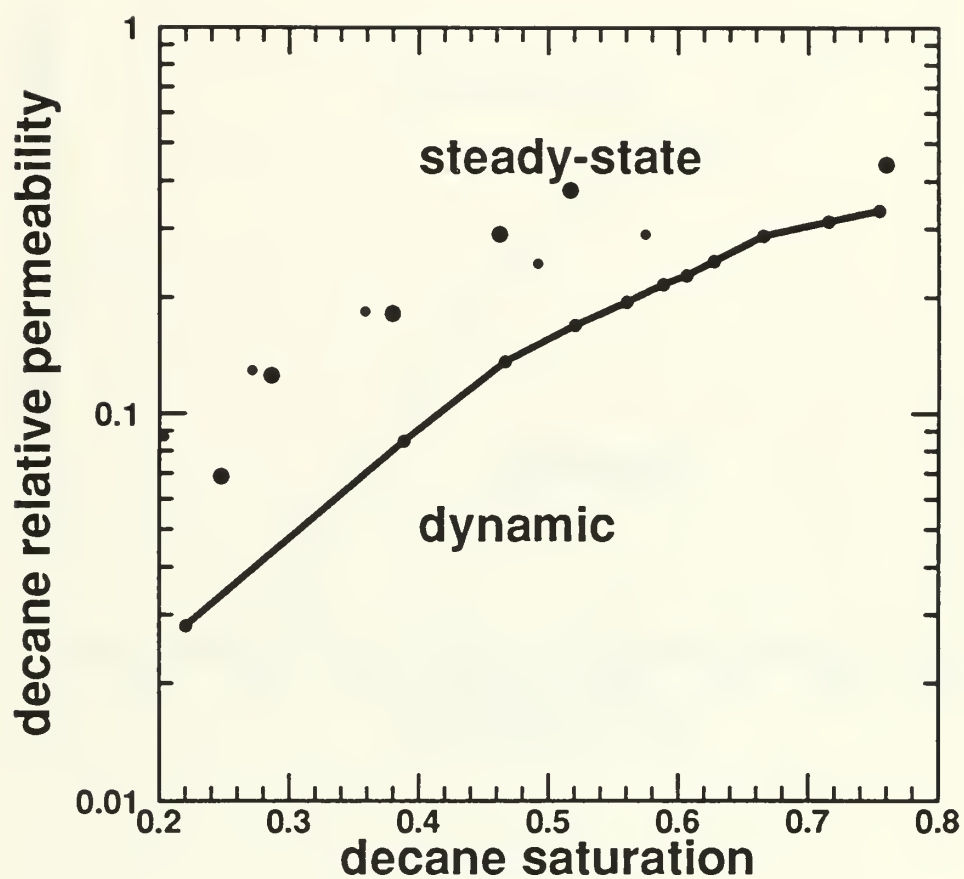


Figure 7.47: Comparison of Dynamic and Steady-State Calculated Relative Decane Permeabilities; Run 8.

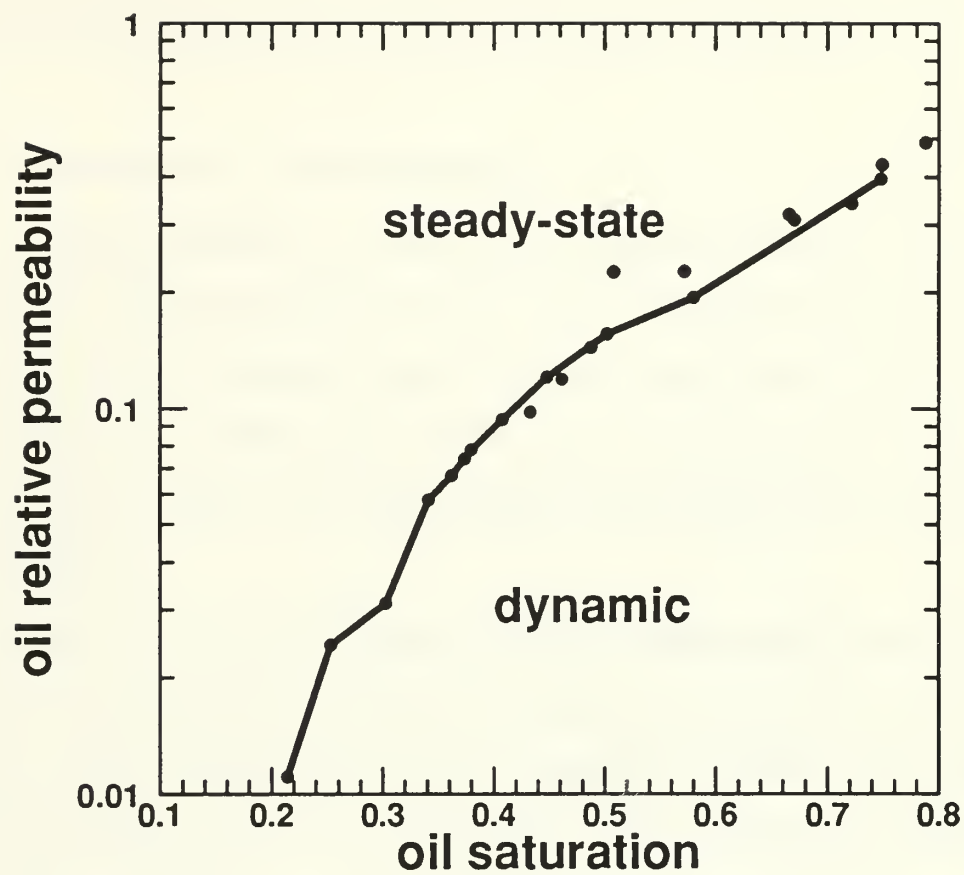


Figure 7.48: Comparison of Dynamic and Steady-State Calculated Relative Oil Permeabilities; Run 8.

consistently higher in the steady-state experiments. The reason for the disparity in the decane relative permeabilities is unclear and requires more research.

7.4 Three-Phase Water Flood Experiments

This section discusses the results of the three-phase dynamic water flood experiments. These are conducted in runs 4 and 5, and at the conclusion of run 8. This series of runs is designed to map the interior region of the ternary diagram. This is attempted by making a series of water floods originating from several points spaced along the residual water saturation line at varying decane and benzyl alcohol (oil) saturations.

Figure 7.49 is the pressure profile of the core linearity check for run 4. The plateaus of the profile show the pressure drop between the labeled core taps. In this linearity test each tap along the core was opened for 5 minutes (300 seconds). Sample time was one second. The core had a maximum pressure difference of 7.2% between zones ΔP_{2-3} and ΔP_{4-5} . Other differences were 1.6% between ΔP_{2-3} and ΔP_{3-4} , and 5.7% between ΔP_{3-4} and ΔP_{4-5} .

Figures 7.50 and 7.51 are the run 4 recovery curves for benzyl alcohol and water with the injected decane. The initials of the fluids identify the recovery curves. The dots on the figures are the actual data points representing the data from each collection vessel. These data are contained in Table A.13 of Appendix A. Breakthrough of the water occurred at approximately 0.39 pore volumes injected as shown by the departure of the water recovery curve from the x-axis and the abrupt changes in the slopes of the decane and benzyl alcohol recovery curves. The almost vertical increase of the slope of the alcohol recovery curve at breakthrough indicates that an oil bank developed during the flood. The tangent to the recovery curve has

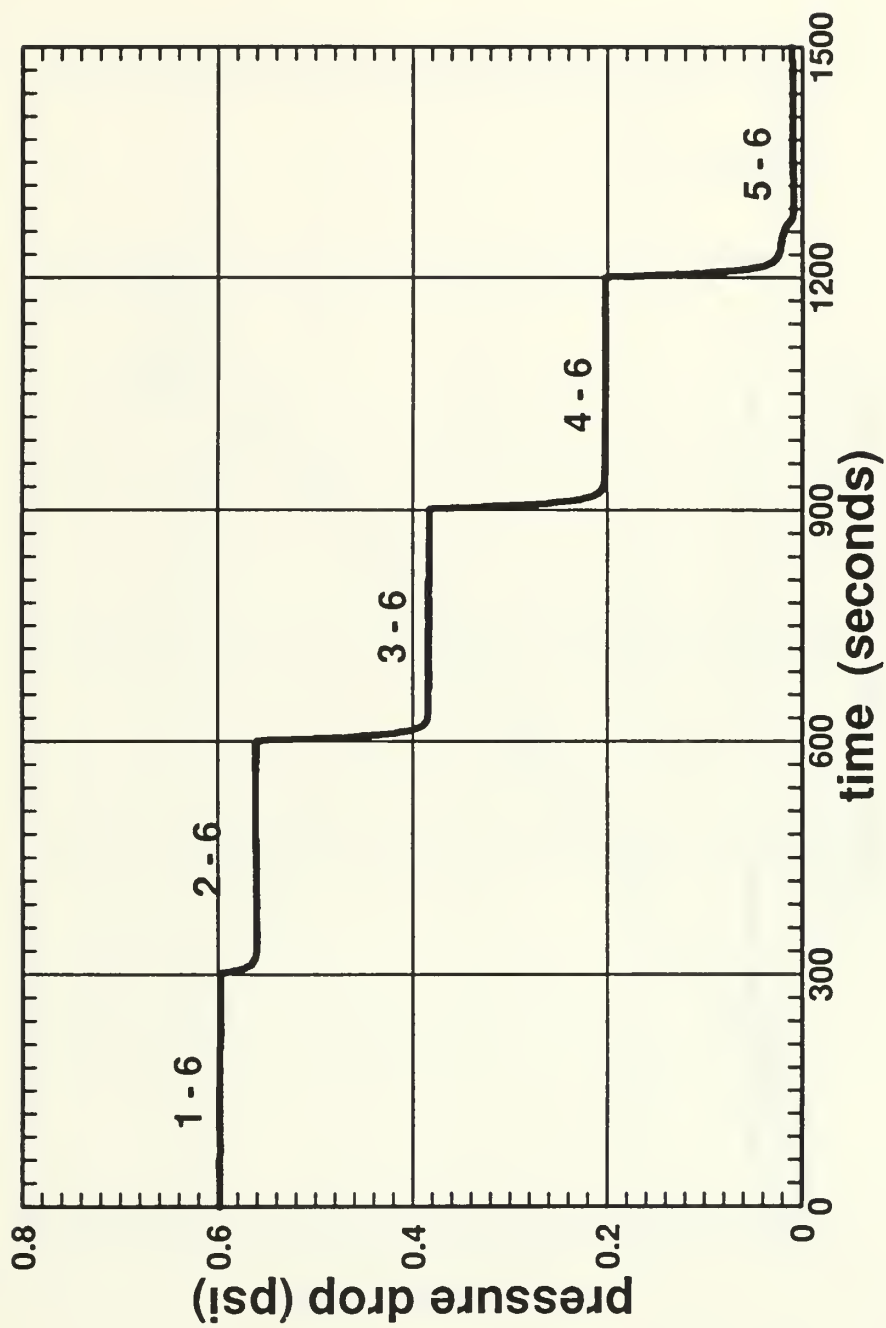


Figure 7.49: Core Linearity Check Pressure Profile; Run 4.

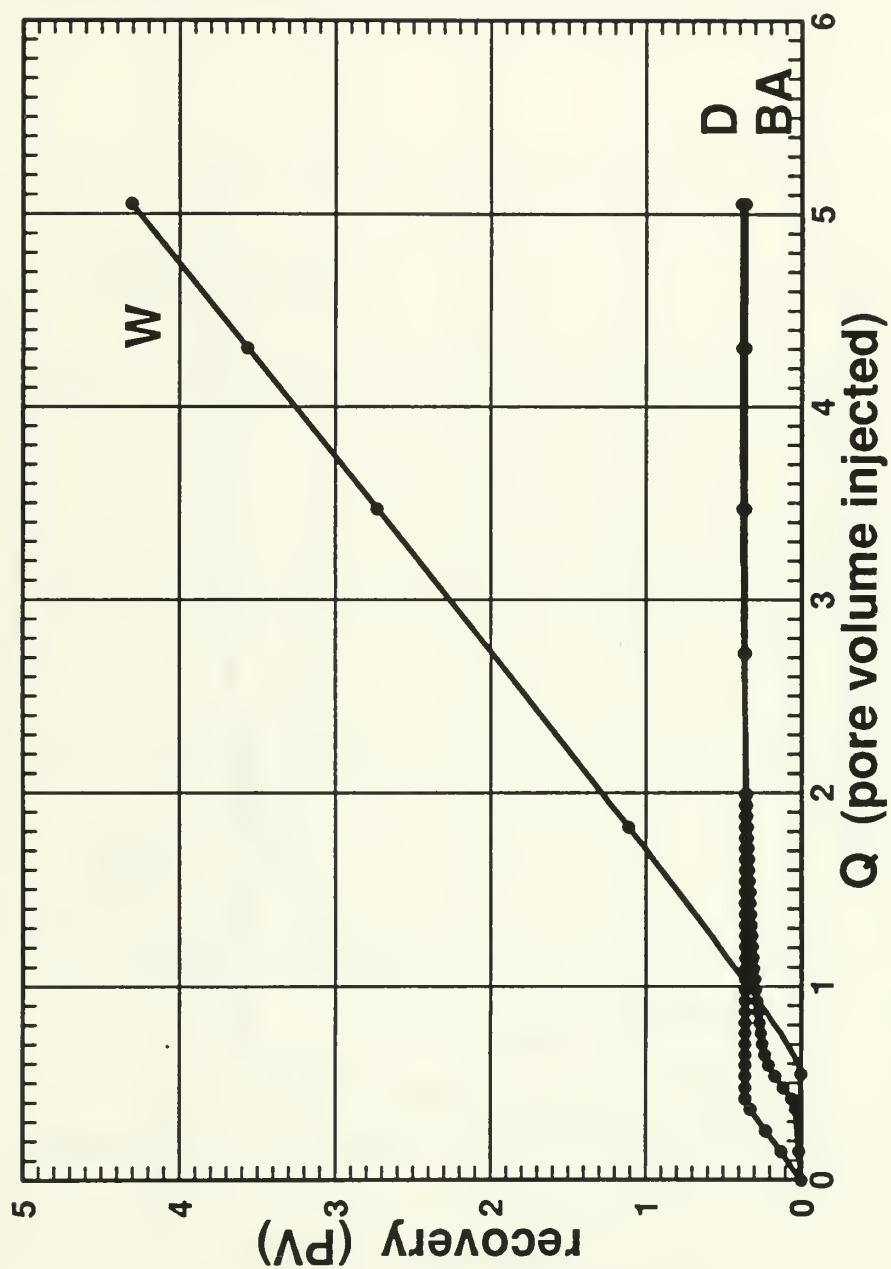


Figure 7.50: Dynamic Flood Recovery Curves; Run 4.

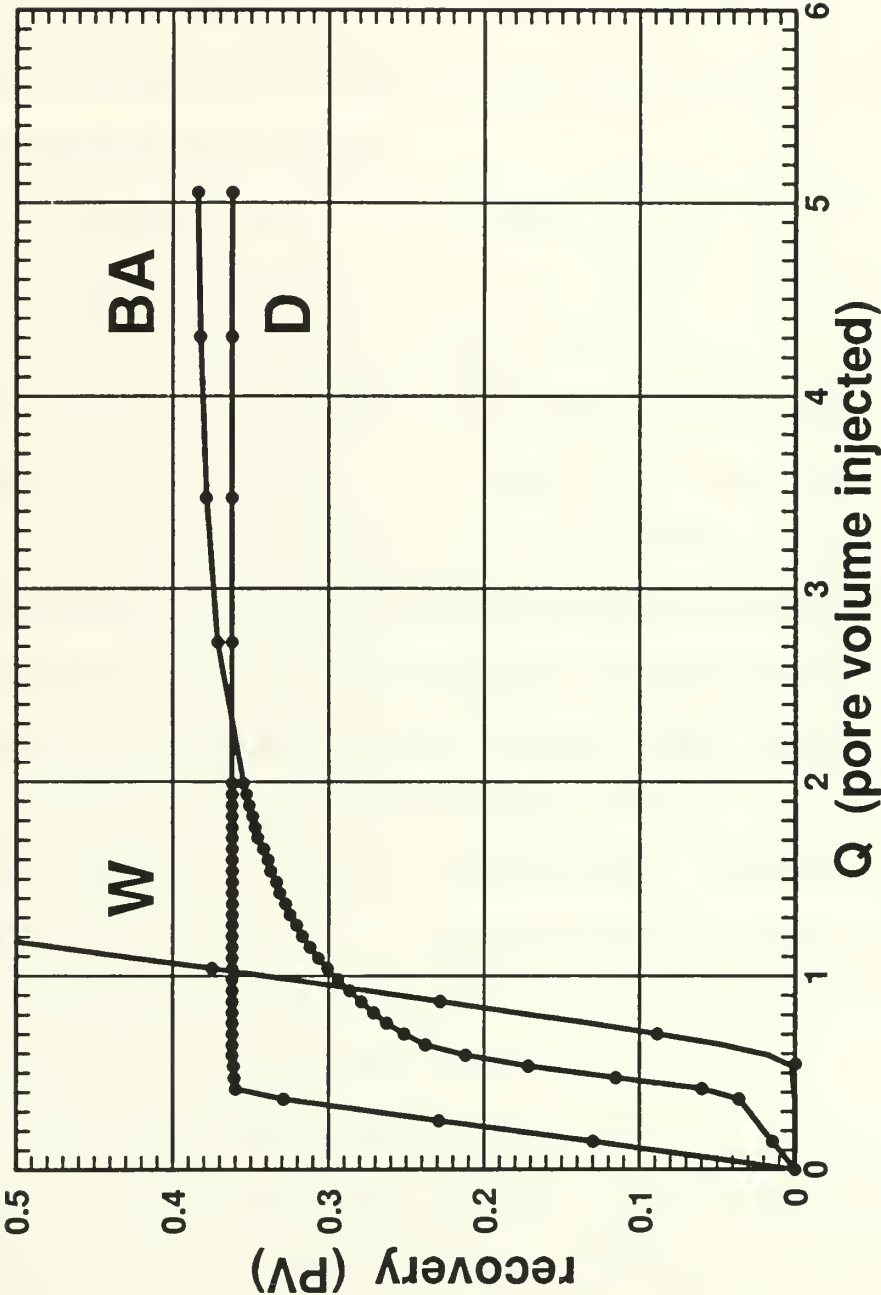


Figure 7.51: Expanded Dynamic Flood Recovery Curves; Run 4.

a negative y-intercept which indicates an increase in core-end oil saturation at breakthrough. The zero slope of the decane recovery curve after breakthrough indicates that the decane was removed from the core with piston like displacement down to a residual decane saturation prior to breakthrough and, therefore, no decane was produced after breakthrough.

The saturation history of run 4 is shown in Figure 7.52. The glass bead pack was flooded with water, point (1), then flooded to residual water saturation, $S_{rw} = 0.99 \%$, with the oil phase (benzyl alcohol) at point (2). The core at residual water saturation was flooded in a steady-state experiment using a specified fractional flow of 10:1 decane to oil to point (3). The saturations at point (3) are $S_d = 49.5 \%$, $S_o = 49.5 \%$, and $S_{rw} = 1.0 \%$. The glass bead pack was then dynamically water flooded. Core-end oil saturation at breakthrough of the Buckley-Leverett shock was $S_o = 85.0 \%$, point (4). The line from point (4) to point (5) represents the continuous saturation trajectory between breakthrough and the final flood conditions at residual oil and decane saturations. The points are the saturations calculated at various pore volumes injected. These data are contained in Table A.14 of Appendix A. The jump in oil saturation values at breakthrough as predicted by the recovery curve of Figure 7.51 is clearly obvious in the oil saturation jump from point (3) to point (4) in Figure 7.52.

The pressure drop normalized to a fixed flow rate versus the pore volumes injected plot for run 4's dynamic water flood is shown as Figure 7.53. The pressure was normalized to the single calculated actual flow set on the water pump. The pressure sample rate was one sample per second. Every one-hundred pressure points were averaged and plotted to make the pressure profile.

Figure 7.54 is the pressure profile of the core linearity check for run 5. The

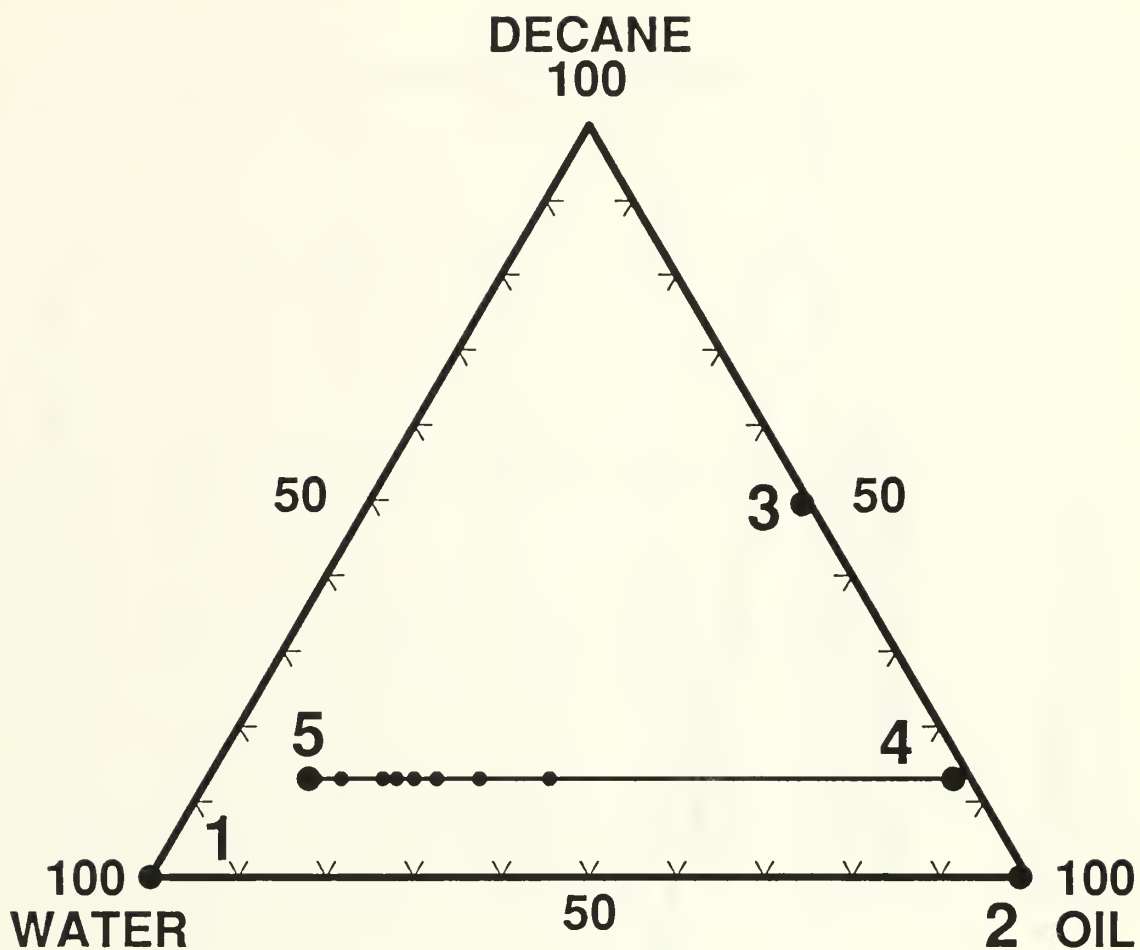


Figure 7.52: Saturation History and Trajectories; Run 4.

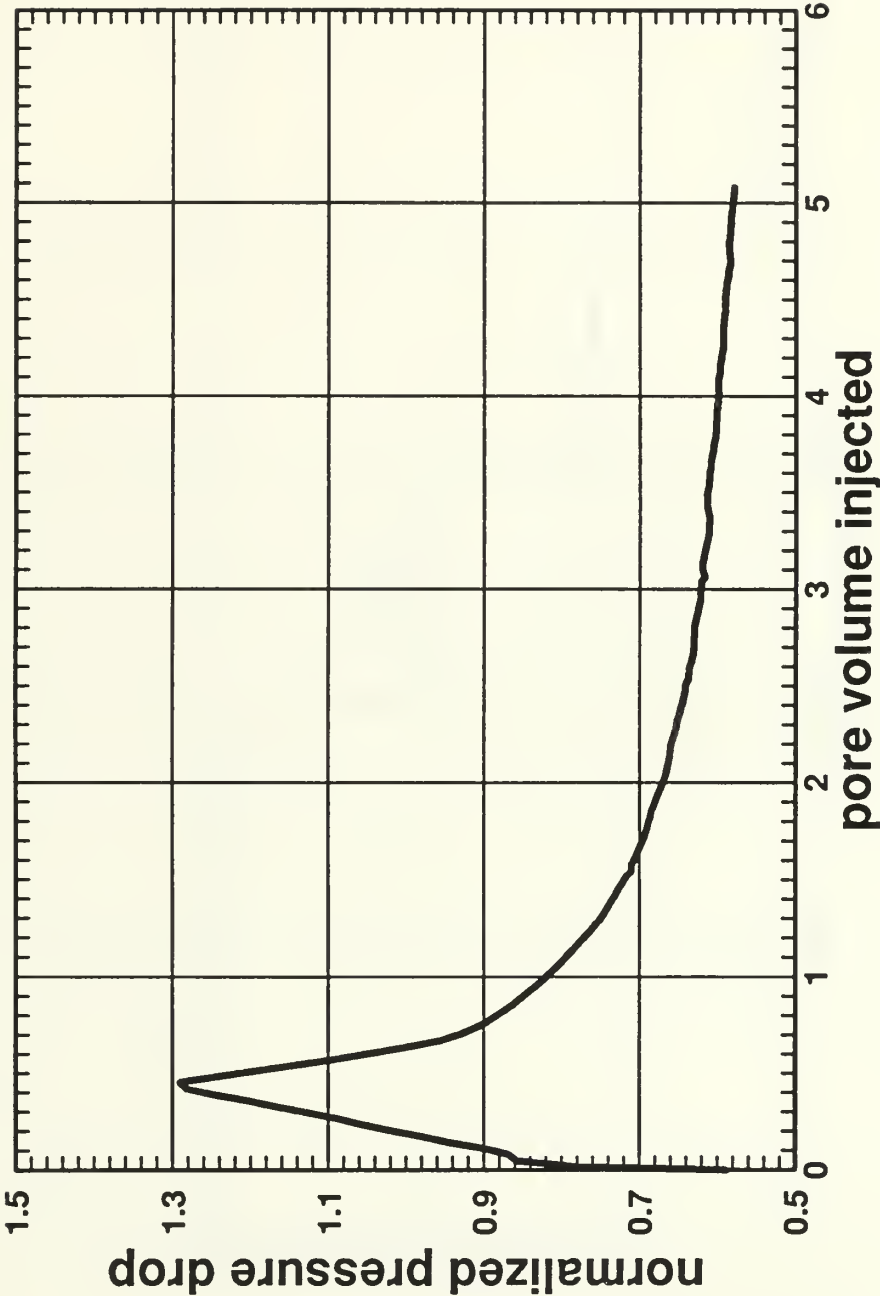


Figure 7.53: Normalized Pressure Drop vs. PVI; Run 4.

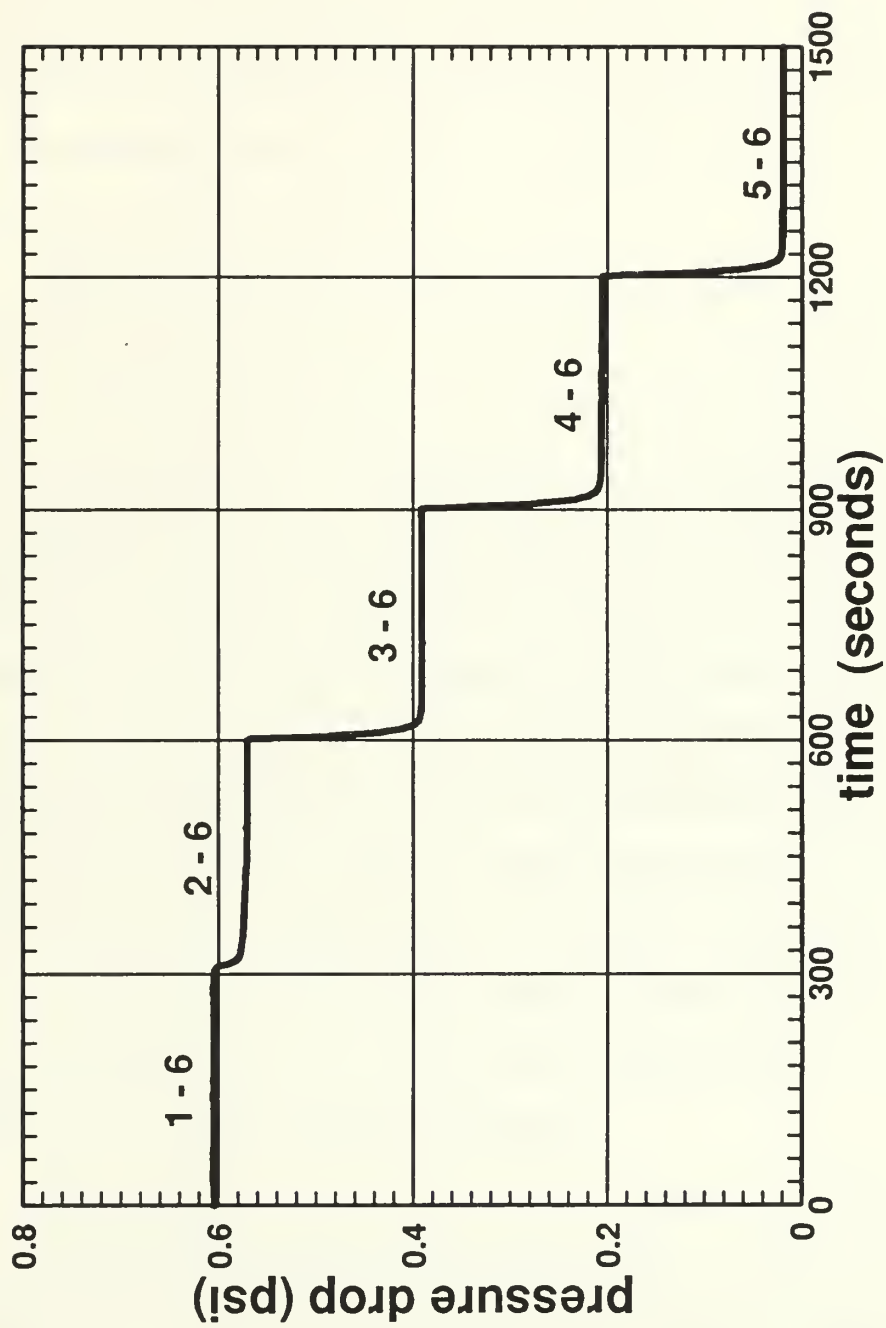


Figure 7.54: Core Linearity Check Pressure Profile; Run 5.

plateaus of the profile show the pressure drop between the labeled core taps. In this linearity test each tap along the core was opened for 5 minutes (300 seconds). Sample time was one second. The core had a maximum pressure difference of 4.2% between zones ΔP_{2-3} and ΔP_{4-5} . Other differences were 3.9% between ΔP_{2-3} and ΔP_{3-4} , and 0.4% between ΔP_{3-4} and ΔP_{4-5} .

Figures 7.55 and 7.56 are the run 5 recovery curves for benzyl alcohol and decane with the injected water. The initials of the fluids identify the recovery curves. The dots on the figures are the actual data points representing the data from each collection vessel. These data are contained in Table A.15 of Appendix A. Breakthrough of the water occurred at approximately 0.46 pore volumes injected as shown by the departure of the water recovery curve from the x-axis and the very abrupt changes in the slopes of the decane and benzyl alcohol recovery curves. The almost vertical increase of the slope of the alcohol recovery curve in Figure 7.56 at breakthrough indicates that an oil bank developed during the flood. The tangent to the recovery curve has a negative y-intercept which indicates an increase in core-end oil saturation at breakthrough. The zero slope of the decane recovery curve after breakthrough indicates that the decane was removed from the core with piston like displacement down to a residual decane saturation prior to breakthrough and hence, none was produced after breakthrough.

The saturation history of run 5 is shown in Figure 7.57. The glass bead pack was flooded with water, point (1), then flooded to residual water saturation, $S_{rw} = 2.1 \%$, with the oil phase (benzyl alcohol) at point (2). The core at residual water saturation was steady-state flooded with a specified fractional flow of 20:1 decane to oil to point (3). The saturations at point (3) are $S_d = 58.5 \%$, $S_o = 39.4 \%$, and $S_{rw} = 2.1 \%$. The glass bead pack was then dynamically water

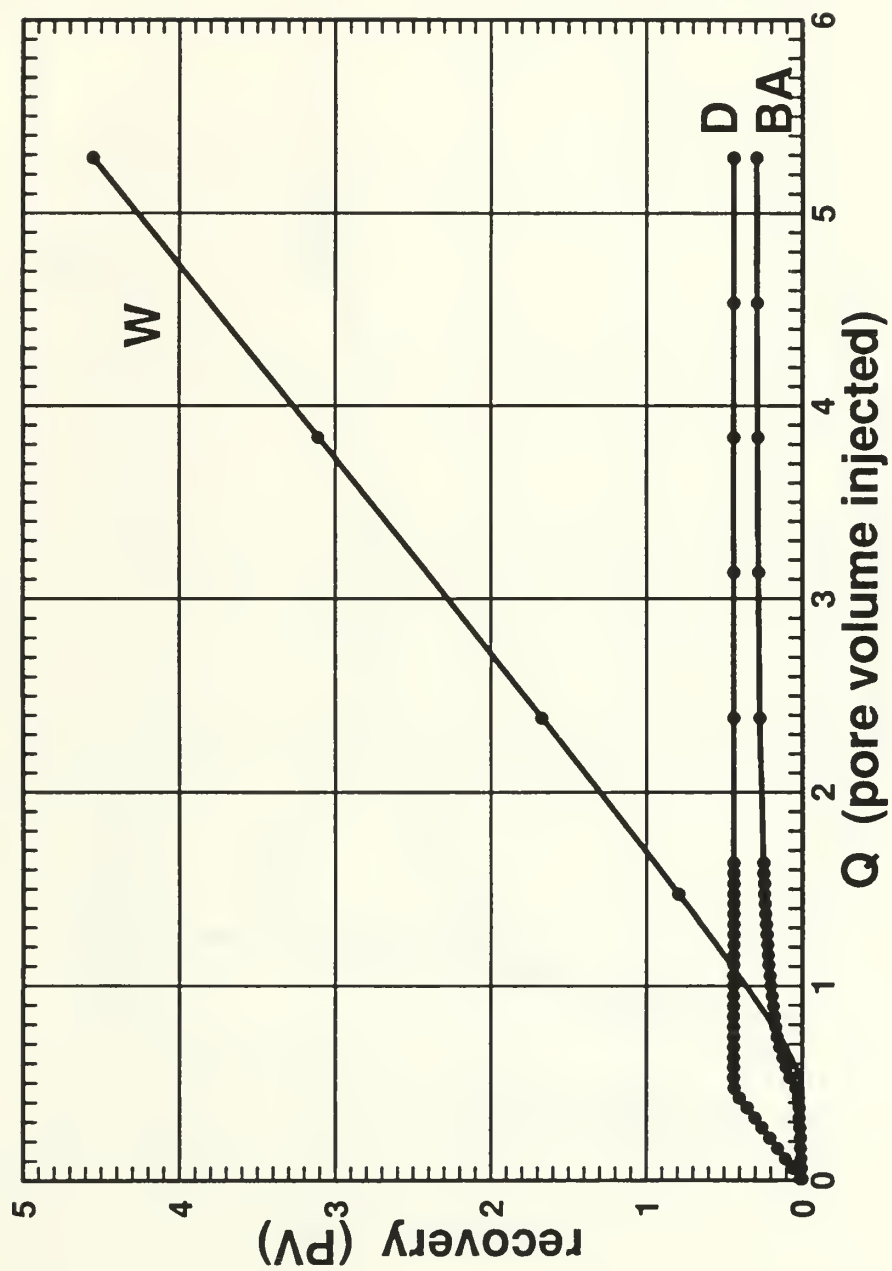


Figure 7.55: Dynamic Flood Recovery Curves; Run 5.

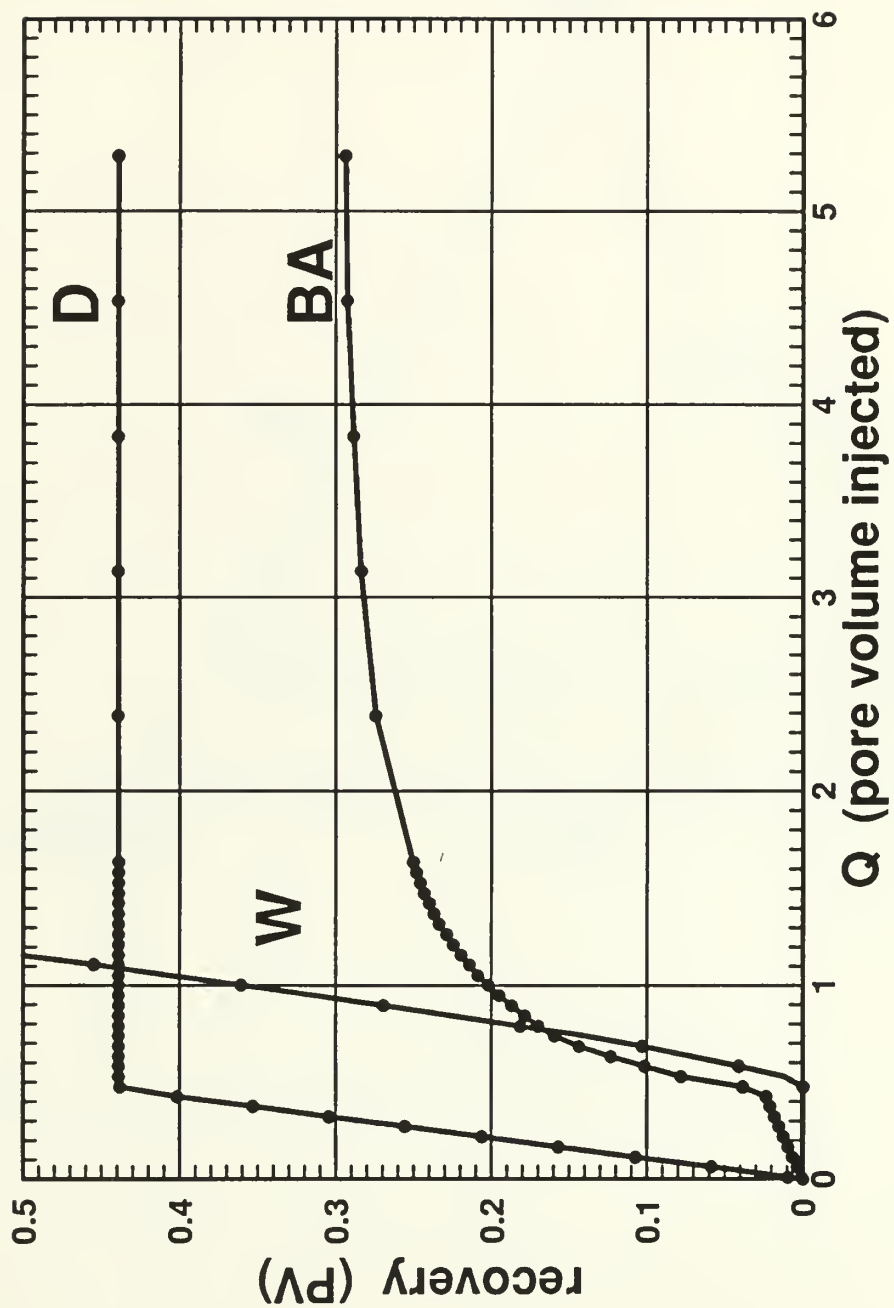


Figure 7.56: Expanded Dynamic Flood Recovery Curves; Run 5.

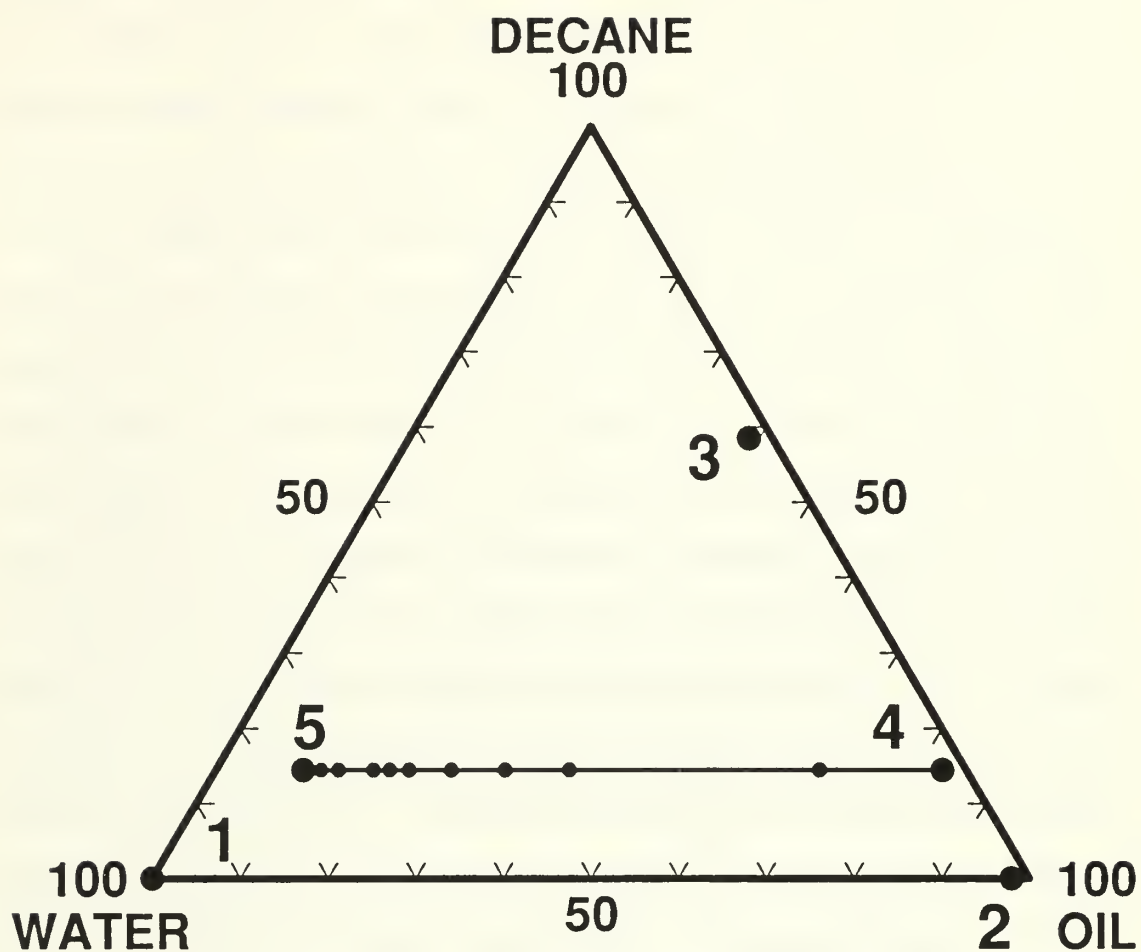


Figure 7.57: Saturation History and Trajectories; Run 5.

flooded. Core-end oil saturation at breakthrough of the Buckley-Leverett shock was $S_o = 82.8\%$, point (4). The line from point (4) to point (5) represents the continuous saturation trajectory between breakthrough and the final flood conditions at residual oil and decane saturations. The dots are the saturations calculated at various pore volumes injected. These data are contained in Table A.16 of Appendix A. The oil bank saturation jump predicted by the recovery curve of Figure 7.56 is clearly obvious in the oil saturation jump from point (3) to point (4) in Figure 7.57. This trajectory, and that in Figure 7.52, differ in two ways from the water flood of the two-phase water-oil experiment at residual decane saturation in run 9, shown in Figure 7.27. The first difference is that there is a Buckley-Leverett jump along the constant decane saturation line in Figure 7.27, and the Buckley-Leverett shock in Figures 7.52 and 7.57 occurs along the residual water saturation line. This means that there is a continuous saturation trajectory along the residual decane saturation line in Figures 7.52 and 7.57. Along this line there can be continuous relative permeability measurements. In Figure 7.27 the Buckley-Leverett jump prohibits a continuous measurement of relative permeabilities. The second difference is that the residual decane saturation line in Figure 7.27 is lower than the residual decane saturation lines in Figures 7.52 and 7.57.

The pressure drop normalized to a fixed flow rate versus the pore volumes injected plot for run 5's dynamic water flood is shown as Figure 7.58. The pressure was normalized to the single calculated actual flow set on the water pump. The pressure sample rate was one sample per second. Every one-hundred pressure points were averaged and plotted to make the pressure profile.

Oil relative permeabilities calculated from the data of the dynamic water floods of runs 4 and 5 are plotted in Figure 7.59. Water relative permeabilities calculated

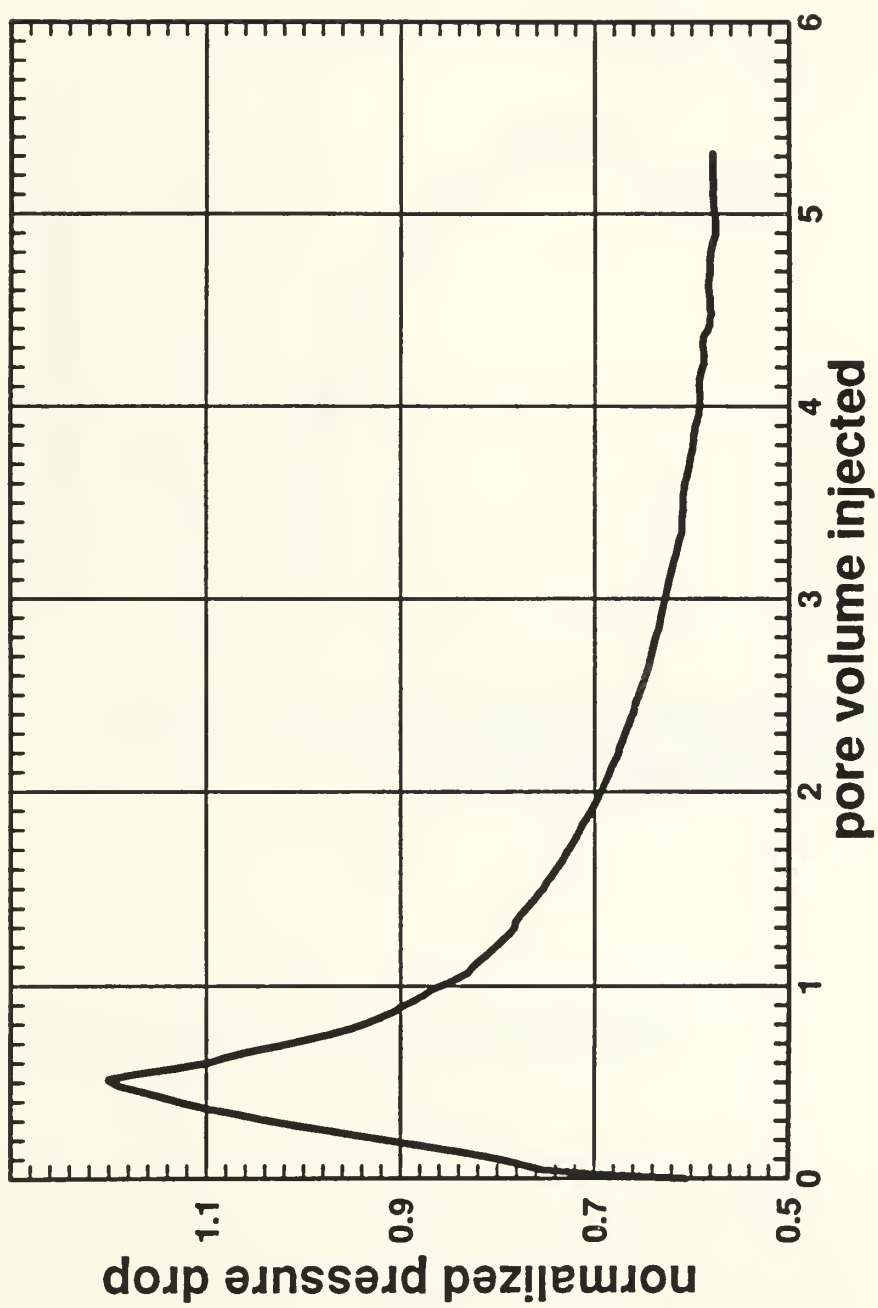


Figure 7.58: Normalized Pressure Drop vs. PVI; Run 5.

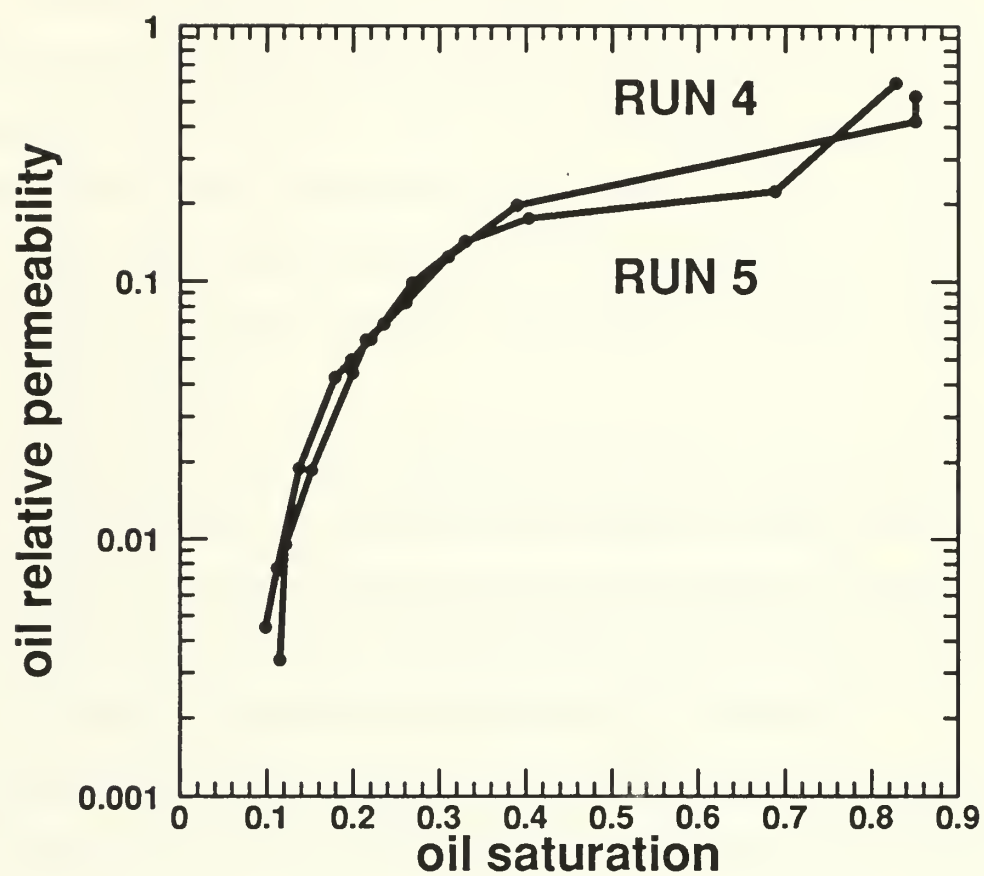


Figure 7.59: Oil Relative Permeabilities; Runs 4 and 5.

from the data of the dynamic water floods of runs 4 and 5 are plotted in Figure 7.60. As can be seen from these two figures, there is a very good match of the permeability data from runs 4 and 5. Figure 7.61 shows the oil and water relative permeabilities from the dynamic water floods of runs 4 and 5 in the conventional Cartesian plot of relative permeabilities. The points in Figures 7.59 through 7.61 are the actual relative permeability values obtained from the data at various pore volumes injected. The data for Figures 7.59 through 7.61 is listed in Table A.14 and A.16 of Appendix A.

As discussed in Section 7.3, the final portion of run 8 was a dynamic water flood of the glass bead pack from the initial conditions of residual water and oil saturations in the presence of decane down to the final conditions of residual oil and decane in the presence of water. The initial and final points of this dynamic water flood were shown to be points (5) and (6) respectively on Figure 7.35.

Figures 7.62 and 7.63 are the run 8 dynamic water flood recovery curves for benzyl alcohol and decane with the injected water. The initials of the fluids identify the recovery curves. The dots on the figures are the actual data points representing the data from each collection vessel. These data are contained in Table A.17 of Appendix A. Breakthrough of the water occurred at approximately 0.56 pore volumes injected as shown by the departure of the water recovery curve from the x-axis and the very abrupt change in the slope of the decane recovery curve. The small increase of the slope of the alcohol recovery curve at breakthrough indicates that a small oil bank developed during the flood. The tangent to the recovery curve has a negative y-intercept which indicates a slight increase in core-end oil saturation at breakthrough. As with the recovery curves of the decane in runs 4 and 5, the zero slope of the decane recovery curve after breakthrough indi-

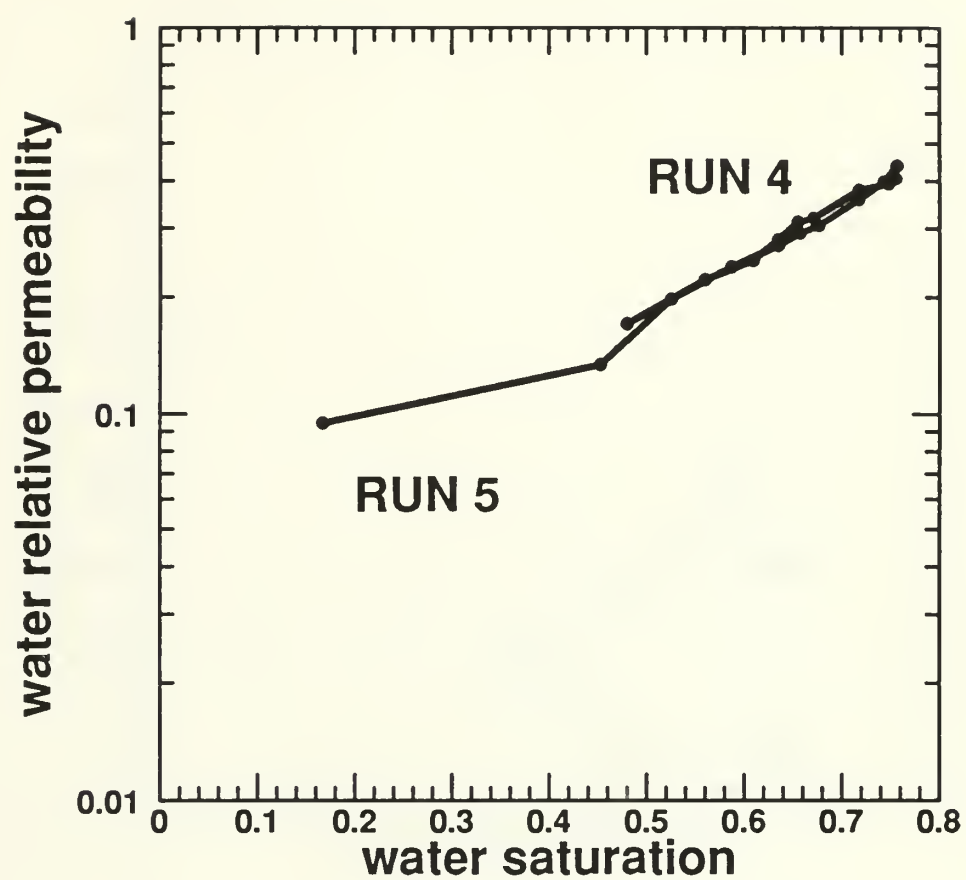


Figure 7.60: Water Relative Permeabilities; Runs 4 and 5.

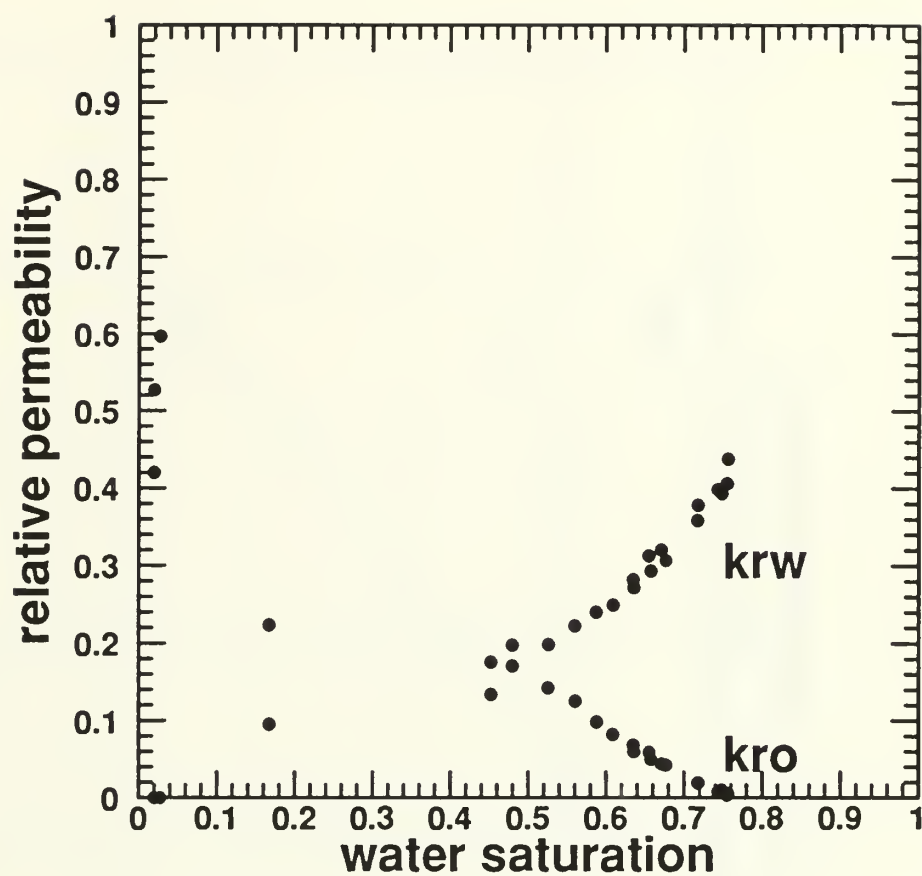


Figure 7.61: Oil and Water Relative Permeabilities; Runs 4 and 5.

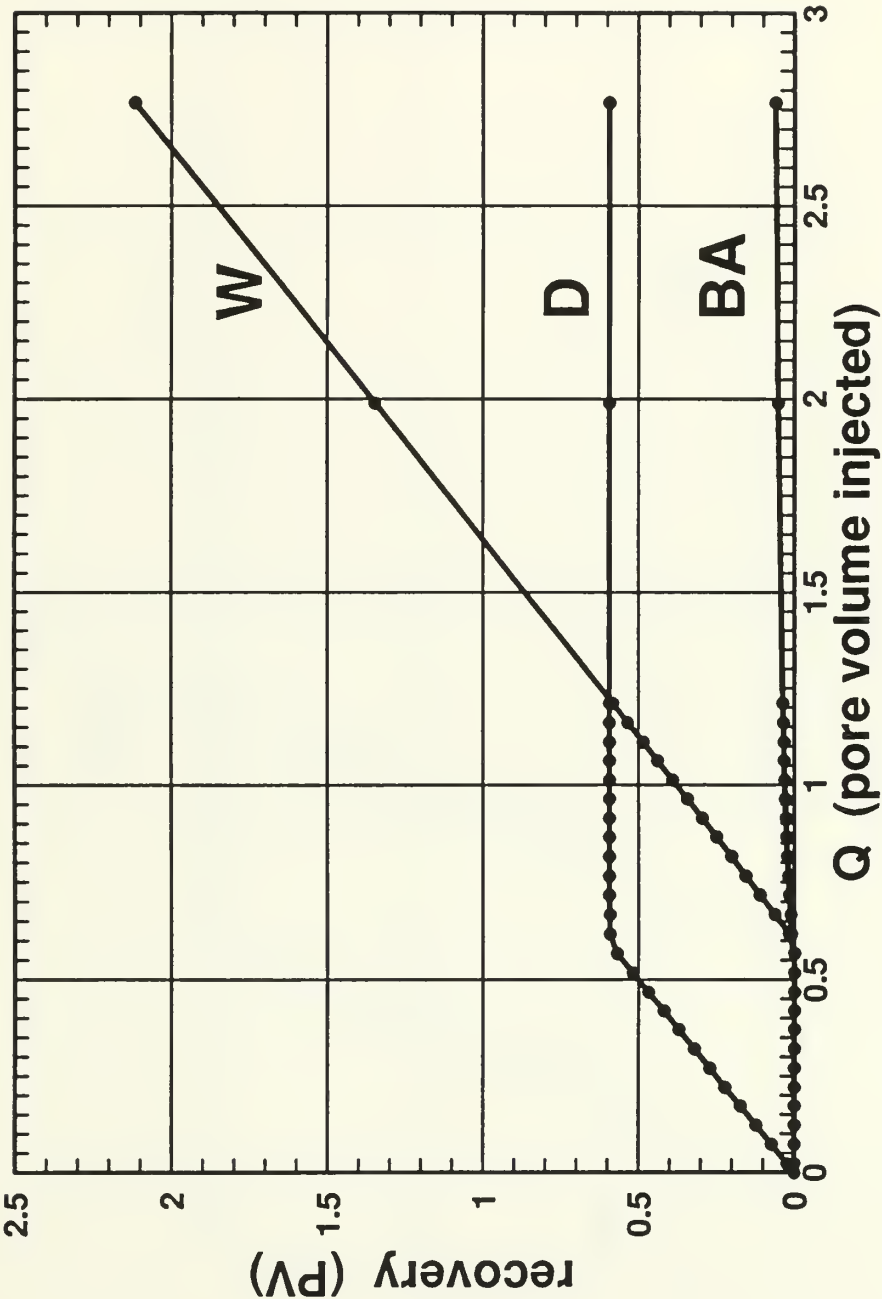


Figure 7.62: Dynamic Water Flood Recovery Curves; Run 8.

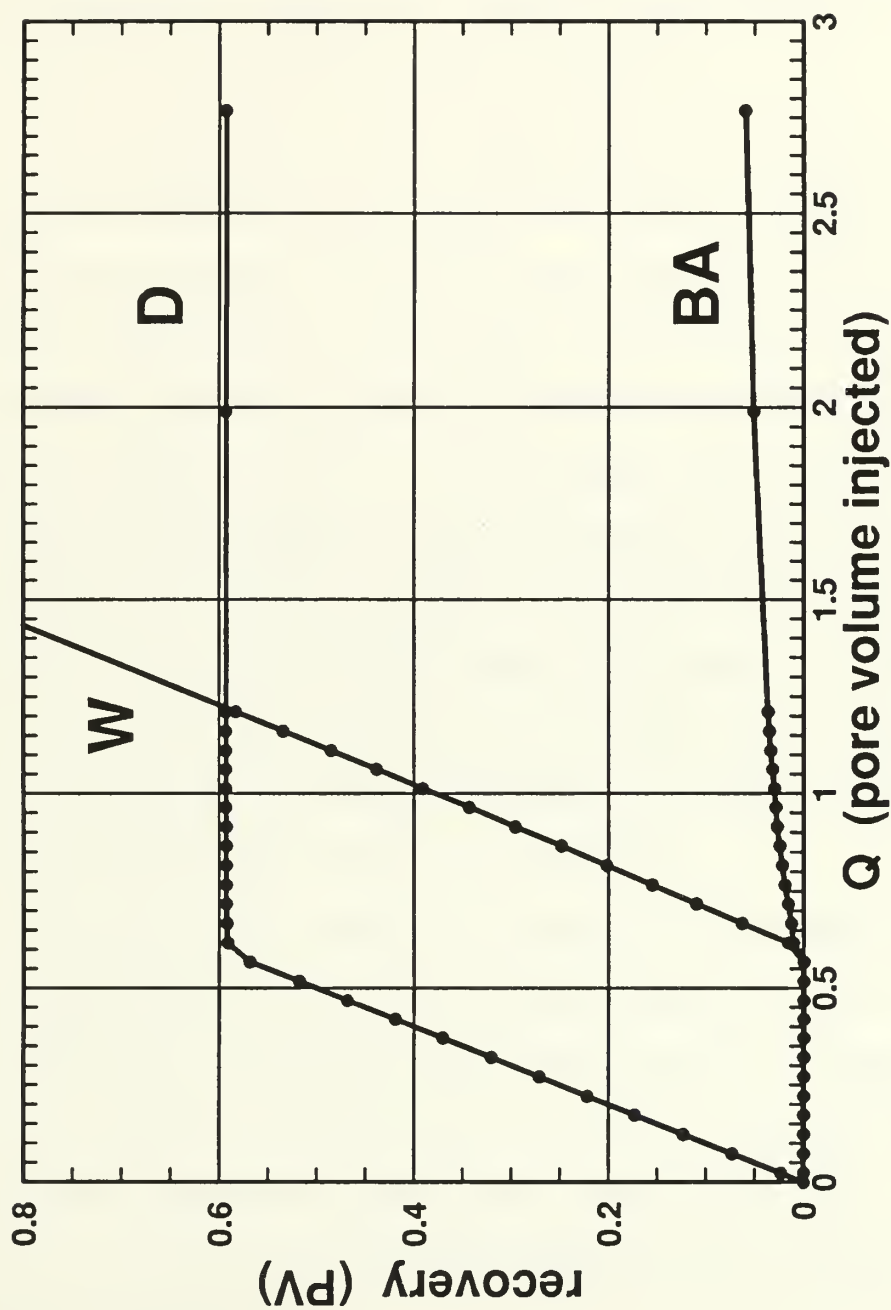


Figure 7.63: Expanded Dynamic Water Flood Recovery Curves; Run 8.

cates that the decane was removed from the core with piston like displacement down to a residual decane saturation prior to breakthrough, and therefore, no decane was produced after breakthrough. It should be noted that the oil bank formed in runs 4 and 5 is more significant than the bank of run 8.

The saturation history of run 8's dynamic water flood is shown in Figure 7.64. The glass bead pack was taken from the final conditions of residual oil and water in the presence of decane after the run 8 dynamic decane flood, point (1), to residual oil and decane saturation in the presence of water, point (3) through a dynamic water flood. Core-end oil saturation at breakthrough of the Buckley-Leverett shock, point (2), was $S_o = 20.7 \%$. The line from point (2) to point (3) represents the continuous saturation trajectory between breakthrough and the final flood conditions at residual oil and decane saturations. The small oil bank saturation increase predicted by the recovery curve of Figure 7.63 is seen in the oil saturation jump from point (1) to point (2). No decane was produced between points (2) and (3). The dots represent the saturations calculated at various pore volumes injected. These data are contained in Table A.18 of Appendix A.

The pressure drop normalized to a fixed flow rate versus the pore volumes injected plot for run 8's dynamic water flood is shown as Figure 7.65. The pressure was normalized to the single calculated actual flow set on the water pump. The pressure sample rate was one sample per second. Every one-hundred pressure points were averaged and plotted to make the pressure profile. The very small slope of the curve after breakthrough corresponds to the very little amount of oil produced after breakthrough.

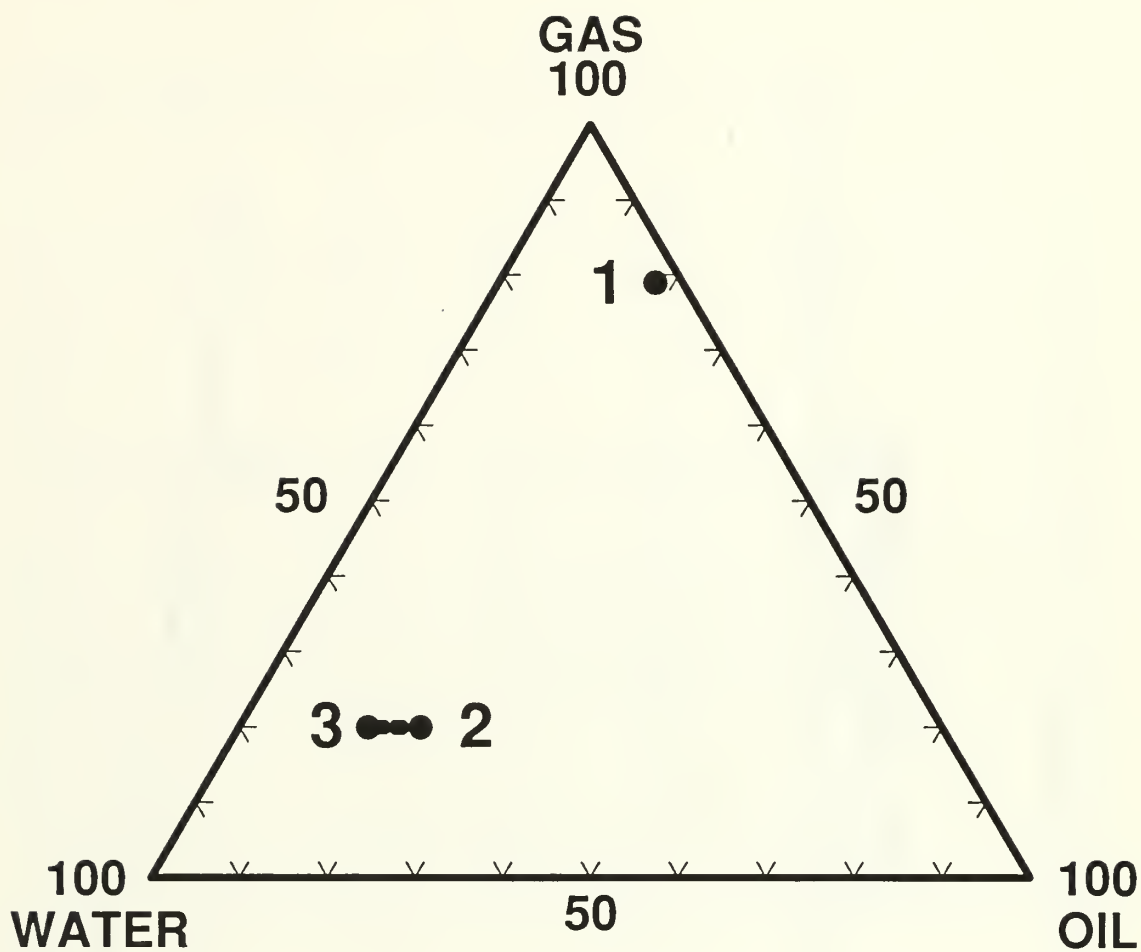


Figure 7.64: Saturation History and Trajectories; Run 8 - Dynamic Water Flood.

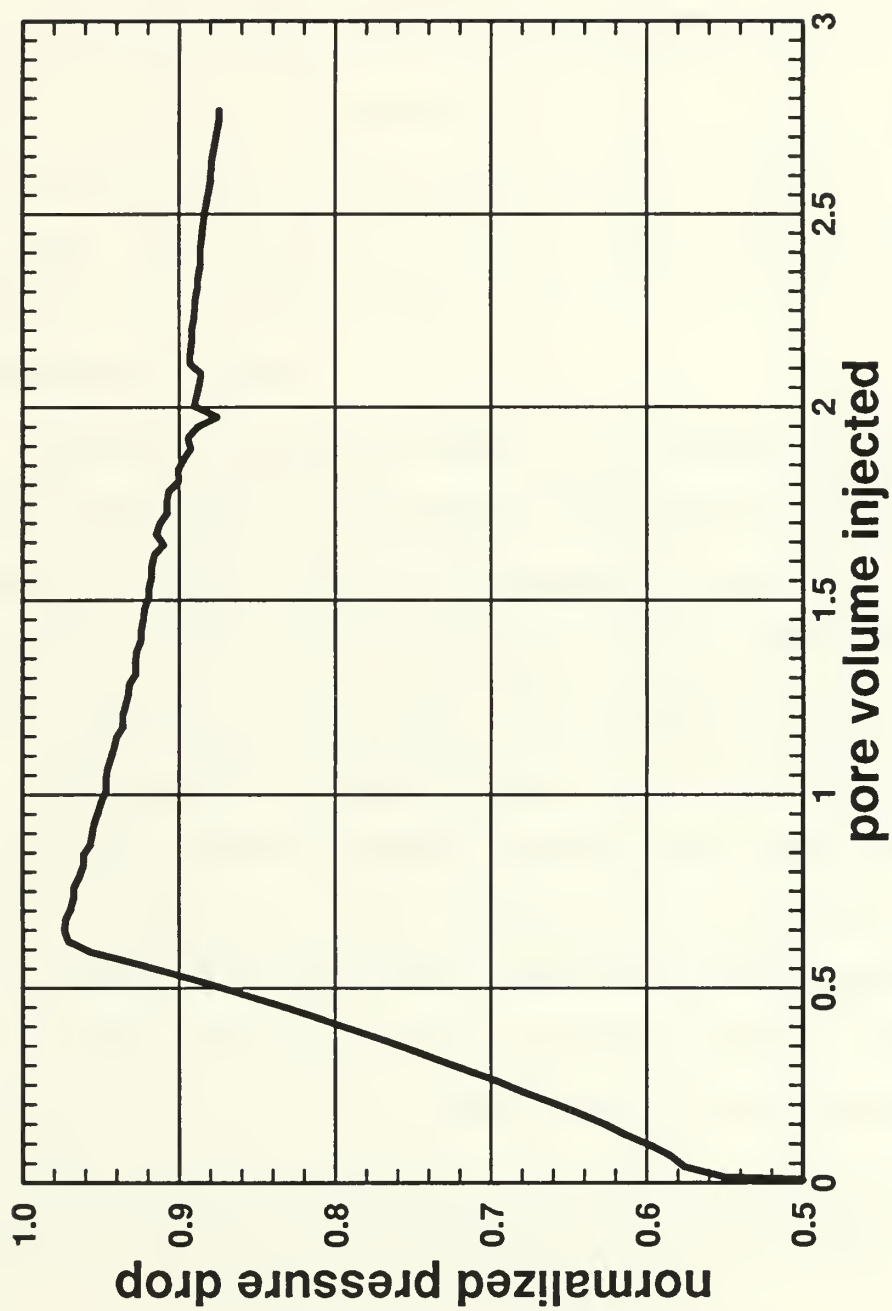


Figure 7.65: Normalized Pressure Drop vs. PVI; Run 8 - Dynamic Water Flood.

7.5 Unacceptable Core Linearity Runs

Runs 6 and 7 were not continued after initial core flooding because of core linearity problems. Figure 7.66 is the pressure profile of the core linearity check for run 6. The plateaus of the profile show the pressure drop between the labeled core taps. In this linearity test each tap along the core was opened for five minutes (300 seconds). Sample time was one second. The core had a maximum pressure difference of over 400% between zones ΔP_{2-3} and ΔP_{4-5} . This exceeded the allowed 10% difference.

Figure 7.67 is the pressure profile of the core linearity check for run 7. The plateaus of the profile show the pressure drop between the labeled core taps. In this linearity test each tap along the core was opened for five minutes (300 seconds). Sample time was one second. The core had a maximum pressure difference of over 220% between zones ΔP_{2-3} and ΔP_{4-5} . This exceeded the allowed 10% difference.

The permeability nonlinearity of these packs is probably caused by settling of the glass beads and fluid bypassing the glass bead pack along the pack/case interface. This explanation is further substantiated by the following two observations. While flowing water through the core, tapping the core lightly produced a reduction in the pressure differential read out, this could be caused by unsettling the glass bead pack. When the cores were opened to remove the glass beads and clean the core, there was a void approximately 1/4-inch deep at the upstream end of the core, this would have allowed the glass bead packs to expand and unsettle.

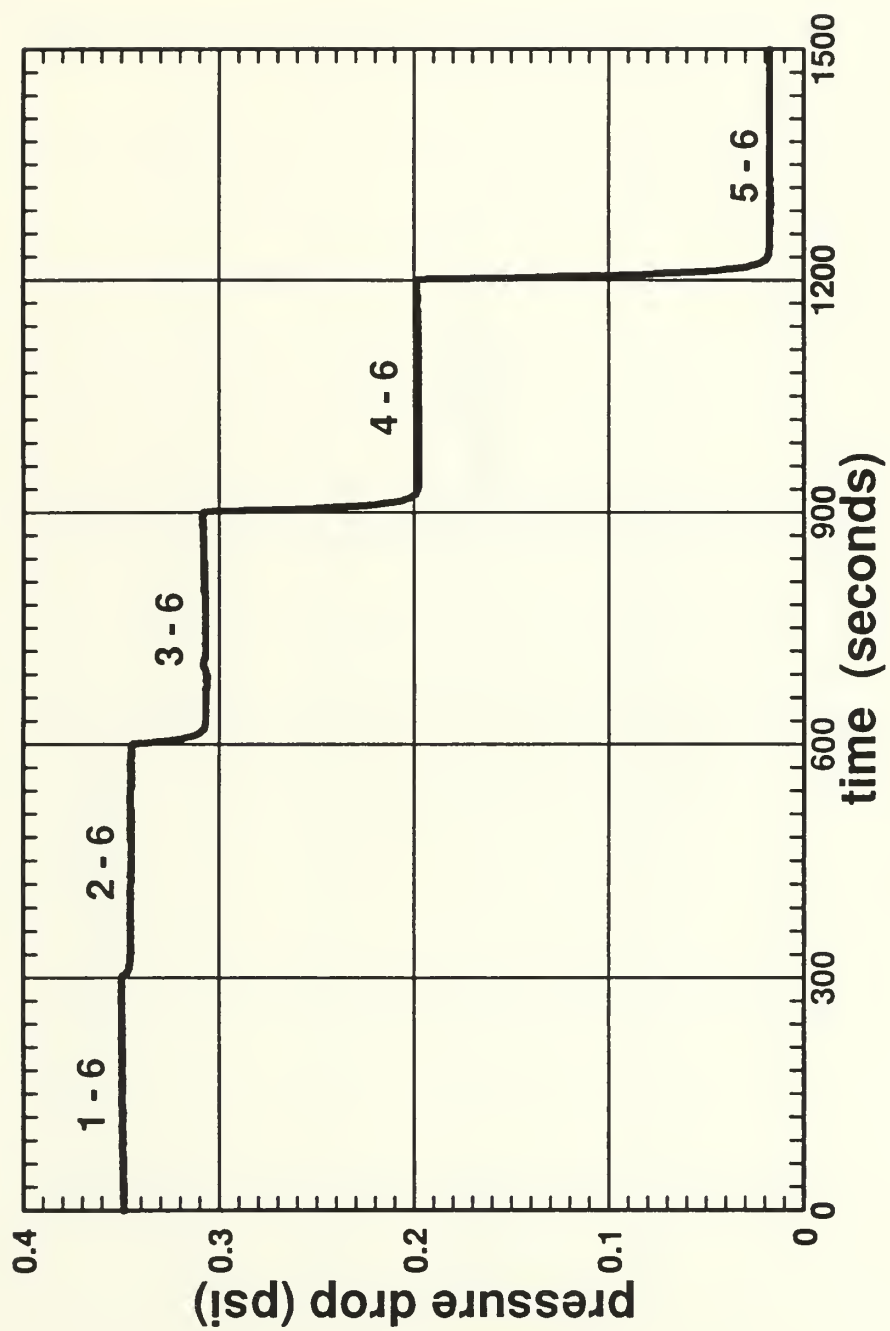


Figure 7.66: Core Linearity Check Pressure Profile; Run 6.

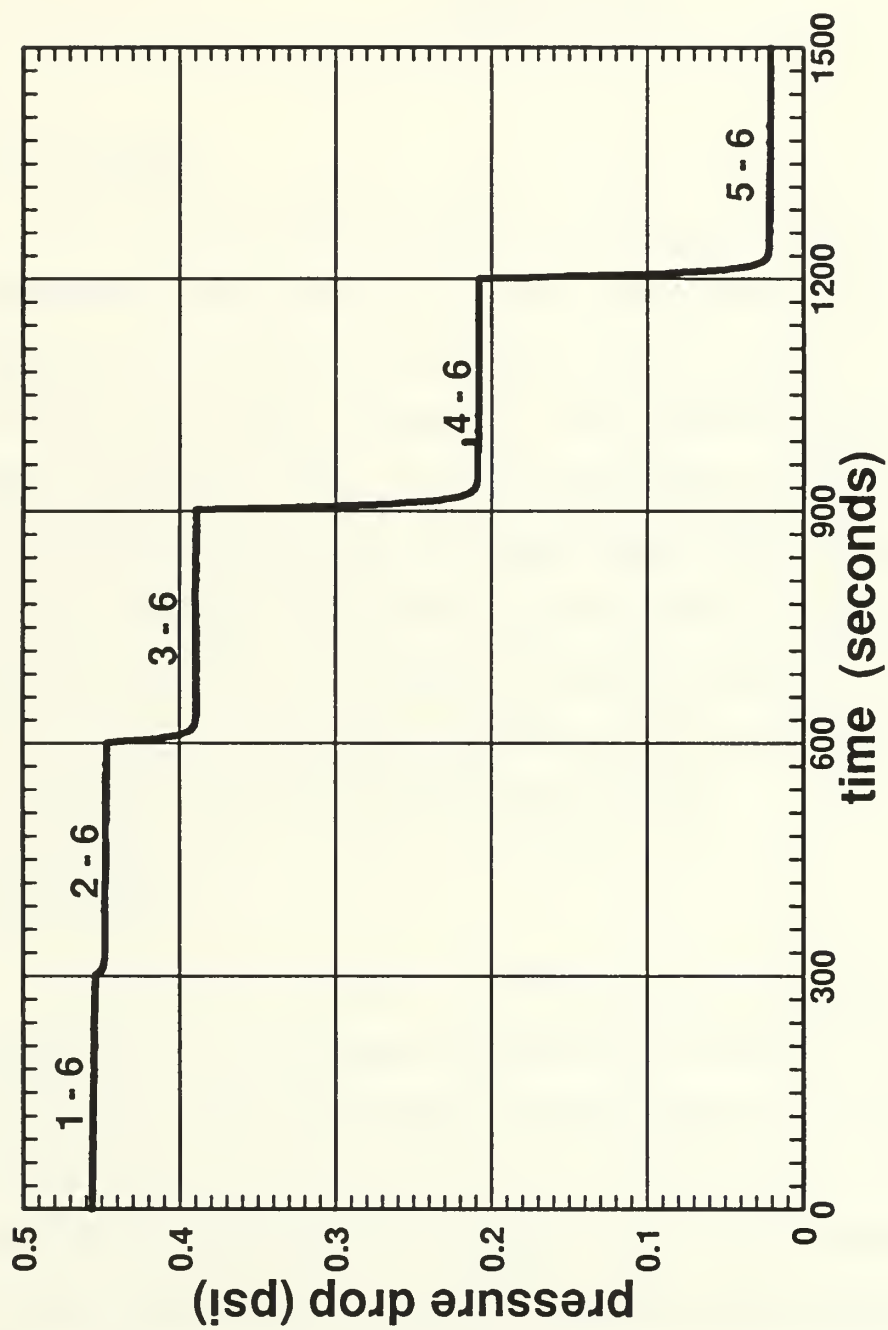


Figure 7.67: Core Linearity Check Pressure Profile; Run 7.

Chapter 8

DISCUSSION

8.1 Verification

The initial portion of the research is concerned with decane flooding and the verification of previous work. This work is accomplished in runs 2 and 3. The uncertainty in the linearity of the core used in run 2 (see Figure 7.1), resulted in run 3 being used to verify the apparatus. Run 3 reproduced results and trends of Grader and O'Meara (1988). The initial core saturation of run 3 is very close to run 15 of the work reported by Grader and O'Meara (1988). The saturation trajectory of run 3 (Figure 7.9) indicates a good match with the saturation trajectory of their (1988) run 15. This comparison of saturation trajectories is shown in Figure 8.1. In Figure 8.1, the saturation trajectories of run 3 and Grader and O'Meara's run 15 are represented by curves A and B respectively.

8.2 Apparatus

The apparatus is capable of the flexibility that was designed into it. Both steady-state and non-steady-state experiments are conducted under a variety of injected fluid scenarios. The apparatus showed the ability to reproduce results. An example of this is seen by the repeat of run 9's first dynamic water flood in the second run 9 water flood. The comparison of the relative permeabilities of these two runs (Figure 7.26), the comparison of the pressure drops normalized to the variable flow rate (Figures 7.18 and 7.24), and the comparison of the recovery curves (Figures 7.16 and 7.22) indicate close agreement.

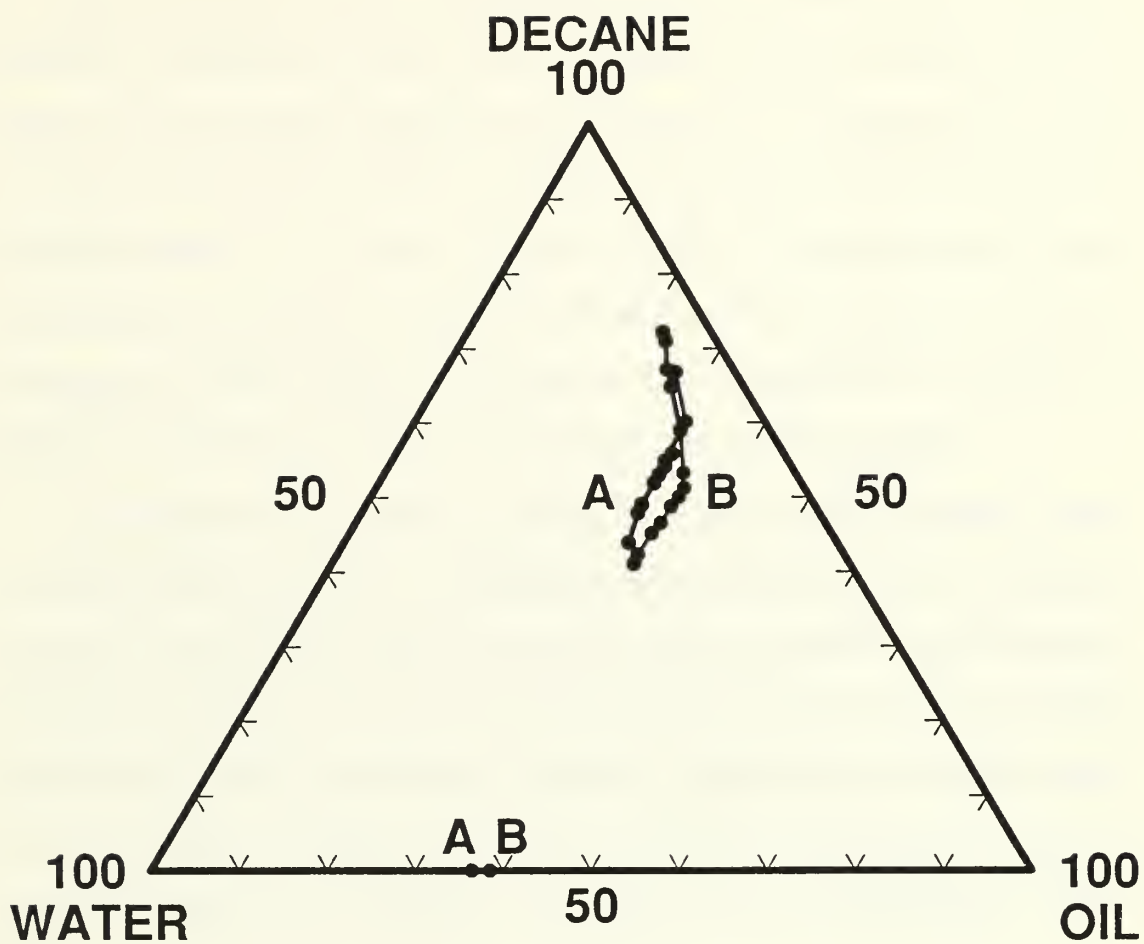


Figure 8.1: Comparison of Saturation Trajectories;
Run 3 (marked as A) vs. Grader and O'Meara (1988) Run 15
(marked as B).

Some limitations shown by the apparatus are seen in the inability to obtain a continuous three-phase recovery curve. This differs from the pressure recovery curve where a data point is obtainable every second with very good resolution. The pressure recovery curve is nearly continuous. A source of error and a bottleneck in the data analysis is the fact that the data analysis is not automated. Recovery curve and normalized pressure curve slopes are taken by hand. Future improvements to the apparatus should include the addition of these modifications to expedite the analysis and also reduce some of the error associated with hand analysis.

Achieving uniform packing of the glass bead core is the most difficult step in the experimental procedure. The acceptable linear pressure drop of an individual core did not mean that the core is the same in terms of porosity and absolute permeability as other cores. This variance among the cores should account for most of the difference between similar terms calculated in different runs. It cannot account for the difference of similar terms calculated within the same run, i.e. using the same core. Table A.19 of Appendix A lists some of the core characteristics of each run.

8.3 Exploratory Findings

The dynamic water floods of runs 4, 5, 8, and 9 are the new areas of investigation conducted by this research. The objective of mapping relative permeabilities in the interior region of the three-phase ternary diagram is not achievable through dynamic water floods. The flooding of the glass bead pack at residual water saturation and several combinations of decane and benzyl alcohol saturation, resulted in the development of an oil bank and subsequent bypassing of the interior region of the ternary diagram during the flood. As can be seen on the dynamic flood recovery curves of runs 4 and 5 (Figures 7.51 and 7.56), the water flood displaced

the decane to its dynamic residual saturation at breakthrough. The Buckley-Leverett oil saturation jump at breakthrough, caused by the development of the oil bank, can be seen on the saturation trajectories of runs 4 and 5 (Figures 7.52 and 7.57). Figures 7.52 and 7.57 clearly show that the interior region of the ternary diagram is bypassed.

During the water flood and the development of the oil bank prior to breakthrough, two saturation shocks did not develop as may have been expected. The water saturation behind the oil front is continuous, in other words, at breakthrough both oil and water are produced. The results did not show 100% oil production followed by the appearance of water. Figures 8.2 through 8.4 show the core saturation profiles at breakthrough for runs 4, 5 and 8 respectively. The data for Figures 8.2, 8.3 and 8.4 are contained in Tables A.14, A.16, and A.18, respectively. It may appear in Figure 8.2 that a water shock developed. This is not the case, however, as the recovery data in Table A.13 shows that a small amount of water is produced at breakthrough. The resolution of the graph is such that one cannot see the water saturation increase until the dimensionless position of 0.72. The increased initial saturation of the benzyl alcohol may be the cause of the apparent lack of initial water production in run 4. Figures 8.2 through 8.4 show that a significant oil bank is developed, even in the case of Figure 8.4 where the water flood was initiated at a low benzyl alcohol saturation.

The development of the oil bank, and the resulting increase in oil saturation at breakthrough in runs 4 and 5, enabled the relative permeabilities to be measured along a continuous saturation trajectory. This is in contrast to the water flood experiment at residual decane saturation conducted in run 9. This experiment had a jump in the saturation trajectory along the residual decane saturation line resulting

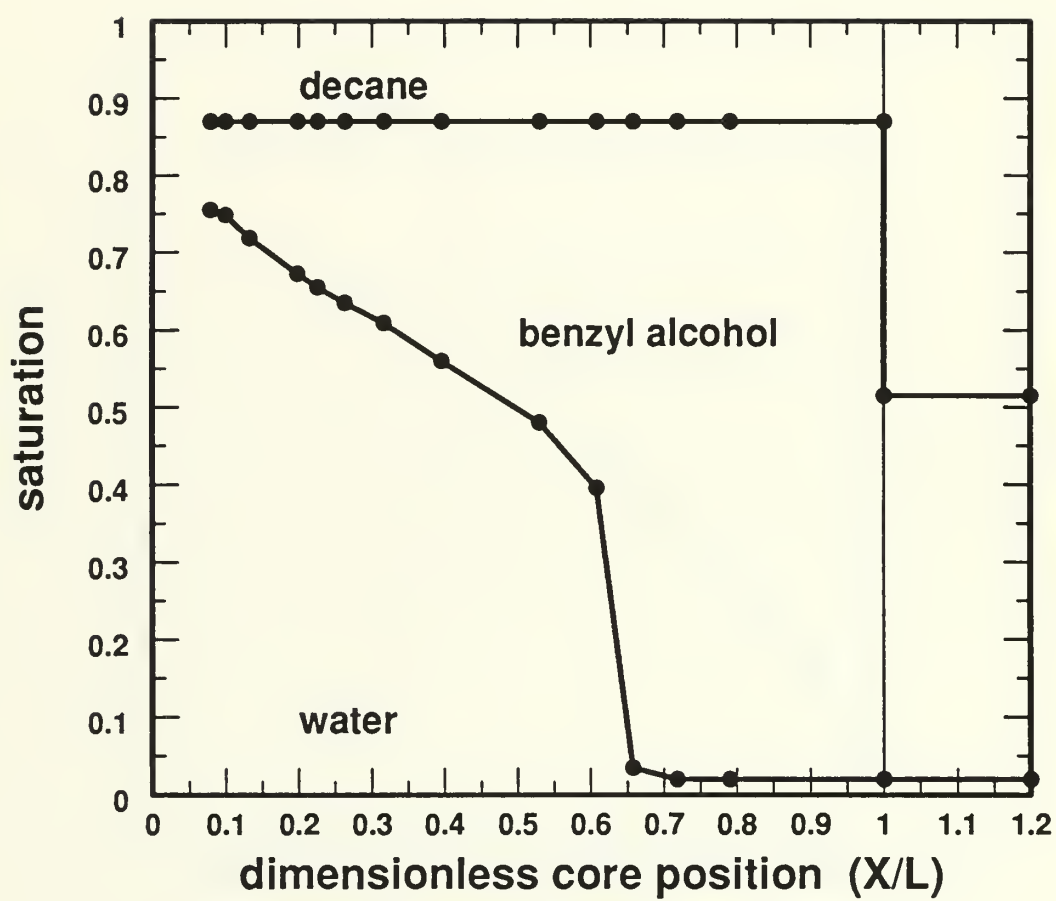


Figure 8.2: Core Saturation Profile at Breakthrough; Run 4

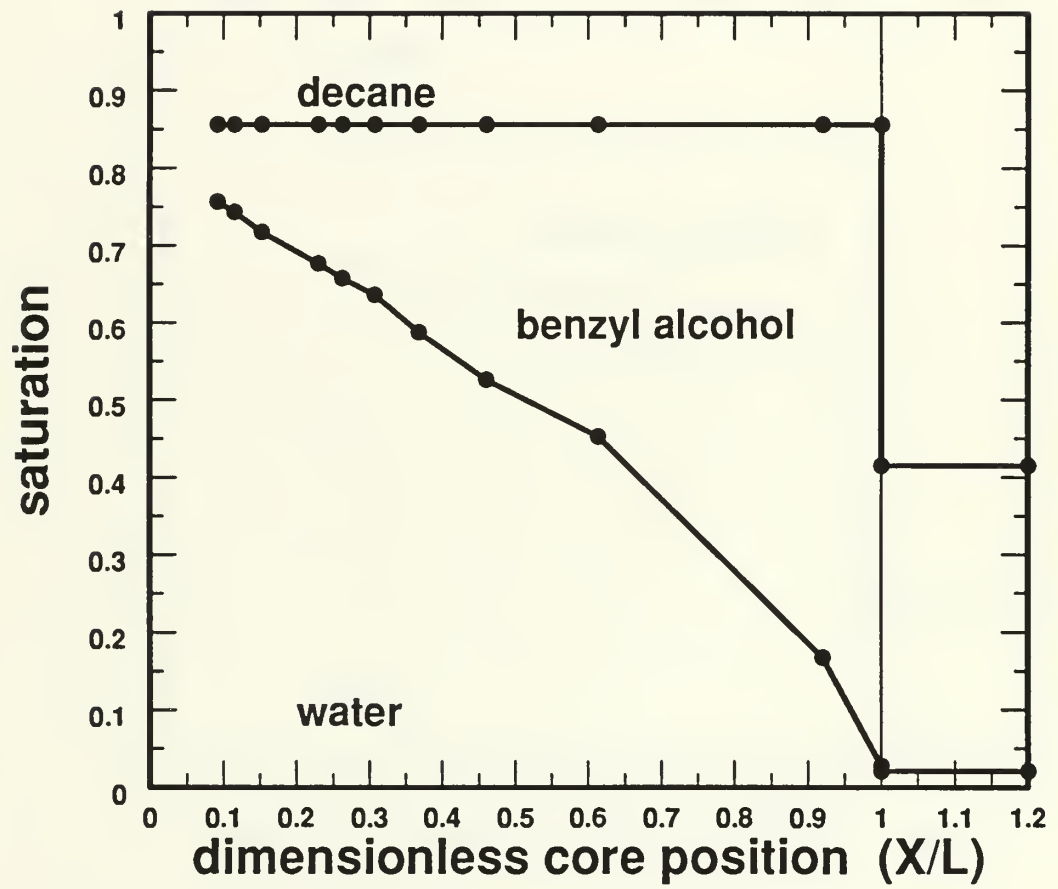


Figure 8.3: Core Saturation Profile at Breakthrough; Run 5

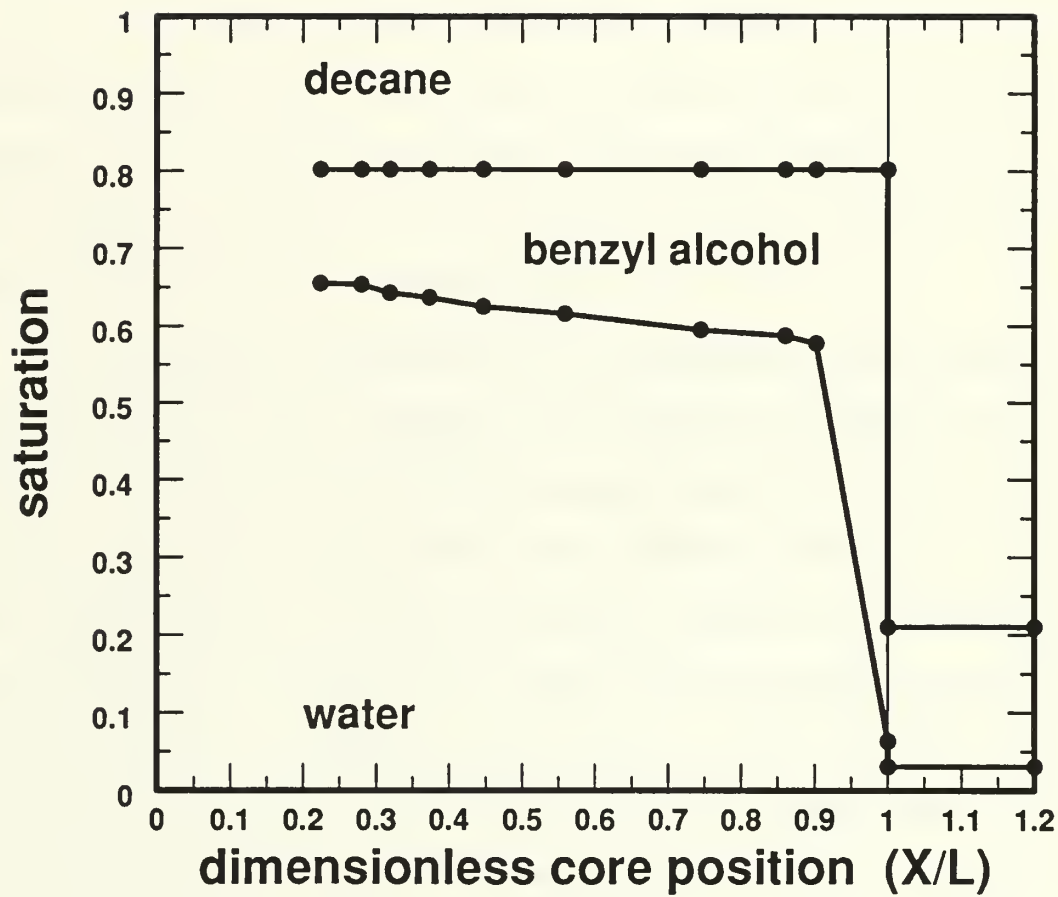


Figure 8.4: Core Saturation Profile at Breakthrough; Run 8

in the inability to dynamically measure the relative permeabilities in that region. These differences can be seen in the saturation trajectories shown in Figures 7.27, 7.52 and 7.57.

Of interest in the comparison of the dynamic water floods of runs 4 and 5 with the water flood of the core at residual decane saturation in run 9, is the difference between the end decane saturations. The residual decane saturation arrived at by steady-state flooding in run 9 is lower than the dynamic residual decane saturation achieved by water flooding in runs 4 and 5. This is seen in Figures 7.52 and 7.57 when compared to Figure 7.27. It is unclear if this is a phenomenological occurrence, or if it is due to experimental error.

There are minimal hysteresis effects in the comparison of the relative permeabilities at residual water saturation in the drainage and imbibition series of steady-state experiments and the drainage dynamic decane flood. As seen in Figure 7.48, the oil relative permeabilities are not noticeably different in any of the runs, whether determined by steady-state or dynamic experiments. The decane relative permeability curve differed slightly in slope during the drainage and imbibition series of steady state experiments as seen in Figure 7.41. When compared with the dynamic flood, the decane relative permeability curves maintained their relative shapes and slopes, but are positioned slightly above the dynamic flood generated curve. This can be seen in Figure 7.47.

Run 9 showed some shifting of the water and benzyl alcohol relative permeability curves when decane is present at residual saturation. As shown in Figure 7.33, the relative permeability curves of both the water and benzyl alcohol in the presence of residual decane (B and D) dropped below the curves generated when just the water and benzyl alcohol are present (A and C). This lower curve shifting

in the presence of decane is expected. The oil curve showed a more pronounced shift than did the water curve in the presence of residual decane. The reason for the increased shift in the oil curve over the water curve is unknown.

8.4 Questions Raised From the Research

Several major questions arose from the project's findings. Future work needs to be done on determining the reason for the development of the oil bank and why there is a change in the residual decane saturation between dynamic and steady-state water floods. Work needs to be done to see if there is some fluid flow mechanism that is responsible for these observations.

The interior of the ternary diagram could not be mapped with dynamic water floods. A topic of future work will be to determine how to map this interior region. Steady-state experiments may be required.

8.5 Implications

The extension of the two-phase theory to three phases is validated by the exact graphical matching of the core-end saturation change between the displaced decane and the oil bank in the dynamic water floods of runs 4 and 5. Examination of Figure 7.51, the expanded recovery curve of run 4's dynamic water flood, is an example of this validation. The y-intercept of the tangent to the oil recovery curve at breakthrough is -0.36 , this represents a saturation increase of 36% in the benzyl alcohol. The extension of the flat decane recovery curve intercepts the y-axis at 0.36 , this indicates a decrease in decane saturation of 36%. The saturation changes are equal, the decane is replaced by the benzyl alcohol. In addition, the independent flow-rate portion of the theory is validated by the unintentional flow-rate change seen in the first two dynamic water floods of run 9. As seen in Figure 7.19, the

normalized pressure profile is not affected by flow-rate changes if they are incorporated into the calculation of Φ . The inclusion of the flow rate in the normalized pressure drop, Φ , is permitted only in the cases where gravity effects are neglected.

This research provides directions for future mapping of the three-phase diagram. If the phenomenon of a self-sharpening oil bank is true, it will have an impact on oil recovery. It may be beneficial to increase the gas saturation in the reservoir prior to a water flood in order to facilitate the development of an oil bank.

Chapter 9

CONCLUSIONS AND RECOMMENDATIONS

An experimental investigation of the simultaneous motion of three phases within porous media is conducted with the purpose of quantifying and qualifying immiscible three-phase relative permeabilities. This research is exploratory in nature and intended to indicate trends, provide a background for further research, and generate generic data for use in any field or discipline dealing with the flow of three phases through a porous medium.

It is found that the interior region of the three-phase ternary diagram cannot be mapped with dynamic water floods when starting at residual water saturation. It is discovered during water floods originating along the residual water iso-saturation line, that an oil bank develops in front of the advancing water front and drives the decane out of the core with piston-like displacement, bypassing the interior region of the diagram. This will have an impact on the future directions taken in mapping the three-phase diagram and may have ramifications in the area of oil recovery.

Grader and O'Meara's extension of the two-phase Welge and JBN dynamic displacement theories to three-phases appears valid. This is shown by the equivalent saturation changes of the decane and benzyl alcohol graphically determined in the dynamic water flood recovery curves of runs 4 and 5.

Directions indicated for future investigation by this research include:

- Perform the experiments, and determine the saturations using the CAT scanner. The independent saturation determination will provide the ultimate validation of the extension of the Welge/JBN theory.

- Attempt to map the interior region of the three-phase diagram by originating the dynamic water flood from a point in the the three-phase diagram where mobile water exists. Conduct dynamic oil floods in an attempt to enter the interior of the diagram. Utilize steady-state experiments to reach saturations in the interior of the diagram unreachable by dynamic floods.
- Conduct more research in the area of the hysteresis experienced during water floods conducted at and above steady-state residual decane saturation.
- Examine the effects of a consolidated core using the same fluids used in the glass bead pack experiments.
- Introduce an actual gas phase, such as nitrogen, into the idealized glass bead packed core and determine the effects of the differing interfacial tensions of the fluids on relative permeability-saturation relationships.

REFERENCES

- Baker, L. E.: "Three-Phase Relative Permeability Correlations," Paper SPE/DOE 17369, presented at the EOR Symposium, Tulsa, OK, April 17-20, 1988.
- Caudle, B.H., Slobod, R.L., and Brownscombe, E.R.: "Further Developments in the Laboratory Determination of Relative Permeability," *Trans. AIME* (1951) 145-150.
- Corey, A. T., Rathjens, C. H., Henderson, J. H., and Wyllie, M. R. J.: "Three-Phase Relative Permeability," *J. Pet. Tech.*, (Nov. 1956) 63-65.
- Darcy, H.: *Les Fontaines Publiques de la Ville de Dijon*, Dalmount, Paris (1856).
- Donaldson, E. C., and Dean, G. W.: "Two- and Three-Phase Relative Permeability Studies," RI6826, USBM (1966), 23 pp.
- Donaldson E. C, and Kayser, B. M: "Three Phase Flow in Porous Media," DOE/BETC/IC-80/4, (April 1981).
- Grader, A.S. and O'Meara, D.J. Jr.: "Dynamic Displacement Measurements of Three-Phase Relative Permeabilities Using Three Immiscible Liquids," paper SPE 18293 presented at the 63th Annual Tech. Conf. and Exhib. of SPE, Oct. 2-5, 1988, Houston, TX.
- Honarpour, M, Koederitz, L, and Harvey, A. H.: "Relative Permeability of Petroleum Reservoirs", CRC Press, 1986, Second Edition.
- Johnson, E. F., Bossler, D. P., and Naumann, V. O.: "Calculation of Relative Permeability from Displacement Experiments," *Trans.*, AIME (1959) 216, 370.
- Jones, S. C., and Roszelle, W. O.: "Graphical Techniques for Determining Relative Permeability from Displacement Experiments," *J. Pet. Tech.*, 5, 807, 1978.
- Leverett, M. C., and Lewis, W. B.: "Steady Flow of Gas-Oil-Water Mixtures Through Unconsolidated Sands," *Trans.*, AIME (1941) 142, 107-116.
- Oak, M. J., Baker, L. E., and Thomas, D. C.: "Three-Phase Relative Permeability of Berea Sandstone," Paper SPE/DOE 17370, presented at the EOR Symposium, Tulsa, OK, April 17-20, 1988.
- Obut, Tina Saxon: "Two-Phase High Velocity Flow Through Porous Media: Near-Wellbore Domain," Master of Science Thesis, Petroleum and Natural Gas Section, The Pennsylvania State University, 1989.
- Saraf, D. N., Batycky, J. P., Jackson, C. H., and Fisher, D. B: "An Experimental Investigation of Three-Phase Flow Water/Oil gas Mixtures Through Water-Wet Sandstones," Paper SPE 10761, presented at the annual California Regional Meeting (March 1983), 24-26.

- Sarem, A. M.: "Three-Phase Relative Permeability Measurements by Unsteady-State Method," *Soc. Pet. Eng. J.*," (Sept. 1966) 6, 199-205.
- Snell, R. W.: "Three-Phase Relative Permeability in an Unconsolidated Sand," *J. Inst. Pet.*, (March 1962) 48, 80-88.
- Welge, H. J.: "Displacement of Oil from Porous Media by Water and Gas," *Trans., AIME* (1950) **198**, 314-316.

Appendix A
TABULATED RUN DATA

Table A.1
Fractional Collection Analysis Summary;
Run 2

tube no.	tube oil vol. (cc)	tube water vol. (cc)	tube decane vol. (cc)	cum. oil vol. (cc)	cum. water vol. (cc)	cum. decane vol. (cc)	total fluid vol. (cc)	oil rec. (PVI)	water rec. (PVI)	decane rec. (PVI)	PVI
1	4.10	2.97	0.	4.10	2.97	0.	7.07	0.03	0.02	0.	0.05
2	4.75	4.05	1.95	8.85	7.02	1.95	17.82	0.07	0.05	0.01	0.13
3	4.30	3.80	2.65	13.15	10.82	4.60	28.57	0.10	0.08	0.03	0.21
4	3.90	3.70	2.80	17.05	14.52	7.40	38.97	0.13	0.11	0.05	0.29
5	3.85	2.85	3.80	20.90	17.37	11.20	49.47	0.16	0.13	0.08	0.37
6	2.80	2.10	5.80	23.70	19.47	17.00	60.17	0.18	0.14	0.13	0.45
7	1.60	2.05	7.35	25.30	21.52	24.35	71.17	0.19	0.16	0.18	0.53
8	1.05	2.15	7.60	26.35	23.67	31.95	81.97	0.20	0.18	0.24	0.61
9	1.10	1.95	7.90	27.45	25.62	39.85	92.92	0.20	0.19	0.30	0.69
10	0.95	1.75	8.30	28.40	27.37	48.15	103.92	0.21	0.20	0.36	0.77
11	1.00	1.30	8.60	29.40	28.67	56.75	114.82	0.22	0.21	0.42	0.85
12	0.80	1.15	8.85	30.20	29.82	65.60	125.62	0.22	0.22	0.49	0.93
13	0.80	1.00	9.05	31.00	30.82	74.65	136.47	0.23	0.23	0.55	1.01
14	0.80	0.90	9.15	31.80	31.72	83.80	147.32	0.24	0.24	0.62	1.09
15	0.62	0.78	9.40	32.42	32.50	93.20	158.12	0.24	0.24	0.69	1.17
16	0.62	0.78	9.55	33.04	33.28	102.75	169.07	0.25	0.25	0.76	1.25
17	0.69	0.56	9.70	33.73	33.84	112.45	180.02	0.25	0.25	0.83	1.34
18	0.45	0.55	9.90	34.18	34.39	122.35	190.92	0.25	0.26	0.91	1.42
19	0.78	0.42	9.80	34.96	34.81	132.15	201.92	0.26	0.26	0.98	1.50
20	0.60	0.35	9.95	35.56	35.16	142.10	212.82	0.26	0.26	1.05	1.58
21	0.40	0.35	10.15	35.96	35.51	152.25	223.72	0.27	0.26	1.13	1.66
22	0.52	0.33	9.95	36.48	35.84	162.20	234.52	0.27	0.27	1.20	1.74
23	0.60	0.35	10.05	37.08	36.19	172.25	245.52	0.28	0.27	1.28	1.82
24	4.60	2.10	93.30	41.68	38.29	265.55	345.52	0.31	0.28	1.97	2.56
25	3.20	1.80	95.00	44.88	40.09	360.55	445.52	0.33	0.30	2.68	3.31
26	1.45	1.45	97.10	46.33	41.54	457.65	545.52	0.34	0.31	3.40	4.05
27	1.60	1.15	97.25	47.93	42.69	554.90	645.52	0.36	0.32	4.12	4.79
28	0.59	0.02	99.39	48.52	42.71	654.29	745.52	0.36	0.32	4.86	5.53
29	1.25	0.14	98.61	49.77	42.85	752.90	845.52	0.37	0.32	5.59	6.28

Table A.2
Relative Permeability Analysis Summary;
Run 2

PVI	S_o	S_w	S_d	$k_{r,o}$	$k_{r,w}$	$k_{r,d}$
0.5	0.3984	0.1635	0.4381	0.1005	0.0324	0.0857
0.75	0.3669	0.2810	0.3941	0.0625	0.0207	0.0999
1.0	0.3479	0.3185	0.3566	0.0463	0.0136	0.1074
1.25	0.3249	0.3470	0.3281	0.0346	0.0100	0.1168
1.5	0.3134	0.3725	0.3141	0.0308	0.0089	0.1240
1.75	0.2989	0.3980	0.3031	0.0245	0.0078	0.1310
2.0	0.2814	0.4155	0.3031	0.0184	0.0079	0.1323
2.5	0.2724	0.4560	0.2716	0.0105	0.0079	0.1346
3.0	0.2649	0.4970	0.2381	0.0144	0.0049	0.1450
4.0	0.2469	0.5445	0.2086	0.0105	0.0031	0.1690
5.0	0.1909	0.6350	0.1741	0.0026	0.0016	0.1850

Table A.3
Fractional Collection Analysis Summary;
Run 3

tube no.	tube oil vol. (cc)	tube water vol. (cc)	tube decane vol. (cc)	cum. oil vol. (cc)	cum. water vol. (cc)	cum. decane vol. (cc)	total fluid vol. (cc)	oil rec. (PVI)	water rec. (PVI)	decane rec. (PVI)	PVI
1	0.89	6.93	0.	0.89	6.93	0.	7.82	0.00	0.05	0.	0.06
2	1.20	10.70	0.	2.09	17.63	0.	19.72	0.02	0.14	0.	0.15
3	1.20	10.70	0.	3.29	28.33	0.	31.62	0.03	0.22	0.	0.25
4	1.15	10.70	0.	4.44	39.03	0.	43.47	0.03	0.30	0.	0.34
5	1.25	10.55	0.	5.69	49.58	0.	55.27	0.04	0.39	0.	0.43
6	1.30	10.30	0.10	6.99	59.88	0.10	66.97	0.05	0.47	0.00	0.52
7	0.35	1.45	10.05	7.34	61.33	10.15	78.82	0.06	0.48	0.08	0.62
8	0.30	1.25	10.30	7.64	62.58	20.45	90.67	0.06	0.49	0.16	0.71
9	0.30	1.00	10.70	7.94	63.58	31.15	102.67	0.06	0.50	0.24	0.80
10	0.20	1.00	10.80	8.14	64.58	41.95	114.67	0.06	0.50	0.33	0.90
11	0.20	0.80	10.95	8.34	65.38	52.90	126.62	0.07	0.51	0.41	0.99
12	0.18	0.72	11.10	8.52	66.10	64.00	138.62	0.07	0.52	0.50	1.08
13	0.18	0.62	11.15	8.70	66.72	75.15	150.57	0.07	0.52	0.59	1.18
14	0.19	0.53	11.23	8.89	67.25	86.38	162.52	0.07	0.53	0.67	1.27
15	0.24	0.47	11.19	9.13	67.72	97.57	174.42	0.07	0.53	0.76	1.36
16	0.19	0.44	11.37	9.32	68.16	108.94	186.42	0.07	0.53	0.85	1.46
17	0.18	0.41	11.36	9.50	68.57	120.30	198.37	0.07	0.54	0.94	1.55
18	0.15	0.37	11.43	9.65	68.94	131.73	210.32	0.08	0.54	1.03	1.64
19	0.19	0.32	11.39	9.84	69.26	143.12	222.22	0.08	0.54	1.12	1.74
20	0.18	0.32	11.50	10.02	69.58	154.62	234.22	0.08	0.54	1.21	1.83
21	0.18	0.31	11.46	10.20	69.89	166.08	246.17	0.08	0.55	1.30	1.92
22	0.20	0.29	11.56	10.40	70.18	177.64	258.22	0.08	0.55	1.39	2.02
23	0.15	0.34	11.51	10.55	70.52	189.15	270.22	0.08	0.55	1.48	2.11
24	0.21	0.29	11.55	10.76	70.81	200.70	282.27	0.08	0.55	1.57	2.21
25	0.35	0.22	11.48	11.11	71.03	212.18	294.32	0.09	0.56	1.66	2.30
26	3.20	1.10	93.20	14.31	72.13	305.38	391.82	0.11	0.56	2.39	3.06
27	2.60	0.70	94.60	16.91	72.83	399.98	489.72	0.13	0.57	3.13	3.83
28	1.55	0.50	95.85	18.46	73.33	495.83	587.62	0.14	0.57	3.87	4.59
29	1.41	0.24	96.25	19.87	73.57	592.08	685.52	0.16	0.57	4.63	5.36
30	1.14	0.30	94.06	21.01	73.87	686.14	781.02	0.16	0.58	5.36	6.10

Table A.4
Relative Permeability Analysis Summary;
Run 3

PVI	S_o	S_w	S_d	$k_{r,o}$	$k_{r,w}$	$k_{r,d}$
0.525	0.3250	0.2360	0.4390	0.0176	0.0172	0.0866
0.75	0.3150	0.2060	0.4790	0.0143	0.0133	0.0996
1.0	0.3140	0.1960	0.4900	0.0120	0.0103	0.1104
1.25	0.3140	0.1670	0.5190	0.0100	0.0069	0.1190
1.5	0.3140	0.1560	0.5300	0.0105	0.0056	0.1258
1.750	0.3150	0.1440	0.5410	0.0120	0.0046	0.1323
2.0	0.3150	0.1270	0.5580	0.0126	0.0037	0.1394
3.0	0.3520	0.1000	0.5480	0.0235	0.0019	0.1520
4.0	0.3090	0.0900	0.6010	0.0234	0.0013	0.1761
5.0	0.2640	0.0680	0.6680	0.0105	0.0004	0.2040

Table A.5
Relative Permeability Analysis Summary;
Run 9 - First Dynamic Water Flood

PVI	S_o	S_w	S_d	$k_{r,o}$	$k_{r,w}$	$k_{r,d}$
0.625	0.4468	0.2786	0.0	0.5532	0.1767	0.0
0.750	0.4048	0.2343	0.0	0.5952	0.2132	0.0
1.000	0.3398	0.1968	0.0	0.6602	0.2992	0.0
1.250	0.3008	0.1578	0.0	0.6992	0.3372	0.0
1.500	0.2748	0.1371	0.0	0.7252	0.3713	0.0
1.750	0.2408	0.1076	0.0	0.7592	0.4210	0.0
2.000	0.2118	0.0829	0.0	0.7882	0.4622	0.0
2.250	0.1988	0.0695	0.0	0.8012	0.4848	0.0
2.500	0.1758	0.0534	0.0	0.8242	0.4957	0.0
3.000	0.1508	0.0389	0.0	0.8492	0.5334	0.0
4.000	0.1158	0.0113	0.0	0.8842	0.5746	0.0

Table A.6
Fractional Collection Analysis Summary
Run 9 - First Dynamic Water Flood

tube no.	tube oil vol. (cc)	tube water vol. (cc)	tube decane vol. (cc)	cum. oil vol. (cc)	cum. water vol. (cc)	cum. decane vol. (cc)	total fluid vol. (cc)	oil rec. (PVI)	water rec. (PVI)	decane rec. (PVI)	PVI
1	2.38	0.	0.	2.38	0.	0.	2.38	0.02	0.	0.	0.02
2	6.70	0.	0.	9.08	0.	0.	9.08	0.07	0.	0.	0.07
3	6.50	0.	0.	15.58	0.	0.	15.58	0.12	0.	0.	0.12
4	6.55	0.	0.	22.13	0.	0.	22.13	0.17	0.	0.	0.17
5	6.70	0.	0.	28.83	0.	0.	28.83	0.22	0.	0.	0.22
6	6.50	0.	0.	35.33	0.	0.	35.33	0.27	0.	0.	0.27
7	6.60	0.	0.	41.93	0.	0.	41.93	0.32	0.	0.	0.32
8	6.75	0.	0.	48.68	0.	0.	48.68	0.37	0.	0.	0.37
9	6.50	0.	0.	55.18	0.	0.	55.18	0.42	0.	0.	0.42
10	6.80	0.	0.	61.98	0.	0.	61.98	0.47	0.	0.	0.47
11	6.70	0.	0.	68.68	0.	0.	68.68	0.52	0.	0.	0.52
12	6.80	0.	0.	75.48	0.	0.	75.48	0.57	0.	0.	0.57
13	6.00	0.80	0.	81.48	0.80	0.	82.28	0.62	0.00	0.	0.62
14	3.35	3.45	0.	84.83	4.25	0.	89.08	0.64	0.03	0.	0.67
15	1.65	4.95	0.	86.48	9.20	0.	95.68	0.66	0.07	0.	0.73
16	1.30	5.30	0.	87.78	14.50	0.	102.28	0.67	0.11	0.	0.78
17	1.20	5.50	0.	88.98	20.00	0.	108.98	0.67	0.15	0.	0.83
18	1.15	5.60	0.	90.13	25.60	0.	115.73	0.68	0.19	0.	0.88
19	1.10	5.65	0.	91.23	31.25	0.	122.48	0.69	0.24	0.	0.93
20	0.96	5.74	0.	92.19	36.99	0.	129.18	0.70	0.28	0.	0.98
21	0.90	5.85	0.	93.09	42.84	0.	135.93	0.71	0.32	0.	1.03
22	0.87	6.08	0.	93.96	48.92	0.	142.88	0.71	0.37	0.	1.08
23	0.71	6.24	0.	94.67	55.16	0.	149.83	0.72	0.42	0.	1.14
24	0.89	5.91	0.	95.56	61.07	0.	156.63	0.72	0.46	0.	1.19
25	0.62	5.13	0.	96.18	66.20	0.	162.38	0.73	0.50	0.	1.23
26	0.52	4.88	0.	96.70	71.08	0.	167.78	0.73	0.54	0.	1.27
27	0.59	4.96	0.	97.29	76.04	0.	173.33	0.74	0.58	0.	1.31
28	0.51	5.09	0.	97.80	81.13	0.	178.93	0.74	0.61	0.	1.36
29	0.41	5.24	0.	98.21	86.37	0.	184.58	0.74	0.65	0.	1.40
30	0.49	5.21	0.	98.70	91.58	0.	190.28	0.75	0.69	0.	1.44
31	0.40	5.30	0.	99.10	96.88	0.	195.98	0.75	0.73	0.	1.49
32	0.46	5.29	0.	99.56	102.17	0.	201.73	0.75	0.77	0.	1.53
33	0.41	5.44	0.	99.97	107.61	0.	207.58	0.76	0.82	0.	1.57
34	0.42	5.48	0.	100.39	113.09	0.	213.48	0.76	0.86	0.	1.62
35	0.43	5.57	0.	100.82	118.66	0.	219.48	0.76	0.90	0.	1.66
36	0.35	5.45	0.	101.17	124.11	0.	225.28	0.77	0.94	0.	1.71
37	1.34	34.16	0.	102.51	158.27	0.	260.78	0.78	1.20	0.	1.98
38	3.50	102.90	0.	106.01	261.17	0.	367.18	0.80	1.98	0.	2.78
39	1.59	107.11	0.	107.60	368.28	0.	475.88	0.82	2.79	0.	3.61
40	0.96	114.34	0.	108.56	482.62	0.	591.18	0.82	3.66	0.	4.48
41	0.49	110.41	0.	109.05	593.03	0.	702.08	0.83	4.49	0.	5.32

Table A.7
Relative Permeability Analysis Summary;
Run 9 - Second Dynamic Water Flood

PVI	S _o	S _w	S _d	k _{r,o}	k _{r,w}	k _{r,d}
0.625	0.5706	0.4819	0.0	0.4294	0.1310	0.0
0.750	0.4306	0.3183	0.0	0.5694	0.2141	0.0
1.000	0.3396	0.2185	0.0	0.6604	0.2820	0.0
1.250	0.2766	0.1594	0.0	0.7234	0.3408	0.0
1.500	0.2396	0.1252	0.0	0.7604	0.3747	0.0
1.750	0.2126	0.0988	0.0	0.7874	0.4086	0.0
2.000	0.1936	0.0807	0.0	0.8064	0.4273	0.0
2.250	0.1756	0.0649	0.0	0.8244	0.4372	0.0
2.500	0.1626	0.0562	0.0	0.8374	0.4530	0.0
3.000	0.1286	0.0331	0.0	0.8714	0.4826	0.0
4.000	0.0916	0.0044	0.0	0.9084	0.5312	0.0

Table A.8
Fractional Collection Analysis Summary
Run 9 - Second Dynamic Water Flood

tube no.	tube oil vol. (cc)	tube water vol. (cc)	tube decane vol. (cc)	cum. oil vol. (cc)	cum. water vol. (cc)	cum. decane vol. (cc)	total fluid vol. (cc)	oil rec. (PVI)	water rec. (PVI)	decane rec. (PVI)	PVI
1	1.07	0.	0.	1.07	0.	0.	1.07	0.00	0.	0.	0.00
2	5.55	0.	0.	6.62	0.	0.	6.62	0.05	0.	0.	0.05
3	5.45	0.	0.	12.07	0.	0.	12.07	0.09	0.	0.	0.09
4	5.65	0.	0.	17.72	0.	0.	17.72	0.13	0.	0.	0.13
5	5.35	0.	0.	23.07	0.	0.	23.07	0.17	0.	0.	0.17
6	5.55	0.	0.	28.62	0.	0.	28.62	0.22	0.	0.	0.22
7	5.55	0.	0.	34.17	0.	0.	34.17	0.26	0.	0.	0.26
8	5.55	0.	0.	39.72	0.	0.	39.72	0.30	0.	0.	0.30
9	5.80	0.	0.	45.52	0.	0.	45.52	0.34	0.	0.	0.34
10	5.74	0.	0.	51.26	0.	0.	51.26	0.39	0.	0.	0.39
11	5.65	0.	0.	56.91	0.	0.	56.91	0.43	0.	0.	0.43
12	5.80	0.	0.	62.71	0.	0.	62.71	0.48	0.	0.	0.48
13	5.70	0.	0.	68.41	0.	0.	68.41	0.52	0.	0.	0.52
14	5.95	0.	0.	74.36	0.	0.	74.36	0.56	0.	0.	0.56
15	5.75	0.10	0.	80.11	0.10	0.	80.21	0.61	0.00	0.	0.61
16	3.40	2.35	0.	83.51	2.45	0.	85.96	0.63	0.02	0.	0.65
17	2.40	3.30	0.	85.91	5.75	0.	91.66	0.65	0.04	0.	0.69
18	1.80	4.00	0.	87.71	9.75	0.	97.46	0.66	0.07	0.	0.74
19	1.35	4.45	0.	89.06	14.20	0.	103.26	0.67	0.11	0.	0.78
20	1.30	4.50	0.	90.36	18.70	0.	109.06	0.68	0.14	0.	0.83
21	1.10	4.63	0.	91.46	23.33	0.	114.79	0.69	0.18	0.	0.87
22	1.10	4.70	0.	92.56	28.03	0.	120.59	0.70	0.21	0.	0.91
23	0.90	4.85	0.	93.46	32.88	0.	126.34	0.71	0.25	0.	0.96
24	1.00	4.65	0.	94.46	37.53	0.	131.99	0.72	0.28	0.	1.00
25	0.85	4.90	0.	95.31	42.43	0.	137.74	0.72	0.32	0.	1.04
26	0.80	5.00	0.	96.11	47.43	0.	143.54	0.73	0.36	0.	1.09
27	0.78	5.02	0.	96.89	52.45	0.	149.34	0.73	0.40	0.	1.13
28	0.68	4.97	0.	97.57	57.42	0.	154.99	0.74	0.44	0.	1.17
29	0.65	5.05	0.	98.22	62.47	0.	160.69	0.74	0.47	0.	1.22
30	0.60	5.25	0.	98.82	67.72	0.	166.54	0.75	0.51	0.	1.26
31	0.55	5.30	0.	99.37	73.02	0.	172.39	0.75	0.55	0.	1.31
32	0.53	5.27	0.	99.90	78.29	0.	178.19	0.76	0.59	0.	1.35
33	0.50	5.35	0.	100.40	83.64	0.	184.04	0.76	0.63	0.	1.39
34	0.50	5.40	0.	100.90	89.04	0.	189.94	0.76	0.67	0.	1.44
35	0.49	5.36	0.	101.39	94.40	0.	195.79	0.77	0.72	0.	1.48
36	0.43	5.57	0.	101.82	99.97	0.	201.79	0.77	0.76	0.	1.53
37	0.35	5.45	0.	102.17	105.42	0.	207.59	0.77	0.80	0.	1.57
38	0.35	5.35	0.	102.52	110.77	0.	213.29	0.78	0.84	0.	1.62
39	4.20	87.32	0.	106.72	198.09	0.	304.81	0.81	1.50	0.	2.31
40	1.75	82.47	0.	108.47	280.56	0.	389.03	0.82	2.13	0.	2.95
41	1.04	94.62	0.	109.51	375.18	0.	484.69	0.83	2.84	0.	3.67
42	0.35	99.15	0.	109.86	474.33	0.	584.19	0.83	3.59	0.	4.43

Table A.9
Relative Permeability Analysis Summary;
Run 9 - Third Dynamic Water Flood

PVI	S_o	S_w	S_d	$k_{r,o}$	$k_{r,w}$	$k_{r,d}$
0.540	0.5809	0.3380	0.0811	0.4025	0.0756	0.0
0.750	0.3659	0.5530	0.0811	0.1982	0.1825	0.0
1.000	0.3059	0.6130	0.0811	0.1511	0.2247	0.0
1.250	0.2509	0.6680	0.0811	0.1058	0.2642	0.0
1.500	0.2239	0.6950	0.0811	0.0904	0.2974	0.0
1.750	0.2039	0.7150	0.0811	0.0768	0.3144	0.0
2.000	0.1739	0.7450	0.0811	0.0523	0.3292	0.0
2.250	0.1529	0.7660	0.0811	0.0397	0.3437	0.0
2.500	0.1349	0.7840	0.0811	0.0296	0.3592	0.0
3.000	0.1229	0.7960	0.0811	0.0250	0.3811	0.0
4.000	0.0829	0.8360	0.0811	0.0062	0.4142	0.0

Table A.10
Fractional Collection Analysis Summary
Run 9 - Third Dynamic Water Flood

tube no.	tube oil vol. (cc)	tube water vol. (cc)	tube decane vol. (cc)	cum. oil vol. (cc)	cum. water vol. (cc)	cum. decane vol. (cc)	total fluid vol. (cc)	oil rec. (PVI)	water rec. (PVI)	decane rec. (PVI)	PVI
1	2.38	0.	0.	2.38	0.	0.	2.38	0.02	0.	0.	0.02
2	6.45	0.	0.	8.83	0.	0.	8.83	0.07	0.	0.	0.07
3	6.60	0.	0.	15.43	0.	0.	15.43	0.12	0.	0.	0.12
4	6.70	0.	0.	22.13	0.	0.	22.13	0.17	0.	0.	0.17
5	6.60	0.	0.	28.73	0.	0.	28.73	0.22	0.	0.	0.22
6	6.65	0.	0.	35.38	0.	0.	35.38	0.27	0.	0.	0.27
7	6.60	0.	0.	41.98	0.	0.	41.98	0.32	0.	0.	0.32
8	6.50	0.	0.	48.48	0.	0.	48.48	0.37	0.	0.	0.37
9	6.75	0.	0.	55.23	0.	0.	55.23	0.42	0.	0.	0.42
10	6.55	0.	0.	61.78	0.	0.	61.78	0.47	0.	0.	0.47
11	6.50	0.	0.	68.28	0.	0.	68.28	0.52	0.	0.	0.52
12	4.90	1.70	0.	73.18	1.70	0.	74.88	0.55	0.01	0.	0.57
13	3.10	3.50	0.	76.28	5.20	0.	81.48	0.58	0.04	0.	0.62
14	2.00	4.70	0.	78.28	9.90	0.	88.18	0.59	0.08	0.	0.67
15	1.69	5.11	0.	79.97	15.01	0.	94.98	0.61	0.11	0.	0.72
16	1.32	5.18	0.	81.29	20.19	0.	101.48	0.62	0.15	0.	0.77
17	1.30	5.30	0.	82.59	25.49	0.	108.08	0.63	0.19	0.	0.82
18	1.17	5.48	0.	83.76	30.97	0.	114.73	0.63	0.23	0.	0.87
19	1.09	5.61	0.	84.85	36.58	0.	121.43	0.64	0.28	0.	0.92
20	0.95	5.65	0.	85.80	42.23	0.	128.03	0.65	0.32	0.	0.97
21	0.87	5.78	0.	86.67	48.01	0.	134.68	0.66	0.36	0.	1.02
22	0.86	5.89	0.	87.53	53.90	0.	141.43	0.66	0.41	0.	1.07
23	0.71	5.99	0.	88.24	59.89	0.	148.13	0.67	0.45	0.	1.12
24	0.68	5.92	0.	88.92	65.81	0.	154.73	0.67	0.50	0.	1.17
25	0.68	6.02	0.	89.60	71.83	0.	161.43	0.68	0.54	0.	1.22
26	0.65	6.05	0.	90.25	77.88	0.	168.13	0.68	0.59	0.	1.27
27	0.50	6.20	0.	90.75	84.08	0.	174.83	0.69	0.64	0.	1.32
28	0.49	6.11	0.	91.24	90.19	0.	181.43	0.69	0.68	0.	1.37
29	0.49	6.21	0.	91.73	96.40	0.	188.13	0.70	0.73	0.	1.43
30	0.45	6.25	0.	92.18	102.65	0.	194.83	0.70	0.78	0.	1.48
31	0.45	6.15	0.	92.63	108.80	0.	201.43	0.70	0.82	0.	1.53
32	0.38	6.27	0.	93.01	115.07	0.	208.08	0.70	0.87	0.	1.58
33	2.40	54.10	0.	95.41	169.17	0.	264.58	0.72	1.28	0.	2.00
34	2.45	91.04	0.	97.86	260.21	0.	358.07	0.74	1.97	0.	2.71
35	1.10	88.35	0.	98.96	348.56	0.	447.52	0.75	2.64	0.	3.39
36	0.75	95.11	0.	99.71	443.67	0.	543.38	0.76	3.36	0.	4.12

Table A.11
Relative Permeability Analysis Summary;
Run 8 - Dynamic Decane Flood

PVI	S_o	S_w	S_d	$k_{r,o}$	$k_{r,w}$	$k_{r,d}$
0.250	0.7481	0.0313	0.2206	0.3949	0.	0.0281
0.500	0.5801	0.0313	0.3886	0.1942	0.	0.0846
0.750	0.5021	0.0313	0.4666	0.1560	0.	0.1361
1.000	0.4481	0.0313	0.5206	0.1206	0.	0.1699
1.250	0.4081	0.0313	0.5606	0.0937	0.	0.1947
1.500	0.3801	0.0313	0.5886	0.0781	0.	0.2163
1.750	0.3621	0.0313	0.6066	0.0671	0.	0.2281
2.000	0.3411	0.0313	0.6276	0.0580	0.	0.2480
3.000	0.3031	0.0313	0.6656	0.0312	0.	0.2879
4.000	0.2531	0.0313	0.7156	0.0243	0.	0.3130
5.000	0.2141	0.0313	0.7546	0.0111	0.	0.3346

Table A.12
Fractional Collection Analysis Summary
Run 8 - Dynamic Decane Flood

tube no.	tube oil vol. (cc)	tube water vol. (cc)	tube decane vol. (cc)	cum. oil vol. (cc)	cum. water vol. (cc)	cum. decane vol. (cc)	total fluid vol. (cc)	oil rec. (PVI)	water rec. (PVI)	decane rec. (PVI)	PVI
1	1.77	0.	0.70	1.77	0.	0.70	2.47	0.01	0.	0.00	0.02
2	6.40	0.	0.20	8.17	0.	0.90	9.07	0.06	0.	0.00	0.07
3	6.40	0.	0.30	14.57	0.	1.20	15.77	0.11	0.	0.00	0.12
4	6.00	0.	0.70	20.57	0.	1.90	22.47	0.15	0.	0.01	0.17
5	5.30	0.	1.20	25.87	0.	3.10	28.97	0.19	0.	0.02	0.22
6	5.30	0.	1.35	31.17	0.	4.45	35.62	0.23	0.	0.03	0.27
7	4.75	0.	1.85	35.92	0.	6.30	42.22	0.27	0.	0.05	0.32
8	4.50	0.	2.20	40.42	0.	8.50	48.92	0.30	0.	0.06	0.37
9	3.70	0.	2.90	44.12	0.	11.40	55.52	0.33	0.	0.09	0.41
10	2.80	0.	3.80	46.92	0.	15.20	62.12	0.35	0.	0.11	0.46
11	2.30	0.	4.30	49.22	0.	19.50	68.72	0.37	0.	0.15	0.51
12	2.00	0.	4.50	51.22	0.	24.00	75.22	0.38	0.	0.18	0.56
13	1.70	0.	4.80	52.92	0.	28.80	81.72	0.39	0.	0.21	0.61
14	1.60	0.	5.05	54.52	0.	33.85	88.37	0.41	0.	0.25	0.66
15	1.40	0.	5.25	55.92	0.	39.10	95.02	0.42	0.	0.29	0.71
16	1.30	0.	5.40	57.22	0.	44.50	101.72	0.43	0.	0.33	0.76
17	1.20	0.	5.55	58.42	0.	50.05	108.47	0.44	0.	0.37	0.81
18	0.99	0.	5.51	59.41	0.	55.56	114.97	0.44	0.	0.41	0.86
19	0.95	0.	5.65	60.36	0.	61.21	121.57	0.45	0.	0.46	0.91
20	0.88	0.	5.72	61.24	0.	66.93	128.17	0.46	0.	0.50	0.96
21	0.88	0.	5.82	62.12	0.	72.75	134.87	0.46	0.	0.54	1.01
22	0.70	0.	5.85	62.82	0.	78.60	141.42	0.47	0.	0.59	1.06
23	0.78	0.	5.97	63.60	0.	84.57	148.17	0.47	0.	0.63	1.11
24	0.65	0.	5.95	64.25	0.	90.52	154.77	0.48	0.	0.68	1.15
25	0.55	0.	5.95	64.80	0.	96.47	161.27	0.48	0.	0.72	1.20
26	0.62	0.	6.03	65.42	0.	102.50	167.92	0.49	0.	0.76	1.25
27	0.60	0.	6.05	66.02	0.	108.55	174.57	0.49	0.	0.81	1.30
28	0.61	0.	6.20	66.63	0.	114.75	181.37	0.50	0.	0.86	1.35
29	0.50	0.	6.00	67.13	0.	120.75	187.87	0.50	0.	0.90	1.40
30	0.49	0.	6.16	67.62	0.	126.91	194.52	0.50	0.	0.95	1.45
31	0.48	0.	6.17	68.10	0.	133.08	201.17	0.51	0.	0.99	1.50
32	0.42	0.	6.13	68.52	0.	139.20	207.72	0.51	0.	1.04	1.55
33	0.40	0.	6.25	68.92	0.	145.45	214.37	0.51	0.	1.09	1.60
34	0.41	0.	6.34	69.33	0.	151.80	221.12	0.52	0.	1.13	1.65
35	0.41	0.	6.34	69.74	0.	158.14	227.87	0.52	0.	1.18	1.70
36	0.39	0.	6.31	70.13	0.	164.45	234.57	0.52	0.	1.23	1.75
37	4.60	0.	95.50	74.73	0.	259.95	334.67	0.56	0.	1.94	2.50
38	3.20	0.	103.40	77.93	0.	363.34	441.27	0.58	0.	2.71	3.29
39	1.70	0.	98.40	79.63	0.	461.74	541.37	0.59	0.	3.45	4.04
40	1.39	0.	98.71	81.02	0.	560.45	641.47	0.60	0.	4.18	4.79
41	0.60	0.	53.80	81.62	0.	614.25	695.87	0.61	0.	4.58	5.19

Table A.13
Fractional Collection Analysis Summary;
Run 4

tube no.	tube oil vol. (cc)	tube water vol. (cc)	tube decane vol. (cc)	cum. oil vol. (cc)	cum. water vol. (cc)	cum. decane vol. (cc)	total fluid vol. (cc)	oil rec. (PVI)	water rec. (PVI)	decane rec. (PVI)	PVI
1	0.42	0.	4.04	0.42	0.	4.04	4.46	0.00	0.	0.03	0.03
2	0.72	0.	6.58	1.14	0.	10.62	11.76	0.00	0.	0.08	0.09
3	0.79	0.	6.46	1.93	0.	17.08	19.01	0.01	0.	0.13	0.14
4	0.66	0.	6.48	2.59	0.	23.56	26.15	0.02	0.	0.18	0.20
5	0.70	0.	6.55	3.29	0.	30.11	33.40	0.03	0.	0.23	0.25
6	0.69	0.	6.56	3.98	0.	36.67	40.65	0.03	0.	0.28	0.31
7	0.78	0.	6.63	4.76	0.	43.30	48.06	0.04	0.	0.33	0.37
8	3.10	0.10	4.05	7.86	0.10	47.35	55.31	0.06	0.00	0.36	0.42
9	7.30	0.10	0.10	15.16	0.20	47.45	62.81	0.12	0.00	0.36	0.48
10	7.40	0.05	0.05	22.56	0.25	47.50	70.31	0.17	0.00	0.36	0.53
11	5.35	2.05	0.10	27.91	2.30	47.60	77.81	0.21	0.02	0.36	0.59
12	3.40	3.90	0.	31.31	6.20	47.60	85.11	0.24	0.05	0.36	0.65
13	1.80	5.45	0.	33.11	11.65	47.60	92.36	0.25	0.09	0.36	0.70
14	1.45	5.85	0.	34.56	17.50	47.60	99.66	0.26	0.13	0.36	0.76
15	1.09	6.21	0.	35.65	23.71	47.60	106.96	0.27	0.18	0.36	0.81
16	1.06	6.34	0.	36.71	30.05	47.60	114.36	0.28	0.23	0.36	0.87
17	1.01	6.34	0.	37.72	36.39	47.60	121.71	0.29	0.28	0.36	0.93
18	0.94	6.46	0.	38.66	42.85	47.60	129.11	0.29	0.33	0.36	0.98
19	0.91	6.49	0.	39.57	49.34	47.60	136.51	0.30	0.38	0.36	1.04
20	0.76	6.64	0.	40.33	55.98	47.60	143.91	0.31	0.43	0.36	1.09
21	0.69	6.66	0.	41.02	62.64	47.60	151.26	0.31	0.48	0.36	1.15
22	0.70	6.60	0.	41.72	69.24	47.60	158.56	0.32	0.53	0.36	1.21
23	0.45	6.90	0.	42.17	76.14	47.60	165.91	0.32	0.58	0.36	1.26
24	0.59	6.76	0.	42.76	82.90	47.60	173.26	0.33	0.63	0.36	1.32
25	0.35	7.05	0.	43.11	89.95	47.60	180.66	0.33	0.68	0.36	1.37
26	0.50	7.00	0.	43.61	96.95	47.60	188.16	0.33	0.74	0.36	1.43
27	0.26	7.19	0.	43.87	104.14	47.60	195.61	0.33	0.79	0.36	1.49
28	0.50	6.95	0.	44.37	111.09	47.60	203.06	0.34	0.84	0.36	1.54
29	0.25	7.10	0.	44.62	118.19	47.60	210.41	0.34	0.90	0.36	1.60
30	0.34	7.06	0.	44.96	125.25	47.60	217.81	0.34	0.95	0.36	1.66
31	0.50	6.85	0.	45.46	132.10	47.60	225.16	0.35	1.00	0.36	1.71
32	0.22	7.08	0.	45.68	139.18	47.60	232.46	0.35	1.06	0.36	1.77
33	0.25	7.15	0.	45.93	146.33	47.60	239.86	0.35	1.11	0.36	1.82
34	0.25	7.20	0.	46.18	153.53	47.60	247.31	0.35	1.17	0.36	1.88
35	0.21	7.24	0.	46.39	160.77	47.60	254.76	0.35	1.22	0.36	1.94
36	0.22	7.23	0.	46.61	168.00	47.60	262.21	0.35	1.28	0.36	1.99
37	2.21	93.71	0.	48.82	261.71	47.60	358.13	0.37	1.99	0.36	2.72
38	0.95	97.09	0.	49.77	358.80	47.60	456.17	0.38	2.73	0.36	3.47
39	0.47	109.83	0.	50.24	468.63	47.60	566.47	0.38	3.56	0.36	4.31
40	0.30	97.74	0.	50.54	566.37	47.60	664.51	0.38	4.31	0.36	5.05

Table A.14
Relative Permeability Analysis Summary;
Run 4

PVI	S_o	S_w	S_d	$k_{r,o}$	$k_{r,w}$	$k_{r,d}$	$\frac{X}{L}$
0.395	0.8500	0.0200	0.1300	0.5267	0.0	0.0	1.0
0.500	0.8500	0.0200	0.1300	0.4201	0.0	0.0	0.79
0.600	0.535	0.3350	0.1300	—	—	—	0.658
0.650	0.474	0.3960	0.1300	—	—	—	0.608
0.750	0.3900	0.4800	0.1300	0.1974	0.1710	0.0	0.53
1.000	0.3100	0.5600	0.1300	0.1246	0.2222	0.0	0.395
1.250	0.2610	0.6090	0.1300	0.0827	0.2490	0.0	0.316
1.500	0.2350	0.6350	0.1300	0.0681	0.2817	0.0	0.263
1.750	0.2150	0.6550	0.1300	0.0591	0.3123	0.0	0.226
2.000	0.1990	0.6710	0.1300	0.0441	0.3200	0.0	0.198
3.000	0.1520	0.7180	0.1300	0.1860	0.3780	0.0	0.132
4.000	0.1220	0.7480	0.1300	0.0095	0.3930	0.0	0.099
5.000	0.1150	0.7550	0.1300	0.0034	0.4060	0.0	0.079

Table A.15
Fractional Collection Analysis Summary;
Run 5

tube no.	tube oil vol. (cc)	tube water vol. (cc)	tube decane vol. (cc)	cum. oil vol. (cc)	cum. water vol. (cc)	cum. decane vol. (cc)	total fluid vol. (cc)	oil rec. (PVI)	water rec. (PVI)	decane rec. (PVI)	PVI
1	0.08	0.	1.09	0.08	0.	1.09	1.17	0.00	0.	0.00	0.00
2	0.40	0.	6.55	0.48	0.	7.64	8.12	0.00	0.	0.06	0.06
3	0.38	0.	6.52	0.86	0.	14.16	15.02	0.00	0.	0.11	0.11
4	0.39	0.	6.61	1.25	0.	20.77	22.02	0.00	0.	0.16	0.16
5	0.40	0.	6.60	1.65	0.	27.37	29.02	0.01	0.	0.20	0.22
6	0.40	0.	6.60	2.05	0.	33.97	36.02	0.02	0.	0.25	0.27
7	0.36	0.	6.49	2.41	0.	40.46	42.87	0.02	0.	0.30	0.32
8	0.38	0.	6.52	2.79	0.	46.98	49.77	0.02	0.	0.35	0.37
9	0.35	0.	6.45	3.14	0.	53.43	56.57	0.02	0.	0.40	0.42
10	2.00	0.	4.90	5.14	0.	58.33	63.47	0.04	0.	0.44	0.48
11	5.30	1.60	0.10	10.44	1.60	58.43	70.47	0.08	0.01	0.44	0.53
12	3.10	3.90	0.	13.54	5.50	58.43	77.47	0.10	0.04	0.44	0.58
13	2.90	4.00	0.	16.44	9.50	58.43	84.37	0.12	0.07	0.44	0.63
14	2.70	4.30	0.	19.14	13.80	58.43	91.37	0.14	0.10	0.44	0.68
15	2.15	4.85	0.	21.29	18.65	58.43	98.37	0.16	0.14	0.44	0.74
16	1.35	5.60	0.	22.64	24.25	58.43	105.32	0.17	0.18	0.44	0.79
17	1.18	5.82	0.	23.82	30.07	58.43	112.32	0.18	0.23	0.44	0.84
18	1.11	5.89	0.	24.93	35.96	58.43	119.32	0.19	0.27	0.44	0.89
19	1.10	6.00	0.	26.03	41.96	58.43	126.42	0.20	0.31	0.44	0.95
20	0.90	6.20	0.	26.93	48.16	58.43	133.52	0.20	0.36	0.44	1.00
21	0.90	6.10	0.	27.83	54.26	58.43	140.52	0.21	0.41	0.44	1.05
22	0.72	6.48	0.	28.55	60.74	58.43	147.72	0.21	0.45	0.44	1.11
23	0.75	6.25	0.	29.30	66.99	58.43	154.72	0.22	0.50	0.44	1.16
24	0.63	6.47	0.	29.93	73.46	58.43	161.82	0.22	0.55	0.44	1.21
25	0.57	6.53	0.	30.50	79.99	58.43	168.92	0.23	0.60	0.44	1.27
26	0.67	6.43	0.	31.17	86.42	58.43	176.02	0.23	0.65	0.44	1.32
27	0.44	6.56	0.	31.61	92.98	58.43	183.02	0.24	0.70	0.44	1.37
28	0.43	6.57	0.	32.04	99.55	58.43	190.02	0.24	0.75	0.44	1.42
29	0.41	6.59	0.	32.45	106.14	58.43	197.02	0.24	0.80	0.44	1.48
30	0.35	6.65	0.	32.80	112.79	58.43	204.02	0.25	0.84	0.44	1.53
31	0.31	6.69	0.	33.11	119.48	58.43	211.02	0.25	0.89	0.44	1.58
32	0.28	6.72	0.	33.39	126.20	58.43	218.02	0.25	0.95	0.44	1.63
33	3.20	96.90	0.	36.59	223.10	58.43	318.12	0.27	1.67	0.44	2.38
34	1.26	99.04	0.	37.85	322.14	58.43	418.42	0.28	2.41	0.44	3.13
35	0.60	92.77	0.	38.45	414.91	58.43	511.79	0.29	3.11	0.44	3.83
36	0.55	92.82	0.	39.00	507.73	58.43	605.16	0.29	3.80	0.44	4.53
37	0.21	100.09	0.	39.21	607.82	58.43	705.46	0.29	4.55	0.44	5.28

Table A.16
Relative Permeability Analysis Summary;
Run 5

PVI	S_o	S_w	S_d	$k_{r,o}$	$k_{r,w}$	$k_{r,d}$	$\frac{X}{L}$
0.460	0.8280	0.0274	0.1446	0.5965	0.0	0.0	1.0
0.500	0.6880	0.1674	0.1446	0.2230	0.0947	0.0	0.920
0.750	0.4030	0.4524	0.1446	0.1756	0.1340	0.0	0.613
1.000	0.3300	0.5254	0.1446	0.1425	0.1978	0.0	0.460
1.250	0.2680	0.5874	0.1446	0.0980	0.2398	0.0	0.368
1.500	0.2200	0.6354	0.1446	0.0594	0.2718	0.0	0.307
1.750	0.1980	0.6574	0.1446	0.0495	0.2929	0.0	0.263
2.000	0.1790	0.6764	0.1446	0.0424	0.3068	0.0	0.230
3.000	0.1380	0.7174	0.1446	0.0189	0.3578	0.0	0.153
4.000	0.1120	0.7434	0.1446	0.0077	0.3980	0.0	0.115
5.000	0.0990	0.7564	0.1446	0.0045	0.4380	0.0	0.092

Table A.17
Fractional Collection Analysis Summary
Run 8 - Dynamic Water Flood

tube no.	tube oil vol. (cc)	tube water vol. (cc)	tube decane vol. (cc)	cum. oil vol. (cc)	cum. water vol. (cc)	cum. decane vol. (cc)	total fluid vol. (cc)	oil rec. (PVI)	water rec. (PVI)	decane rec. (PVI)	PVI
1	0.	0.	3.07	0.	0.	3.07	3.07	0.	0.	0.02	0.02
2	0.	0.	6.70	0.	0.	9.77	9.77	0.	0.	0.07	0.07
3	0.	0.	6.70	0.	0.	16.47	16.47	0.	0.	0.12	0.12
4	0.	0.	6.70	0.	0.	23.17	23.17	0.	0.	0.17	0.17
5	0.	0.	6.55	0.	0.	29.72	29.72	0.	0.	0.22	0.22
6	0.	0.	6.60	0.	0.	36.32	36.32	0.	0.	0.27	0.27
7	0.	0.	6.65	0.	0.	42.97	42.97	0.	0.	0.32	0.32
8	0.	0.	6.70	0.	0.	49.67	49.67	0.	0.	0.37	0.37
9	0.	0.	6.49	0.	0.	56.16	56.16	0.	0.	0.42	0.42
10	0.	0.	6.65	0.	0.	62.81	62.81	0.	0.	0.47	0.47
11	0.	0.	6.60	0.	0.	69.41	69.41	0.	0.	0.52	0.52
12	0.	0.	6.75	0.	0.	76.16	76.16	0.	0.	0.57	0.57
13	1.40	2.10	3.05	1.40	2.10	79.21	82.71	0.01	0.02	0.59	0.62
14	0.32	6.33	0.10	1.72	8.43	79.31	89.46	0.01	0.06	0.59	0.67
15	0.43	6.27	0.10	2.15	14.70	79.41	96.26	0.02	0.11	0.59	0.72
16	0.39	6.11	0.	2.54	20.81	79.41	102.76	0.02	0.16	0.59	0.77
17	0.40	6.25	0.	2.94	27.06	79.41	109.41	0.02	0.20	0.59	0.82
18	0.38	6.27	0.	3.32	33.33	79.41	116.06	0.02	0.25	0.59	0.87
19	0.30	6.30	0.	3.62	39.63	79.41	122.66	0.03	0.30	0.59	0.92
20	0.24	6.31	0.	3.86	45.94	79.41	129.21	0.03	0.34	0.59	0.96
21	0.15	6.40	0.	4.01	52.34	79.41	135.76	0.03	0.39	0.59	1.01
22	0.29	6.36	0.	4.30	58.70	79.41	142.41	0.03	0.44	0.59	1.06
23	0.20	6.35	0.	4.50	65.05	79.41	148.96	0.03	0.49	0.59	1.11
24	0.24	6.51	0.	4.74	71.56	79.41	155.71	0.04	0.53	0.59	1.16
25	0.15	6.55	0.	4.89	78.11	79.41	162.41	0.04	0.58	0.59	1.21
26	2.00	102.22	0.	6.89	180.33	79.41	266.63	0.05	1.35	0.59	1.99
27	1.02	103.20	0.	7.91	283.53	79.41	370.85	0.06	2.12	0.59	2.77

Table A.18
Relative Permeability Analysis Summary;
Run 8 - Dynamic Water Flood

PVI	S_o	S_w	S_d	$k_{r,o}$	$k_{r,w}$	$k_{r,d}$	$\frac{X}{L}$
0.559	0.7400	0.0613	0.1987	—	—	—	1.0
0.620	0.2240	0.5770	0.1987	—	—	—	0.902
0.650	0.2140	0.5873	0.1987	—	—	—	0.86
0.750	0.2069	0.5944	0.1987	0.0736	0.2660	0.0	0.745
1.000	0.1859	0.6154	0.1987	0.0474	0.2758	0.0	0.559
1.250	0.1789	0.6224	0.1987	0.0311	0.2830	0.0	0.447
1.500	0.1649	0.6364	0.1987	0.0240	0.2885	0.0	0.373
1.750	0.1589	0.6424	0.1987	0.0196	0.2927	0.0	0.319
2.000	0.1479	0.6534	0.1987	0.0174	0.2966	0.0	0.280
2.500	0.1469	0.6544	0.1987	0.0130	0.2977	0.0	0.224

Table A.19
Run Core Characteristics

Run no.	Core no.	bead wt. [g]	pore vol. [cc]	porosity %	k _{abs} [darcy]
1	1	541.6	134.1	39.3	—
2	2	533.4	134.7	39.5	43.33
3	1	536.9	128.0	37.5	21.08
4	2	531.5	131.5	38.6	22.92
5	2	535.1	133.5	39.1	22.67
6	1	532.1	135.9	39.9	—
7	1	533.7	134.4	39.4	—
8	2	537.4	134.0	39.3	21.41
9	1	542.6	131.9	38.7	19.57

Appendix B

COMPUTER PROGRAMS

B.1 READPT.BAS

```

10 REM *** CONTINUOUS PRESSURE SAMPLE PROGRAM ***

20 CLS
30 ON ERROR GOTO 500
40 OPEN"COM1:1200,N,8,1,CS,DS,LF"AS#1
50 PRINT#1, "*0100VR"
60 CLOSE#1
80 INPUT "FILENAME FOR RESULTS";FILE$
90 INPUT "ENTER CORE NUMBER:";TYPE$
100 INPUT "WATER RATE IN [CC/MIN]:";RATE1
110 INPUT "BENZYL ALCOHOL RATE IN [CC/MIN]:";RATE2
120 INPUT "DECANE RATE IN [CC/MIN]:";RATE3
130 OPEN FILE$ FOR APPEND AS #2
140 WRITE #2,"DATA FILE: " ,FILE$
150 WRITE #2,"CORE NUMBER: ",TYPE$
160 WRITE #2,"H2O RATE: ",RATE1," BA RATE: ",RATE2," C10 RATE: ",RATE3
170 PRINT ""
180 PRINT "PROGRAM IS STOPPED BY PRESSING 'S' (CAPITAL - S)"
190 PRINT ""
200 PRINT "PRESS ANY KEY TO START"
210 X$ = INKEY$: IF X$ = "" THEN 210

220 REM *** READ INITIAL TEMPERATURE IN DEGREES CENTIGRADE ***

230 OPEN"COM1:1200,N,8,1,CS,DS,LF"AS#1
240 PRINT#1,"*0100Q3"
250 INPUT #1,A$
260 A$ = MID$(A$,6)
270 WRITE #2,"INITIAL TEMPERATURE (C): ",A$
280 PRINT;"INITIAL TEMPERATURE (C): "A$
290 PRINT#1,"*0100P4"

300 REM *** INITIALIZE TIMER ***

310 NOW = TIMER
320 DT = TIMER - NOW

330 REM *** READ PRESSURE VALUES IN PSI ***

```



```
340 INPUT#1,A$
350 A$=MID$(A$,6)
360 WRITE #2,DT,    VAL(A$)
370 PRINT;DT,    A$
380 AA$ = INKEY$: IF AA$ = "S" THEN 400
390 GOTO 320
400 PRINT"PROGRAM STOPPED"
410 REM *** READ FINAL TEMPERATURE ***
420 PRINT#1,"*0100Q3"
430 INPUT#1,A$
440 A$ = MID$(A$,6)
450 WRITE #2,"FINAL TEMPERATURE (C): ",A$
460 PRINT;"FINAL TEMPERATURE:",A$
470 CLOSE #1
480 CLOSE #2
490 END
500 PRINT "ERROR NR";ERR; "ON LINE";ERL
510 RESUME 490
```


B.2 DATAFRAC.F

- c This program does fractional collection analysis calculations
- c for water floods rate.
- c There is a limit of 50 collection containers

```
dimension o(50), w(50), d(50)
dimension Vo(50), Vw(50), Vd(50), Vt(50)
dimension Vto(50), Vtw(50), Vtd(50), Vtt(50)
dimension pvi(50), Itube(50), Ro(50), Rd(50), Rw(50)
```

```
implicit real*8 (a-h,o-z)
```

```
open(unit=3,file='recovdata',status='unknown')
rewind(unit=3)
```

```
open(unit=4,file='recovprint',status='unknown')
rewind(unit=4)
```

```
open(unit=8,file='echodata',status='unknown')
rewind(unit=8)
```

- c Variables are as follows:
- c o = level of the benzyl alcohol in the container
- c w = level of the water in the container
- c d = level of the decane in the container
- c Vo = volume of benzyl alcohol in the container
- c Vw = volume of water in the container
- c Vd = volume of decane in the container
- c Vto = total volume of benzyl alcohol collected
- c Vtw = total volume of water collected
- c Vtd = total volume of decane collected
- c Vtt = total combined volume of fluid collected
- c pvi = pore volumes injected
- c Itube = tube number
- c Ro = oil recovered

- c R_d = decane recovered
- c R_w = water recovered
- c Data must be entered into the data file as follows:
 - c pore volume of core - (porevol)
 - c number of collection samples - (nsamp)
 - c total dead volume of flowing system - (AB)
 - c actual decane flow rate being pumped through system - (qd)
 - c actual oil flow rate being pumped through system - (qo)

```

      read (5,*) porevol
      read (5,*) nsamp
      read (5,*) AB
      read (5,*) qd
      read (5,*) qo

```

- c Determine the fractional flow of the decane and oil
 - $fd = qd / (qd + qo)$
 - $fo = qo / (qd + qo)$
- c Constd and consto are the dead volumes of the decane and oil
 - $constd = ab * fd$
 - $consto = ab * fo$
- c Initialize the Arrays
 - do 10 I = 1,nsamp
 - Itube(I) = 0
 - o(I) = 0.0
 - w(I) = 0.0
 - d(I) = 0.0
 - Vo(I) = 0.0
 - Vw(I) = 0.0
 - Vd(I) = 0.0
 - Vt(I) = 0.0
 - Vtw(I) = 0.0
 - Vto(I) = 0.0
 - Vtd(I) = 0.0
 - Vtt(I) = 0.0
 - pvi(I) = 0.0
 - Ro(I) = 0.0
 - Rd(I) = 0.0


```

        Rw(I) = 0.0
10      continue

c  Read in data
    do 20  I = 1,nsamp
        read (5,*) Itube(I), o(I), w(I), d(I)
20      continue

        I = 1
        Vo(I) = o(I) - consto
        Vto(I) = Vo(I)
        Ro(I) = Vto(I) / porevol
        Vw(I) = w(I) - o(I)
        Vtw(I) = Vw(I)
        Vd(I) = d(I) - w(I) - constd
        Vtd(I) = Vd(I)
        Rd(I) = Vtd(I) / porevol
        Vtt(I) = Vto(I) + Vtw(I) + Vtd(I)
        pvi(I) = Vtt(I) / porevol
        Rw(I) = Vtw(I) / porevol

    do 30  I = 2,nsamp
        Vo(I) = o(I)
        Vto(I) = Vo(I) + Vto(I-1)
        Ro(I) = Vto(I) / porevol
        Vw(I) = w(I) - o(I)
        Vtw(I) = Vw(I) + vtw(I-1)
        Vd(I) = d(I) - w(I)
        Vtd(I) = Vd(I) + Vtd(I-1)
        Rd(I) = Vtd(I) / porevol
        Vtt(I) = Vto(I) + Vtw(I) + Vtd(I)
        pvi(I) = Vtt(I) / porevol
        Rw(I) = Vtw(I) / porevol
30      continue
        ndsamp = nsamp + 1

    write (3,100) ndsamp
    c1 = 0.0

```



```

c2 = 0.0
write (3,101) c1, c2
do 40 j = 1,nsamp
    write (3, 101) pvi(j), Ro(j)
40    continue

    write (3,110) ndsamp
    write (3,101) c1, c2
    do 50 j = 1,nsamp
        write (3, 101) pvi(j), Rd(j)
50    continue

    write (3,120) ndsamp
    write (3,101) c1, c2
    do 60 j = 1,nsamp
        write (3, 101) pvi(j), Rw(j)
60    continue

    write(3,124) 0
    write(4,125)
    write(8,126)
    write(4,150)
    write(8,150)
    write(4,130)
    write(8,131)
    do 80 I = 1,nsamp
        write(4,140) Itube(I), Vo(I), Vw(I), Vd(I),
$           Vto(I), Vtw(I), Vtd(I), Vtt(I), Ro(I), Rw(I),
$           Rd(I), pvi(I)
        write(8,141) Itube(I), o(I), w(I), d(I)
80    continue

    stop
100   format (I5,'      Ro data')
101   format (f12.5,5x,f12.5)
110   format (I5,'      Rd data')
120   format (I5,'      Rw data')
124   format (I5)
125   format ('fractional collection analysis')

```



```
126  format ('fractional collection data ')
130  format (' #   Vo    Vw    Vd    Vto    Vtw    Vtd    Vtt    Ro
      $ Rw  Rd  PVI')
131  format (' #       o       w       d       ')
140  format (I2,1x,f5.2,1x,6(f6.2,1x),4(f5.2))
141  format (I3,1x,3(f7.3,1x))
150  format (' ')
      end
```


B.3 PVST.F

- c This program takes the raw pressure vs time data and averages each
- c " n " number of up to " Istop " number of raw data points for
- c fixed injection flow rates.
- c The pore volume and flow rate must be provided under the parameters

```
implicit real*8 (a-h,o-z)
```

```
dimension time(500), press(500)
```

```
dimension pvi(500), phi(500)
```

```
dimension avetime(500), avepress(500)
```

```
parameter ( n = 100, Istop = 10100)
```

```
parameter ( q = 2.2175, porevol = 134.01)
```

```
open(unit=3,file='pvivsqr',status='unknown')
```

```
rewind(unit=3)
```

```
open(unit=4,file='pvst',status='unknown')
```

```
rewind(unit=3)
```

```
Icount = 0
```

```
npoin = 0
```

```
read(5,*) time(1), press(1)
```

```
1 sumtime = 0.00
```

```
sumpress = 0.00
```

```
ncount = 0
```

```
do 10 I = 1,n
```

```
    Icount = Icount + 1
```

```
    ncount = ncount + 1
```

```
    read(5,*) time(I), press(I)
```

```
    sumtime = sumtime + time(I)
```

```
    sumpress = sumpress + press(I)
```

```
    if (Icount .GE. Istop) go to 20
```

```
10 continue
```

```
20 npoin = npoin + 1
```

```
avetime(npoin) = sumtime / (ncount * 60.0)
```

```
avepress(npoin) = sumpress / ncount
```

```
phi(npoin) = avepress(npoin) / q
```

```
pvi(npoin) = (avetime(npoin) * q) / (porevol)
```



```
      if (Icount .GE. Istop) go to 30
      go to 1
30      write(3,101) npoint
      write(4,101) npoint
      do 40 I = 1,npoint
         write(3,100) pvi(I) , phi(I)
         write(4,100) avetime(I), avepress(I)
40      continue
100     format(f16.8,3x,f16.8)
101     format(I6)
      end
```


B.4 VARIQ.F

- c This program determines the normalized pressure profile vs pore
- c volumes injected for varying flow rates.
- c The program first does fractional collection analysis
- c calculations for water floods then calls the subroutine fixflow
- c which determines the normalized pressure profile for varying flow
- c rates by determining the flow rate for each collection time.
- c There is a limit of 50 collection containers

```
dimension o(50), w(50), d(50)
dimension Vo(50), Vw(50), Vd(50), Vt(50)
dimension Vto(50), Vtw(50), Vtd(50), Vtt(50)
dimension pvi(50), Itube(50), Ro(50), Rd(50), Rw(50)
common/a/ ctime(50), q(50)
```

```
implicit real*8 (a-h,o-z)
```

```
open(unit=7,file='datafrac',status='old',access='unknown')
rewind(unit=7)
```

```
open(unit=3,file='recovdata',status='unknown')
rewind(unit=3)
```

```
open(unit=4,file='recovprint',status='unknown')
rewind(unit=4)
```

```
open(unit=8,file='echodata',status='unknown')
rewind(unit=8)
```

- c Variables are as follows:
- c o = level of the benzyl alcohol in the container
- c w = level of the water in the container
- c d = level of the decane in the container
- c Vo = volume of benzyl alcohol in the container
- c Vw = volume of water in the container
- c Vd = volume of decane in the container

- c V_{to} = total volume of benzyl alcohol collected
- c V_{tw} = total volume of water collected
- c V_{td} = total volume of decane collected

- c V_{tt} = total combined volume of fluid collected

- c p_{vi} = pore volumes injected
- c I_{tube} = tube number
- c R_o = oil recovered
- c R_d = decane recovered
- c R_w = water recovered

- c Data must be entered into the data file as follows:
 - c pore volume of core - (porevol)
 - c number of collection samples - (nsamp)
 - c total dead volume of flowing system - (AB)
 - c actual decane flow rate being pumped through system - (qd)
 - c actual oil flow rate being pumped through system - (qo)

```

      read (7,*) porevol
      read (7,*) nsamp
      read (7,*) AB
      read (7,*) qd
      read (7,*) qo
      
```

- c Determine the fractional flow of the decane and oil
 - $fd = qd / (qd + qo)$
 - $fo = qo / (qd + qo)$

- c Constd and consto are the dead volumes of the decane and oil
 - $constd = ab * fd$
 - $consto = ab * fo$

```

do 10 I = 1,nsamp
  Itube(I) = 0
  o(I) = 0.0
  w(I) = 0.0
  d(I) = 0.0
  Vo(I) = 0.0
  Vw(I) = 0.0
      
```



```

Vd(I) = 0.0
Vt(I) = 0.0
Vtw(I) = 0.0
Vto(I) = 0.0
Vtd(I) = 0.0
Vtt(I) = 0.0
pvi(I) = 0.0
Ro(I) = 0.0
Rd(I) = 0.0
Rw(I) = 0.0
Vt(I) = 0.0
q(I) = 0.0
10   continue

do 20 I = 1,nsamp
    read (7,*) Itube(I), o(I), w(I), d(I), ctime(I)
20   continue

I = 1
Vo(I) = o(I) - consto
Voa = o(I)
Vto(I) = Vo(I)
Ro(I) = Vto(I) / porevol
Vw(I) = w(I) - o(I)
Vwa = w(I) - o(I)
Vtw(I) = Vw(I)
Vd(I) = d(I) - w(I) - constd
Vda = d(I) - w(I)
Vtd(I) = Vd(I)
Rd(I) = Vtd(I) / porevol
Vtt(I) = Vto(I) + Vtw(I) + Vtd(I)
pvi(I) = Vtt(I) / porevol
Rw(I) = Vtw(I) / porevol
Vt(I) = Vo(I) + Vw(I) + Vd(I)
q(I) = (Voa + Vwa + Vda) / ctime(I)

do 30 I = 2,nsamp
    Vo(I) = o(I)
    Vto(I) = Vo(I) + Vto(I-1)

```



```

Ro(I) = Vto(I) / porevol
Vw(I) = w(I) - o(I)
Vtw(I) = Vw(I) + vtw(I-1)
Vd(I) = d(I) - w(I)
Vtd(I) = Vd(I) + Vtd(I-1)
Rd(I) = Vtd(I) / porevol
Vtt(I) = Vto(I) + Vtw(I) + Vtd(I)
pvi(I) = Vtt(I) / porevol
Rw(I) = Vtw(I) / porevol
Vt(I) = Vo(I) + Vw(I) + Vd(I)
q(I) = Vt(I) / ctime(I)

```

```

30      continue

```

```

      ndsamp = nsamp + 1

```

```

      write (3,100) ndsamp
      c1 = 0.0
      c2 = 0.0
      write (3,101) c1, c2
      do 40 j = 1,nsamp
        write (3, 101) pvi(j), Ro(j)

```

```

40      continue

```

```

      write (3,110) ndsamp
      write (3,101) c1, c2
      do 50 j = 1,nsamp
        write (3, 101) pvi(j), Rd(j)

```

```

50      continue

```

```

      write (3,120) ndsamp
      write (3,101) c1, c2
      do 60 j = 1,nsamp
        write (3, 101) pvi(j), Rw(j)

```

```

60      continue

```

```

      write(3,124) 0
      write(4,125)
      write(8,126)

```



```

        write(4,150)
        write(8,150)
        write(4,130)
        write(8,131)
        do 80 I = 1,nsamp
            write(4,140) Itube(I), Vo(I), Vw(I), Vd(I),
$           Vto(I), Vtw(I), Vtd(I), Vtt(I), Ro(I), Rw(I),
$           Rd(I), pvi(I)
            write(8,141) Itube(I), o(I), w(I), d(I)
80      continue

        call fixflow

        stop
100     format (I5,'      Ro data')
101         format (f12.5,5x,f12.5)
110     format (I5,'      Rd data')
120     format (I5,'      Rw data')
124     format (I5)
125     format ('fractional collection analysis')
126     format ('fractional collection data ')
130     format (' #   Vo    Vw    Vd   Vto   Vtw   Vtd   Vtt   Ro
$   Rw   Rd   PVI')
131     format (' #       o       w       d   ')
140     format (I2,1x,f5.2,1x,6(f6.2,1x),4(f5.2))
141     format (I3,1x,3(f7.3,1x))
150     format (' ')
        end

c*****
c*****

        subroutine fixflow

c  This program takes the raw pressure vs time data and averages each
c  " n " number of up to " Istop " number of raw data points to give
c  a managable data file for the graphs

c  This program also adjusts the pressure time data to account for the
c  delay in starting the run and the dead volume of the core

```



```
implicit real*8 (a-h,o-z)
```

```
dimension phi(2000), pvi(2000)
```

```
common/a/ ctime(50), q(50)
```

c set the pore volume of the core: "porevol"

c set the constant displacing fluid flow rate: "qf"

c set the delta time (seconds) from the start of the data file

c until the beginning of the run: "deltat"

c set the flowing dead volume of the core: "Vdead"

```
parameter ( porevol = 131.97)
```

```
parameter ( qf= 2.2175)
```

```
parameter ( deltat = 103.0)
```

```
parameter ( Vdead = 1.82)
```

```
parameter ( n = 100, Istop = 19400)
```

c data.in contains the pressure time data from the run

```
open(unit=11,file='data.in',status='old',access='unknown')
```

```
rewind(unit=11)
```

c fig.data is the output file that contains the corrected normalized

c pressure and pore volume injected data

```
open(unit=12,file='fig.data',status='unknown')
```

```
rewind(unit=12)
```

c calculate the time adjustment: tadj

```
tadj = deltat + 60.0 * (Vdead / q(1))
```

c set initial values

c Icount = number of actual data points read

```
Icount = 0
```


c Npoint = number of points recorded for graphing

Npoint = 0

c ntube = collection tube that data are for

ntube = 1

c runtime = cumulative time of the run

runtime = 0.0

c tubetime = cumulative run time that the tube "ntube" was collected

coltime = ctime(ntube)

c Vinj = cumulative fluid volume injected into the core

c corrected for Vdead and time

Vinj = 0.0

c Vinjole = cumulative fluid volume injected into the core

c at the beginning of the averaging period

Vinjold = 0.0

c Vave = average volume injected into core during a time period

Vave = 0.0

c rtold = runtime at the beginning of the time step

rtold = 0.0

c qave = average flowrat during the time step

qave = 0.0

c ctime(I) = collection time of tube "I"

c q(I) = flowrate of tube "I"

c told = last time point read

c dT = time difference between last time read and current time read


```

        do 999 j = 1,38
999      continue

1       read(11,*) t, p

        told = t
        Icount = Icount + 1
        t = t - tadj
        if (Icount .GE. Istop) go to 20

        if (t .lt. 0.00000) go to 1
        Npoint = Npoint + 1

        phi(Npoint) = p / (q(ntube))
        pvi(Npoint) = 0.0

c      start loop to determine pvi vs normalized pressure

5       sumpress = 0.00
        rtold = runtime
        Vinjold = Vinj

        Vave = 0.0
        ncount = 0
        do 10 I = 1,n
            Icount = Icount + 1
            ncount = ncount + 1
            read(11,*) t, p
            dT = dabs((t - told)/60.0)
            runtime = runtime + dT
            told = t

7       if (runtime .gt. coltime) then
            ntube = ntube + 1
            coltime = coltime + ctime(ntube)
            go to 7
        end if

        Vinj = Vinj + dT * q(ntube)
        Vave = (Vave + dT * q(ntube)) / float(I)
        gave = (Vinj - Vinjold) / (dabs(runtime - rtold))

```



```

        sumpress = sumpress + p
        if (Icount .GE. Istop) go to 20
10      continue
20      Vave = Vave + Vinjold
        avepress = sumpress / ncount
        Npoint = Npoint + 1

        phi(Npoint) = avepress / qave
        pvi(Npoint) = (Vave) / (porevol)
        if (Icount .LT. Istop) go to 5

c  print data

        write(12,100) Npoint
        do 30 I = 1,Npoint
            write(12,200) pvi(I), phi(I)
30      continue
100     format(I5)
200     format(f16.8,3x,f16.8)
        return
        end

```


Thesis

T4174 Thomas

c.1 Three-phase dynamic
displacement measurements
of relative permeability
in porous media using
three immiscible liquids.

Thesis

T4174 Thomas

c.1 Three-phase dynamic
displacement measurements
of relative permeability
in porous media using
three immiscible liquids.





3 2768 00005685 7